Lecture Note on

Sediment Transport and Scour

Subhasish Dey

Department of Civil Engineering
Indian Institute of Technology
Kharagpur
India

2006

Preface

The purpose of this lecture note is to describe the basic mechanics of sediment transport in rivers and scour at various flow obstacles. The background of the audiences should have a basic course in fluid mechanics or hydraulics in undergraduate level. Brief description of different chapters of the lecture note is given below:

- **Chapter 1** deals with the fundamentals in fluid mechanics emphasizing on the Reynolds and bed shear stresses induced by the flow over a sedimentary bed.
- **Chapter 2** presents various concepts of the threshold or beginning of sediment motion.
- **Chapter 3** discusses different bed-load transport theories, which are used to estimate the bed-load transport rate in rivers.
- **Chapter 4** provides the detailed mechanism of suspended-load transport, which is considered to be one of the most important issues of sediment transport.
- **Chapter 5** furnishes the details of bed-forms that are often formed in riverbeds.
- **Chapter 6** gives a comprehensive review on scour within contractions, scour below pipelines, scour downstream of structures, and scour at piers and abutments.

Subhasish Dey 27 November 2006

Associate Professor, Department of Civil Engineering
Indian Institute of Technology
Kharagpur 721302
West Bengal
India

Email: sdey@iitkgp.ac.in
Fax: +91 3222 282254
Phone: +91 3222 283418 (Off), +91 3222 283419 (Res)
Personal homepage: http://www.geocities.com/dr_sdey

Contents

Chapter 1

Flow Characteristics

1.1 General

This chapter summarizes some fundamental principles in fluid mechanics applied to the sediment-laden flows in loose boundary open channels.

1.2 Types of Flow

In general, the fluid flow can be distinguished as laminar flow and turbulent flow. *Laminar flow* occurs at relatively low velocity and it is visualized as layered flow in which layers of fluid slide smoothly over each other with different flow velocities without microscopic mixing of fluid particles normal to the direction of flow. As the flow velocity exceeds a certain value, the flow loses its stability resulting in the sudden formation of eddies which spread throughout the flow region. Such highly irregular, random and fluctuating flow is called *turbulent flow*. The typical characteristic of the turbulent flow is that the velocity and the pressure at a fixed point in space do not remain constant at time but fluctuate very irregularly with high frequency. Flows in rivers and channels are turbulent, in general.

In turbulent flow, it is convenient to describe the hydrodynamic quantities by separating the time-averaged values from their fluctuations. Such decomposition of an instantaneous value of a hydrodynamic quantity is called the *Reynolds decomposition*. Fig. 1.1 illustrates the decomposition of u-component of velocity.

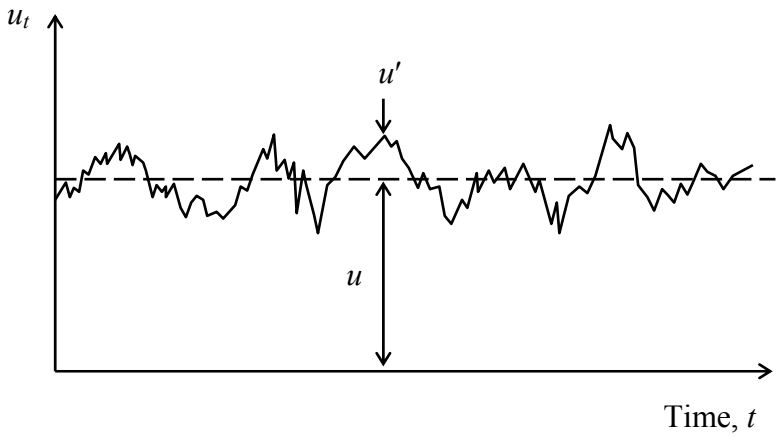

Fig. 1.1 Time series of u_t

The instantaneous velocity components (u_t, v_t, w_t) in the Cartesian coordinate system (x, y, z) and the pressure intensity p_t are given by

$$u_t = u + u' \tag{1.1a}$$

$$v_t = v + v' \tag{1.1b}$$

$$w_t = w + w' \tag{1.1c}$$

$$p_t = p + p' \tag{1.1d}$$

where u, v, w = time-averaged velocities in (x, y, z); u', v', w' = fluctuations of u, v, w; p = time-averaged pressure intensity; and p' = fluctuations of p.

The time-averaged value of a hydrodynamic quantity, say u, is given by

$$u = \frac{1}{t_1}\int_{t_0}^{t_0+t_1} u_t\, dt \tag{1.2}$$

where t_0 = any arbitrary time; and t_1 = time over which the mean is taken. The time t_1 is taken as a sufficiently long interval of time in order to obtain the time independent quantities. Thus, the time-averaged values of all the fluctuations are equal to zero. Similarly, the time-averaged values of the derivatives of velocity fluctuations also vanish.

$$\overline{u'} = \overline{v'} = \overline{w'} = \overline{p'} = 0 \tag{1.3a}$$

$$\overline{\frac{\partial u'}{\partial x}} = \overline{\frac{\partial^2 u'}{\partial x^2}} = \overline{\frac{\partial uu'}{\partial x^2}} = \cdots\cdots = 0 \tag{1.3b}$$

However, the quadratic terms resulting from the products of cross-velocity fluctuations such as $\overline{u'u'}$, $\overline{u'v'}$, and $\partial\overline{u'v'}/\partial x$ do not reduce to zero.

It is pertinent to mention that, in turbulent flow, the velocity fluctuations (u', v', w') influence the time-averaged velocity components (u, v, w), so that (u, v, w) exhibits an apparent increase in the resistance to deformation, which is called as *turbulent stresses* or *Reynolds stresses*.

The following relationships are known as the *Reynolds conditions* (Note: Bar denotes time-averaging), written with two quantities, say, E and G

$$\overline{E+G} = \overline{E} + \overline{G} \tag{1.4a}$$

$$\overline{\text{constant} \times E} = \text{constant} \times \overline{E} \tag{1.4b}$$

$$\overline{\text{constant}} = \text{constant} \tag{1.4c}$$

$$\overline{\frac{\partial E}{\partial s_1}} = \frac{\partial \overline{E}}{\partial s_1} \tag{1.4d}$$

$$\overline{\overline{E}\cdot G} = \overline{E}\cdot\overline{G} \tag{1.4e}$$

$$\overline{\overline{E}} = \overline{E} \tag{1.4f}$$

$$\overline{E'} = 0 \tag{1.4g}$$

$$\overline{\overline{E}\cdot\overline{G}} = \overline{E}\cdot\overline{G} \tag{1.4h}$$

$$\overline{\overline{E}\cdot G'} = \overline{E}\cdot\overline{G}' = 0 \tag{1.4i}$$

where s_1 = space and time coordinate, that is (x, y, z, t).

1.3 Reynolds Equations and Reynolds Stresses

The Navier-Stokes and the continuity equations for an incompressible fluid flow in the Cartesian coordinate system are

$$\frac{\partial u_t}{\partial t} + u_t\frac{\partial u_t}{\partial x} + v_t\frac{\partial u_t}{\partial y} + w_t\frac{\partial u_t}{\partial z} = g_x - \frac{1}{\rho}\frac{\partial p}{\partial x} + \nu\left(\frac{\partial^2 u_t}{\partial x^2} + \frac{\partial^2 u_t}{\partial y^2} + \frac{\partial^2 u_t}{\partial z^2}\right) \tag{1.5a}$$

$$\frac{\partial v_t}{\partial t} + u_t \frac{\partial v_t}{\partial x} + v_t \frac{\partial v_t}{\partial y} + w_t \frac{\partial v_t}{\partial z} = g_y - \frac{1}{\rho}\frac{\partial p}{\partial y} + \nu\left(\frac{\partial^2 v_t}{\partial x^2} + \frac{\partial^2 v_t}{\partial y^2} + \frac{\partial^2 v_t}{\partial z^2}\right) \tag{1.5b}$$

$$\frac{\partial w_t}{\partial t} + u_t \frac{\partial w_t}{\partial x} + v_t \frac{\partial w_t}{\partial y} + w_t \frac{\partial w_t}{\partial z} = g_z - \frac{1}{\rho}\frac{\partial p}{\partial z} + \nu\left(\frac{\partial^2 w_t}{\partial x^2} + \frac{\partial^2 w_t}{\partial y^2} + \frac{\partial^2 w_t}{\partial z^2}\right) \tag{1.5c}$$

$$\frac{\partial u_t}{\partial x} + \frac{\partial v_t}{\partial y} + \frac{\partial w_t}{\partial z} = 0 \tag{1.5d}$$

where g_x, g_y, g_z = components of gravity in (x, y, z); ρ = mass density of fluid; and ν = kinematic viscosity of fluid. Here, Eqs. (1.5a) - (1.5c) represent the equations of motion and Eq. (1.5d) represents the continuity equation. Eqs. (1.5a) - (1.5d) can be rewritten as

$$\frac{\partial u_t}{\partial t} + \frac{\partial (u_t^2)}{\partial x} + \frac{\partial (u_t v_t)}{\partial y} + \frac{\partial (u_t w_t)}{\partial z} = g_x - \frac{1}{\rho}\frac{\partial p}{\partial x} + \nu\left(\frac{\partial^2 u_t}{\partial x^2} + \frac{\partial^2 u_t}{\partial y^2} + \frac{\partial^2 u_t}{\partial z^2}\right) \tag{1.6a}$$

$$\frac{\partial v_t}{\partial t} + \frac{\partial (v_t u_t)}{\partial x} + \frac{\partial (v_t^2)}{\partial y} + \frac{\partial (v_t w_t)}{\partial z} = g_y - \frac{1}{\rho}\frac{\partial p}{\partial y} + \nu\left(\frac{\partial^2 v_t}{\partial x^2} + \frac{\partial^2 v_t}{\partial y^2} + \frac{\partial^2 v_t}{\partial z^2}\right) \tag{1.6b}$$

$$\frac{\partial w_t}{\partial t} + \frac{\partial (w_t u_t)}{\partial x} + \frac{\partial (w_t v_t)}{\partial y} + \frac{\partial (w_t^2)}{\partial z} = g_z - \frac{1}{\rho}\frac{\partial p}{\partial z} + \nu\left(\frac{\partial^2 w_t}{\partial x^2} + \frac{\partial^2 w_t}{\partial y^2} + \frac{\partial^2 w_t}{\partial z^2}\right) \tag{1.6c}$$

$$\frac{\partial u_t}{\partial x} + \frac{\partial v_t}{\partial y} + \frac{\partial w_t}{\partial z} = 0 \tag{1.6d}$$

Using Reynolds decomposition [Eq. (1.1)] into Eqs. (1.6a) - (1.6d), taking into account the Reynolds conditions [Eqs. (1.4a) – (1.4i)], yield

$$\frac{\partial u}{\partial t} + u\frac{\partial u}{\partial x} + v\frac{\partial u}{\partial y} + w\frac{\partial u}{\partial z} = g_x - \frac{1}{\rho}\frac{\partial p}{\partial x} + \nu\nabla^2 u - \left(\frac{\partial \overline{u'u'}}{\partial x} + \frac{\partial \overline{u'v'}}{\partial y} + \frac{\partial \overline{u'w'}}{\partial z}\right) \tag{1.7a}$$

$$\frac{\partial v}{\partial t} + u\frac{\partial v}{\partial x} + v\frac{\partial v}{\partial y} + w\frac{\partial v}{\partial z} = g_y - \frac{1}{\rho}\frac{\partial p}{\partial y} + \nu\nabla^2 v - \left(\frac{\partial \overline{v'u'}}{\partial x} + \frac{\partial \overline{v'v'}}{\partial y} + \frac{\partial \overline{v'w'}}{\partial z}\right) \tag{1.7b}$$

$$\frac{\partial w}{\partial t} + u\frac{\partial w}{\partial x} + v\frac{\partial w}{\partial y} + w\frac{\partial w}{\partial z} = g_z - \frac{1}{\rho}\frac{\partial p}{\partial z} + \nu\nabla^2 w - \left(\frac{\partial \overline{w'u'}}{\partial x} + \frac{\partial \overline{w'v'}}{\partial y} + \frac{\partial \overline{w'w'}}{\partial z}\right) \tag{1.7c}$$

$$\frac{\partial u}{\partial x} + \frac{\partial v}{\partial y} + \frac{\partial w}{\partial z} = 0 \tag{1.7d}$$

where $\nabla^2 = \frac{\partial^2}{\partial x^2} + \frac{\partial^2}{\partial y^2} + \frac{\partial^2}{\partial z^2}$.

Subtracting Eq. (1.7d) from Eq. (1.6d), gives the continuity equation for fluctuating part

$$\frac{\partial u'}{\partial x} + \frac{\partial v'}{\partial y} + \frac{\partial w'}{\partial z} = 0 \tag{1.8}$$

Thus, the time-averaged velocity components and their fluctuations satisfy the continuity equation. Eqs. (1.7a) - (1.7c) are identical with Eqs. (1.5a) - (1.5c) if (u_t, v_t, w_t) are replaced by (u, v, w), except the last terms. These last terms are obtained from three cross products of velocity fluctuations and provide additional stresses developed due to turbulence. Hence,

they are called as *turbulent shear stresses* or *Reynolds stresses* and can be expressed as a stress tensor called *Reynolds stress tensor* given as

$$\begin{pmatrix} \sigma_u & \tau_{uv} & \tau_{uw} \\ \tau_{vu} & \sigma_v & \tau_{vw} \\ \tau_{wu} & \tau_{wv} & \sigma_w \end{pmatrix} = -\rho \begin{pmatrix} \overline{u'u'} & \overline{u'v'} & \overline{u'w'} \\ \overline{v'u'} & \overline{v'v'} & \overline{v'w'} \\ \overline{w'u'} & \overline{w'v'} & \overline{w'w'} \end{pmatrix} \tag{1.9}$$

where σ_u, σ_v, σ_w = normal stresses in (x, y, z) directions; and τ_{uv}, τ_{uw}, τ_{vu}, τ_{vw}, τ_{wu}, τ_{wu} = shear stresses. These Reynolds stresses are developed due to turbulent fluctuations and are given by the time-averaged values of the quadratic terms in the turbulent fluctuations. As these terms are added to the ordinary viscous stresses in the laminar flow and have a similar influence on the flow, it is often called *eddy viscosity*. In general, these Reynolds stresses far outweigh the viscous stresses in turbulent flow.

1.4 Reynolds Stress Distribution in Open Channel Flow

For a steady flow having zero-pressure gradient in the x-direction (with streamwise slope θ), the basic equations are continuity equation and two components of Reynolds equations. The continuity equation is automatically satisfied. The z-component of Reynolds equation [Eq. (1.7c)] gives an equation for the Reynolds stress $-\rho\overline{w'w'}$. On the other hand, the x-component of Reynolds equation [Eq. (1.7a)] reduces to

$$\frac{\partial u}{\partial t} + u\frac{\partial u}{\partial x} + w\frac{\partial u}{\partial z} = g_x - \frac{1}{\rho}\frac{\partial p}{\partial x} + \nu\left(\frac{\partial^2 u}{\partial x^2} + \frac{\partial^2 u}{\partial z^2}\right) - \left(\frac{\partial \overline{u'u'}}{\partial x} + \frac{\partial \overline{u'w'}}{\partial z}\right) \tag{1.10}$$

The valid conditions are $\partial u/\partial t = 0$; $w = 0$; $g_x = -g\sin\theta$; $\partial p/\partial x = 0$; and $u = u(z)$; where g = gravitational acceleration. Also, $\partial u/\partial x = 0$ for uniform flow. Therefore, Eq. (1.10) becomes

$$\mu\frac{d^2u}{dz^2} + \frac{d(-\rho\overline{u'w'})}{dz} = \rho g\frac{dh}{dx} \tag{1.11}$$

where μ = dynamic viscosity of fluid, that is $\rho\nu$. Eq. (1.11) can be written as

$$\frac{d}{dz}\left[\mu\frac{du}{dz} + (-\rho\overline{u'w'})\right] = \frac{\tau_0}{h} \tag{1.12}$$

where τ_0 = bed shear stress, that is $\rho g h(dh/dx)$.

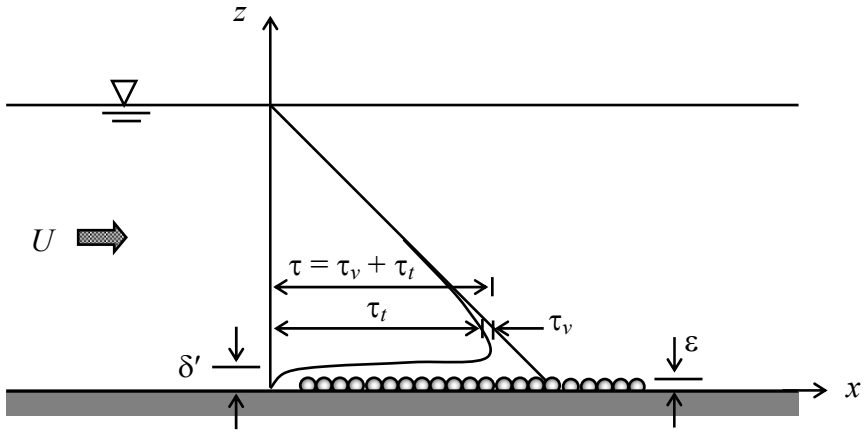

Fig. 1.2 Shear stress components and distribution

The terms inside the parenthesis in LHS of Eq. (1.12) are expressed as

$$\mu \frac{du}{dz} + (-\rho \overline{u'w'}) = \tau_v + \tau_t = \tau \tag{1.13}$$

where τ_v = shear stress due to viscosity, that is $\mu(du/dz)$; τ_t = shear stress due to turbulence or Reynolds stress, that is $-\rho \overline{u'w'}$; and τ = total shear stress. Therefore, Eq. (1.12) becomes

$$d\tau/dz = \tau_0 / h \tag{1.14}$$

Integrating Eq. (1.14) yields

$$\tau = [1 - (z/h)]\tau_0 \tag{1.15}$$

Fig. 1.2 gives the vertical distribution of shear stress.

1.5 Classical Turbulence Theory

As the phenomenon of turbulence is complex, no theory is available to describe the phenomena completely. All existing theories are based on the semi-empirical hypothesis, which establish relationship between the Reynolds stresses caused by the exchange of momentum and the time-averaged velocities. The basic theories proposed by Prandtl and von Karman are given below:

1.5.1 *Prandtl's Mixing-Length Theory*

Prandtl introduced the mixing-length concept in order to calculate the turbulent shear stress or Reynolds stress. He simulated the momentum exchange on a macro-scale to that of the molecular motion of a gas to explain the mixing phenomenon induced by the turbulence in a fluid flow; and thus established the *mixing-length theory*.

When the fluid flows over a solid boundary in turbulent motion, the fluid particles unite into elements called *eddies* or *parcels*. These elements move both in longitudinal and transverse directions. During the motion of element, there is no momentum transfer. Fig. 1.3 shows such a fluid element located in layer 1, having velocity u_1, moves to layer 2, having velocity u_2, due to eddy motion. The velocity of element is still u_1, when it just arrives at layer 2, and decreases to u_2 sometime later by the momentum exchange with the fluid in layer 2. This action will speed up the fluid in layer 2, which cause the development of turbulent shear stress τ_t acting on layer 2 while accelerating layer 2. The horizontal instantaneous velocity fluctuation of the fluid element in layer 2 is given by

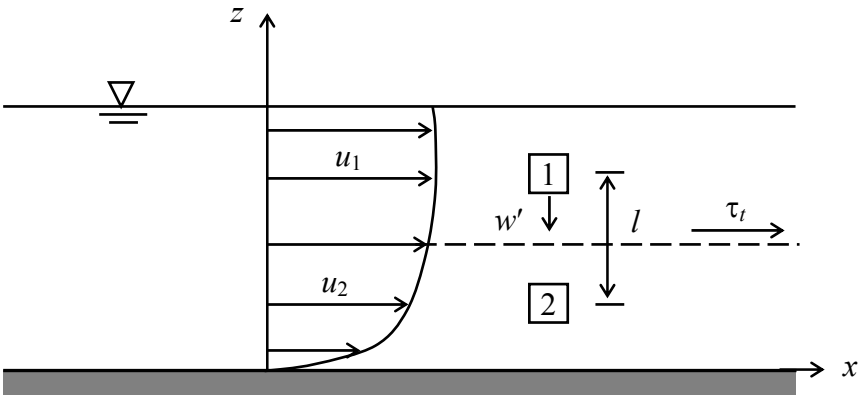

Fig. 1.3 Sketch showing the mixing-length in turbulent flow

$$u' = u_2 - u_1 = l\frac{du}{dz} \tag{1.16}$$

where l = mixing length. Following the hypothesis of Prandtl that the vertical velocity fluctuation w' is of the same order of magnitude of u'

$$w' = -l\frac{du}{dz} \tag{1.17}$$

Here, the negative sign is due to downward movement of fluid element. The turbulent shear stress or Reynolds stress τ_t now becomes

$$\tau_t = -\rho\overline{u'w'} = \rho l^2\left(\frac{du}{dz}\right)^2 \tag{1.18}$$

This yields the turbulent model of the mixing-length

$$\tau_t = \rho l^2\left|\frac{du}{dz}\right|\left(\frac{du}{dz}\right) \tag{1.19}$$

$$\tau_t = \rho\varepsilon_m\frac{du}{dz} \tag{1.20}$$

where ε_m = kinematic eddy viscosity, that is $l^2(du/dz)$. Using Eq. (1.20) into Eq. (1.13) yields

$$\tau = (\mu + \rho\varepsilon_m)\frac{du}{dz} = \rho(\nu + \varepsilon_m)\frac{du}{dz} \tag{1.21}$$

According to Prandtl, the mixing-length l is proportional to the distance z from the boundary. For a smooth flow (laminar flow), l must vanish, as the transverse motion of fluid is inhibited. The relationship between l and z is given by

$$l = \kappa z \tag{1.22}$$

where κ = von Karmans constant, determined from the experiments.

1.5.2 *Similarity Hypothesis of Turbulent Flow after von Karman*

von Karman (1930) developed an important relationship for the mixing-length l based on the similarity hypothesis. His assumed: (1) except in a region near the boundary, turbulence phenomena are not affected by the viscosity; and (2) the basic pattern of turbulence at different positions are similar, i.e. they differ only in scales of time and length. In other words, the mixing-length l is a function of the distribution of the mean motion in the turbulent flow, while it is indirectly related to the distance z from the boundary. Using the similarity hypothesis, von Karman suggested the mixing-length as

$$l = \kappa\frac{du/dz}{d^2u/dz^2} \tag{1.23}$$

Eq. (1.23) indicates that the mixing-length is a local function and depends only on velocity distribution in the neighborhood of a particular point.

1.6 Classification of Flow Layer

The fluid flow over a solid boundary is classified into different flow layers (Fig. 1.4):

1. *Viscous sub-layer*: A thin layer just adjacent to the boundary. The flow in this layer is fully laminar, and turbulence is totally absent.

2. *Transition-layer or buffer-layer*: In this layer both viscous and turbulence effects exist.
3. *Turbulent logarithmic-layer*: A layer in which viscous shear stress is negligible and the shear stress is due to the turbulence only.
4. *Turbulent outer-layer*: In this layer, velocities are almost constant because of the presence of large eddies, which produce strong mixing of flow. This layer possesses approximately 80 % to 90 % of the flow region.

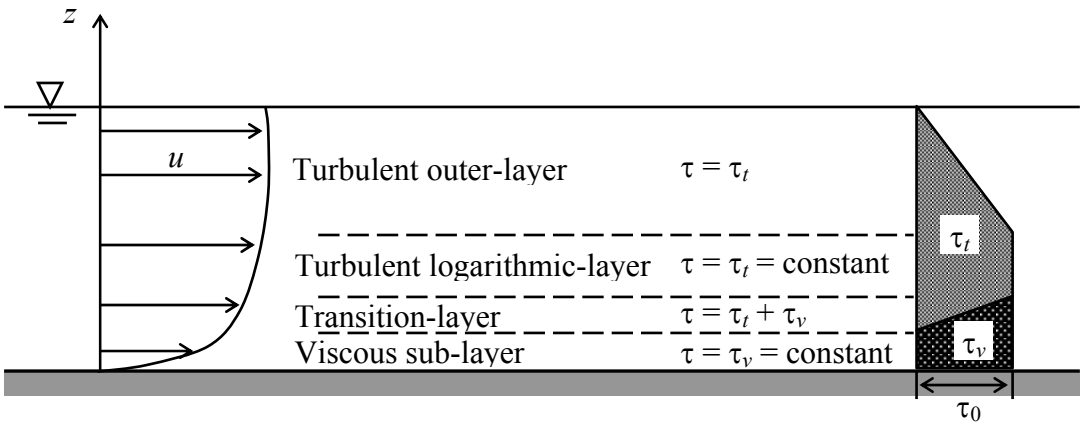

Fig. 1.4 Classification of flow region (layer thickness not to scale)

By the modification of the mixing-length after Prandtl, the logarithmic velocity profile is applicable to both the buffer- and turbulent outer-layers. On the other hand, in the viscous sub-layer, the boundary roughness plays a role on the velocity distribution, which was first observed by Nikuradse (1933), who introduced the concept of equivalent roughness ε, called *Nikuradse's equivalent roughness*. Based on the experimental data, the flow is classified as follows:

1. *Hydraulically smooth flow* ($R_* \leq 5$): Bed roughness is much smaller than the thickness of viscous sub-layer δ′ and hence will not affect the velocity distribution.
2. *Hydraulically rough flow* ($R_* \geq 70$): Bed roughness is so large that it produces eddies near the boundary and viscous sub-layer no longer exists.
3. *Hydraulically transitional flow* ($5 < R_* < 70$): The velocity distribution is affected by both the bed roughness and the viscosity.

where R_* = shear Reynolds number, that is $u_*\varepsilon/\nu$; and u_* = shear velocity, that is $(\tau_0/\rho)^{0.5}$. Fig. 1.5 presents the effect of bed roughness on the flow field.

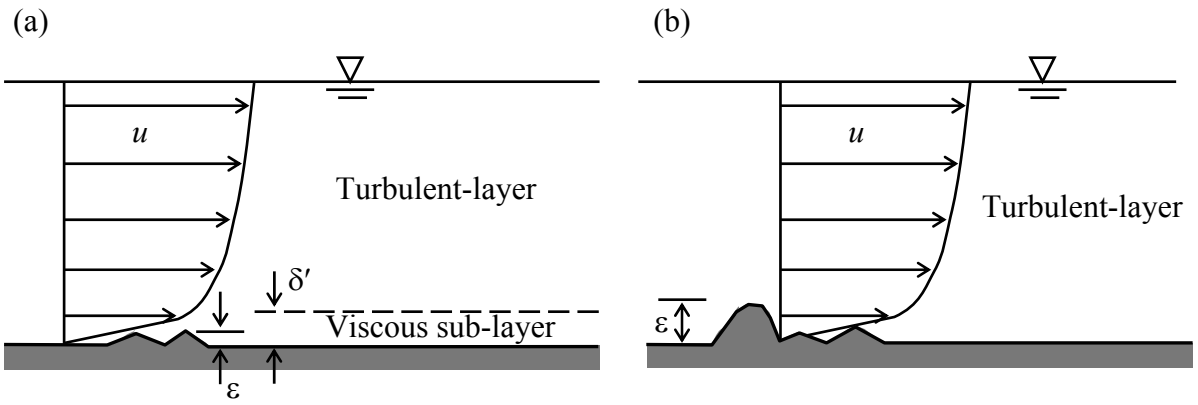

Fig. 1.5 (a) hydraulically smooth flow and (b) hydraulically rough flow

1.7 Velocity Distributions

The flow zone over a boundary is characterized by the two-layer: an *inner-layer* where the flow is directly affected by the bed roughness and an *outer-layer* where the bed roughness indirectly influences the flow. The inner-layer consists of viscous sub-layer and transition- or buffer-layer. On the other hand, the outer-layer is divided into turbulent logarithmic-layer and turbulent outer-layers. Fig. 1.6 depicts the velocity profiles in different layers over a smooth boundary. The velocity distributions in different layers are given in the succeeding sub-sections.

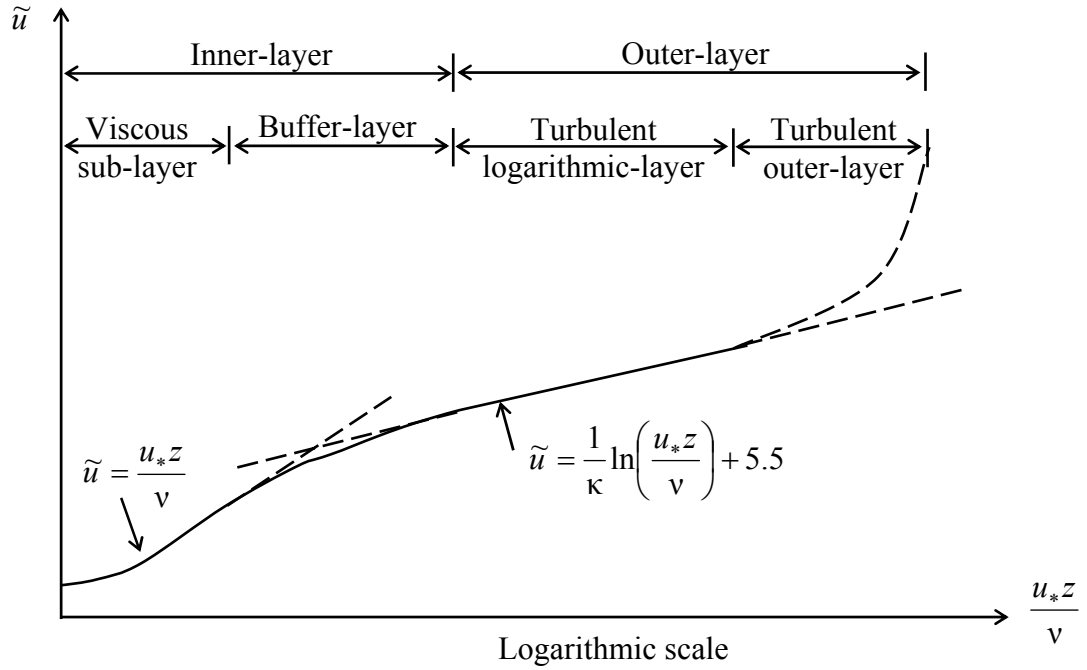

Fig. 1.6 Velocity profiles in different layers

1.7.1 *Linear-Law in Viscous Sub-Layer*

In case of hydraulically smooth flow, the viscous shear stress is constant (Fig. 1.4) and equal to bed shear stress τ_0. That is

$$\tau_v = \rho\nu\frac{du}{dz} = \tau_0 \tag{1.24}$$

$$du = \frac{u_*^2}{\nu}dz \tag{1.25}$$

Integrating and using no-slip condition at the boundary, that is $u\big|_{z=0} = 0$, yields

$$\widetilde{u} = \frac{u_* z}{\nu} \tag{1.26}$$

where $\widetilde{u} = u/u_*$. Thus, there is a linear velocity distribution in the viscous sub-layer as shown in Fig. 1.6. Eq. (1.26) is valid for the range $0 < u_* z/\nu \leq 5$.

1.7.2 *Logarithmic-Law in Turbulent-Layer*

In the turbulent-layer, the total shear stress τ contains only the turbulent shear stress τ_t (Fig. 1.4). According to Prandtl's mixing-length theory, one gets

$$\tau_t = \rho l^2 \left(\frac{du}{dz}\right)^2 = \tau_0 \tag{1.27}$$

Putting $l = \kappa z$, yields

$$du = \frac{u_*}{\kappa z} dz \tag{1.28}$$

Integration of Eq. (1.28) gives the logarithmic velocity distribution

$$\tilde{u} = \frac{1}{\kappa} \ln z + \text{constant} \tag{1.29}$$

Using the boundary condition $u = 0$ and $z = z_0$, that is zero-velocity level, gives

$$\tilde{u} = \frac{1}{\kappa} \ln\left(\frac{z}{z_0}\right) \tag{1.30}$$

According to Nikuradse's study on pipe flows, the expressions for z_0 are

$$z_0 = 0.11\frac{\nu}{u_*} \qquad \text{for smooth flow } R_* \le 5 \tag{1.31a}$$

$$z_0 = 0.033\varepsilon \qquad \text{for rough flow } R_* \ge 70 \tag{1.31b}$$

$$z_0 = 0.11\frac{\nu}{u_*} + 0.033\varepsilon \qquad \text{for transition } 5 < R_* < 70 \tag{1.31c}$$

The ASCE Task Force on Friction Factor in Open Channels (1963) reported that for open channel roughness similar to that encountered in pipes, the resistance equations similar to those of pipe flows are adequate. Therefore, for the flow over a smooth boundary, such as a plane bed surface having median particle size less than 0.25 mm, using Eq. (1.31a) into Eq. (1.30) yields

$$\tilde{u} = \frac{1}{\kappa} \ln\left(\frac{u_* z}{\nu}\right) + 5.5 \tag{1.32}$$

On the other hand, for the flow over a rough boundary, such as gravel-beds, which are often encountered in hilly rivers, Eq. (1.29) reduces to

$$\tilde{u} = \frac{1}{\kappa} \ln \tilde{z} + B_r \tag{1.33}$$

where $\tilde{z} = z/\varepsilon$; B_r = constant of integration, that is $-(1/\kappa)\ln \tilde{z}_0$; and $\tilde{z}_0 = z_0/\varepsilon$. Importantly, it is uncertain to consider the traditional value of the von Karman constant κ as 0.41 for mobile boundaries, as was done by Kironoto and Graf (1994) and Song et al. (1994); because Nikora and Goring (2000) reported that the value of κ goes down when the bed is mobile. Therefore, it is essential to estimate κ from the concept of the mixing-length using the experimental data. The schematic view of the flow over a gravel-bed is shown in Fig. 1.7.

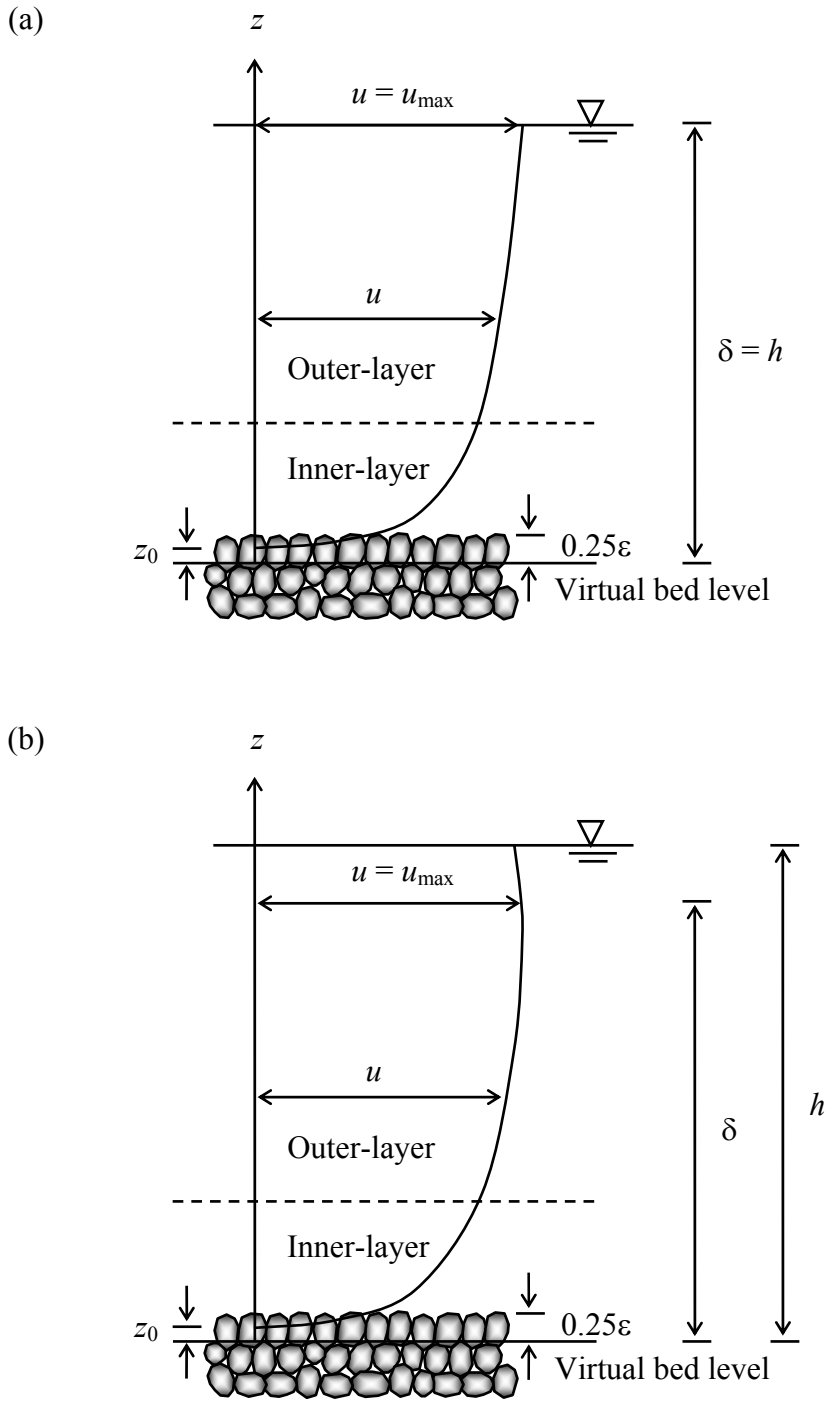

Fig. 1.7 Schematic velocity profiles on gravel-beds: (a) wide channel and (b) deep channel

To calculate the mixing-length l from Eq. (1.19), Raikar (2006) used the measured velocity profiles to determine the velocity gradients du/dz by smooth curve fitting to the data, while he obtained the Reynolds stresses τ directly from the measured Reynolds stress distributions. The variation of nondimensional mixing-length $\hat{l}$ (= l/δ) with nondimensional flow depth $\hat{z}_1$ (= z/δ) is shown in Fig. 1.8, where δ is the normal distance of the occurrence of maximum velocity from the virtual bed level, that is the boundary-layer thickness. In the inner-layer, all the experimental data of gravel-beds (under the near-threshold condition) collapse reasonably on a single band, and the mixing-length $\hat{l}$ increases linearly with an increase in flow depth $\hat{z}_1$ up to $\hat{z}_1 = 0.23$, being in conformity with the Prandtl's hypothesis. The average value of

the von Karman constant κ (and their standard deviation) obtained from the slope of the fitted straight line is 0.35 (± 0.003) and the upper-limit of the inner-layer is $\hat{z}_1 = 0.23$ (within this limit, l is linear with z). The value of κ is slightly less than that of von Karman's 0.41 and greater than that of Nikora and Goring's (2000) 0.29 for mobile gravel-beds. Hence, it corroborates that the unrest condition of the surface particles at near-threshold is the principal cause of the reduction of the value of κ. However, the upper-limit of the inner-layer obtained as $\hat{z}_1 = 0.23$, in this study, is slightly higher, since $\hat{z}_1 = 0.2$ is the traditional upper-limit (Nezu and Nakagawa 1993). Beyond $\hat{z}_1 = 0.23$, the mean trend of the curve is nonlinear becoming almost constant at $\hat{l} \approx 0.11$ towards the free surface. The data trend of Nezu and Rodi (1986) and Cardoso et al. (1989) were similar as well towards the free surface. In $\hat{z}_1 >$ 0.23, the data shows a considerable scatter, which is also evident in Nezu and Nakagawa (1993), Kironoto and Graf (1994), and Song et al. (1994).

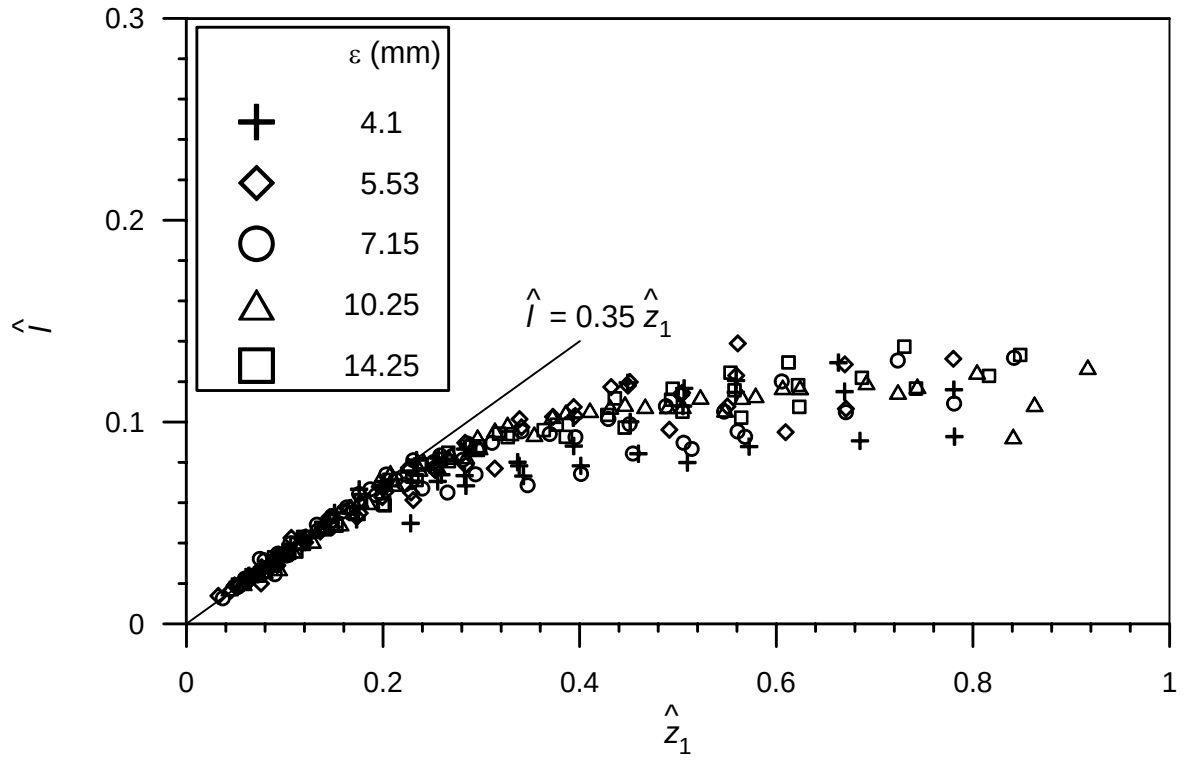

Fig. 1.8 Mixing-length as a function of flow depth (Raikar 2006)

The average value of B_r (and their standard deviation) obtained by Raikar (2006) for gravel-beds under the near-threshold condition is 7.8 (±0.37). It is less than those reported in the literature for rough boundary streams, for instance, 8.5 (±0.15) of Reynolds (1974), 8.47 (±0.9) of Kironoto and Graf (1994) and 8.42 (±0.22) of Song et al. (1994). In Nikora and Goring (2000), the values of B_r are rather high. Importantly, in flows with unrest surface particles at the near-threshold condition, there prevails a tendency of decreasing value of B_r.

1.7.3 *Law of Wake in Turbulent Outer-Layer (Coles Law)*

In the outer-layer (in the vicinity of the free surface) the velocity profile deviates from the logarithmic-law, as the distance from the boundary increases ($u_* z/\nu > 1000$) as shown in Fig. 1.6 by the broken line. The reason for this departure is owing to the assumption of constant

shear stress throughout the fluid and mixing-length. Coles (1956) suggested the complete description of the velocity distribution u, including the law of the wake as

$$\tilde{u} = \left[\frac{1}{\kappa}\ln\left(\frac{u_* z}{\nu}\right) + 5.5\right] + \frac{2\Pi}{\kappa}\sin^2\left(\frac{\pi}{2}\hat{z}_1\right) \quad \text{for smooth flow} \qquad (1.34a)$$

$$\tilde{u} = \frac{1}{\kappa}\ln\tilde{z} + B_r + \frac{2\Pi}{\kappa}\sin^2\left(\frac{\pi}{2}\hat{z}_1\right) \quad \text{for rough flow} \qquad (1.34b)$$

where Π = Coles' wake parameter. The last term describes the velocity enhancement in the turbulent outer-layer and is called the *wake function*. The wake function is zero near the boundary and increases gradually towards the free surface and reaches a maximum value of $2\Pi/\kappa$.

The usual form of the Coles' law of the wake is in terms of velocity defect that would require information on the maximum velocity of a vertical distribution of velocity. Thus, Raikar used the experimental velocity distributions to estimate the wake parameter Π from Eq. (1.34b) for gravel-beds under the near-threshold condition. The average value of Π (and their standard deviation) calculated is 0.11 (± 0.026). Due to the feeble movement of the surface particles at the near-threshold condition, the value of Π is slightly greater than those of fixed rough boundaries, for example, 0.09 of Kironoto and Graf (1994) and 0.08 of Song et al. (1994). The lone case of negative value of Π (= -0.03) for a gravel-bed of ε = 23 mm was reported by Kironoto and Graf (1994). In contrast, for smooth boundary streams, the values of Π are relatively high. Coleman (1981) found an average value of Π as 0.19, Nezu and Rodi (1986) obtained as 0.2, Steffler et al. (1985) reported as 0.08 - 0.15 and Kirkgöz (1989) observed as 0.1. Coleman (1981) and Nezu and Rodi (1986) studied the flow with reasonably high Reynolds numbers. However, for low flow Reynolds numbers, the value of Π goes as high as 0.23 (Dong et al. 1991; Nezu and Nakagawa 1993; Nikora and Goring 2000).

1.8 Turbulence Characteristics in Flow over Loose Beds

The fluctuating velocity is one of the most important characteristics of turbulence, and hence, its measurement has received top priority in the studies of turbulence. In recent years, acoustic Doppler velocimeter (ADV) and laser Doppler anemometer (LDA) are being used to measure the turbulent characteristics in fluid flows.

The turbulence fluctuations are presented in the form of root-mean-square (RMS) termed *turbulence intensity*. The root-mean-square values of turbulent fluctuations in streamwise u^+ [= $(\overline{u'u'})^{0.5}$] and vertical w^+ [= $(\overline{w'w'})^{0.5}$] directions are written in nondimensional form dividing by either the shear velocity u_* or the depth-averaged flow velocity U. The experimental results of Grass (1971) are shown in Fig. 1.9. The conclusions of the results are as follows:

- The turbulence intensity is zero at a boundary and increases rapidly to reach its peak value within a slight distance from the boundary. Away from the boundary, in the main flow region, the turbulence intensity is less and nearly constant.
- In the main flow region, the vertical fluctuations approach shear velocity, $w^+/u_* \approx 1$, while the streamwise fluctuations are slightly greater than the shear velocity.
- The boundary roughness has no effect on the intensity of the fluctuations in the main flow region. However, close to the boundary, the turbulent fluctuations are influenced by the boundary roughness. More the boundary roughness lesser the streamwise turbulence fluctuations and greater is the vertical turbulence fluctuations.

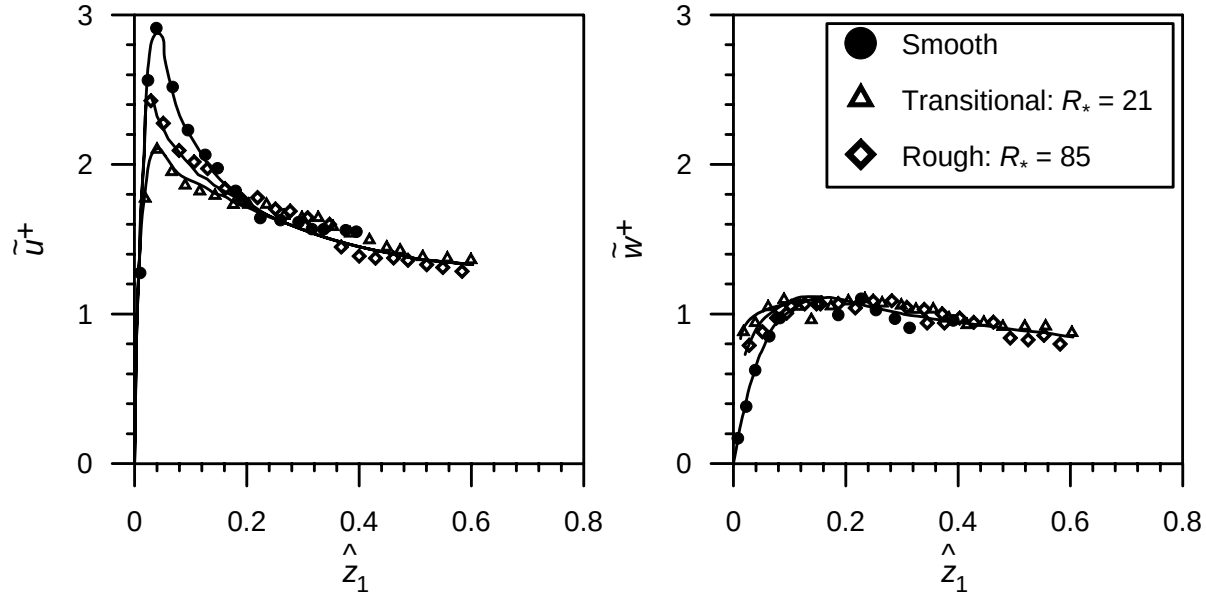

Fig. 1.9 Turbulence quantities (Grass 1971)

Nezu (1977) suggested the following exponential-law for the nondimensional streamwise and vertical turbulence intensities:

$$\tilde{u}^+ = B_u \exp(-C_u \hat{z}_1) \tag{1.35a}$$

$$\tilde{w}^+ = B_w \exp(-C_w \hat{z}_1) \tag{1.35b}$$

where $\tilde{u}^+ = u^+/u_*$; $\tilde{w}^+ = w^+/u_*$; $w^+ = (\overline{w'w'})^{0.5}$; and B_u, B_w, C_u, and C_w = constants. The values of the constants were obtained from the experimental data, as given in Table 1. Also, Fig. 1.10 shows more distributions of $\tilde{u}^+$ and $\tilde{w}^+$ over gravel-beds under the near-threshold condition as obtained by Raikar (2006). In addition, Nikora and Goring (1998) proposed the logarithmic-law of turbulence intensities for mobile gravel-beds as:

$$\tilde{u}^{+2} = 1.9 + 1.32 \ln \hat{z}_1 \tag{1.36a}$$

$$\tilde{w}^{+2} = 0.59 + 0.22 \ln \hat{z}_1 \tag{1.36b}$$

It is evident from Fig. 1.10 that $\tilde{u}^+$ and $\tilde{w}^+$ for mobile beds (Nikora and Goring 1998) are greater than those for beds under near-threshold condition (Raikar 2006).

Table 1. Constants of Exponential-Law for Turbulent Intensities

Source	B_u	C_u	B_w	C_w	Boundary condition
Nezu (1977)	2.3	1	1.27	1	Smooth and rough
Nezu and Rodi (1986)	2.26	0.88	1.23	0.67	Smooth and rough
Cardoso et al. (1989)	2.28	1.08	-	-	Smooth
Kironoto and Graf (1994)	2.04	0.97	1.14	0.76	Rough
Raikar (2006)	2.07	0.95	1.17	0.69	Rough

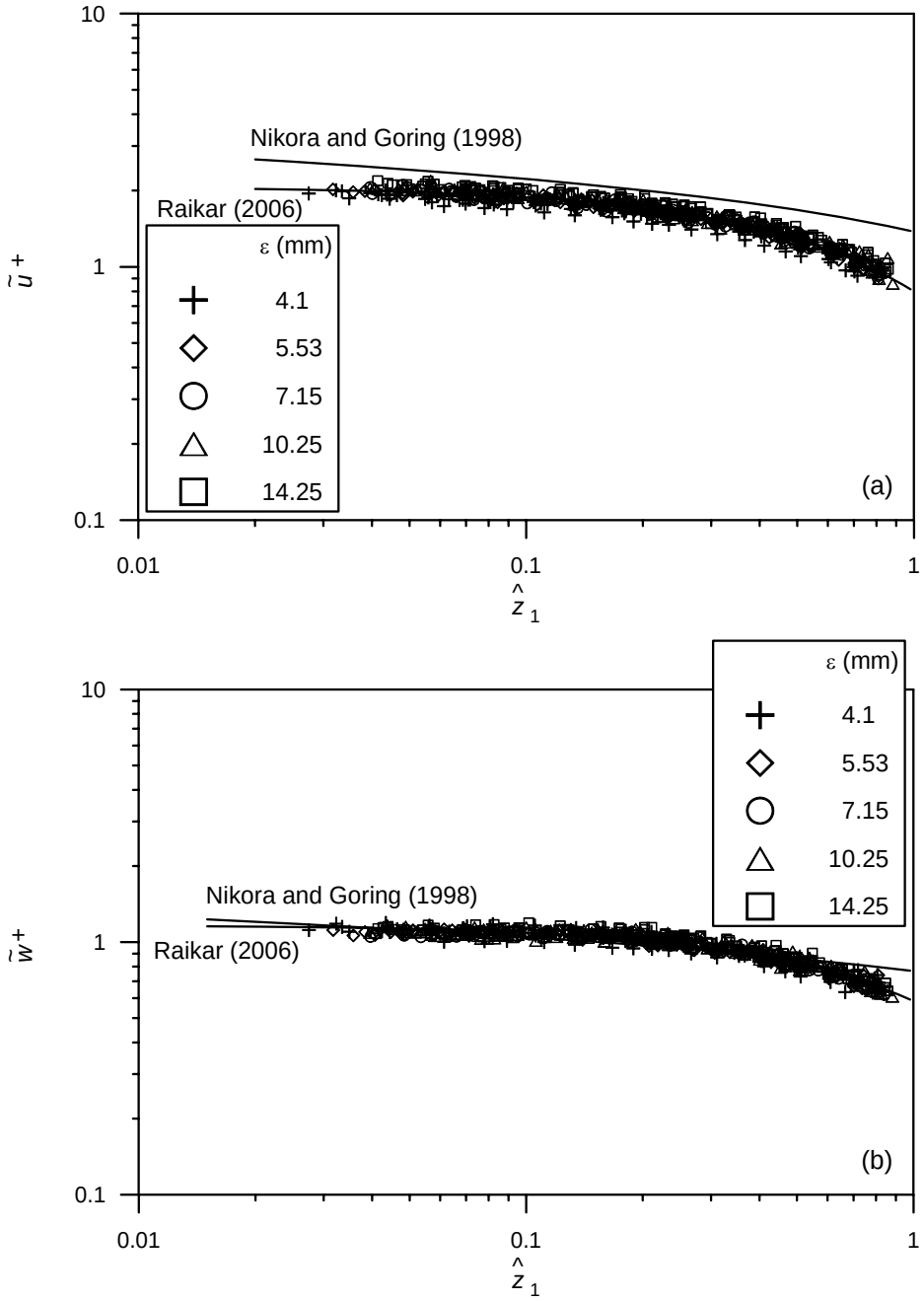

Fig. 1.10 Variations of (a) $\tilde{u}^+$ with $\hat{z}_1$ and (b) $\tilde{w}^+$ with $\hat{z}_1$ for different ε after Nikora and Goring (1998) and Raikar (2006), and a comparison with the experimental data of Raikar (2006) for gravel-beds under near-threshold condition

1.9 Experimental Determination of Bed Shear Stress

- The shear velocity u_* [$= (\tau_0/\rho)^{0.5}$] and hence bed shear stress τ_0 can be determined from the well-known Clauser method, applying the least square fitting of Eq. (1.32) or Eq. (1.33) to the experimental data in the inner-layer ($\tilde{z} < 0.2$).
- The bed shear stress τ_0 can be obtained from the Reynolds stress profiles extending them on the boundary, that is $\tau_0 = \tau\big|_{z=z_0}$.

- The bed shear stress τ_0 can be calculated from the bed-slope S, as $\tau_0 = \rho g h S$.

1.10 Bed Shear in a Rectangular Channel with Rough Bed and Smooth Walls

The equation of bed shear stress τ_b (in the preceding, the symbol τ_0 has been used for bed shear stress) as a function of dynamic pressure is used here. It is

$$\tau_b = \frac{f_b}{8} \rho U_b^2 \tag{1.37}$$

where f = friction factor. Subscript b refers to the quantities associated with the bed. The Colebrook-White equation, used to evaluate f_b, is given below:

$$\frac{1}{\sqrt{f_b}} = -0.86 \ln\left(\frac{\varepsilon P_b}{14.8 A_b} + \frac{2.51}{R_b \sqrt{f_b}} \right) \tag{1.38}$$

where A = flow area; P = wetted perimeter; and R = Reynolds number of flow. In a rectangular channel or an experimental flume, the bed is rough consisting of sediment particles and the sidewalls are smooth. Therefore, f_w is considerably different from f_b, where subscript w refers to the quantities associated with the smooth walls. Consequently, τ_w is significantly different from τ_b. Vanoni's (1975) method of *side-wall correction* is applied here owing to the smooth wall and rough bed for a cross-section of the channel. Using the continuity equation, the discharge Q is

$$Q = AU = A_w U_w + A_b U_b \tag{1.39}$$

The mean velocity U, considered same as U_w and U_b, can be computed once Q is known. The equation of force along streamwise direction is given by

$$-A \frac{dp}{dx} = \rho \frac{f}{8} U^2 P = \rho \frac{f_w}{8} U_w^2 P_w + \rho \frac{f_b}{8} U_b^2 P_b \tag{1.40}$$

where dp/dx = streamwise pressure gradient. Using $U = U_w = U_b$ into Eq. (1.40), one gets

$$Pf = P_w f_w + P_b f_b \tag{1.41}$$

As the hydraulic grade line is same for the smooth wall and the rough bed regions, equating forces to the wall and bed regions, one can write

$$\frac{Pf}{A} = \frac{P_w f_w}{A_w} = \frac{P_b f_b}{A_b} \tag{1.42}$$

The Reynolds numbers of flow for different regions are

$$R = \frac{4UA}{\nu P}, \quad R_w = \frac{4UA_w}{\nu P_w}, \quad R_b = \frac{4UA_b}{\nu P_b} \tag{1.43}$$

Using Eq. (1.43) into Eq. (1.42), one gets

$$\frac{R}{f} = \frac{R_w}{f_w} = \frac{R_b}{f_b} \tag{1.44}$$

As the wall is smooth, Blasius equation can be used to evaluate f_w. It is

$$f_w = \frac{0.316}{R_w^{0.25}} \tag{1.45}$$

Using Eqs. (1.39) - (1.45), the following equation is obtained as

$$f_b = 0.316 R_b \left(\frac{4UA}{\nu P_w} - \frac{R_b P_b}{P_w} \right)^{-1.25} \tag{1.46}$$

Again, using Eq. (1.43) into Eq. (1.38), the Colebrook-White equation becomes

$$\frac{1}{\sqrt{f_b}} = -0.86 \ln \left(\frac{\varepsilon U}{3.7 \nu R_b} + \frac{2.51}{R_b \sqrt{f_b}} \right) \tag{1.47}$$

Here, ε can be assumed as d_{50}, as was done by Dey (2003). For given data of A, V, P, P_w, P_b, ν, ρ and d_{50}, the unknowns R_b and f_b can be determined numerically solving Eqs. (1.46) and (1.47). Then, Eq. (1.37) is used to estimate the bed shear stress τ_b.

1.11 Stresses in Nonuniform Unsteady Flow: Dey and Lambert's Approach

Dey and Lambert (2005) obtained the expressions for the Reynolds and bed shear stresses for nonuniform unsteady flow in open channels, assuming universal velocity distribution law and using the two-dimensional Reynolds and continuity equations.

The Reynolds equation for two-dimensional nonuniform unsteady flow in open channels is

$$\overline{u}\,\overline{u}_x + \overline{w}\,\overline{u}_z + \overline{u}_t = \frac{1}{\rho}\left(-p_x + \tau_z\right) \tag{1.48}$$

where $\overline{u}$ and $\overline{w}$ = time-averaged point velocities in streamwise x and normal z directions, respectively; x and z = distances in streamwise and normal directions, respectively; t = time; and τ = Reynolds stress at any depth z, that is $-\rho\overline{u'w'}$. The subscripts refer to the partial derivatives.

The time-averaged point velocity components and the Reynolds stress are

$$\overline{u} = U\psi(\eta, t) \tag{1.49a}$$

$$\overline{w} = U\varphi(\eta, t) \tag{1.49b}$$

$$\tau = -\rho\overline{u'w'} = \tau\big|_{z=a}\,\xi(\eta, t) \tag{1.50}$$

where U = depth-averaged velocity; $\tau\big|_{z=a}$ = bed shear stress; a = zero-velocity level, that is $z\big|_{\overline{u}=0}$, being equal to 0.033ε; ε = equivalent roughness assumed as d (Dey 2003); $\eta = z/h$; and h = flow depth. The Prandtl-von Karman universal (logarithmic) velocity distribution law is

$$\overline{u} = \frac{1}{\kappa}\sqrt{\frac{\tau\big|_{z=a}}{\rho}}\ln\left(\frac{z}{a}\right) \tag{1.51}$$

where κ = von Karman constant being 0.4. The depth-averaged velocity U can be given by

$$U = \frac{1}{h-a}\int_a^h \overline{u}\,dz = \frac{\beta}{\kappa}\sqrt{\frac{\tau\big|_{z=a}}{\rho}} \tag{1.52}$$

where $\beta = -[\ln e^{1/(1-e)} + 1]$; and $e = a/h$. Differentiating Eqs. (1.49a) and (1.50), one can write

$$\overline{u}_x = \psi U_x - \frac{U}{h}\eta\psi_\eta h_x \tag{1.53}$$

$$\overline{u}_z = \frac{U}{h}\psi_\eta \tag{1.54}$$

$$\tau_z = \frac{\tau\big|_{z=a}}{h}\xi_\eta \tag{1.55}$$

$$\overline{u}_t = \psi U_t - \frac{U}{h}\eta\psi_\eta h_t + U\psi_t \tag{1.56}$$

Differentiating Eq. (1.49b), one gets

$$\overline{w}_z = \frac{U}{h}\varphi_\eta \tag{1.57}$$

Using continuity equation of time-averaged point velocity components, that is $\overline{u}_x + \overline{w}_z = 0$, and Eq. (1.53), one can write

$$\varphi_\eta = \eta\psi_\eta h_x - \frac{h}{U}\psi U_x \tag{1.58}$$

Integrating Eq. (1.58), one obtains

$$\varphi = h_x\int_e^\eta \eta\psi_\eta d\eta - \frac{h}{U}U_x\int_e^\eta \psi\, d\eta = \psi\,\eta\, h_x - \frac{1}{U}(hU_x + Uh_x)\int_e^\eta \psi\, d\eta \tag{1.59}$$

The continuity equation for depth-averaged nonuniform unsteady flow in open channels is

$$hU_x + Uh_x + h_t = 0 \tag{1.60}$$

Using Eq. (1.60) into Eq. (1.59), the expression of φ becomes

$$\varphi = \psi\,\eta\, h_x + \frac{1}{U}h_t\int_e^\eta \psi\, d\eta \tag{1.61}$$

Inserting Eq. (1.61) into Eq. (1.49b), one gets

$$\overline{w} = \overline{u}\eta h_x + h_t\int_e^\eta \psi\, d\eta \tag{1.62}$$

Substituting Eqs. (1.49a), (1.49b), (1.53) - (1.56) and (1.62) into Eq. (1.48), one obtains

$$U\psi^2 U_x + \psi U_t - \frac{U}{h}\left(\eta - \int_e^\eta \psi\, d\eta\right)\psi_\eta h_t + U\psi_t = \frac{1}{\rho}\left(-p_x + \frac{\tau\big|_{z=a}}{h}\xi_\eta\right) \tag{1.63}$$

The piezometric pressure gradient is given by

$$p_x = -\rho g(S - h_x) \tag{1.64}$$

The Saint Venant equation of motion for nonuniform unsteady flow in open channels is

$$\frac{U}{g}U_x + h_x - S + \frac{\tau\big|_{z=a}}{\rho g h} + \frac{1}{g}U_t = 0 \tag{1.65}$$

For simplicity, the momentum correction factor is assumed to be unity in Eq. (1.65), as it varies from 1.01 to 1.1 in straight open channels. Rearranging Eq. (1.65), one can write

$$\frac{\rho hU}{\tau\big|_{z=a}}U_x = -\frac{\rho g h}{\tau\big|_{z=a}}\left(h_x - S + \frac{1}{g}U_t\right) - 1 = -\lambda - 1 \tag{1.66}$$

where λ = streamwise pressure gradient parameter, which is given by

$$\lambda = \frac{\rho g h}{\tau\big|_{z=a}}\left(h_x - S + \frac{1}{g}U_t\right) \tag{1.67}$$

In Eq. (1.67), for steady flow $U_t = 0$; and for uniform flow $h_x = 0$. In accelerating and decelerating flows $\lambda < -1$ and $\lambda > -1$, respectively.

Using Eqs. (1.66) and (1.67) into Eq. (1.63) yields

$$-(\lambda+1)\psi^2 + (\psi-1)\frac{\rho h}{\tau\big|_{z=a}}U_t - \left(\eta - \int_e^{\eta}\psi\, d\eta\right)\frac{\rho U}{\tau\big|_{z=a}}\psi_\eta h_t + \frac{\rho h}{\tau\big|_{z=a}}U\psi_t = -\lambda + \xi_\eta \tag{1.68}$$

Dividing Eq. (1.51) by Eq. (1.52) and equating to Eq. (1.49a), one can write

$$\frac{\overline{u}}{U} = \frac{1}{\beta}\ln\left(\frac{\eta}{e}\right) = \psi \tag{1.69}$$

Eq. (1.69) represents the velocity profile characteristics that remain independent of time ($\psi_t = 0$). Substituting Eq. (1.69) into Eq. (1.68) and making $\psi_t = 0$, one obtains

$$\xi_\eta = \lambda - (\lambda+1)\frac{1}{\beta^2}\ln^2\left(\frac{\eta}{e}\right) + \left[\frac{1}{\beta}\ln\left(\frac{\eta}{e}\right) - 1\right]\frac{\rho h}{\tau\big|_{z=a}}U_t - \frac{1}{\beta}\left\{1 - \frac{1}{\beta}\left[\ln\left(\frac{\eta}{e}\right) + \frac{e}{\eta} - 1\right]\right\}\frac{\rho U}{\tau\big|_{z=a}}h_t \tag{1.70}$$

At the bed ($\eta = e$), the above equation becomes

$$\xi_\eta\big|_{\eta=e} = \lambda - \frac{\rho h}{\tau\big|_{z=a}}U_t - \frac{1}{\beta}\cdot\frac{\rho U}{\tau\big|_{z=a}}h_t \tag{1.71}$$

Integrating Eq. (1.71) and using the boundary condition $\xi\big|_{\eta=e} = 1$, yields

$$\xi = 1 + \lambda(\eta - e) - (\lambda+1)\frac{1}{\beta^2}\left\{\eta\ln^2\left(\frac{\eta}{e}\right) - 2\left[\eta\ln\left(\frac{\eta}{e}\right) - \eta + e\right]\right\}$$

$$+\left[\frac{\eta}{\beta}\ln\left(\frac{\eta}{e}\right) - \left(1+\frac{1}{\beta}\right)(\eta - e)\right]\frac{\rho h}{\tau\big|_{z=a}}U_t + \frac{1}{\beta}\left[\frac{\eta+e}{\beta}\ln\left(\frac{\eta}{e}\right) - \left(1+\frac{2}{\beta}\right)(\eta-e)\right]\frac{\rho U}{\tau\big|_{z=a}}h_t \tag{1.72}$$

Substituting λ from Eq. (1.67) and U_x from Eq. (1.60) into Eq. (1.72), the equation of nondimensional Reynolds stress for nonuniform unsteady flow in open channels is obtained as

$$\xi = 1 + (\eta - e)\frac{\rho g h}{\tau\big|_{z=a}}(h_x - S) - \frac{1}{\beta^2}\left\{\eta\ln^2\left(\frac{\eta}{e}\right) - 2\left[\eta\ln\left(\frac{\eta}{e}\right) - \eta + e\right]\right\}\frac{\rho U}{\tau\big|_{z=a}}(Uh_x + h_t)$$

$$+\frac{1}{\beta}\left[\eta\ln\left(\frac{\eta}{e}\right) - \eta + e\right]\frac{\rho h}{\tau\big|_{z=a}}U_t + \frac{1}{\beta}\left[\frac{\eta+e}{\beta}\ln\left(\frac{\eta}{e}\right) - \left(1+\frac{2}{\beta}\right)(\eta-e)\right]\frac{\rho U}{\tau\big|_{z=a}}h_t \tag{1.73}$$

The bed shear stress $\tau\big|_{z=a}$ can be obtained from Eq. (1.73) using the boundary condition $\tau\big|_{z=h} = 0$ as

$$\tau\big|_{z=a} = -(1-e)\rho g h(h_x - S) + \frac{1}{\beta^2}[\ln^2 e + 2(\ln e + 1 - e)]\rho U(Uh_x + h_t) + \frac{1}{\beta}(\ln e + 1 - e)\rho h U_t$$

$$+\frac{1}{\beta}\left[\frac{1+e}{\beta}\ln\varepsilon+\left(1+\frac{2}{\beta}\right)(1-e)\right]\rho U h_t \tag{1.74}$$

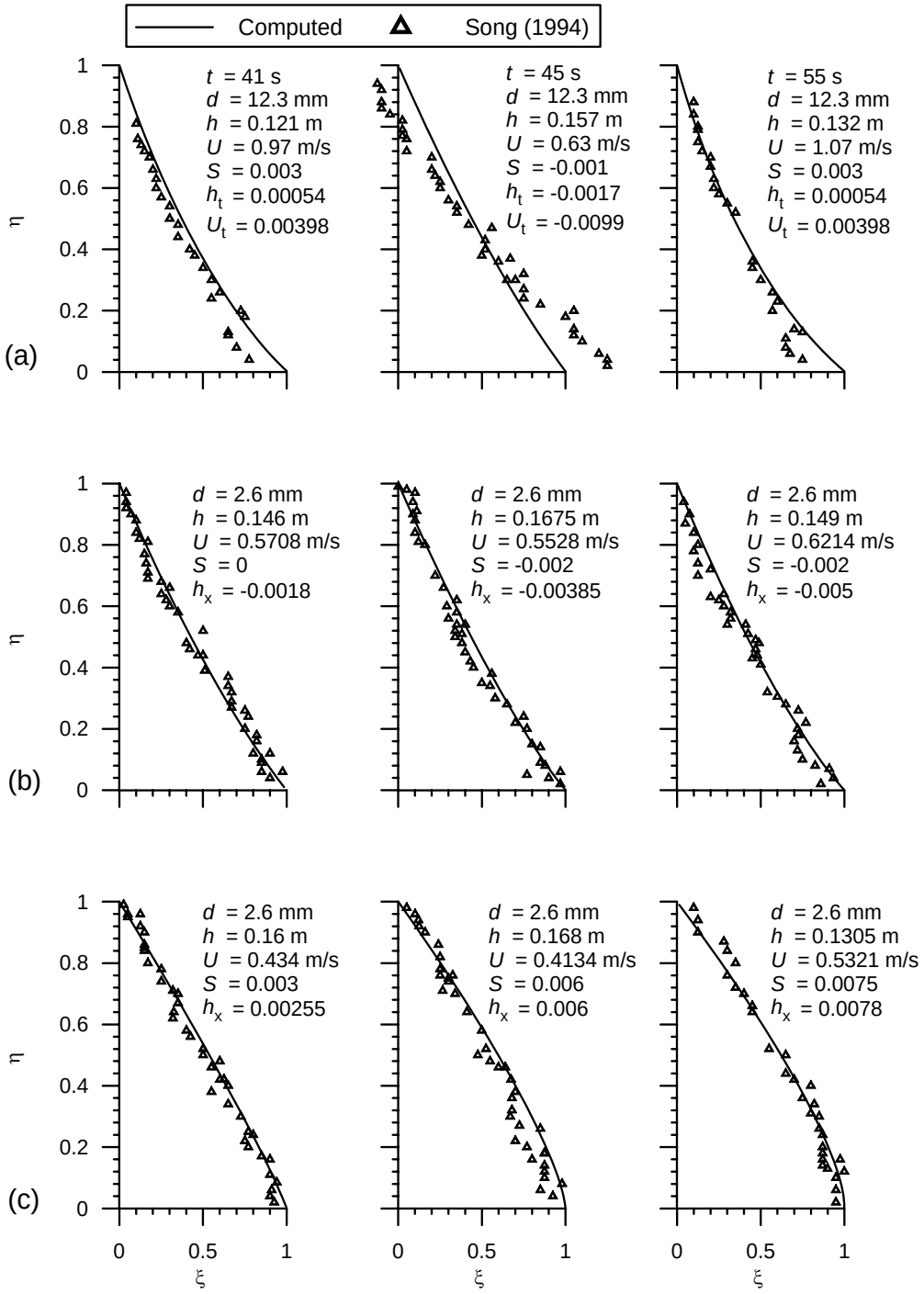

Fig. 1.11 Nondimensional Reynolds stress profiles and comparisons with the data of Song (1994): (a) unsteady; (b) nonuniform accelerating and (c) nonuniform decelerating flows

Using Eqs. (1.73) and (1.74), the equation of Reynolds stress $\tau\big|_{z=z}$ can be obtained as

$$\tau\big|_{z=z} = -(1-\eta)\rho g h(h_x - S) - \frac{1}{\beta^2}\left\{\eta \ln^2\left(\frac{\eta}{e}\right) - \ln^2 e - 2\left[\eta \ln\left(\frac{\eta}{e}\right) + \ln e + 1 - \eta\right]\right\}\rho U(Uh_x + h_t)$$

$$+\frac{1}{\beta}\left[\eta \ln\left(\frac{\eta}{e}\right) + \ln e + 1 - \eta\right]\rho h U_t + \frac{1}{\beta}\left\{\frac{1}{\beta}\left[(\eta + e)\ln\left(\frac{\eta}{e}\right) + (1+e)\ln e\right] + \left(1 + \frac{2}{\beta}\right)(1-\eta)\right\}\rho U h_t \tag{1.75}$$

The distribution of Reynolds stress in nondimensional and dimensional forms can be computed using Eqs. (1.73) and (1.75), respectively, if d, h, U, S, h_x, h_t, U_t and $\tau\big|_{z=a}$ are known. However, Eq. (1.74) can be used to estimate the bed shear stress $\tau\big|_{z=a}$. Figs. 1.11(a-c) present curves η versus ξ computed using Eq. (1.73), where the values of $\tau\big|_{z=a}$ were calculated from Eq. (1.74). The computed curves are in good agreement with the experimental data of Song (1994) for unsteady and nonuniform flows in open channels.

1.12 References

ASCE Task Force on Friction Factor in Open Channels. (1963). "Friction factor in open channels." *J. Hydraul. Div.*, *Am. Soc. Civ. Eng.*, 89(2), 97-143.

Cardoso, A. H., Graf, W. H., and Gust, G. (1989). "Uniform flow in smooth open-channel." *J. Hydraul. Res.*, 27(5), 603-616.

Coleman, N. L. (1981). "Velocity profiles with suspended sediment." *J. Hydraul. Res.*, 19(3), 211-229.

Coles, D. (1956). "The law of the wake in a turbulent boundary layer." *J. Fluids Mech.*, 1, 191-226.

Dey, S. (2003). "Threshold of sediment motion on combined transverse and longitudinal sloping beds." *J. Hydraul. Res.*, 41(4), 405-415.

Dey, S., and Lambert, M. F. (2005). "Reynolds stress and bed shear in nonuniform-unsteady open channel flow." *J. Hydraul. Eng.*, 131(7), 610-614.

Dong, Z., Wang, J., Chen, C., and Xia, Z. (1991). "Turbulence characteristics of open-channel flows over rough beds." *Proc. 24th IAHR Congr.*, Delft, The Netherlands, C33-C40.

Grass, A. J. (1971). "Structural features of turbulent flow over smooth and rough boundaries." *J. Fluid Mech.*, 50, 233-255.

Kirkgöz, M. S. (1989). "Turbulence velocity profiles for smooth and rough open-channel flow." *J. Hydraul. Eng.*, 115(11), 1543-1561.

Kironoto, B. A., and Graf, W. H. (1994). "Turbulence characteristics in rough uniform open-channel flow." *Proc. Inst. Civ. Eng.*, *Water*, *Maritime Energ.*, London, UK, 106(Dec.), 333-344.

Nezu, I. (1977). Turbulent structure in open channel flows. *PhD thesis*, Kyoto University, Japan.

Nezu, I., and Nakagawa, H. (1993). *Turbulence in open-channel flows*. Balkema, Rotterdam, The Netherlands.

Nezu, I., and Rodi, W. (1986). "Open-channel flow measurements with a laser Doppler anemometer." *J. Hydraul. Eng.*, 112(5), 335-355.

Nikora, V., and Goring, D. (1998). "Spectral scaling for gravel-bed open-channel flows." *Proc. NATO Advanced Research Workshop on Stochastic Models of Hydrological Processes and their Applications to Problems of Environmental Preservation*, Water Problems Institute, Moscow, Russia, 239-245.

Nikora, V., and Goring, D. (2000). "Flow turbulence over fixed and weakly mobile gravel beds." *J. Hydraul. Eng.*, 126(9), 679-690.

Nikuradse, J. (1933). "Stromungsgesetze in rauhen rohren." *Verein Deutscher Ingenieure, Forschungsheft* 361.

Raikar, R. V. (2006). "Characteristics of flow over gravel-beds and scour within contractions and at piers." *PhD thesis*, Indian Institute of Technology, Kharagpur, India.

Reynolds, J. A. (1974). *Turbulent flows in engineering*. John Wiley, London, UK.

Song, T. (1994). "Velocity and turbulence distribution in nonuniform and unsteady open-channel flow." *Doctoral dissertation*, Ecole Polytechnique Federale de Lausanne, Lausanne, Switzerland.

Song, T., Graf, W. H., and Lemmin, U. (1994). "Uniform flow in open channels with movable gravel bed." *J. Hydraul. Res.*, 32(6), 861–876.

Steffler, P. M., Rajaratnam, N., and Peterson, A. W. (1985). "LDA measurements in open channel." *J. Hydraul. Eng.*, 111(1), 119-130.

Vanoni, V. A. (1975). "Sedimentation engineering." *ASCE Manual No. 54*. ASCE, New York, USA.

von Karman, T. (1930). "Mechanische aehnlichkeit und turbulenz." *Proc., 3rd Int. Congr. Appl. Mech.*, Stockholm, Sweden, 1, 85-93.

Chapter 2

Sediment Threshold

2.1 General

When a stream-flow takes place over a loose sedimentary bed, hydrodynamic forces are exerted on the sediment particles at the bed surface. An increase in flow velocity causes an increase in the magnitude of hydrodynamic forces. Hence, sediment particles start to move if a situation is eventually reached when the hydrodynamic forces induced by the flow exceed a certain limiting value. The initial movement of sediment particles is frequently called *incipient motion*. The condition being just sufficient to initiate sediment motion is termed *threshold* or *critical condition*. The threshold of sediment motion in open channels having erodible bed is an important component of the management of river systems and occupies the central position of the sediment transport theory. If the stream flow is further increased, then sediment transport takes place. A review on sediment threshold is available in Graf (1971), Yalin (1972), Raudkivi (1998), Yang (1996) and Chien and Wan (1999).

2.2 Sediment Properties

The result of the sieve analysis of adequate number of representative sediment samples is presented as a *frequency curve* (also known as *probability density function curve*) [Fig. 2.1(a)] or as a *cumulative frequency curve* (also known as *particle size distribution curve*) [Fig. 2.1(b)]. In the frequency curve, in Fig. 2.1(a), the abscissa represents the particle diameter d and the ordinate the concentration of the total sample contained in the corresponding intervals of the diameter d. Very often the distribution curve of sediments approaches the log-normal probability curve when plotted, as shown in Fig. 2.1(a), so that the distribution function is log-normal and is given by

$$f(d) = \frac{1}{\sqrt{2\pi} d \ln(\sigma_g)} \exp\left\{ -0.5 \left[\frac{\ln(d / d_{50})}{\ln(\sigma_g)} \right]^2 \right\} \tag{2.1}$$

where σ_g = geometric standard deviation, given by $(d_{84}/d_{16})^{0.5}$; and d_{50} = median particle diameter or 50 percent finer (by weight) particle diameter. Similarly, d_{84} and d_{16} are 84 and 16 percent finer diameters, respectively. For uniformly graded sediments, σ_g is less than 1.4. In the cumulative frequency curve [Fig. 2.1(b)], the ordinate indicates how much percent (by weight) of the total sample is finer than the diameter d of the abscissa.

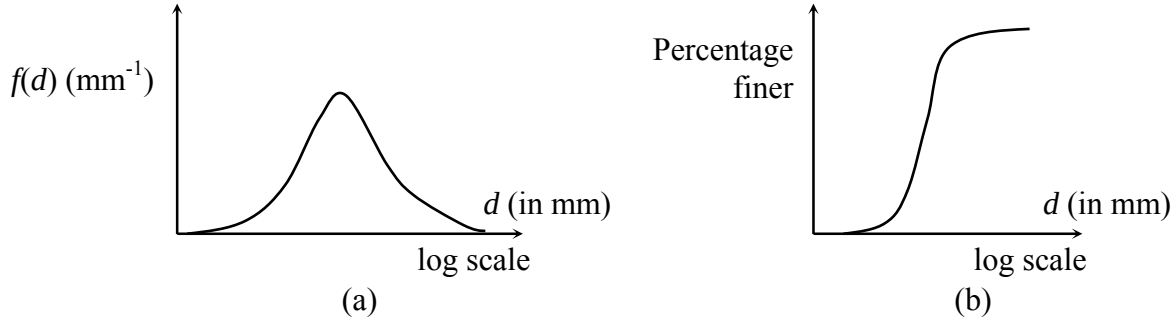

Fig. 2.1 (a) Frequency curve and (b) cumulative frequency curve

2.3 Definitions of Sediment Threshold

The first type of definition is based on sediment flux. Shields (1936) put forward a concept of sediment threshold that the bed shear stress has a value for which the extrapolated sediment flux becomes zero. On the other hand, USWES (1936) set a concept of sediment threshold that the tractive force brings about *general motion* of bed particles. For sediment particles less than 0.6 mm, this concept was found to be inadequate and general motion was redefined that sediment in motion should reasonably be represented by all sizes of bed particles and that sediment flux should exceed 4.1×10^{-4} kg/sm. The second type of definition is based on bed particle motion. Kramer (1935) indicated four different bed shear stress conditions for sedimentary bed for which:

1. No particles are in motion, termed *no transport*.
2. A few of the smallest particles are in motion at isolated zones, termed *weak transport*.
3. Many particles of mean size are in motion, termed *medium transport*.
4. Particles of all sizes are in motion at all points and at all times, termed *general transport*.

However, Kramer (1935) pointed out the difficulty of setting up clear limits between these regimes but defined threshold bed shear stress to be that stress initiating *general transport*. Vanoni (1964) proposed that the sediment threshold is the condition of particle motion in every two seconds at any location of a bed.

2.4 Competent Velocity Concept

A competent bed velocity or competent mean velocity is a velocity at particle level or mean velocity, which is just enough to move the particles of a given size. Though most of the early investigators provided valuable information regarding competency, many of them had not clearly reported the exact particle size and location of the bed velocity being taken. Goncharov (1964) defined the threshold velocity as detachment velocity (U_n), which was defined as the lowest average velocity at which individual particles continually detaches from the bed for which the mean value of the fluctuating lift force nearly equals the submerged weight of particle in fluid. He gave an equation as

$$U_n = \log(8.8h/d)\sqrt{0.57\Delta gd} \tag{2.2}$$

where h = flow depth; d = representative particle diameter, that is median particle diameter; g = acceleration due to gravity; $\Delta = s - 1$; s = relative density of sediment particles, that is ρ_s/ρ; ρ_s = mass density of sediment; and ρ = mass density of fluid.

Carstens (1966) reported an equation of critical or threshold velocity u_{cr} at the particle level having analyzed a large number of published data on threshold of sediment motion. It is

$$u_{cr}^2/\Delta gd \approx 3.61(\tan\varphi\cos\theta - \sin\theta) \tag{2.3}$$

where φ = angle of repose of sediment; and θ = angle made by the streamwise sloping bed with the horizontal.

Neill (1968) presented a conservative design curve for the movement of coarse uniform gravel in terms of average threshold velocity U_{cr} and represented it in an equation as

$$U_{cr}^2/\Delta gd = 2(h/d)^{1/3} \tag{2.4}$$

Zanke (1977) proposed the following equation:

$$U_{cr} = 2.8\sqrt{\Delta g d} + 14.7 c_1 \nu / d \tag{2.5}$$

where c_1 = a coefficient for cohesiveness varying from 1 for non-cohesive to 0.1 for cohesive sediments; and ν = kinematic viscosity of fluid. Many researchers have validly criticized the use of critical velocity equation as a criterion for threshold of sediment motion. The unanswered question is as to what is meant by competent velocity at particle level u_{cr} and average velocity for threshold condition U_{cr}. This confusion has led the hydraulicians to accept a more satisfactory quantity, the bed shear stress as a sediment threshold. Nevertheless, Yang (1973) developed a promising model for the estimation of average velocity for sediment threshold.

2.4.1 Yang's Competent Velocity Model

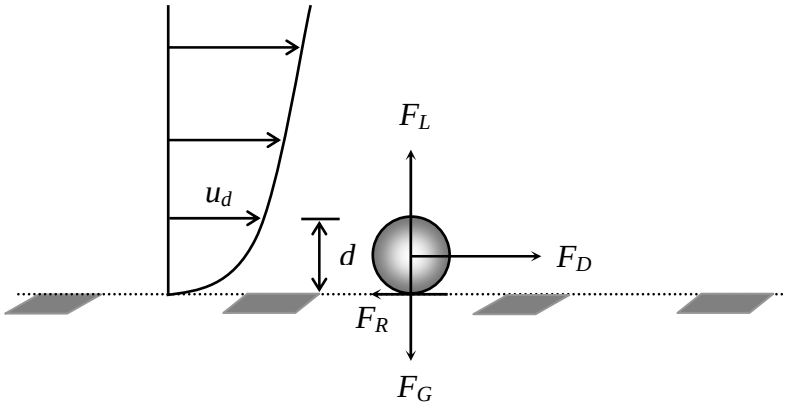

Fig. 2.2 Forces acting on a spherical sediment particle at the bottom of an open channel

The forces acting on a spherical sediment particle at the bottom of an open channel, as considered by Yang (1973), are shown in Fig. 2.2. The drag force F_D is expressed as

$$F_D = C_D \frac{\pi}{8} d^2 \rho u_d^2 \tag{2.6}$$

where C_D = drag coefficient; and u_d = velocity at a distance d above the bed.

The terminal fall velocity w_{ss} of a spherical particle is reached when there is a balance between the drag force F_D and submerged weight F_G of the particle. Thus, one can write

$$C_{D1} \frac{\pi}{8} d^2 \rho w_{ss}^2 = \frac{\pi}{6} d^3 (\rho_s - \rho) g \; (= F_G) \tag{2.7}$$

where C_{D1} = drag coefficient at w_{ss}, assumed as $\psi_1 C_D$. Eliminating C_D from Eqs. (2.6) and (2.7), the drag force becomes

$$F_D = \frac{\pi}{6 \psi_1 w_{ss}^2} d^3 (\rho_s - \rho) g u_d^2 \tag{2.8}$$

Considering the logarithmic law for velocity distribution, velocity at particle level u_d and depth-averaged velocity U are obtained as:

$$u_d = B_r u_* \tag{2.9a}$$

$$U = u_* \left[5.75 \left(\log \frac{h}{d} - 1 \right) + B_r \right] \tag{2.9b}$$

where B_r = roughness function; and u_* = shear velocity. Using Eqs. (2.9a) and (2.9b) into Eq. (2.8), yields

$$F_D = \frac{\pi}{6\psi_1} d^3(\rho_s - \rho) g \left(\frac{U}{w_{ss}}\right)^2 \frac{B_r^2}{\left[5.75\left(\log\frac{h}{d} - 1\right) + B_r\right]^2} \tag{2.10}$$

The lift force F_L acting on the particle is given by

$$F_L = C_L \frac{\pi}{8} d^2 \rho u_d^2 \tag{2.11}$$

where C_L = lift coefficient, assumed as C_D/ψ_2.

Thus, using Eqs. (2.9a) and (2.9b) into Eq. (2.11), yields

$$F_L = \frac{\pi}{6\psi_1\psi_2} d^3(\rho_s - \rho) g \left(\frac{U}{w_{ss}}\right)^2 \frac{B_r^2}{\left[5.75\left(\log\frac{h}{d} - 1\right) + B_r\right]^2} \tag{2.12}$$

The drag force F_D is balanced by the resistance force F_R. Thus, one can write

$$F_D = F_R = \psi_3 (F_G - F_L) \tag{2.13}$$

where ψ_3 = friction coefficient.

Inserting Eqs. (2.7), (2.10) and (2.12) in Eq. (2.13), one gets the equation of average critical or threshold velocity U_c as

$$\frac{U_c}{w_{ss}} = \sqrt{\frac{\psi_1\psi_2\psi_3}{\psi_2 + \psi_3}} \left[\frac{5.75}{B_r}\left(\log\frac{h}{d} - 1\right) + 1\right] \tag{2.14}$$

Yang (1973) gave the equations for both smooth and rough boundaries as follows:

$$\frac{U_c}{w_{ss}} = \frac{2.5}{\log R_* - 0.06} + 0.66 \qquad \text{for } 0 < R_* < 70 \tag{2.15}$$

$$\frac{U_c}{w_{ss}} = 2.05 \qquad \text{for } R_* \geq 70 \tag{2.16}$$

where R_* = particle Reynolds number, that is $u_* d/\nu$.

2.5 Lift Force Concept

Principally the lift force may arise for two reasons:

- First suppose that the particle under consideration rests on the bottom of a channel. This is the zone where the velocity gradient is the steepest; thus a pressure difference is set up which results in lifting of the particle.
- Secondly, the same particle might experience lift because of the upward velocity component adjacent to the bed as a result of turbulence.

Now, if the magnitude of the lift becomes equal to the submerged weight, the smallest drag force would suffice to cause a threshold motion.

Jeffreys (1929) showed that the classical hydrodynamics provides a simple explanation of lifting and carrying solid particles in fluid. Assuming a potential flow over a circular cylinder with its major axis perpendicular to the flow, lift takes place if

$$(3+\pi^2)U^2 > 9\Delta g r_1 \tag{2.17}$$

where r_1 = radius of the cylinder. On experimental verification of the above model, it was felt that modified factors must be taken, since the two-dimensional model behaves in different way for flow past a particle in three-dimension. The shortcoming of Jeffreys' model is that the drag forces are totally discarded.

Reitz (1936) discussed a similar idea and suggested to express the beginning of sediment motion with a lift model. Circulation and viscosity are important parameters of this investigation.

Lane and Kalinske (1939) stressed on turbulence for the determination of lift and assumed that: 1. only particles having a settling velocity smaller than the instantaneous turbulent fluctuations at bed experience lift; 2. the velocity fluctuations vary according to the normal error law; and 3. the turbulent fluctuations and shear velocities are related.

White (1940) carried out a single experiment and found that the lift on an individual particle is very small compared to its weight.

Einstein and El-Samni (1949) measured the lift force directly as a pressure difference. They carried out experiments using plastic spherical balls (d = 0.225 ft) and gravel (d_{50} = 0.225 ft) having considerable spread of particle size. They proposed

$$f_L = 0.5 C_L \rho u_{0.35d}^2 \tag{2.18}$$

where f_L = lift force per unit area of the particle; C_L = lift coefficient assumed as 0.178; and $u_{0.35d}$ = measured velocity of flow at a distance of 0.35 diameter from the theoretical wall. They also investigated the turbulent fluctuations on the lift. These experiments gave a constant average lift force with random fluctuations superimposed, following the normal error law.

Iwagaki (1956) worked on the problem of sediment threshold using the shear stress concept. His analysis with and without considering lift does not change the critical tractive force significantly, thereby concluding that the lift force is secondary.

The results of the study of Einstein and El-Samni (1949) were used by the Task Committee (1966), who calculated f_L/τ_c; where τ_c = threshold bed shear stress. This ratio was found to be about 2.5, giving strong indication that the lift forces are of considerable importance in the initial motion mechanism. However, once the particle is displaced, lift force tends to diminish and drag force to increase, as pointed out by Chepil (1961).

Coleman (1967) studied the lift forces acting on a sphere placed on a hypothetical streambed. Data for plastic and steel spheres were examined and lift coefficient versus Reynolds number plot was obtained. For Reynolds number less than 100, the negative values of lift force could not be explained.

Although the lift forces obviously contribute to the sediment threshold problem, no critical lift criterion has been presented as yet which could be a ready reference for the determination of the sediment threshold condition. It was seen that besides the lift force, the drag force always exists to contribute towards the threshold movement of the bed sediment.

2.6 Threshold Shear Stress Concept

2.6.1 Empirical Equations of Threshold Shear Stress

Several attempts have been made in laboratory and field studies to relate the threshold bed shear stress and sediment properties. Kramer (1935) carried out experiments in a flume using quartz particles of relative density 2.7. On the basis of these experiments and data available from other sources, he proposed

$$\tau_c = 29\sqrt{(\rho_s - \rho) g\, d / M} \tag{2.19}$$

where τ_c = threshold or critical bed shear stress (in g/m^2); M = uniformity coefficient of Kramer; and d is in mm. Eq. (2.19) is based on d ranging from 0.24 mm to 6.52 mm and the uniformity coefficient varying from 0.265 to 1. USWES (1936) recommended the formula as

$$\tau_c = 0.285\sqrt{\Delta\, d / M} \tag{2.20}$$

where τ_c is in Pa; and d is in mm. This relationship is valid for d ranging from 0.205 mm to 4.077 mm and M ranging from 0.280 to 0.643.

Leliavsky (1966) gave a simple threshold bed shear stress equation as

$$\tau_c = 166\, d \tag{2.21}$$

where τ_c is in g/m^2; and d is in mm. It can be seen that none of the formulae account for the effect of fluid viscosity, and further each of these formulae gives results that differ from each other considerably. This discrepancy might be a result of variation in the definition of sediment threshold. However, the empirical formulae can estimate the approximate threshold bed shear stress but their use is not recommended since more reliable methods are available.

2.6.2 Theoretical and Semi-Theoretical Analyses

2.6.2.1 Shields Diagram

Fig. 2.3 shows the steady state flow over a bed composed of noncohesive sediment particles. These particles do not move at very low velocity. As the flow velocity increases to a certain value, the driving forces on the sediment particles exceeds the stabilizing forces, and the sediment starts to move. Shields (1936) was the pioneer to present a semi-theoretical solution to the sediment threshold problem. The threshold of sediment particle motion is governed by the ratio of the driving (as drag force) to the stabilizing forces.

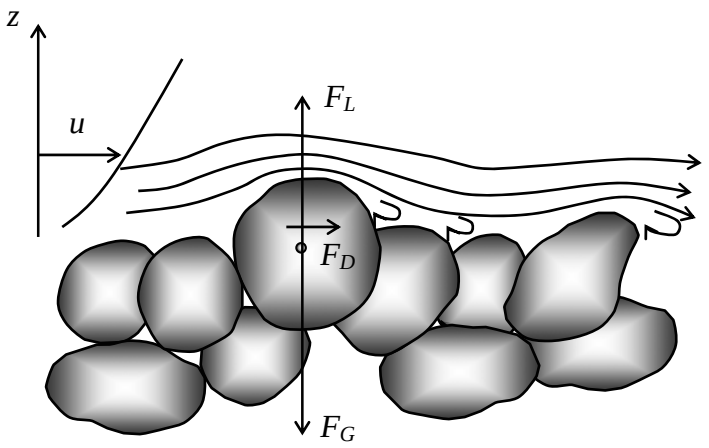

Fig. 2.3 Forces acting on a sediment particle resting on bed

The driving force is the drag force F_D due to flow exerted on the sediment particle and is given by

$$F_D = C_D \frac{1}{2} \rho u^2 A = f_1\left(a_1, \frac{ud}{\nu}\right) \tag{2.22}$$

where u = velocity at elevation $z = a_2 d$; A = frontal area of the particle; and a_1 = particle shape factor. The velocity distributions for the flow over rough and smooth boundaries have the form as

$$\frac{u}{u_*} = 5.75 \log \frac{z}{k_s} + \frac{z u_*}{\nu} = 5.75 \log a_2 + f_2\left(\frac{u_* d}{\nu}\right) \tag{2.23}$$

where k_s = roughness height being proportional to d. Thus, the drag force is

$$F_D = \tau_0 d^2 = f_3(a_1, a_2, R_*) \tag{2.24}$$

The resistance to motion F_R was assumed to be dependent only upon the bed roughness and the submerged weight F_G of the particle. That is

$$F_R = a_3 \Delta \rho g d^3 \tag{2.25}$$

where a_3 = roughness factor.

At the incipient condition, when the sediment particle is about to move, $u_* \rightarrow u_{*c}$ (that is the critical shear velocity), then the drag force is balanced by the resistance. Therefore, one can write

$$F_D = F_R \tag{2.26}$$

Rearranging the terms

$$\frac{u_{*c}^2}{\Delta g d} = \frac{\tau_c}{\Delta \rho g d} = f(R_*) \tag{2.27}$$

The Shields parameter Θ is defined as

$$\Theta = \frac{u_*^2}{\Delta g d} \tag{2.28}$$

Therefore, Eq. (2.27) is expressed as a critical Shields parameter Θ_c that is

$$\Theta_c = f(R_*) \tag{2.29}$$

Fig. 2.4 shows the Shields' experimental results which relate critical Shields parameter Θ_c and R_* and is known as *Shields diagram*. The threshold of sediment motion occurs when $\Theta > \Theta_c$ or $\tau_0 > \tau_c$ or $u_* > u_{*c}$. The Fig. 2.4 depicts three distinct zones:

1. Hydraulically smooth flow for $R_* \leq 2$: In this case, d is much smaller than the thickness of viscous sub-layer; and experimentally it was found that $\Theta_c = 0.1/R_*$.
2. Hydraulically rough flow for $R_* \geq 500$: The viscous sub-layer does not exist. The critical Shields parameter Θ_c is independent of the fluid viscosity and has a constant value of 0.056.
3. Hydraulically transitional flow for $2 \leq R_* \leq 500$: Sediment particles are of the order of the thickness of viscous sub-layer. There is a minimum value of Θ_c of 0.032 corresponding to $R_* = 10$.

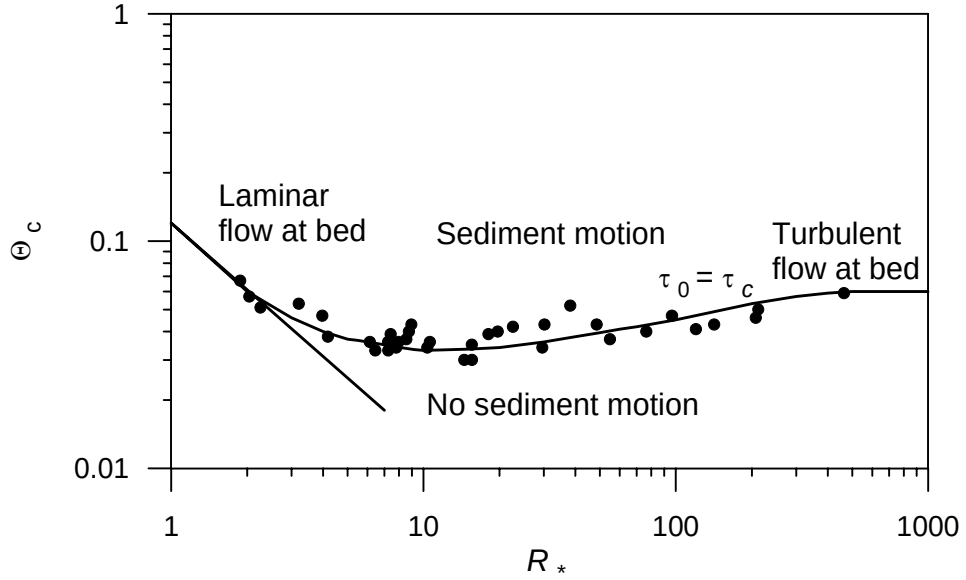

Fig. 2.4 Shields parameter Θ_c as a function of particle Reynolds number R_*

The drawback of the Shields theory is that the viscous sub-layer does not have any effect on the velocity distribution when $R_* \geq 70$, but his diagram shows that Θ_c still varies with R_* when the latter is greater than seventy. Furthermore, Shields used the bed shear stress and the shear velocity in his diagram as dependent and independent variables, which is not appropriate as they are interchangeable. Consequently the threshold bed shear stress must be determined through trial and error method. However, van Rijn (1984) gave the empirical equations of the Shields curve as

$$\Theta_c(D_* \leq 4) = 0.24 / D_* \tag{2.30a}$$

$$\Theta_c(4 < D_* \leq 10) = 0.14 / D_*^{0.64} \tag{2.30b}$$

$$\Theta_c(10 < D_* \leq 20) = 0.04 / D_*^{0.1} \tag{2.30c}$$

$$\Theta_c(20 < D_* \leq 150) = 0.013 D_*^{0.29} \tag{2.30d}$$

$$\Theta_c(D_* > 150) = 0.055 \tag{2.30e}$$

where D_* = particle parameter, that is $d(\Delta g/\nu^2)^{1/3}$. Also, Julien (1998) proposed the empirical equations of the Shields curve as a function particle parameter and angle of repose as

$$\Theta_c(D_* \leq 0.3) = 0.5 \tan\varphi \tag{2.31a}$$

$$\Theta_c(0.3 < D_* \leq 19) = 0.25 \tan\varphi / D_*^{0.6} \tag{2.31b}$$

$$\Theta_c(19 < D_* \leq 50) = 0.013 D_*^{0.4} \tan\varphi \tag{2.31c}$$

$$\Theta_c(D_* > 50) = 0.06 \tan\varphi \tag{2.31d}$$

2.6.2.2 White's Analysis

If one neglects the lift force, at limiting equilibrium the drag force (shear drag) is balanced by the frictional resistance. White (1940) classified high-speed case ($R_* \geq 3.5$) and low-speed case ($R_* < 3.5$).

High-Speed Case ($R_* \geq 3.5$):

High flow velocity is required to move larger sediment particles, where the drag due to skin friction is negligible as compared to the drag due to pressure difference. If p_f is the packing coefficient defined by Nd^2, where N is the number of particles per unit area, the shear drag per particle (that is τ_0/N) is given by $\tau_0 d^2/p_f$. At limiting equilibrium of a particle resting on a horizontal bed, the shear drag is balanced by the product of the submerged weight of the particle and the frictional coefficient $\tan\varphi$. Therefore, one gets

$$\Theta_c = \frac{\pi}{6} p_f \tan\varphi \tag{2.32}$$

In Eq. (2.32), White introduced a factor termed *turbulence factor* T_f, which is the ratio of the instantaneous bed shear stress to the mean bed shear stress. Hence, Eq. (2.32) becomes

$$\Theta_c = \frac{\pi}{6} p_f T_f \tan\varphi \tag{2.33}$$

He experimentally obtained $p_f = 0.4$ and $T_f = 4$ for fully developed turbulent flow.

Low-Speed Case ($R_* < 3.5$):

Low flow velocity is required to move smaller sediment particles, where the drag due to pressure difference acting on the particle is very small as compared to the viscous force. However, the upper portion of the particle is exposed to the aforementioned shear drag that acts above the center of gravity of the particle. This effect is taken into account introducing a coefficient α_f. Therefore, the equation of sediment threshold is

$$\Theta_c = \frac{\pi}{6} p_f \alpha_f \tan\varphi \tag{2.34}$$

He experimentally obtained $p_f\alpha_f = 0.34$ as an average value.

2.6.2.3 Wilberg and Smith's Approach

On a horizontal bed, the expression for the force balance given by Wiberg and Smith (1987) becomes

$$(F_G - F_L)\tan\varphi = F_D \tag{2.35}$$

They expressed the submerged weight of the particle F_G, drag force F_D and lift force F_L as follows

$$F_G = \Delta\rho g V \tag{2.36}$$

$$F_D = C_D \frac{1}{2}\rho u^2 A_x = C_D \frac{1}{2}\tau_0[f^2(z/z_0)]A_x \tag{2.37}$$

$$F_L = C_L \frac{1}{2}\rho(u_T^2 - u_B^2)A_x = C_L \frac{1}{2}\tau_0[f^2(z_T/z_0) - f^2(z_B/z_0)]A_x \tag{2.38}$$

where V = volume of the particle; A_x = frontal area of the particle; u = velocity at z above the bed; z_0 = zero-velocity level; u_T = velocity at the top of the particle; u_B = velocity at the bottom of the particle; z_T = height of the top point of the particle from the bed; and z_B = height of the bottom point of the particle from the bed. They assumed the bed level passing through the mid points (those are the contact points) of the bed particles.

Using Eqs. (2.36) – (2.38), the following expression for Θ_c is obtained:

$$\Theta_c = \frac{2}{C_D \alpha_0} \cdot \frac{1}{f^2(z/z_0)} \cdot \frac{\tan\varphi}{1 + (F_L/F_D)_c \tan\varphi} \tag{2.39}$$

where $\alpha_0 = A_x d/V$. They used C_D as a function of particle Reynolds number (Schlichting 1960), $C_L = 0.2$ and $\cos\varphi = [(d/k_s) + z_*]/[(d/k_s) + 1]$. For natural sands, $z_* = -0.02$. For smooth regime ($R_* < 3$) and transitional regime ($3 \le R_* < 100$), Reichardt's (1951) equation of velocity distribution was used (see Eq. 2.72), while for rough regime ($R_* \ge 100$), universal logarithmic velocity distribution (see Eq. 2.75) was taken into consideration. Fig. 2.5 shows Θ_c as a function of R_* for different d/k_s.

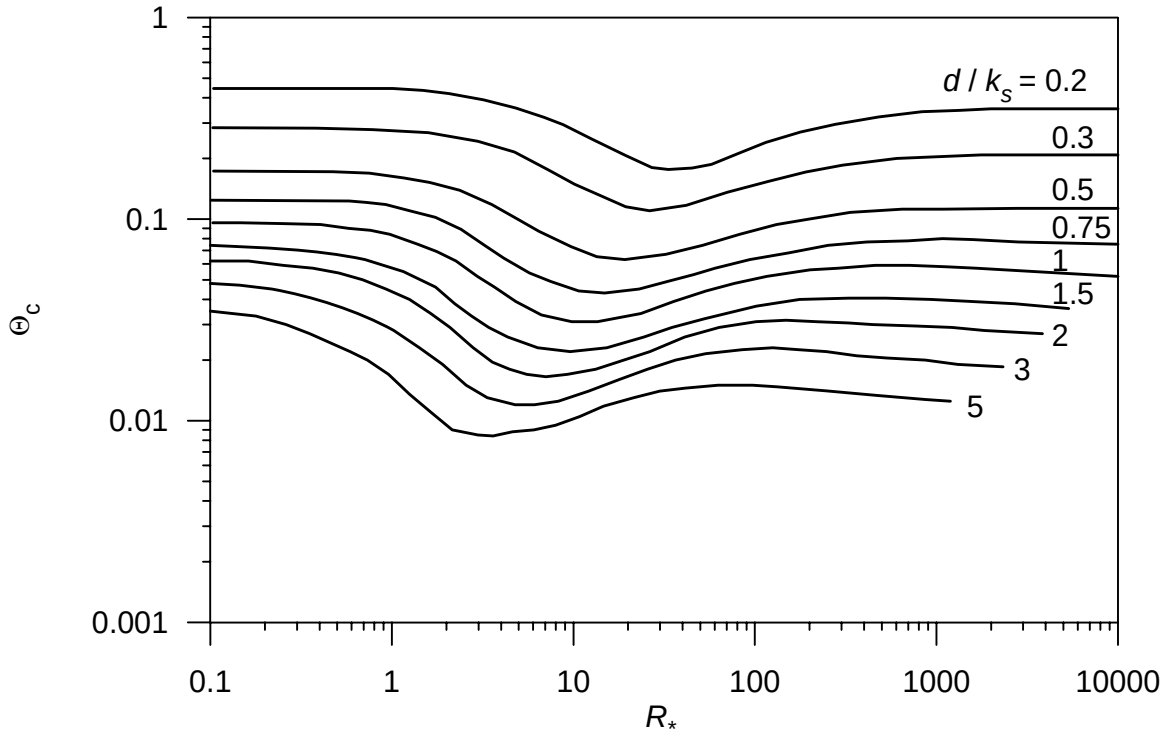

Fig. 2.5 Θ_c as a function of R_* for different d/k_s

2.6.2.4 Equations of Other Investigators

Kurihara (1948) extended the work of White (1940). He considered the bed shear stress to be a sum of the time-averaged bed shear stress due to main flow and the bed shear stress resulting from turbulent fluctuations. He obtained an expression for turbulence factor T_f in terms of R_*, turbulence intensity and the probability of bed shear stress increment. Since his theoretical equations were quite complicated, he proposed the following empirical equations of threshold bed shear stress:

$$\Theta_c(X_2 \le 0.1) = (0.047 \log X_2 - 0.023)\beta_2 \tag{2.40a}$$

$$\Theta_c(0.1 < X_2 \le 0.25) = (0.01 \log X_2 + 0.034)\beta_2 \tag{2.40b}$$

$$\Theta_c(X_2 > 0.25) = (0.0517 \log X_2 + 0.057)\beta_2 \tag{2.40c}$$

where $X_2 \approx 4.67\times10^{-3}[\Delta g/(\nu^2\beta_2)]^{1/3} d$; $\beta_2 = (M + 2)/(1 + 2M)$; and M = uniformity coefficient of Kramer (1935) varying from 0.265 to 1.

Iwagaki (1956) considered the equilibrium of a single spherical particle, placed on a rough surface and found the conditions necessary for the equilibrium of a particle. However, in practice, this condition seldom occurs because of the existence of other particles. The theoretical equation given by Iwagaki (1956) is of the form

$$\Theta_c = \frac{\tan\varphi}{\varepsilon_s \Psi_s R_*} \tag{2.41}$$

where ε_s = empirical coefficient to take care of the sheltering effect; and Ψ_s = function of R_*.

Egiazaroff (1965) presented yet another derivation for Θ_c as a function of R_*. The essential feature of his analysis is the assumption that at threshold condition, the velocity at an elevation of $0.63d$ (above the bottom of particle) equals the fall velocity w_{ss} of particle. He gave the equation as

$$\Theta_c = \frac{1.33}{C_D[a_r + 5.75\log(0.63)]} \tag{2.42}$$

where $a_r = 8.5$; and C_D = drag coefficient = 0.4 for large R_*, and both a_r and C_D increase for low R_*. His results do not agree quantitatively with the Shields curve.

Mantz (1977) proposed the extended Shields diagram for flat sedimentary bed to obtain the condition of maximum stability (Fig. 2.6). Yalin and Karahan (1979) presented a graphical presentation of Θ_c versus R_*, using a large volume of data collected by various investigators (Fig. 2.6). Their curve is regarded as a superior curve to the more commonly used Shields curve.

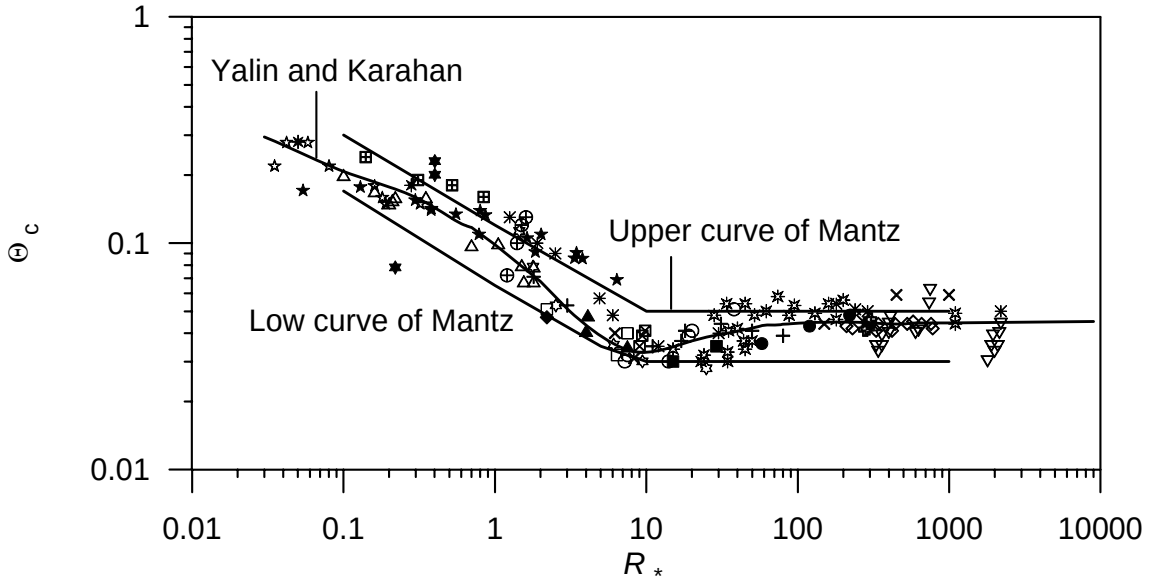

Fig. 2.6 Curves (Θ_c versus R_*) of Mantz (1977) and Yalin and Karahan (1979)

Soulsby and Whitehouse (1997) presented the critical Shields parameter Θ_c in terms of the dimensionless particle size D_* to avoid the trial and error estimation of τ_c. It is

$$\Theta_c = \frac{0.24}{D_*} + 0.055\,[1 - \exp(-0.02D_*)] \tag{2.43}$$

2.7 Probabilistic Concept

The threshold of sediment motion is probabilistic in nature. It depends on the location of a specific particle with respect to other particles of different sizes and their orientations. It also depends on the instantaneous strength of turbulence. The concept gives the mean condition that there is a fifty percent chance for a given particle to move under specific flow and sediment conditions.

Gessler (1970) measured the probability that particles of a specific size stay. It was shown that the probability of a given particle to stay depends strongly on the Shields parameter and weakly on particle Reynolds number. The ratio τ_c/τ_0 is directly related to the probability that a sediment particle stays. It can be used to determine the particle size distribution in the armor layer. Thus

$$P_0(d) = \int_{d_{\min}}^{d} p_0(d)dd \tag{2.44}$$

where p_0 = frequency function of the original distribution. The armor layer particle size frequency is

$$p_a(d) = k_1 q p_0(d) \tag{2.45}$$

where q = probability for a particle size d to stay; and k_1 = constant. The quantity q varies with the particle size d that can be determined by

$$\int_{d_{\min}}^{d_{\max}} p_a(d)dd = 1 \tag{2.46}$$

The expression for particle size distribution of the armor layer is

$$P(d) = \frac{\int_{d_{\min}}^{d} q p_0(d)dd}{\int_{d_{\min}}^{d_{\max}} q p_0(d)dd} \tag{2.47}$$

The expression for particle size distribution of the moving particles is

$$P(d) = \frac{\int_{d_{\min}}^{d} (1-q) p_0(d)dd}{\int_{d_{\min}}^{d_{\max}} (1-q) p_0(d)dd} \tag{2.48}$$

The most detailed experimental observations on the bed shear stress fluctuation carried out so far are due to Grass (1970). He pointed out that for any given area of a flat bed there is a random distribution of bed shear stresses due to stream flow. In addition, there is a second independent random distribution of bed shear stress for the same area, at which the bed particles move. To be more explicit, when these two distributions start to develop, the bed particles, which require the least bed shear stress to move, are disturbed during the peaks of the velocity bursts.

2.8 Dey's Sediment Threshold Model

In a unidirectional steady-uniform flow over a sedimentary bed, the most stable three-dimensional configuration of a spherical solitary sediment particle of diameter D resting over three closely packed spherical particles of identical diameter d forming the sediment bed is shown in Fig. 2.7. Depending on the orientation of the bed particles, the solitary particle has a tendency either to roll over the valley formed by the two particles or to roll over the summit of a single particle due to the hydrodynamic forces.

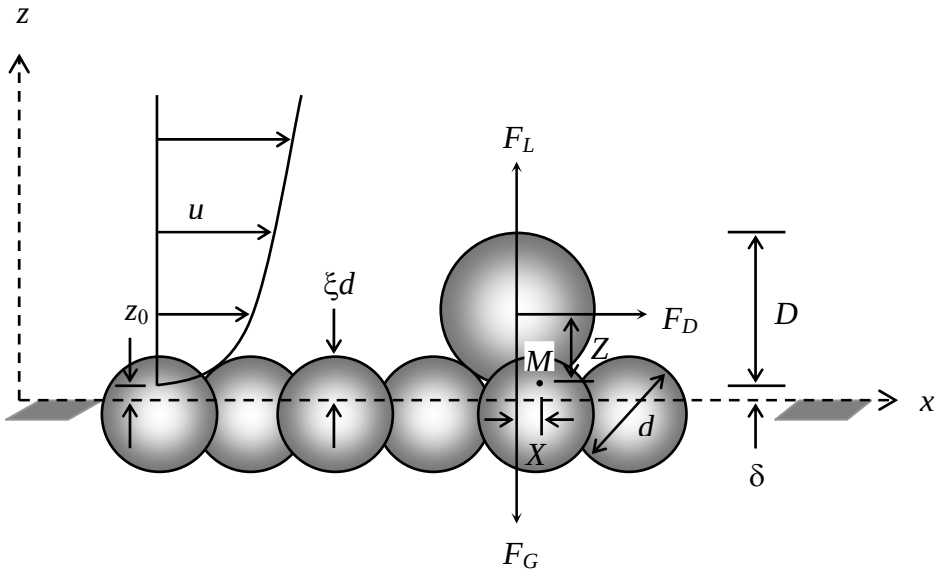

Fig. 2.7 Diagrammatic presentation of forces acting on a spherical solitary particle

When the solitary particle is about to dislodge downstream from its original position, the equation of moment about the point of contact *M* of the solitary particle downstream is

$$(F_L - F_G)X + F_D Z = 0 \tag{2.49}$$

where *X* and *Z* = horizontal and vertical lever arms, respectively (Fig. 2.7). The expressions of *X* and *Z* given by Dey et al. (1999) [also see Dey (1999)] are

$$X = \frac{\sqrt{3}}{4} \cdot \frac{Dd}{D+d} \tag{2.50}$$

$$Z = \frac{1}{2\sqrt{3}} \cdot \frac{D}{D+d}(3D^2 + 6Dd - d^2)^{0.5} \tag{2.51}$$

The submerged weight of the solitary particle is

$$F_G = \frac{\pi}{6} D^3 (\rho_s - \rho) g \tag{2.52}$$

The drag force developed due to pressure and viscous skin frictional forces is given by

$$F_D = C_D \frac{\pi}{8} D^2 \rho u_m^2 \tag{2.53}$$

where C_D = drag coefficient; and u_m = mean flow velocity received by the frontal area (the projected area of the particle being right angles to the direction of flow) of the solitary particle. The empirical equation of the drag coefficient C_D given by Morsi and Alexander (1972) is used. It is

$$C_D = a + bR^{-1} + cR^{-2} \tag{2.54}$$

where *R* = flow Reynolds number at particle level (= $u_m D/\nu$); and *a*, *b* and *c* = coefficients dependent on *R*.

The lift force, caused by the velocity gradient, in a shear flow is termed *lift due to shear effect* (F_{Ls}). For a sphere in a viscous flow, Saffman (1968) proposed the following equation:

$$F_{Ls} = C_L \rho D^2 u_m \left(\nu \frac{\partial u}{\partial z} \right)^{0.5} \tag{2.55}$$

where $\partial u/\partial z$ = velocity gradient; and u = time-averaged flow velocity at z.

For low particle Reynolds number R_*, Eq. (2.55) is applicable. However, for large Reynolds number ($R_* > 3$), the solitary particle spins into the groove, formed by the three closely packed bed particles, just before dislodging downstream from its original position due to large velocity gradient (differential velocity in the vertical direction owing to considerable velocity difference between the bottom and top points of the solitary particle) at the particle level (Dey et al. 1999). To be more explicit, the hydrodynamic force acting on the upper portion of particle is significantly greater than that acting on the lower portion of particle, resulting in a turning moment to the particle. Therefore, the inclusion of slip-spinning mode is significant in the analysis of the threshold of sediment motion. The lift force, caused by the spinning mode of particle, is termed *lift due to Magnus effect* (F_{Lm}). Rubinow and Keller (1961) formulated it as

$$F_{Lm} = \mathrm{C}_L \rho D^3 u_m \omega \tag{2.56}$$

where ω = angular velocity of spinning particle. According to Saffman (1965), the maximum angular velocity achieved by a solitary particle equals $0.5\partial u/\partial z$. Thus, Eq. (2.56) is rewritten as

$$F_{Lm} = 0.5 C_L \rho D^3 u_m \frac{\partial u}{\partial z} \tag{2.57}$$

The total lift force F_L, a combination of F_{Ls} and F_{Lm}, is expressed as

$$F_L = C_L \rho D^2 u_m \left(\frac{\partial u}{\partial z} \right)^{0.5} \left[\nu^{0.5} + 0.5 f(R_*) D \left(\frac{\partial u}{\partial z} \right)^{0.5} \right] \tag{2.58}$$

where $f(R_*) = 1$ for $R_* \geq 3$; $f(R_*) = 0$ for $R_* < 3$; and R_* is the particle Reynolds number ($= u_* d/\nu$). For low values of R_* ($R_* < 3$), particles do not spin.

Using Eqs. (2.50) - (2.53) and (2.58) into Eq. (2.49), the equation of the threshold of sediment motion is obtained as

$$\Theta_c = \frac{2\pi \hat{d}}{\pi C_D \hat{u}_m^2 (3 + 6\hat{d} - \hat{d}^2)^{0.5} + 6 C_L \hat{d} \hat{u}_m (\partial \hat{u}/\partial \hat{z}) \{2[(R_*/\hat{d}) \partial \hat{u}/\partial \hat{z}]^{-0.5} + f(R_*)\}} \tag{2.59}$$

where $\hat{u}_m = u_m/u_*$; $\hat{d} = d/D$; $\hat{u} = u/u_*$; and $\hat{z} = z/D$.

The accuracy of the results obtained from the model is highly dependent on the accurate determination of $\hat{d}$ which is not an easy task through field measurement of a sedimentary bed. To avoid this difficulty, $\hat{d}$ is determined from the information on angle of repose of bed sediments, using the expression given by Ippen and Eagleson (1955) for the spherical sediments as

$$\hat{d} = \frac{2 \tan\varphi \, [6 \tan\varphi + (48 \tan^2 \varphi + 27)^{0.5}]}{4 \tan^2 \varphi + 9} \tag{2.60}$$

where φ = angle of repose.

The threshold of sediment motion over sedimentary bed is controlled by the applied instantaneous shear stress at the bed due to the turbulent fluctuations. The most important

event for the threshold of sediment motion is the sweep event, which has a dominant role in entraining the sediment particles at the bed. The sweep event applies shear in the direction of the flow and provides additional forces to the viscous shear stress. Keshavarzy and Ball (1996) reported that the magnitude of instantaneous bed shear stress in a sweep event is much larger than the time-averaged bed shear stress. Thus, they proposed the following equation of total bed shear velocity for rough-turbulent regime:

$$u_{*t} = (1 + p\sqrt{\alpha - 1}\cos\psi)\, u_* = \eta_t u_* \tag{2.61}$$

where u_{*t} = total shear velocity (= $u_* + u_t$); u_t = instantaneous shear velocity [= $u_* p(\alpha - 1)^{0.5}\cos\psi$ or $(\tau_t/\rho)^{0.5}$]; τ_t = instantaneous bed shear stress; p = probability of occurring sweep event; $\alpha = \tau_t/\tau_0$; and ψ = sweep angle. Therefore, Θ_c calculated from Eq. (2.59) is modified as

$$\Theta_c = \Theta_c(\text{Eq. } 2.59)/\eta_t^2 \tag{2.62}$$

Keshavarzy and Ball (1996) observed experimentally that the frequency of sweep event p and the sweep angle ψ are 30 percent and 22°, respectively, in the vicinity of the bed. In smooth regime, η_t is considered as unity. To solve Eq. (2.62), one needs additional information as given below.

The particle parameter $\tilde{d}$ is given by $(d/\nu)[gd(\rho_s-\rho)/\rho]^{0.5}$. The following equation is used to compute $\tilde{d}$:

$$\tilde{d} = R_*(\hat{d}/\Theta_c)^{0.5} \tag{2.63}$$

The virtual bed level is considered to be at a depth of ξd below the top of the bed particles (Fig. 2.7). Thus, the normal distance δ between the virtual bed level and the bottom level of the solitary sediment particle given by Dey et al. (1999) is

$$\delta = \frac{1}{2\sqrt{3}}(3D^2 + 6Dd - d^2)^{0.5} - \frac{1}{2}(D + d) + \xi d \tag{2.64}$$

According to van Rijn (1984), $\xi = 0.25$.

The mean velocity of flow received by the frontal area of the solitary particle is given by

$$u_m = \frac{2\zeta}{A}\int_{\varepsilon}^{D+\delta} u[(z-\delta)(D+\delta-z)]^{0.5}\, dz \tag{2.65}$$

where A = frontal area of the solitary particle exposed to the flow, that is $(\pi D^2/4)\{1-\arccos(1-2\hat{h}) + 2(1-2\hat{h})[\hat{h}(1-\hat{h})]^{0.5}\}$; $\hat{h} = h/D$; $h = \varepsilon - \delta$; ζ = coefficient being less than unity; and ε = normal distance between the bottom level of the solitary particle or zero-velocity level and the virtual bed level. The introduction of ζ is pertinent here because the summits of the bed particles upstream of the solitary particle obstruct the flow velocity to some extent. It was found that the value of ζ being 0.5 produced satisfactory results. The normalized mean velocity $\hat{u}_m$ is obtained as

$$\hat{u}_m = \frac{2\zeta}{\hat{A}}\int_{\hat{\varepsilon}}^{1+\hat{\delta}} \hat{u}[(\hat{z}-\hat{\delta})(1+\hat{\delta}-\hat{z})]^{0.5}\, d\tilde{z} \tag{2.66}$$

where $\hat{A} = A/D^2$; $\hat{\delta} = \delta/D$; and $\hat{\varepsilon} = \varepsilon/D$.

The velocity gradient $\partial u/\partial z$ can be obtained as follows:

$$\frac{\partial u}{\partial z} = \frac{1}{D+\delta-\varepsilon}\int_{\varepsilon}^{D+\delta}\frac{\partial u}{\partial z}dz = \frac{u_{D+\delta}-u_{\varepsilon}}{D+\delta-\varepsilon} \tag{2.67}$$

Thus, the normalized velocity gradient $\partial\hat{u}/\partial\hat{z}$ is given by

$$\frac{\partial \hat{u}}{\partial \hat{z}} = \frac{\hat{u}_{1+\hat{\delta}}-\hat{u}_{\hat{\varepsilon}}}{1+\hat{\delta}-\hat{\varepsilon}} \tag{2.68}$$

Case 1 ($R_* < 3$): The flow is hydraulically smooth when R_* is less than three because the bed roughness lies within the viscous sub-layer (Schlichting 1960).

It is assumed that the velocity distribution of the flow is solely linear for $R_* < 3$. Hence, the expression for the velocity distribution is

$$\hat{u} = \frac{zu_*}{\nu} \tag{2.69}$$

Thus, the mean flow velocity $\hat{u}_m$ obtained using Eq. (2.69) is

$$\hat{u}_m = \frac{2\zeta R_*}{\hat{A}\hat{d}}\int_{\hat{\varepsilon}}^{1+\hat{\delta}}[(\hat{z}-\hat{\delta})(1+\hat{\delta}-\hat{z})]^{0.5}\,\hat{z}d\hat{z} \tag{2.70}$$

where $\hat{\varepsilon} = 0$ if $\hat{\delta} \le 0$ and $\hat{\varepsilon} = \hat{\delta}$ if $\hat{\delta} > 0$.

The velocity gradient determined using Eq. (2.70) is

$$\frac{\partial \hat{u}}{\partial \hat{z}} = \frac{R_*}{\hat{d}} \tag{2.71}$$

Case 2 ($3 \le R_* \le 70$): The range of particle Reynolds number $3 \le R_* \le 70$ can be considered as transitional regime (Schlichting 1960).

The equation of the velocity distribution for transitional regime proposed by Reichardt (1951) is used. It is

$$\hat{u} = \frac{1}{\kappa}\left\{\ln\left(1+\frac{\kappa\hat{z}R_*}{\hat{d}}\right)-\left[1-\exp\left(-\frac{\hat{z}R_*}{11.6\hat{d}}\right)-\frac{\hat{z}R_*}{11.6\hat{d}}\exp\left(-\frac{\hat{z}R_*}{3\hat{d}}\right)\right]\ln\left(\frac{\kappa\hat{z}_0R_*}{\hat{d}}\right)\right\} \tag{2.72}$$

where κ = von Karman constant (= 0.4); z_0 = zero-velocity level above the virtual bed level (= $0.033k_s$); and k_s = equivalent roughness height of Nikuradse, assumed as d (Wiberg and Smith 1987).

The mean flow velocity $\hat{u}_m$ determined using Eq. (2.72) is

$$\hat{u}_m = \frac{2\zeta}{\kappa\hat{A}}\int_{\hat{\varepsilon}}^{1+\hat{\delta}}[(\hat{z}-\hat{\delta})(1+\hat{\delta}-\hat{z})]^{0.5}\left\{\ln\left(1+\frac{\kappa\hat{z}R_*}{\hat{d}}\right)\right.$$
$$\left.-\left[1-\exp\left(-\frac{\hat{z}R_*}{11.6\hat{d}}\right)-\frac{\hat{z}R_*}{11.6\hat{d}}\exp\left(-\frac{\hat{z}R_*}{3\hat{d}}\right)\right]\ln\left(\frac{\kappa\hat{z}_0R_*}{\hat{d}}\right)\right\}d\hat{z} \tag{2.73}$$

where $\hat{\varepsilon} = \hat{z}_0$ if $(\hat{z}_0 - \hat{\delta}) \ge 0$ and $\hat{\varepsilon} = \hat{\delta}$ if $(\hat{z}_0 - \hat{\delta}) < 0$.

The velocity gradient obtained using Eq. (2.72) is

$$\frac{\partial \hat{u}}{\partial \hat{z}} = \frac{1}{\kappa(1+\hat{\delta}-\hat{\varepsilon})}\left\{\ln\left[1+\frac{\kappa(1+\hat{\delta})R_*}{\hat{d}}\right]-\ln\left(1+\frac{\kappa\hat{\varepsilon}R_*}{\hat{d}}\right)\right\}+\frac{1}{\kappa(1+\hat{\delta}-\hat{\varepsilon})}\left\{\exp\left[-\frac{(1+\hat{\delta})R_*}{11.6\hat{d}}\right]\right.$$
$$\left.-\exp\left(-\frac{\hat{\varepsilon}R_*}{11.6\hat{d}}\right)+\frac{(1+\hat{\delta})R_*}{11.6\hat{d}}\exp\left[-\frac{(1+\hat{\delta})R_*}{3\hat{d}}\right]-\left(\frac{\hat{\varepsilon}R_*}{11.6\hat{d}}\right)\exp\left(-\frac{\hat{\varepsilon}R_*}{3\hat{d}}\right)\right\}\ln\left(\frac{\kappa\hat{z}_0R_*}{\hat{d}}\right) \quad (2.74)$$

Case 3 ($R_* > 70$): The flow over a sedimentary bed is completely rough when R_* exceeds a value of seventy (Schlichting 1960).

The universal logarithmic velocity distribution in rough regime is given below:

$$\hat{u} = \frac{1}{\kappa}\ln\left(\frac{z}{z_0}\right) \quad (2.75)$$

The mean flow velocity $\hat{u}_m$ derived using Eq. (2.75) is

$$\hat{u}_m = \frac{2\zeta}{\kappa\hat{A}}\int_{\hat{\varepsilon}}^{1+\hat{\delta}}[(\hat{z}-\hat{\delta})(1+\hat{\delta}-\hat{z})]^{0.5}\ln\left(\frac{\hat{z}}{\hat{z}_0}\right)d\hat{z} \quad (2.76)$$

The velocity gradient can be determined using Eq. (2.75) as

$$\frac{\partial \hat{u}}{\partial \hat{z}} = \frac{1}{\kappa(1+\hat{\delta}-\hat{\varepsilon})}\ln\left(\frac{1+\hat{\delta}}{\hat{\varepsilon}}\right) \quad (2.77)$$

Simpson's rule can be applied to solve Eqs. (2.70), (2.73) and (2.76).

As the exact expression for the lift coefficient C_L as a function of R_* is not available, Eq. (2.62) is required to be calibrated extensively. The experimental data (Θ_c and R_*) on sediment threshold reported by Gilbert (1914), Casey (1935), Kramer (1935), Shields (1936), USWES (1936), White (1940), Vanoni (1946), Meyer-Peter and Müller (1948), Iwagaki (1956), Neill (1967), Grass (1970), White (1970), Karahan (1975), Mantz (1977) and Yalin and Karahan (1979) are used to calibrate Eq. (2.62), using C_L a free parameter. Fig. 2.8 shows the dependency of C_L on R_*. The negative values of C_L for low range of R_* ($R_* < 3$) were also reported by Watters and Rao (1971) and Davies and Samad (1978).

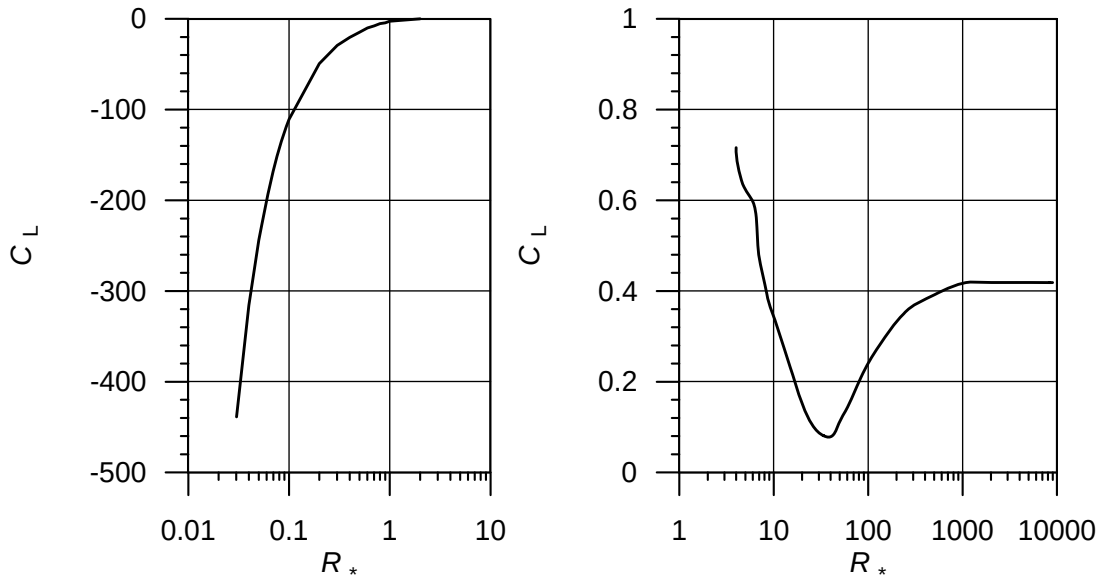

Fig. 2.8 Dependency of C_L on R_*

The dependency of Θ_c on particle parameter $\tilde{d}$ for different φ is presented in Fig. 2.9, that enables direct estimation of Θ_c.

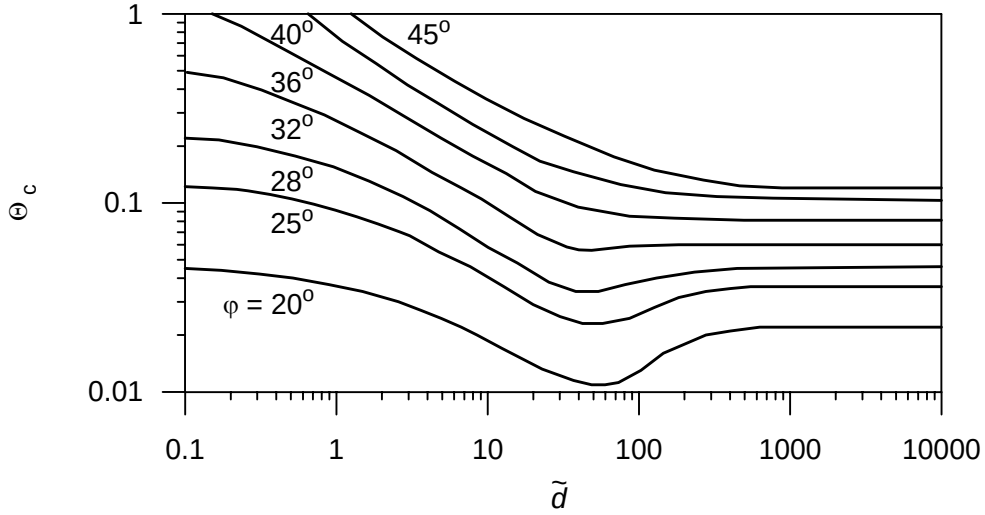

Fig. 2.9 Dependency of Θ_c on particle parameter $\tilde{d}$ for different φ

2.9 Sediment Threshold on Arbitrary Sloping Beds: Dey's Approach

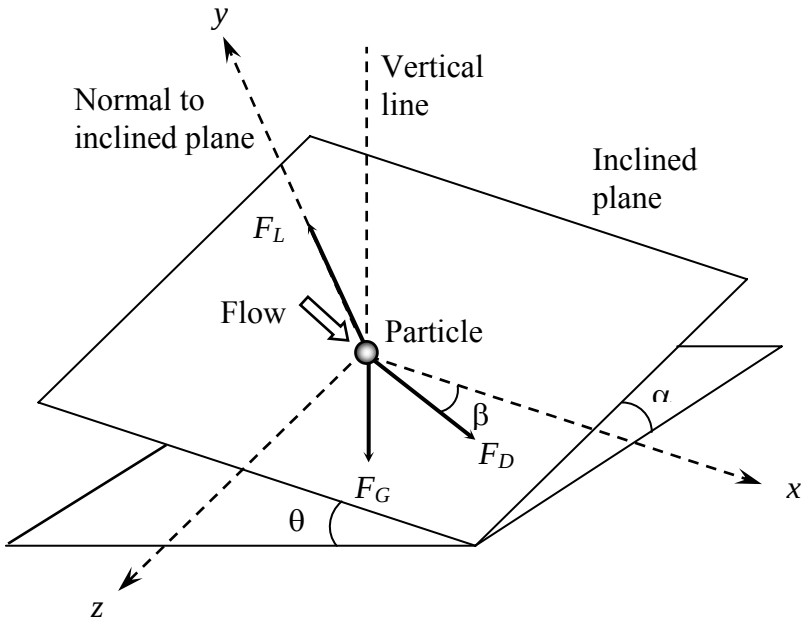

Fig. 2.10 Forces acting on a sediment particle lying on an arbitrary sloping bed

Dey (2003) considered the force acting on a spherical sediment particle placed on a bed having an arbitrary bed slope as shown in Fig. 2.10. When the solitary particle is about to move downstream from its original position, the equation of force balance is

$$F_s^2 = (F_D \cos\beta + F_G \sin\theta)^2 + (F_D \sin\beta + F_G \sin\alpha)^2 \qquad (2.78)$$

where F_s = static Coulomb friction force between the particle and the bed; θ = longitudinal bed angle with the horizontal; α = transverse bed angle with the horizontal; and β = angle of inclination of flow with respect to the longitudinal axis of the channel (positive downward).

The submerged weight of the particle is

$$F_G = \frac{\pi}{6} d^3 (\rho_s - \rho) g \tag{2.79}$$

The static Coulomb friction force is equated to

$$F_s = (F_G \sqrt{\cos^2 \theta - \sin^2 \alpha} - F_L) \mu_c \tag{2.80}$$

where μ_c = static Coulomb friction factor at threshold condition, such that $\arctan(\mu_c) = \varphi$. Equating Eqs. (2.78) and (2.80), one gets

$$F_D^2 + 2F_G(\cos\beta \sin\theta + \sin\beta \sin\alpha) + F_G^2(\sin^2\theta + \sin^2\alpha) - (F_G \sqrt{\cos^2 \theta - \sin^2 \alpha} - F_L)^2 \tan^2 \varphi = 0 \tag{2.81}$$

Normalizing the above equation, one can write

$$(1 - \eta^2 \tan^2 \varphi)\Theta_{cs}^2 + \frac{2}{\hat{F}_D}(\cos\beta \sin\theta + \sin\beta \sin\alpha + \eta \tan^2 \varphi \sqrt{\cos^2 \theta - \sin^2 \alpha}\, \hat{\Theta}_{cs} - \frac{1}{\hat{F}_D}[(\cos^2 \theta - \sin^2 \alpha) \tan^2 \varphi - \sin^2 \theta - \sin^2 \alpha] = 0 \tag{2.82}$$

where $\eta = F_L/F_D$; Θ_{cs} = Shields parameter on an arbitrarily sloping bed, that is $\rho u_{*s}^2/[(\rho_s - \rho)gd]$ or $\tau_{0bs}/[(\rho_s - \rho)gd]$; u_{*s} = critical shear velocity on a sloping bed, that is $(\tau_{0s}/\rho)^{0.5}$; τ_{0s} = critical bed shear stress on a sloping bed; and $\hat{F}_D = 6F_D/(\pi\rho d^2 u_{*s}^2)$. The value of η proposed by Chepil (1958) is as 0.85. The positive solution of Eq. (2.82) is

$$\Theta_{cs} = \frac{1}{(1 - \eta^2 \tan^2 \varphi)\hat{F}_D}\{-(\cos\beta \sin\theta + \sin\beta \sin\alpha + \eta \tan^2 \varphi \sqrt{\cos^2 \theta - \sin^2 \alpha}) + [(\cos\beta \sin\theta + \sin\beta \sin\alpha + \eta \tan^2 \varphi \sqrt{\cos^2 \theta - \sin^2 \alpha})^2 + (1 - \eta^2 \tan^2 \varphi)(\cos^2 \theta \tan^2 \varphi - \sin^2 \alpha \tan^2 \varphi - \sin^2 \theta - \sin^2 \alpha)]^{0.5}\} \tag{2.83}$$

For a horizontal bed, θ and α become zero and Eq. (2.83) reduces to

$$\hat{\Theta}_c = \frac{\tan \varphi}{(1 + \eta \tan \varphi)\hat{F}_D} \tag{2.84}$$

Dividing Eq. (2.83) by Eq. (2.84), yields

$$\tilde{\Theta}_{cs} = \frac{1}{(1 - \eta \tan \varphi) \tan \varphi}\{-(\cos\beta \sin\theta + \sin\beta \sin\alpha + \eta \tan^2 \varphi \sqrt{\cos^2 \theta - \sin^2 \alpha}) + [(\cos\beta \sin\theta + \sin\beta \sin\alpha + \eta \tan^2 \varphi \sqrt{\cos^2 \theta - \sin^2 \alpha})^2 + (1 - \eta^2 \tan^2 \varphi)(\cos^2 \theta \tan^2 \varphi - \sin^2 \alpha \tan^2 \varphi - \sin^2 \theta - \sin^2 \alpha)]^{0.5}\} \tag{2.85}$$

where $\tilde{\Theta}_{cs}$ = critical bed shear stress ratio, that is τ_{0s}/τ_0. However, in general, the flow through a river or a channel is in the longitudinal direction. Therefore, the equation of $\tilde{\Theta}_{cs}$ for this type of flow can be obtained using $\beta = 0$ in Eq. (2.85) as

$$\widetilde{\Theta}_{cs} = \frac{1}{(1-\eta\tan\varphi)\tan\varphi}\{-(\sin\theta+\eta\tan^2\varphi\sqrt{\cos^2\theta-\sin^2\alpha}) + [(\sin\theta+\eta\tan^2\varphi\sqrt{\cos^2\theta-\sin^2\alpha})^2 + (1-\eta^2\tan^2\varphi)(\cos^2\theta\tan^2\varphi-\sin^2\alpha\tan^2\varphi-\sin^2\theta-\sin^2\alpha)]^{0.5}\} \quad (2.86)$$

For transverse bed slopes, using $\theta = 0$ and $\eta = 0$, Eq. (2.86) becomes

$$\widetilde{\Theta}_{c\alpha} = \cos\alpha\sqrt{1-\frac{\tan^2\alpha}{\tan^2\varphi}} \quad (2.87)$$

where $\widetilde{\Theta}_{c\alpha} = \tau_{0\alpha}/\tau_0$; and $\tau_{0\alpha}$ = bed shear stress on a transversely sloping bed.

On the other hand, for longitudinal bed slopes, using $\alpha = 0$, Eq. (2.86) becomes

$$\widetilde{\Theta}_{c\theta} = \cos\theta\left(1-\frac{\tan\theta}{\tan\varphi}\right) \quad (2.88)$$

where $\widetilde{\Theta}_{c\theta} = \tau_{0\theta}/\tau_0$; and $\tau_{0\theta}$ = bed shear stress on a longitudinally sloping bed.

Also, van Rijn (1993) and Dey (2004) proposed that critical bed shear stress on an arbitrary sloping bed is given by $\tau_{0b} = \tau_0\widetilde{\Theta}_{c\alpha}\widetilde{\Theta}_{c\theta}$.

2.10 Streambed Armoring

When the sediment transport capacity of a channel exceeds the rate of sediment supply by the approaching flow, the channel bed starts to degrade. Because of the nonuniformity of the bed sediment, finer sediment is transported at a faster rate than the coarser sediment, and the remaining bed sediment becomes coarser. This coarsening process stops until a layer of coarse sediment completely develops to cover the streambed protecting the finer sediments beneath it from being transported. Once this process is completed, the streambed is *armored* and the coarse layer is called the *armor-layer* (Fig. 2.11). Due to the variation of flow condition of a natural riverbed, usually more than one layer of armoring particles are required to protect finer sediment beneath it. Borah (1989) and Froehlich (1995) reported that the natural armor-layer thickness is one to three times the armoring particle sizes.

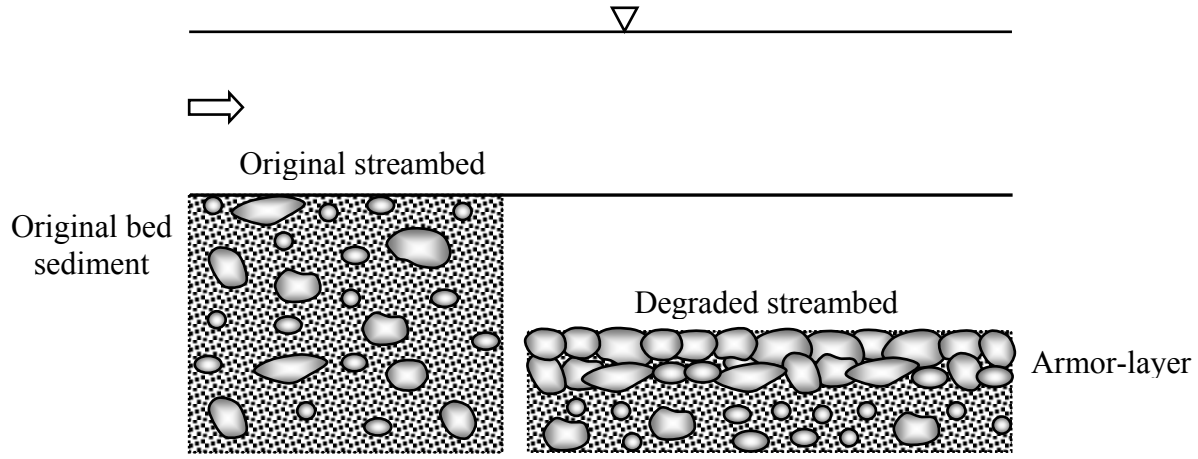

Fig. 2.11 Definition sketch of streambed armoring

2.11 References

Borah, D. K. (1989). "Scour-depth prediction under armoring conditions." *J. Hydraul. Eng.*, 115(10), 1421-1425.

Carstens, M. R. (1966). "An analytical and experimental study of bed ripples under water waves." *Quart. Reports 8 and 9*, Georgia Institute of Technology, School of Civil Engineering, Atlanta, USA.

Casey, H. J. (1935). "Über die geschiebebewegung." *PhD thesis*, Teknikal Hochschule-Scharlottenburg, Berlin, Germany.

Chepil, W. S. (1958). "The use of evenly spaced hemispheres to evaluate aerodynamic force on a soil surface." *Trans. Am. Geophy. Union*, 39(3), 397-404.

Chepil, W. S. (1961). "The use of spheres to measure lift and drag on wind-eroded soil grains." *Proc. Soil Sci. Soc, Am.*, 25(5), 343-345.

Chien, N., and Wan, Z. (1999). *Mechanics of sediment transport*. ASCE Press, Virginia, USA.

Coleman, N. L. (1967). "A theoretical and experimental study of drag and lift forces acting on a sphere resting on a hypothetical stream bed." *Proc. XII IAHR Congr.*, Fort Collins, Colorado, 3, 185-192.

Davies, T. R. H., and Samad, M. F. A. (1978). "Fluid dynamic lift on a bed particle." *J. Hydraul. Div.*, *Am. Soc. Civ. Eng.*, 104(8), 1171-1182.

Dey, S. (1999). "Sediment threshold." *Appl. Math. Modelling*, 23(5), 399-417.

Dey, S. (2003). "Threshold of sediment motion on combined transverse and longitudinal sloping beds." *J. Hydraul. Res.*, 41(4), 405-415.

Dey, S. (2004). "Critical bed shear for initial movement of sediments on a combined lateral and longitudinal slope." *Nordic Hydrol.*, 35(2), 153-164.

Dey, S., Dey Sarker, H. K., and Debnath, K. (1999). "Sediment threshold under stream flow on horizontal and sloping beds." *J. Eng. Mech.*, *Am. Soc. Civ. Eng.*, 125(5), 545-553.

Egiazaroff, J. V. (1965). "Calculation of non-uniform sediment concentrations." *J. Hydraul. Div.*, *Am. Soc. Civ. Eng.*, 91(4), 225-247.

Einstein, H. A., and El-Samni, E. A. (1949). "Hydrodynamic forces on rough wall." *Rev. Modern Phys.*, *Am. Inst. of Phys.*, 21(3), 520-524.

Froehlich, D. C. (1995). "Armor-limited clear-water contraction scour at bridges." *J. Hydraul. Eng.*, 121(6), 490-493.

Gessler, J. (1970). "Self-stabilizing tendencies of alluvial channels." *J. Waterways Harbors Div.*, *Am. Soc. Civ. Eng.*, 96(2), 235-249.

Gilbert, G. K. (1914). "Transportation of debris by running water." *Prof. Paper No. 86*, United States Geological Survey, Washington D.C, USA.

Goncharov, V. N. (1964). *Dynamics of channel flow*. Israel Programme for Scientific Translation, Moscow, Russia.

Graf, W. H. (1971). *Hydraulics of sediment transport*. McGraw-Hill, New York, USA.

Grass, A. J. (1970). "Initial instability of fine bed sand." *J. Hydraul. Div.*, *Am. Soc. Civ. Eng.*, 96(3), 619-632.

Ippen, A. T., and Eagleson, P. S. (1955). "A study of sediment sorting by waves shoaling on a plane beach." *Tech. Memo. No. 63*, US Army Corps Engineers, Beach Erosion Board.

Iwagaki, Y. (1956). "Fundamental study on critical tractive force." *Trans. Jap. Soc. Civ. Eng.*, 41, 1-21.

Jeffreys, H. (1929). "On the transport of sediments in stream." *Proc. Camb. Phil. Soc*., 25, 272 .

Julien, P. Y. (1998). *Erosion and sedimentation*. Cambridge University Press, Cambridge, UK.

Karahan, E. (1975). "Initiation of motion for uniform and non-uniform materials." *PhD thesis*, Technical University, Istanbul, Turkey.

Keshavarzy, A., and Ball, J. E. (1996). "Characteristics of turbulent shear stress applied to bed particles in an open channel flow." *Proc. VII IAHR Int. Symp. Stochastic Hydr. 96*, 451-458.

Kramer, H. (1935). "Sand mixtures and sand movement in fluvial levels." *Trans. Am. Soc. Civ. Eng.*, 100, 798-838.

Kurihara, M. (1948). "On the critical tractive force." *Rep. No.* 3, Vol. 4, Research Institute for Hydraulic Engineering.

Lane, E. W., and Kalinske, A. A. (1939). "The relation of suspended to bed materials in river." *Trans. Am. Geophys. Union*, 20, 637.

Leliavsky, S. (1966). *An introduction to fluvial hydraulics*. Dover, New York.

Mantz, P. A. (1977). "Incipient transport of fine grains and flanks by fluids-extended Shields diagram." *J. Hydraul. Div., Am. Soc. Civ. Eng.*, 103(6), 601-615.

Meyer-Peter, E., and Müller, R. (1948). "Formulas for bed-load transport." *Proc. II IAHR Congr*., Stockholm, Sweden, 39-64.

Morsi, S. A., and Alexander, A. J. (1972). "An investigation of particle trajectories in two-phase flow systems." *J. Fluid Mech*., 55, 193-208.

Neill, C. R. (1967). "Mean velocity criterion for scour of course uniform bed material." *Proc. XII IAHR Congr*., Fort Collins, Colorado, USA, 3, 46-54.

Neill, C. R. (1968). "Note on initial movement of coarse uniform bed-material." *J. Hydraul. Res.*, 6(2), 173-176.

Raudkivi, A. J. (1998). *Loose boundary hydraulics*. A. A. Balkama, Rotterdam, The Netherlands.

Reichardt, H. (1951). "Vollstandige darstellung der turbulenten geschwindig-keitsverteilung in glatten leitungen." *Z. Angew. Math. Mech.*, 31(7), 208-219.

Reitz, W. (1936). "Uber geschiebebewegung." *Wasserwirtsch. und Tech.*, 28-30.

Rubinow, S. I., and Keller, J. B. (1961). "The transverse force on a spinning sphere moving in a viscous fluid." *J. Fluid Mech*., 11, 447-459.

Saffman, P. G. (1965). "The lift on a small sphere in a slow shear flow." *J. Fluid Mech*., 22, 385-400.

Saffman, P. G. (1968). "Corrigendum, the lift on a small sphere in a slow shear flow." *J. Fluid Mech*., 31, 624.

Schlichting, H. (1960). *Boundary layer theory*. McGraw-Hill Book Companies, New York, USA.

Shields, A. (1936). "Application of similarity principles and turbulence research to bed-load movement." *Mitteilunger der Preussischen Versuchsanstalt für Wasserbau und Schiffbau,* Berlin, Germany, 26, 5-24.

Soulsby, R. L., and Whitehouse, R. J. S. (1997). "Threshold of sediment motion in coastal Environments." *Proc. Combined Australasian Coastal Eng. and Port Conf.*, Christchurch, New Zealand, 149-154.

Task Committee. (1966). "Sediment transportation mechanics: Initiation of motion." *J. Hydraul. Div.*, *Am. Soc. Civ. Eng.*, 92(2), 291-314.

USWES. (1936). "Flume tests made to develop a synthetic sand which will not form ripples when used in movable bed models." *Tech. Memo. 99-1*, United States Waterways Experiment Station, Vieksburg, Mississippi, USA.

Vanoni, V. A. (1946). "Transport of suspended sediment by water." *Trans. Am. Soc. Civ. Eng.*, 111, 67-102.

Vanoni, V. A. (1964). "Measurements of critical shear stress." *Rep. No. KH-R*-7, California Institute of Technology, USA.

van Rijn, L. C. (1984). "Sediment transport, part I: bed-load transport." *J. Hydraul. Eng*., 110(10), 1431-1456.

van Rijn, L. C. (1993). *Principles of sediment transport in rivers, estuaries and coastal seas*. Aqua Publications, The Netherlands.

Watters, G. Z., and Rao, M. V. P. (1971). "Hydrodynamic effects of seepage on bed particles." *J. Hydraul. Div.*, *Am. Soc. Civ. Eng.*, 97(3), 421-439.

White, C. M. (1940). "The equilibrium of grains on the bed of a stream." *Phil. Trans. Royal Soc*., 174A, 322-338.

White, S. J. (1970). "Plane bed thresholds of fine grained sediments." *Nature*, 228(Oct.), 152-153.

Wiberg, P. L., and Smith, J. D. (1987). "Calculations of the critical shear stress for motion of uniform and heterogeneous sediments." *Wat. Resour. Res*., 23(8), 1471-1480.

Yalin, M. S. (1972). *Mechanics of sediment transport*. Pergamon Press, Braunschweig, Germany.

Yalin, M. S., and Karahan, E. (1979). "Inception of sediment transport." *J. Hydraul. Div.*, *Am. Soc. Civ. Eng.*, 105(11), 1433-1443.

Yang, C. T. (1973). "Incipient motion and sediment transport." *J. Hydraul. Div.*, *Am. Soc. Civ. Eng.*, 99(10), 1679-1704.

Yang, C. T. (1996). *Sediment transport: theory and practice*. McGraw-Hill Book Companies, Singapore.

Zanke, U. (1977). "Neuer Ansatz zur Berechnung des Transportbeginns von Sedimenten unter Stromungseinfluss." *Mitt. Des Franzius-Institut,* Techn. Univ. Hannover, Germany, Heft 46.

Chapter 3

Bed-Load Transport

3.1 General

Transport as *bed-load* is the mode of transport of sediments where the sediment particles glide, roll or briefly jump, but stay very close to the bed, which they may leave very temporarily. The displacement of the particle is intermittent; as the random concept of the turbulence plays an important role. It is useful to give limiting values for the separation of different modes of transport:

$$u_* / w_{ss} \geq 0.1 \qquad \text{bed-load transport} \qquad (3.1a)$$

$$u_* / w_{ss} \geq 0.4 \qquad \text{suspended-load transport} \qquad (3.1b)$$

where u_* = shear velocity; and w_{ss} = settling or terminal velocity of particles. Fig. 3.1 presents different modes of sediment transport.

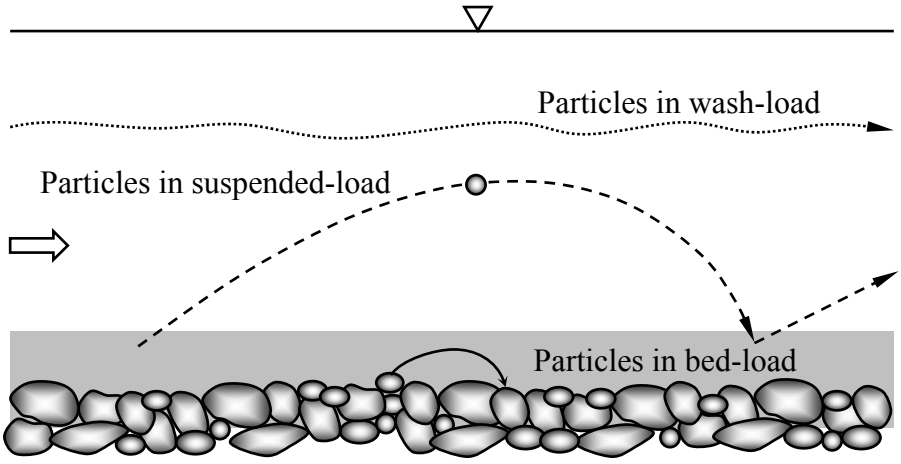

Fig. 3.1 Schematic of different modes of sediment transport

On the other hand, when the particles stay occasionally in contact with the bed and displace them by making more or less large jumps to remain often surrounded by fluid, the mode of transport is termed *suspended-load*. This type of transport concerns the relatively finer particles. However, the mode of transport of very fine particles is as *wash-load*, where the particles almost never in contact with the bed being washed through the zone of flow. A review on bed-load transport is available in Graf (1971), Yalin (1972), Raudkivi (1998), Yang (1996), and Chien and Wan (1999).

3.2 DuBoys' Approach

DuBoys (1879) assumed that the sediment moves in layer having a thickness $\Delta\varepsilon$. These layers move because of the tractive force given by bed shear stress $\tau_0 = (\rho g h S)$ is applied to them, where ρ = mass density of fluid; g = gravitational acceleration; h = flow depth; S = streamwise bed slope. Fig. 3.2 shows the definition sketch of DuBoys model. The top layer is one where the tractive force balances the resistance force between these layers, such that

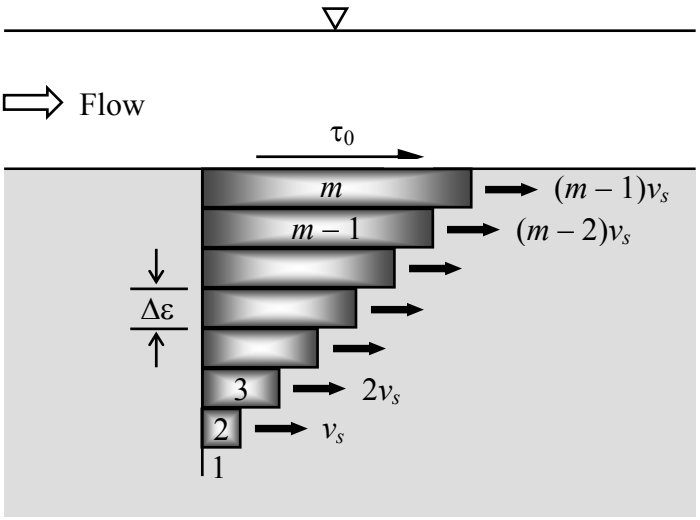

Fig. 3.2 Definition sketch of DuBoys bed-load model

$$\tau_0 = \rho g h S = \mu m \Delta\varepsilon(\rho_s - \rho)g \tag{3.2}$$

where μ = frictional coefficient; m = number of layers; and ρ_s = mass density of sediment. The fastest moving layer is the top layer and moves with the velocity of $(m - 1)v_s$. If the layer between first and m-th moves according to a linear velocity distribution, then the amount of sediment (in volume per unit time and width i.e. m^3/sm) is given by

$$q_b = \Delta\varepsilon v_s m(m-1)/2 \tag{3.3}$$

The critical condition at which sediment motion is just about to begin is given by $m = 1$; then Eq. (3.2) becomes

$$\tau_c = \mu\Delta\varepsilon(\rho_s - \rho)g \tag{3.4}$$

This, in turn, results in the relationship of

$$\tau_0 = m\tau_c \tag{3.5}$$

It is introduced into Eq (3.3) and the following is obtained:

$$q_b = \left[\frac{\Delta\varepsilon v_s}{2\tau_c^2}\right]\tau_0(\tau_0 - \tau_c) \tag{3.6}$$

DuBoys (1879) referred the first term within the square bracket in RHS of Eq. (3.6) as a characteristic of sediment coefficient and gave it a symbol χ (chi). Thus, the equation becomes

$$q_b = \chi\tau_0(\tau_0 - \tau_c) \tag{3.7}$$

Straub [see Rouse (1950)] related χ to the particle size d (in SI units) (0.125 mm < d < 4 mm) as

$$\chi = 6.89 \times 10^{-6} / d^{0.75} \tag{3.8}$$

Other empirical equations of DuBuys type proposed by various investigators are given below:

Schoklitsch (1934) proposed a bed-load equation for particle size 0.305 mm < d < 7.02 mm

$$g_b = \frac{7000}{d_{50}^{0.5}} S^{1.5}(q - q_c) \tag{3.9}$$

where g_b = bed-load transport rate in weight per unit width; q = flow rate per unit width; and $q_c = 1.944\times10^{-5}/S^{1.33}$ (m^3/sm). Schoklitsch later modified the equation for $d \geq 0.6$ mm as

$$g_b = 2500S^{1.5}(q - q_c) \tag{3.10}$$

where $q_c = h_c^{5/3}S^{1/2}/n = 0.26\Delta^{3/5}d^{3/2}/S^{7/6}$; n = Manning coefficient; h_c = critical flow depth; $\Delta = s - 1$; and s = relative density of sediment.

Shields (1936) put forward the bed-load equation as

$$q_b = 10\frac{qS}{s}(\Theta - \Theta_c) \tag{3.11}$$

where Θ and Θ_c = Shields and critical Shields parameters, respectively. The Shields parameter is given by $\Theta = \tau_0/(\Delta\rho g d)$ and Θ_c corresponds to τ_c. In terms of g_b, Eq. (3.11) becomes

$$g_b = 10\frac{\rho g q S}{s}(\Theta - \Theta_c) \tag{3.12}$$

Meyer-Peter (1951) gave the following equations of bed-load in terms of q_b and g_b:

$$q_b = 8(\Delta g d^3)^{0.5}(\Theta - \Theta_c)^{1.5} \tag{3.13a}$$

$$g_b = 8\rho_s g(\Delta g d^3)^{0.5}(\Theta - \Theta_c)^{1.5} \tag{3.13b}$$

For gravel-bed rivers, Parker (1979) proposes

$$q_b = 11.2(\Delta g d^3)^{0.5}\frac{(\Theta - 0.03)^{4.5}}{\Theta^3} \tag{3.14}$$

Nielson's (1992) equation of sand and gravels (0.69 mm $\leq d \leq$ 28.7 mm) transport is

$$q_b = (\Delta g d^3)^{0.5}\Theta(12\Theta - 0.05) \tag{3.15}$$

Note: $\Phi = q_b/(\Delta g d^3)^{0.5} = g_b/[(\rho_s g)(\Delta g d^3)^{0.5}] = g_{bs}(s/\Delta)/[(\rho_s g)(\Delta g d^3)^{0.5}]$, where g_{bs} = bed-load transport rate in submerged weight per unit width.

3.3 Einstein's Bed-Load Function

Einstein (1950) developed a bed-load transport model based on the probabilistic concept.

Rate of Deposition:

The average traveling distance L_0 is the distance that a particle travels from its starting point until it is deposited on the bed. The step length of a particle diameter d can be expressed as λd and for spherical particles, $\lambda = 100$. If after a particle travels a step length, it falls on the bed at a point where a local lift force is greater than the submerged weight of the particle, and the particle does not stop moving but travels a second step length. If p is the probability of the lift force being greater than the submerged weight, $n(1 - p)$ particles deposit on the bed after traveling a step length, where n is the number of particles in motion. Thus, only np particles continue moving. After traveling the second step length, $np(1 - p)$ more particles stop moving and only np^2 particles remain in motion. In this way, all n particles stop on the bed after some time elapses. The traveling distance can be determined as:

$$L_0 = \sum_{n=0}^{\infty}(1-p)\,p^n\,(n+1)\lambda d = \frac{\lambda d}{1-p} \tag{3.16}$$

The particles passing a section (across the flow) per unit time deposit within a length of the channel that is equal to L_0, no matter from where they started moving. If g_b represents the rate of bed-load transport in dry weight, than the rate of deposition on unit area = $g_b/(L_0\times 1) = g_b(1-p)/(\lambda d)$.

Rate of Erosion:

The number of particles per unit area can be estimated as $1/(A_1 d^2)$, and their total weight is $A_2\rho_s g d^3/(A_1 d^2)$. If p is the probability for a particle to begin to move, sediment with a total weight of $(A_2\rho_s g/A_1)pd$ is eroded from the bed per unit time, where A_1 and A_2 are coefficients related to the shape of the particles.

Exchange time or time for a particle to be removed is assumed proportional to the time for a particle to fall a length of one diameter in still fluid. Thus, it is

$$t \sim \frac{d}{w_{ss}} = A_3\,(d/\Delta g)^{0.5} \tag{3.17}$$

where A_3 = constant of time scale. Therefore, the rate of erosion per unit area of the bed surface is $(A_2\rho_s g/A_1)pd/[A_3(d/\Delta g)^{0.5}] = \rho_s\Delta^{0.5} g^{1.5} p d^{0.5}[A_2/(A_1 A_3)]$

Equilibrium of Sediment Transport:

Sediment transport is in equilibrium if the amount of sediment eroded from the bed is equal to the amount of sediment deposited on the bed for a given time. Thus, equilibrium equation is given by

$$\frac{g_b(1-p)}{\lambda d} = \rho_s\Delta^{0.5} g^{1.5} p d^{0.5}\,\frac{A_2}{A_1 A_3} \tag{3.18}$$

Eq. (3.18) can be rewritten as

$$\frac{p}{1-p} = A_*\Phi \tag{3.19}$$

where $A_* = A_1 A_3/(\lambda A_2)$; and $\Phi = g_b/(\rho_s\Delta^{0.5} g^{1.5} d^{1.5})$. The parameter Φ is called *bed-load transport intensity* and the probability is given by

$$p = \frac{A_*\Phi}{1 + A_*\Phi} \tag{3.20}$$

Probability Determination:

The submerged weight of particle F_G is

$$F_G = A_2(\rho_s - \rho)g d^3 \tag{3.21}$$

The lift force F_L is given by

$$F_L = \frac{1}{2} C_L A_1 d^2 \rho u_b^2 \tag{3.22}$$

where C_L = lift coefficient; and u_b = effective velocity at the edge of the viscous sub-layer.

Einstein and El-Samni (1949) found that for uniform sediment, if the velocity at an elevation $z = 0.35X$ is taken as the effective velocity u_b in Eq. (3.22), the distribution of fluctuating lift force follows the normal distribution with a standard deviation equal to half the mean value and $C_L = 0.178$. The effective velocity u_b is expressed as $u_b/u_* = 5.75 \log[(30.2)(0.35X/\Delta_k)]$, where $X(\Delta_k/\delta > 1.8) = 0.77\Delta_k$; $X(\Delta_k/\delta < 1.8) = 1.39\delta$; Δ_k = apparent roughness ($= k_s/x$); and δ = viscour sub-layer thickness ($= 11.6\nu/u_*$). The apparent roughness Δ_k can be obtained from the curve given by Einstein (1950) (Fig. 3.3).

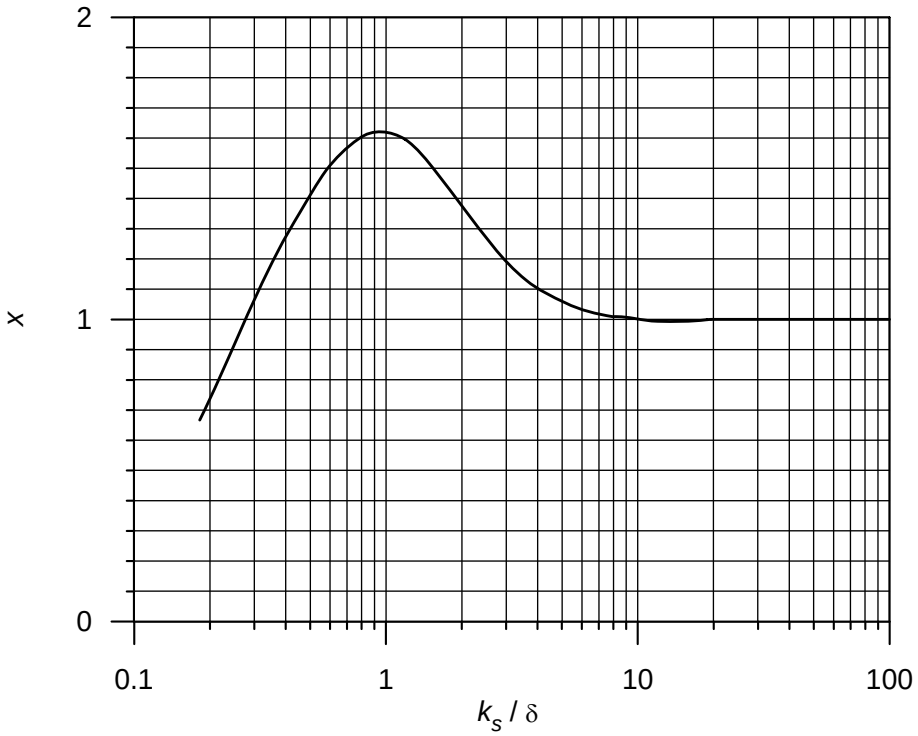

Fig. 3.3 Variation of correction factor x with k_s/δ, where k_s is the equivalent roughness height of Nikuradse ($= d_{65}$)

Hence, the lift force can be expressed as

$$F_L = 0.178 A_1 d^2 \frac{1}{2} \rho 5.75^2 g R_b' S \log^2(10.6X/\Delta_k)(1+\eta) \tag{3.23}$$

where R_b' = hydraulic radius due to grain roughness; such that shear velocity $u_* = (g R_b' S)^{0.5}$. The random function η represents the fluctuating component of the lift force being distributed according to the normal error law, where the standard deviation η_0 is a universal constant of $\eta_0 = 0.5$.

$$\eta = \eta_0 \eta_* \tag{3.24}$$

where η_* = nondimensional number that represents the fluctuation of the lift force that can be expressed as

$$F_L = \frac{0.178 A_1 5.75^2}{2} \rho d^2 g R_b' S \log^2(10.6X/\Delta_k)(1+\eta_*\eta_0) \tag{3.25}$$

The term probability p of erosion is expressed as the ratio of the submerged weight F_G to the instantaneous lift F_L, which has to be smaller than unity, that is

$$1 > \frac{F_G}{F_L} = \left(\frac{1}{1+\eta_0\eta_*}\right)\left(\frac{\Delta d}{R_b' S}\right)\left(\frac{2A_2}{0.178A_1 5.75^2}\right)\frac{1}{\log^2(10.6X/\Delta_k)} \tag{3.26}$$

Using different symbols, Eq. (3.26) becomes

$$1 > \left(\frac{1}{1+\eta_0\eta_*}\right)\frac{\Psi B}{\beta_x^2} \tag{3.27}$$

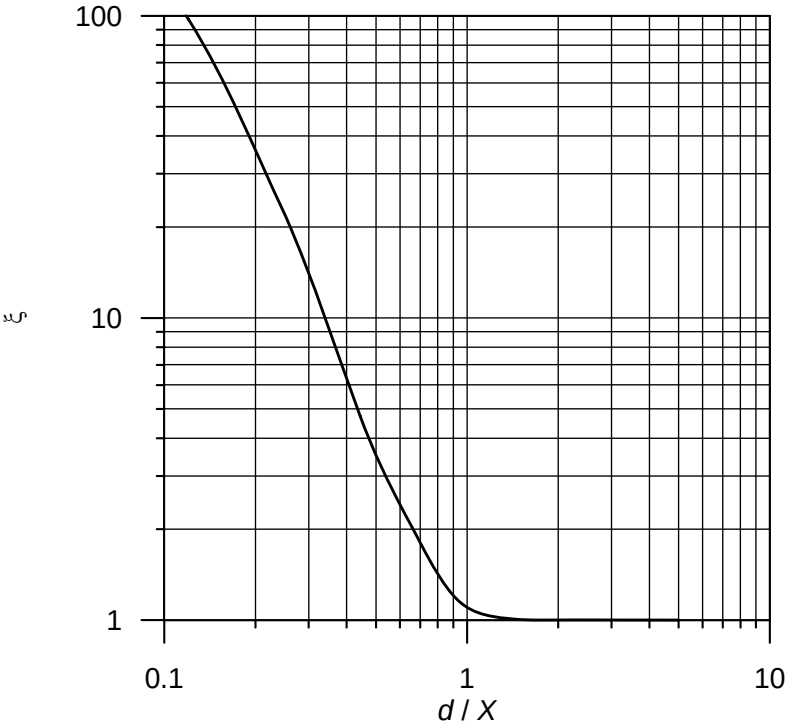

Fig. 3.4 Variation of hiding factor ξ with d/X

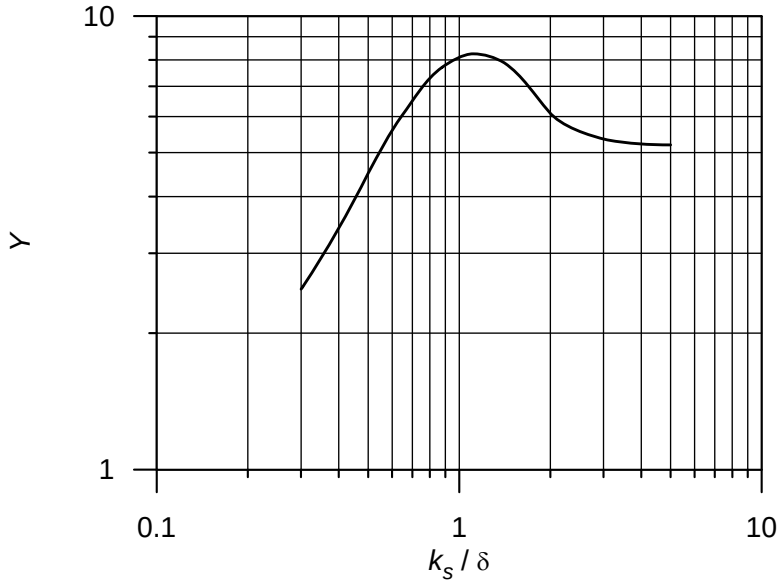

Fig. 3.5 Variation of lift correction factor Y with k_s/δ

where Ψ = flow intensity, that is $\Delta d/(R_b' S)$; $B = 2A_2/(0.178A_1 5.75^2)$; and $\beta_x = \log(10.6X/\Delta_k)$. Einstein (1950) suggested two correction factors ξ and Y termed *hiding factor* and *lift correction factor*, respectively, which were determined by him experimentally. Small particles in the sediment mass seem to hide between larger ones or in the viscous sub-layer, such that their lift must be corrected by ξ^{-1}. The hiding factor ξ of sediment particles is a function of d/X (see Fig. 3.4), where X is the characteristic distance. The lift correction factor Y describes the change of lift coefficient in the sediment mass having different roughness and is a function of k_s/δ (see Fig. 3.5). The fluctuation of the lift force is caused by the fluctuation of the velocity. Whether the fluctuation of velocity is positive or negative, the lift force is always positive. Thus, the inequality for the lift force can be modified as

$$\left|1 + \eta_0 \eta_*\right| > \xi Y B' \frac{\Psi \beta^2}{\beta_x^2} \tag{3.28}$$

where $B' = B/\beta^2$; and $\beta = \log(10.6)$. After rearranging, it becomes

$$\left|\eta_* + \frac{1}{\eta_0}\right| > \frac{B'\Psi_*}{\eta_0} = B_*\Psi_* \tag{3.29}$$

where $\Psi_* = \xi Y \Psi(\beta/\beta_x)^2$; and $B_* = B'/\eta_0$.

The threshold or critical condition for particles to be removed from the bed is

$$\eta_* = \pm B_*\Psi_* - \frac{1}{\eta_0} \tag{3.30}$$

Between the two values, no bed-load motion occurs. Therefore, the probability p of motion becomes

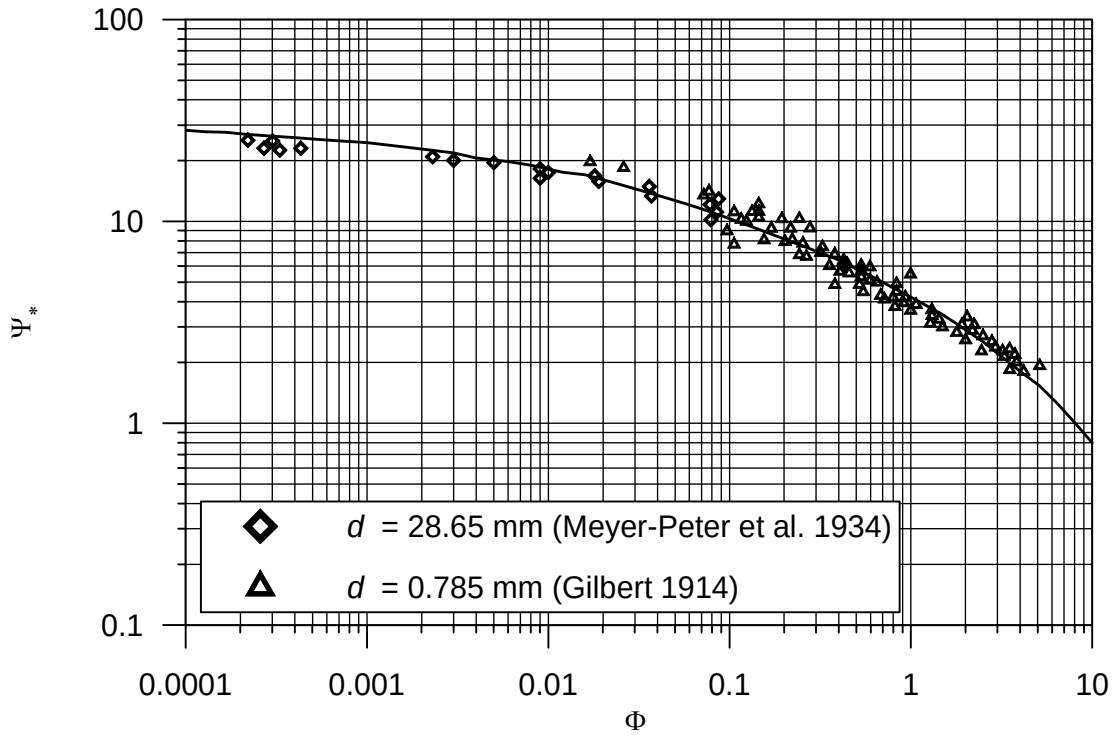

Fig. 3.6 Variation of Ψ_* with Φ obtained from Einstein's (1950) Eq. (3.32)

$$p = 1 - \frac{1}{\sqrt{\pi}} \int_{-B_*\Psi_* - \frac{1}{\eta_0}}^{B_*\Psi_* - \frac{1}{\eta_0}} \exp(-t^2)dt \tag{3.31}$$

Equating Eqs. (3.20) and (3.31), the bed-load equation becomes

$$1 - \frac{1}{\sqrt{\pi}} \int_{-B_*\Psi_* - \frac{1}{\eta_0}}^{B_*\Psi_* - \frac{1}{\eta_0}} \exp(-t^2)dt = \frac{A_*\Phi}{1 + A_*\Phi} \tag{3.32}$$

Experimentally determined constants are: $1/\eta_0 = 2$, $A_* = 43.5$ and $B_* = 1/7$. Variation of Ψ_* with Φ obtained from Eq. (3.32) is shown in Fig. 3.6.

3.4 Yalin's Bed-Load Equation

Yalin (1972) proposed a bed-load transport model based on the analysis of forces acting on a sediment particle. The equations of force acting on a sediment particle in the streamwise and normal directions are

$$F_x = m' \frac{du_{bx}}{dt} \tag{3.33a}$$

$$-F_z - F_G = m' \frac{du_{bz}}{dt} \tag{3.33b}$$

where F_x and F_z = force components of flow acting on a particle in the streamwise direction and normal directions, respectively; u_{bx} and u_{bz} = velocity components of a sediment particle in the streamwise and normal directions, respectively; and m' = submerged mass of the sediment particle. The force components F_x and F_z are given by

$$F_x = \frac{\pi}{8} C_{Dx} \rho d^2 (u - u_{bx})^2 \tag{3.34a}$$

$$F_z = \frac{\pi}{8} C_{Dz} \rho d^2 u_{bz}^2 \tag{3.34b}$$

where u = flow velocity received by the particle.

A particle jumps up from the bed under the action of a lift force F_L. The lift force then decreases with distance from the bed and is equal to F_G at an elevation where the particle reaches its maximum vertical velocity component. The maximum vertical velocity component can be obtained from the following equation:

$$-F_z - F_G + F_L = m' \frac{du_{bz}}{dt} \tag{3.35}$$

This equation represents the initial condition of Eq. (3.33b). To solve these equations, Yalin made the following assumptions:

- $F_L/F_G \sim \exp(-z/d)$,
- C_{Dx} and C_{Dz} are constants, and

- u/u_* is constant at the bed.

In this process, he obtained an expression for u_{bx}, and then he determined its average value $\overline{u}_b$ over the time when it is in motion. It is given by

$$\overline{u}_b = u_* C_1 \left[1 - \frac{1}{a_1 s_1} \ln(1 + a_1 s_1) \right] \tag{3.36}$$

where $s_1 = (\Theta - \Theta_c)/\Theta_c$; $a_1 = 2.45\Theta_c^{0.5}/s^{0.4}$; and C_1 = a constant to be determined. The parameter Θ, being the Shields parameter, is reciprocal of the parameter Ψ. He determined the submerged weight of the bed-load per unit area W_s from the dimensional analysis. It follows

$$\frac{W_s}{(\rho_s - \rho) g d} = f_1(\Theta, R_*) \tag{3.37}$$

where $\Theta = \rho g R_b S/(\Delta \rho g d)$; R_b = hydraulic radius; $R_* = u_* d/\nu$; and ν = kinematic viscosity of fluid.

The particle Reynolds number can be expressed as

$$R_* = \sqrt{\frac{\Delta g d^3}{\nu^2} \Theta} \tag{3.38}$$

Therefore, Eq. (3.37) can be rewritten as

$$\frac{W_s}{(\rho_s - \rho) g d} = f_2\left(\Theta, \frac{\Delta g d^3}{\nu^2} \right) \tag{3.39}$$

At the initiation of bed-load motion, $W_s = 0$, and

$$f_2\left(\Theta_c, \frac{\Delta g d^3}{\nu^2} \right) = 0 \tag{3.40}$$

Combining Eqs. (3.39) and (3.40), yields

$$\frac{W_s}{(\rho_s - \rho) g d} = f_2(\Theta, \Theta_c) \tag{3.41}$$

Yalin assumed

$$\frac{W_s}{(\rho_s - \rho) g d} = C_2 s_1 \tag{3.42}$$

where C_2 = constant to be determined.

Substituting Eqs. (3.36) and (3.42) into Eqs. (3.33a) and (3.33b) and determining the constants from the measured data, the bed-load transport rate g_b in weight per unit time and width is given by $g_b = g_{bs}(s/\Delta) = W_s \overline{u}_b (s/\Delta)$. Thus, the bed-load equation of Yalin (1972) is

$$g_b = 0.635 \rho g s d u_* s_1 \left[1 - \frac{1}{a_1 s_1} \ln(1 + a_1 s_1) \right] \tag{3.43}$$

3.5 Bagnold's Approach

Bagnold (1973) assumed that to sustain the saltation of a particle, the flowing fluid must act on the particle so as to provide a momentum component $m'u'$ with the time interval Δt between successive collisions of the particle with the bed. Here, m' is the submerged mass and $-u'$ is the reduction in particle velocity in the flow direction because of its collision with the bed.

Therefore, the flow exerts a force on the particle with a component in the flow direction as

$$F_x = \frac{m'u'}{\Delta t} = \frac{F_G u'}{g\Delta t} \tag{3.44}$$

If u_b is the average velocity of the particle, then the work done by the flowing fluid on the particle is $F_x u_b$. Also, the energy consumed in unit time by the flow is $F_G u_b \tan\varphi$, where φ is the frictional angle. Combining them one gets

$$\frac{F_x}{F_G} = \tan\varphi = \frac{u'}{g\Delta t} \tag{3.45}$$

In reality, the force exerted on the particle varies with the distance of the particle from the bed. The distance z_n is the location at which the particle is acted upon by a force equal to F_x. If the flow velocity at z_n is u_n, then the difference of u_n and u_b is u_r (= $u_n - u_b$). If many particles move along the bed, then

$$Tu_b = F_G u_b \tan\varphi = g_{bs} \tan\varphi \tag{3.46}$$

where T = shear stress for maintaining sediment motion at $z = z_n$. So, the bed-load (in submerged weight) transport rate is

$$g_{bs} = \frac{T}{\tan\varphi}(u_n - u_r) \tag{3.47}$$

Using a coefficient a, the shear stress T is given by

$$T = a\tau_0 \tag{3.48}$$

If the flow velocity follows the logarithmic law in the zone $z > z_n$, and the velocity at an elevation $0.4h$ from the bed is taken to be the average velocity, then

$$u_n = U - 5.75u_* \log\frac{0.4h}{z_n} \tag{3.49}$$

where u = depth-averaged velocity; and h = flow depth.

Using Eqs. (3.48) and (3.49) into Eq. (3.47), one gets

$$g_{bs} = \frac{a\tau_0}{\tan\varphi}\left[U - 5.75u_* \log\left(\frac{0.4h}{z_n}\right) - u_r\right] \tag{3.50}$$

Determination of a:

Bagnold assumed a as follows:

$$a = \frac{u_* - u_{*c}}{u_*} \tag{3.51}$$

where u_{*c} = critical shear velocity for the particle motion.

Determination of u_r:

The force exerted on a particle by the flow can be expressed as

$$F_x = \frac{1}{2} C_{Dx} \frac{\pi}{4} d^2 \rho u_r^2 = F_G \tan\varphi \tag{3.52}$$

where C_{Dx} = drag coefficient.

For a particle falling in still fluid, a force F_z acts on the particle. If the submerged weight of the particle is balanced by this force, the particle falls at a constant velocity w_{ss}. Then

$$F_z = \frac{1}{2} C_{Dz} \frac{\pi}{4} d^2 \rho w_{ss}^2 = F_G \tag{3.53}$$

where C_{Dz} = drag coefficient for a settling particle. From Eqs. (3.52) and (3.53), one gets

$$u_r = w_{ss} (C_{Dz} \tan\varphi / C_{Dx})^{0.5} \tag{3.54}$$

It was found from the measured data that $C_{Dz} \approx C_{Dx}$ and $\tan^{0.5}\varphi \approx 1$. Therefore, Eq. (3.54) becomes

$$u_r = w_{ss} \tag{3.55}$$

Determination of z_n:

If no sand dunes form, the average elevation of the saltating particles is proportional to their diameter. Thus

$$z_n = m_1 d \tag{3.56}$$

where $m_1 = K_1 (u_*/u_{*c})^{0.6}$ being dependent on the flow intensity.

In the laboratory, $K_1 = 0.4$ was found by Francis (1973). In rivers, it becomes 2.8 for sands and 7.3 - 9.1 for gravels (Bagnold 1977).

Therefore, the equation of bed-load transport rate obtained by Bagnold is

$$g_b = \frac{u_* - u_{*c}}{u_*} \cdot \frac{\tau_0 s U}{\Delta \tan\varphi} \left[1 - 5.75 \left(\frac{u_*}{U} \right) \log \left(\frac{0.4h}{m_1 d} \right) - \left(\frac{w_{ss}}{U} \right) \right] \tag{3.57}$$

Note: $g_b = g_{bs}(s/\Delta)$.

3.6 Engelund and Fredsøe's Bed-Load Equation

Engelund and Fredsøe (1976) developed the bed-load transport model for the flow conditions close to the threshold of sediment motion.

The bed-load particles are transported with a mean transport velocity $\overline{u}_b$, when they are moving. Herby, the tractive or agitation force is given by

$$F_D = \frac{1}{2} \rho C_D \frac{\pi}{4} d^2 (\alpha u_* - \overline{u}_b)^2 \tag{3.58}$$

where C_D = drag coefficient; and αu_* = flow velocity at the bed particle level. If the particle is at a distance of one to two particle diameters above the bed, α = 6 to 10.

The stabilizing frictional force on the moving particle is

$$F_s = \Delta\rho g \frac{\pi d^3}{6} \mu_d \tag{3.59}$$

where μ_d = dynamic friction angle for the bed sediment.

For the equilibrium, the tractive force and the frictional force are equal. Thus

$$\frac{1}{2}\rho C_D \frac{\pi}{4} d^2 (\alpha u_* - \overline{u}_b)^2 = \Delta\rho g \frac{\pi d^3}{6} \mu_d \tag{3.60}$$

It gives

$$\frac{\overline{u}_b}{u_*} = \alpha \left[1 - \left(\frac{\Theta_0}{\Theta} \right)^{0.5} \right] \tag{3.61}$$

where $\Theta_0 = 4\mu_d/(3\alpha^2 C_D)$.

In fact, Θ_c is the critical value for the initial movement of a particle in a compactly arranged bed, and Θ_0 is the critical value for a particle protruding from the bed surface. Therefore, Θ_0 is smaller then Θ_c. It was observed from the measured data that $\Theta_0 = 0.5\Theta_c$.

Thus, Eq. (3.61) becomes

$$\frac{\overline{u}_b}{u_*} = \alpha \left[1 - 0.7 \left(\frac{\Theta_c}{\Theta} \right)^{0.5} \right] \tag{3.62}$$

For a sandy riverbed, $\alpha = 10$. Engelund and Fredsøe (1976) treated sediment particles as spheres of diameter d, so that there are approximately $1/d^2$ spherical particles in a unit area of bed surface. For a certain flow intensity, the portion of the particles on the bed surface that are moving is p (probability).

Hence, the rate of bed-load transport is given by

$$g_b = \frac{\pi}{6} d^3 \rho_s g \frac{p}{d^2} \overline{u}_b \tag{3.63}$$

Using Eq. (3.62) into Eq. (3.63), yields

$$g_b = 10 \frac{\pi}{6} d^3 \rho_s g \frac{p}{d^2} \left[1 - 0.7 \left(\frac{\Theta_c}{\Theta} \right)^{0.5} \right] u_* \tag{3.64}$$

According to Bagnold, the shear stress of flow is composed of particle shear stress τ and fluid shear stress τ'. Furthermore, he suggested that the fluid shear stress τ' equals the critical bed shear stress for initiation of motion of bed particles. Hence

$$\tau = \tau_c + T = \tau_c + nF_x \tag{3.65}$$

where n = number of particles moving per unit area of bed surface; and F_x = drag force acting on the particles. Engelund assumed

$$F_x = \frac{\pi d^3}{6} \Delta\rho g \mu_d \tag{3.66}$$

Eq. (3.65) leads to

$$\Theta = \Theta_c + \frac{\pi}{6} \mu_d (nd^2) = \Theta_c + \frac{\pi}{6} \mu_d p \tag{3.67}$$

where $p = nd^2$. Thus, p is obtained as

$$p = \frac{6}{\pi\mu_d}(\Theta - \Theta_c) \tag{3.68}$$

Therefore, the bed-load transport rate equation is

$$g_b = 10\frac{d}{\mu_d}\rho_s g\frac{u_*}{\Theta^{0.5}}(\Theta - \Theta_c)(\Theta^{0.5} - 0.7\Theta_c^{0.5}) \tag{3.69}$$

3.7 Transformation and Comparison of Bed-Load Equations

Meyer-Peter Equation:

Eq. (3.13b) can be expressed according to Chien (1954) as

$$\Phi = 8\left(\frac{1}{\Psi} - 0.047\right)^{1.5} \tag{3.70}$$

For initiation of bed-load transport ($\Phi \to 0$), $\Theta_c = 0.047$; and for a high bed-load transport rate ($\Theta >> \Theta_c$), $\Phi = 8/\psi^{1.5}$.

Einstein Equation:

Eq. (3.32) is written for $1/\eta_0 = 2$, $A_* = 43.5$ and $B_* = 1/7$ as

$$1 - \frac{1}{\sqrt{\pi}}\int_{-0.143\Psi-2}^{0.143\Psi-2}\exp(-t^2)dt = \frac{43.5\Phi}{1+43.5\Phi} \tag{3.71}$$

Yalin Equation:

Eq. (3.43) is transformed as

$$\Phi = 0.635\frac{s_1}{\Psi}\left[1 - \frac{1}{a_1 s_1}\ln(1 + a_1 s_1)\right] \tag{3.72}$$

For initiation of bed-load transport $\Theta \to \Theta_c$ (or very small) and $a_1 s_1$ is also small. Hence, one can write

$$\frac{1}{a_1 s_1}\ln(1 + a_1 s_1) \approx 1 - \frac{a_1 s_1}{2} \tag{3.73}$$

The bed-load transport rate equation becomes

$$\Phi = 0.78 s^{0.4}\frac{\Psi_c^{1.5}}{\Psi^{0.5}}\left(\frac{1}{\Psi} - \frac{1}{\Psi_c}\right)^2 \tag{3.74}$$

For a high intensity bed-load transport rate, Θ is large, and $a_1 s_1 \to \infty$. Hence, it one gets

$$\ln(1 + a_1 s_1) \to 0 \tag{3.75}$$

The bed-load transport rate equation becomes

$$\Phi = \frac{0.635}{\Psi^{1.5}}(\Psi_c - \Psi) \tag{3.76}$$

Bagnold Equation:

Eq. (3.57) is transformed as

$$\Phi = \frac{1}{\Psi}\left(\frac{1}{\Psi^{0.5}} - \frac{1}{\Psi_c^{0.5}}\right)\left[\frac{1}{\tan\varphi}\left(5.75\log 30.2\frac{m_1 d}{h} - \frac{w_{ss}}{u_*}\right)\right] \tag{3.77}$$

Engelund and Fredsøe Equation:

Assuming $\mu_d = 0.8$ (as obtained commonly for river sands), Eq. (3.69) can be expressed as

$$\Phi = 11.6\left(\frac{1}{\Psi} - \frac{1}{\Psi_c}\right)\left(\frac{1}{\Psi^{0.5}} - \frac{0.7}{\Psi_c^{0.5}}\right) \tag{3.78}$$

For a high bed-load transport rate $\Theta >> \Theta_c$, $\Phi = 11.6/\psi^{1.5}$.

Comparative Results:

Fig. 3.7 shows a comparison of the equations of Meyer-Peter, Einstein, Yalin and Bagnold. In the Bagnold equation, tanφ is used as 0.63. The Φ-ψ relationships for particle size of 0.2 mm and 2 mm are given and they give similar results. The curve for Bagnold equation is the average of the two cases. In general, Fig. 3.7 shows that for $\psi > 2$, the Meyer-Peter, Einstein, and Bagnold equations are close together, while Yalin equation yields smaller values for the bed-load transport rate. However, Engelund and Fredsøe equation is good for the bed-load near threshold condition.

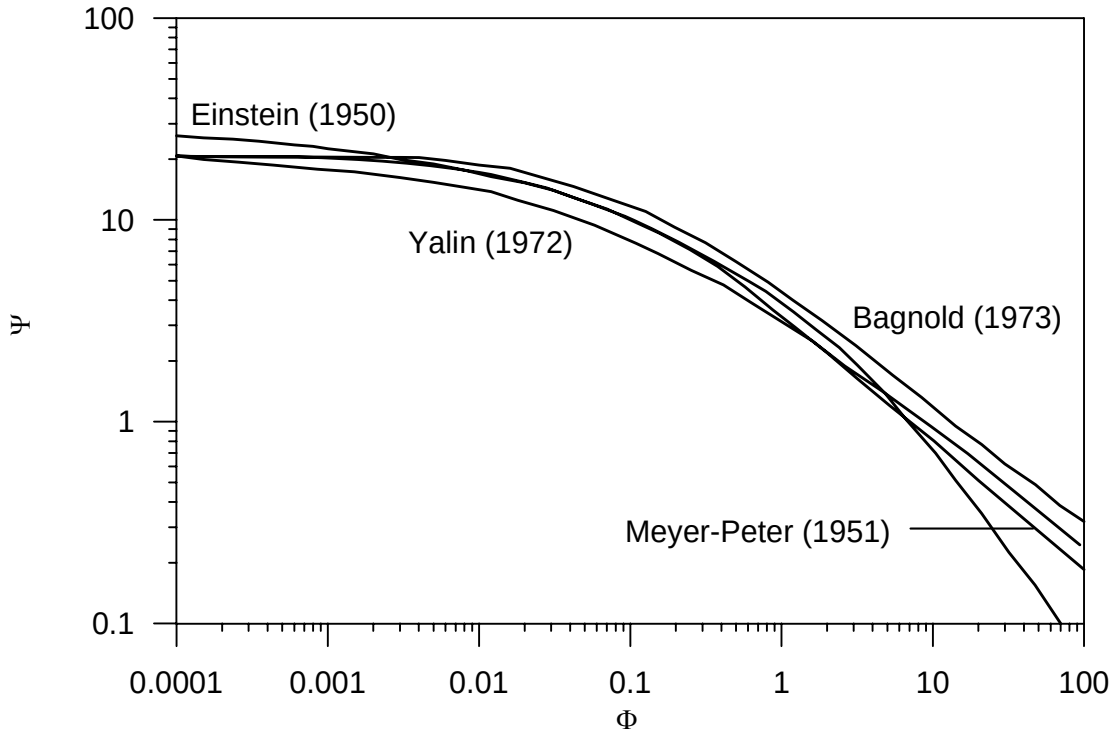

Fig. 3.7 Comparison of the equations of Meyer-Peter, Einstein, Yalin and Bagnold

3.8 Characteristics of Particle Saltations

According to Francis (1973) and Abbott and Francis (1977), the general characteristics of particle saltations is described as follows:

The saltation mode of transport is confined to a layer with a maximum thickness of about ten particle diameters, where the particle motion is dominated by the gravitational forces, although the particle motion may be initiated by the instantaneous turbulent impulses during upward burst of fluid or just by the effect of shear in the sense that a particle in a sheared flow experiences a lift force due to the velocity gradient near the bed. The particles receive their momentum directly from the flow pressure and viscous skin friction. On the rising part of the trajectory, both the vertical component of the fluid drag force and the gravitational force are directed downwards. During the falling part of the trajectory, the vertical component of the fluid drag force opposes the gravitational force. The lift force is always directed upwards as long as the particle velocity lags behind the fluid velocity.

When a particle strikes the bed, it may either impact onto the surface or rebound off the surface particles. During the impact of a particle with the bed, most of its momentum is dissipated by the particles of the bed in a sequence of more or less horizontal impulses that may initiate the rolling mode of transport known as *surface creep*.

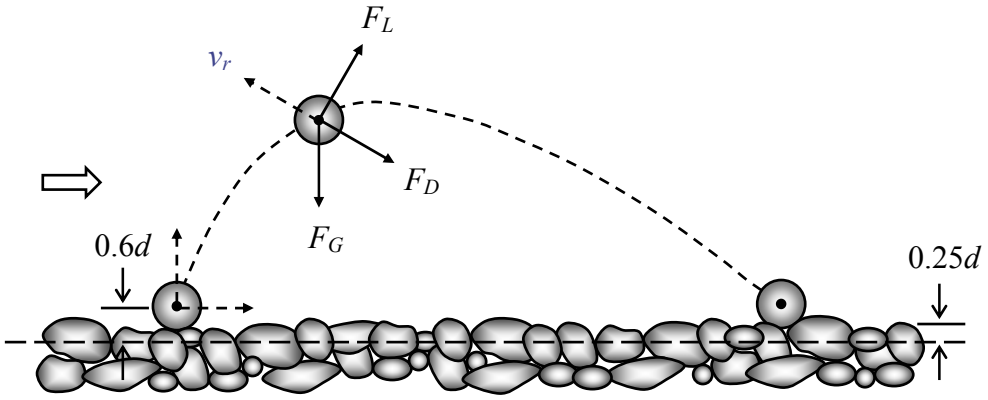

Fig. 3.8 Definition sketch of particle saltation

Equations of Motion:

The forces acting on a saltating particle are shown in Fig. 3.8. The direction of the drag force F_D is opposed to the direction of the particle velocity v_r relative to the flow, while the lift component is in the normal direction. Assuming the spherical particles and the forces due to fluid acceleration are of a second order (Hinze 1975), the equations of motion, according to White and Schultz (1977), can be written as

$$m_a \ddot{x} - F_L\left(\frac{\dot{z}}{v_r}\right) - F_D\left(\frac{u-\dot{x}}{v_r}\right) = 0 \tag{3.79a}$$

$$m_a \ddot{z} - F_L\left(\frac{u-\dot{x}}{v_r}\right) + F_D\left(\frac{\dot{z}}{v_r}\right) + F_G = 0 \tag{3.79b}$$

where m_a = particle mass and added fluid mass; v_r = particle velocity relative to the flow, that is $[(u - \dot{x})^2 + \dot{z}^2]^{0.5}$; u = local flow velocity; $\dot{x}$ and $\dot{z}$ = streamwise and vertical particle velocities, respectively; and $\ddot{x}$ and $\ddot{z}$ = streamwise and vertical particle accelerations, respectively.

The total mass of the spherical particle can be represented by

$$m_a = \frac{1}{6}(\rho_s + \alpha_m \rho)\pi d^3 \tag{3.80}$$

where α_m = added mass coefficient. Assuming potential flow, the added mass α_m of a perfect sphere is exactly equal to the half the mass of the fluid displaced by the sphere. When the flow is separated from the solid sphere, α_m may be different. However, the value of α_m may be considered as 0.5.

The drag force F_D, which is caused by pressure and viscous skin friction, is expressed as

$$F_D = \frac{1}{2} C_D \frac{\pi d^2}{4} \rho v_r^2 \tag{3.81}$$

The drag coefficient C_D can be determined from the empirical expressions given by Morsi and Alexander (1972).

The lift force in a shear flow is caused by the velocity gradient present in the flow (shear flow) and by the spinning motion of the particle (Magnus effect). For a sphere moving in a viscous flow, Saffman (1968) derived the lift due to shear as

$$F_L(\text{shear lift}) = C_L \rho \nu^{0.5} d^2 v_r \left(\frac{\partial u}{\partial z}\right)^{0.5} \tag{3.82}$$

The lift force due to spinning motion in a viscous flow determined by Rubinow and Keller (1961) is given by

$$F_L(\text{Magnus lift}) = C_L \rho d^3 v_r \omega \tag{3.83}$$

where ω = angular velocity of the particle.

The submerged weight of the particle is

$$F_G = \frac{\pi}{6} d^3 \Delta\rho g \tag{3.84}$$

The velocity distribution in flow assumed to follow the logarithmic law is given by

$$u = \frac{u_*}{\kappa} \ln\left(\frac{z}{z_0}\right) \tag{3.85}$$

where κ = von Karman constant (= 0.4); z_0 = zero-velocity level, that is $0.11(\nu/u_*) + 0.03k_s$.

Boundary Conditions and Solution Scheme:

The bed level is assumed at a distance of $0.25d$ below the top level of the bed particles, as shown in Fig. 3.8. The initial position of the particle is $0.6d$ above the bed level. According to the experiments of Francis (1973) and Abbott and Francis (1977), $\dot{x} = \dot{z} = 2u_*$. Eqs. (3.79a) and (3.79b) can be transformed to a system of ordinary simultaneous differential equations of the first order. This system can be solved numerically by means of an automatic step-change differential equation solver.

3.9 References

Abbott, J. E., and Francis, J. R. D. (1977). "Saltation and suspension trajectories of solid grains in a water stream." *Proc. Royal Soc.*, 284A, 225-254.

Bagnold, R. A. (1973). "The nature of saltation and of bed load transport in water." *Proc. Royal Soc.*, 332A, 473-504.

Bagnold, R. A. (1977). "Bed load transport by natural rivers." *Wat. Resour. Res.*, 13(2), 303-312.

Chien, N. (1954). "Meyer-Peter formula for bed load transport and Einstein bed load function." *Missouri River Division Sediment Series No. 7*, Missouri River Division, Corps Engineers.

Chien, N., and Wan, Z. (1999). *Mechanics of sediment transport*. ASCE Press, Virginia, USA.

DuBoys, M. P. (1879). "Le rhone et les rivieres a lit affouillable." *Annales des Ponts et Chaussés*, 18(Series 5), 141-195.

Einstein, H. A. (1950). "The bed-load function for sediment transportation in open channel flows." *Tech. Bulletin No. 1026*, US Department of Agriculture.

Einstein, H. A., and El-Samni, E. A. (1949). "Hydrodynamic forces on rough wall." *Rev. Modern Phys.*, *Am. Inst. of Phys.*, 21(3), 520-524.

Engelund, F., and Fredsøe, J. (1976). "A sediment transport model for straight alluvial channels." *Nordic Hydrol.*, 7, 293-306.

Francis, J. R. D. (1973). "Experiments on the motion of solitary grains along the bed of a water stream." *Proc. Royal Soc.*, 332A, 443-471.

Gilbert, G. K. (1914). "Transportation of debris by running water." *Prof. Paper No. 86*, United States Geological Survey, Washington D.C, USA.

Graf, W. H. (1971). *Hydraulics of sediment transport*. McGraw-Hill, New York, USA.

Hinze, J. O. (1975). *Turbulence*. McGraw-Hill, New York, USA.

Meyer-Peter, E. (1951). "Transport des matières solides en general et problèmes speciaux." *Bulletin Genie Civil d'Hydraul. Fluviale*, Tome V.

Meyer-Peter, E., Favre, H., and Einstein, H. A. (1934). "Neuere versuchsresultate über den geschiebetrieb." *Schweiz. Bauzeitung*, 103(13).

Morsi, S. A., and Alexander, A. J. (1972). "An investigation of particle trajectories in two-phase flow systems." *J. Fluid Mech*., 55, 193-208.

Nielson, P. (1993). "Turbulence effects on the settling of suspended particles." *J. Sediment. Petrol.*, 63, 835-838.

Parker, G. (1979). "Hydraulic geometry of active gravel rivers." *J. Hydraul. Div.*, *Am. Soc. Civ. Eng.*, 105(9), 1185-1201.

Raudkivi, A. J. (1998). *Loose boundary hydraulics*. A. A. Balkama, Rotterdam, The Netherlands.

Rouse, H. (1950). *Engineering hydraulics.* Wiley, New York, USA.

Rubinow, S. I., and Keller, J. B. (1961). "The transverse force on a spinning sphere moving in a viscous fluid." *J. Fluid Mech*., 11, 447-459.

Saffman, P. G. (1968). "Corrigendum, the lift on a small sphere in a slow shear flow." *J. Fluid Mech*., 31, 624.

Schoklitsch, A. (1934). "Geschiebetrieb und geschiebefracht." *Wasserkraft und Wasserwirtschaft*, Jahrgang 39, Heft 4.

Shields, A. (1936). “Application of similarity principles and turbulence research to bed-load movement.” *Mitteilunger der Preussischen Versuchsanstalt für Wasserbau und Schiffbau,* Berlin, Germany, 26, 5-24.

White, B. R., and Schultz, J. C. (1977). “Magnus effect in saltation.” *J. Fluid Mech.*, 81, 497-512.

Yalin, M. S. (1972). *Mechanics of sediment transport*. Pergamon Press, Braunschweig, Germany.

Yang, C. T. (1996). *Sediment transport: theory and practice*. McGraw-Hill Book Companies, Singapore.

Chapter 4

Suspended-Load Transport

4.1 General

Diffusion of turbulent flow results in exchange of both momentum and sediment particles between layers of the flow. If the fall velocity of a sediment particle is small enough, sediment can move in suspension. Therefore, *suspended-load* refers to sediment particles that are supported by the upward component of turbulent flow and stay in suspension for an appreciable period of time. The suspended-load transport rate can be determined as

$$q_s = \int_a^h cudz \tag{4.1a}$$

$$g_s = \rho_s g \int_a^h cudz \tag{4.1b}$$

where q_s = suspended-load transport in volume per unit time and width; g_s = suspended-load transport in weight per unit time and width; u = time-averaged velocity at an elevation z; c = concentration by volume at an elevation z; a = thickness of bed-load transport; h = flow depth; ρ_s = mass density of sediment; and g = gravitational acceleration. A review on suspended-load transport is available in Graf (1971), Yalin (1972), Raudkivi (1998), Yang (1996), Fredsøe and Deigaard (1992) and Chien and Wan (1999).

4.2 Diffusion Theory of Suspension

The solutions developed for molecular diffusion are by analogy important for turbulent diffusion. Analysis of molecular diffusion is based on the continuum hypothesis and Fick's law

$$P = -\varepsilon_m \frac{\partial C}{\partial z} \tag{4.2}$$

where P = rate at which the quantity is transported across unit area normal to z-direction; ε_m = diffusion coefficient; and C = concentration of the quantity transported by diffusion. Introducing the requirement of the conservation of matter, Eq. (4.2) becomes

$$\frac{\partial C}{\partial t} = -\frac{\partial P}{\partial z} = \varepsilon_m \frac{\partial^2 C}{\partial z^2} \tag{4.3}$$

where t = time. Eq. (4.3) has a solution

$$C(z,t) = \frac{B}{t^{0.5}} \exp\left(-\frac{z^2}{4\varepsilon_m t}\right) \tag{4.4}$$

where B = integration constant. In presence of flow, the Fick's law is generalized to $\partial C/\partial t + \nabla\cdot(Cu) = \varepsilon_m \nabla^2 C$, and then for incompressible flow, it becomes $\partial C/\partial t + u\cdot\nabla C = \varepsilon_m \nabla^2 C$ or

$$\frac{\partial C}{\partial t} + u\frac{\partial C}{\partial x} + v\frac{\partial C}{\partial y} + w\frac{\partial C}{\partial z} = \varepsilon_m \frac{\partial^2 C}{\partial x^2} + \varepsilon_m \frac{\partial^2 C}{\partial y^2} + \varepsilon_m \frac{\partial^2 C}{\partial z^2} \tag{4.5}$$

In tensor form, Eq. (4.5) becomes

$$\frac{\partial C}{\partial t} = -u_i \frac{\partial C}{\partial x_i} + \varepsilon_m \frac{\partial^2 C}{\partial x_i \partial x_i} \tag{4.6}$$

where x_i = rectangular coordinate system for i = 1, 2 and 3. Here, ε_m refers to molecular diffusion. For dispersion in a turbulent flow field, $C = \overline{C} + C'$ and $u_i = \overline{u}_i + u_i'$, where $\overline{C}$ and $\overline{u}_i$ = time-averaged concentration and velocity at a given point; and C' and u_i' = fluctuations of C and u_i, respectively. Substituting C and u_i in Eq. (4.6) and using the Reynolds conditions, one obtains

$$\frac{\partial \overline{C}}{\partial t} = -\overline{u}_i \frac{\partial \overline{C}}{\partial x_i} - \frac{\partial}{\partial x_i}(\overline{C'u_i'}) + \varepsilon_m \frac{\partial^2 \overline{C}}{\partial x_i \partial x_i} \tag{4.7}$$

Elder (1959) found it convenient to define a coefficient of turbulent diffusion such that

$$(\varepsilon_t)_{ij} \frac{\partial \overline{C}}{\partial x_j} = -\overline{C'u_i'} \tag{4.8}$$

Under the assumption that molecular and turbulent diffusions are independent and thus additive, one gets

$$\varepsilon_{ij}(x_i) = (\varepsilon_t)_{ij} + \varepsilon_m \tag{4.9}$$

Importantly, in open channel flow, the turbulent diffusivity is usually considerably larger than the molecular one. The bar over a quantity denoting the time-averaged value is no longer required and therefore dropped, and the scalar ε_i replaces ε_{ij} that refers to as the diffusion tensor, by taking the axes of the coordinate system as the principal axes of the diffusion tensor. Introducing these into Eq. (4.7), yields

$$\frac{\partial C}{\partial t} = -u_i \frac{\partial C}{\partial x_i} + \frac{\partial}{\partial x_i}\left(\varepsilon_i \frac{\partial C}{\partial x_i}\right) \tag{4.10}$$

4.2.1 Vertical Distribution of Suspended Particles

The concept of an analogy between the process of mass and momentum transfer in a turbulent flow is known as the *Reynolds analogy.* Considering the transfer of momentum and mass in x_3-direction, one can write

$$\text{Momentum flux} = \rho(\varepsilon_M + \nu)\frac{\partial u_3}{\partial x_3} = \rho\varepsilon_M \frac{\partial u_3}{\partial x_3} \tag{4.11a}$$

$$\text{Mass flux} = (\varepsilon_t + \varepsilon_m)\frac{\partial C}{\partial x_3} = \varepsilon_3 \frac{\partial C}{\partial x_3} \tag{4.11b}$$

where ρ = mass density of fluid; and ν = kinematic viscosity of fluid. Under the assumption that $\varepsilon_M > \nu$ and $\varepsilon_m > \varepsilon_t$, the Reynolds analogy is valid if the mechanisms which control both the mass and momentum transfers are in fact identical. As this is most likely the case, one can use ε_M and ε_3 interchangeable in the x_3-direction, or

$$\varepsilon_M = \varepsilon_3 \tag{4.12}$$

If and only if the solid particles follow the motion of the fluid particles, equality between the diffusivity of fluid mass ε_3 and the diffusivity of suspended solid mass ε_{s3} exists. Therefore, in more generalized way, it is given by

$$\varepsilon_{s3} = \beta\varepsilon_3 \tag{4.13}$$

where β = factor of proportionality. Experimental data revealed that β is approximately unity.

4.2.2 Uniform Turbulence Distribution at Steady-State Condition

For steady condition $\partial C/\partial t = 0$. Assuming sediment concentration (by weight) $C = C(z)$ and ε_s (ε_{s3} replaced by ε_s) being independent of z, Eq. (4.10) can be expressed as:

$$0 = Cw_{ss} + \varepsilon_s \frac{dC}{dz} \tag{4.14}$$

where w_{ss} = settling velocity of the sediment particles.

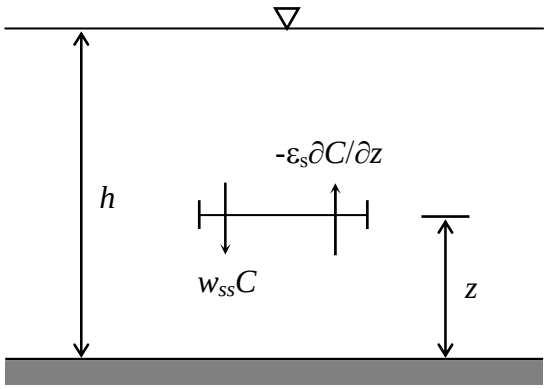

Fig. 4.1 Settling and diffusion of sediment

Eq. (4.14) represents the equilibrium of the sediment suspension that exists by balancing the upward rate of sediment motion due to turbulent diffusion and the downward volumetric rate of sediment transfer per unit area (parallel to the bed) due to gravity (Fig. 4.1). The solution of Eq. (4.14) is

$$\frac{C}{C_a} = \exp\left[-\frac{w_{ss}(z-a)}{\varepsilon_s}\right] \tag{4.15}$$

where C_a = a reference concentration (by weight) at a distance a from the bed.

Note: For high concentration, Eq. (4.14) must be modified to take into account the sediment particles occupy a certain fraction of the total volume. This implies that when a certain volume of sediment $w_{ss}C$ settles through a unit area, this volume is replaced from below by the fluid and sediment. Here, the concentration is also approximately C, so the volume of sediment transported up through the unit area is $C(w_{ss}C)$. Hence, Eq. (4.14) becomes

$$0 = C(1-C)w_{ss} + \varepsilon_s \frac{dC}{dz} \tag{4.16}$$

4.2.3 Nonuniform Turbulence Distribution at Steady-State Condition

Separating the variables, Eq. (4.14) can be rearranged as

$$\frac{dC}{C} + w_{ss}\frac{dz}{\varepsilon_s} = 0 \tag{4.17}$$

In the above equation, the diffusivity of solid particles ε_s is given as a function of z, that is $\varepsilon_s = \varepsilon_s(z)$. Integration of Eq. (4.17) yields

$$C = C_a \exp\left(-w_{ss}\int_a^z \frac{dz}{\varepsilon_s}\right) \tag{4.18}$$

For turbulent flow, the Reynolds stress τ can be expressed as

$$\tau = \varepsilon\rho\frac{du}{dz} \tag{4.19}$$

where ε = kinematic eddy viscosity of fluid or momentum diffusion coefficient of fluid. The Reynolds stress distribution along z is given by

$$\tau = \tau_0\left(1 - \frac{z}{h}\right) \tag{4.20}$$

where τ_0 = bed shear stress. Assuming that the logarithmic velocity distribution is valid, one can write

$$\frac{du}{dz} = \frac{u_*}{\kappa z} \tag{4.21}$$

where u_* = shear velocity; and κ = von Karman constant (= 0.4). From Eq. (4.19) – (4.21), one gets

$$\varepsilon_z = \kappa u_*(h - z)\frac{z}{h} \tag{4.22}$$

Eq. (4.13) suggests that

$$\varepsilon_s = \beta\kappa u_*(h - z)\frac{z}{h} \tag{4.23}$$

Experimental data showed that $\beta \approx 1$. Therefore, inserting ε_s from Eq. (4.23) to Eq. (4.18) and performing the integration, yields

$$\frac{C}{C_a} = \left(\frac{h - z}{z}\cdot\frac{a}{h - a}\right)^{\zeta} \tag{4.24}$$

where $\zeta = w_{ss}/(\kappa u_*)$. This equation of concentration distribution was introduced by Rouse (1937). It can be used to calculate the concentration of a given settling velocity w_{ss} of the sediment size at any distance z from the bed if a reference concentration C_a at a distance a is known. Therefore, the suspended-load transport rate of sediment is given by

$$g_s = \int_a^h Cu\,dz \tag{4.25}$$

The vertical distribution of suspended sediment concentration according to Eq. (4.24) is presented in Fig. 4.2, where experimental data of Vanoni (1946) are used for the validation. It should be noted that the concentration C decreases with the distance from the bed. Mathematically, at the bed ($z = 0$), the concentration C becomes infinity breaking down Eq. (4.24). Einstein et al. (1940) suggested that the suspension is not possible in the so-called *bed-layer*, which has a thickness of two-particle diameters. For low values of ζ, the sediment

distribution is nearly uniform, while for large values of ζ, little sediment is found at the free surface. The particle size, expressed as the settling velocity w_{ss}, is directly responsible for the kind of distribution.

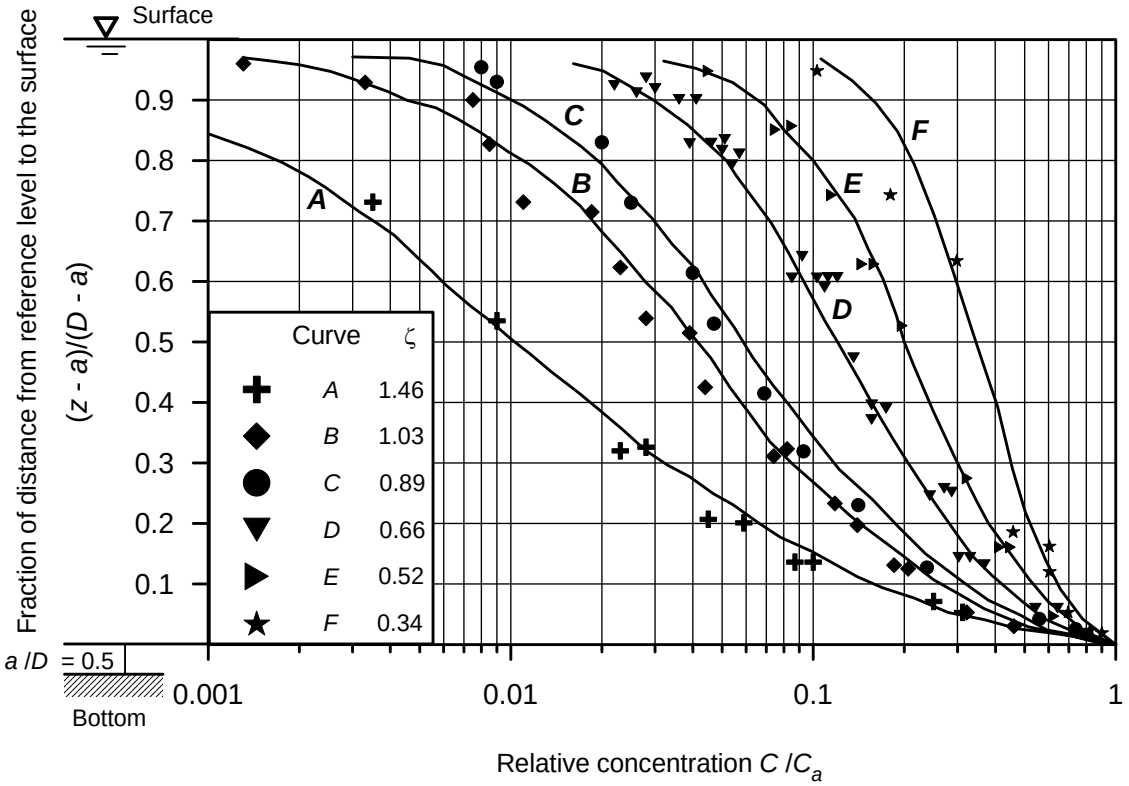

Fig. 4.2 Vertical distribution of suspended sediment concentration

Estimation of C_a:

The depth a and concentration C_a in Eq. (4.24) are called as *reference elevation* and *reference sediment concentration*, respectively. The reference elevation a is the boundary between the bed-load and the suspended-load. Bijker (1971) suggests that a is taken as the bed roughness k_s and relates C_a to the bed-load transport q_b. It is assumed that bed-load transport takes place in the bed-load layer from $z = 0$ to $z = a = k_s$, and in this layer, there is a constant sediment concentration C_a. He argues that in hydraulically rough flow there is still a viscous sub-layer, which starts from $z = 0$ to $z = z_\delta$ where the linear velocity distribution is tangent with the logarithmic velocity distribution. Note the thickness of the viscous sub-layer is much smaller than that in hydraulically smooth flow. He estimated the depth-averaged velocity $\overline{u}_a$ up to depth $z = a$ (= k_s) as $\overline{u}_a \approx 6.34u_*$. Given bed-load $q_b = C_a \overline{u}_a k_s$, the sediment concentration C_a is estimated as $C_a = q_b/(6.34u_* k_s)$.

4.2.4 Sediment Concentration at Free Surface

According to Eq. (4.24), the sediment concentration C at the free surface $z = h$ is zero. However, this result does not agree with the observations of natural rivers. The diffusivity of fluid (or momentum exchange coefficient) ε_z is zero at free surface, but the diffusivity of sediment (or sediment exchange coefficient) ε_s is finite there. For momentum exchange, the relationship of the Reynolds stress $\tau = \rho \overline{u'w'}$ holds, and it shows that the stress τ is generated by the momentum exchange only at the position where u' and w' have certain degree of

correlation that is given by $\overline{u'w'}/(\sqrt{u'u'}\sqrt{w'w'})$. In contrast, sediment suspension depends primarily on w', which is much less than u'. Hence, even if u' and w' are not correlated, sediment can still be transported. Therefore, although the momentum exchange coefficient ε_z is zero at $z = h$, sediment exchange can take place and can produce some sediment at that level. Importantly, at the free surface the logarithmic law of velocity distribution does not hold. Instead the following equation makes possible to estimate the velocity near the free surface

$$\frac{u_{\max} - u}{u_*} = \frac{2}{\kappa}\operatorname{arctanh}\left(\frac{h-z}{h}\right)^{1.5} \tag{4.26}$$

where $u_{\max}$ = maximum value of u which occurs at $z = h$. The mixing length l and the momentum exchange coefficient ε_z are then as follows:

$$l = \frac{\kappa}{3}h\left[1-\left(\frac{h-z}{h}\right)^3\right] \tag{4.27}$$

$$\varepsilon_z = \frac{\kappa}{3}u_* h\sqrt{\frac{h-z}{h}}\left[1-\left(\frac{h-z}{h}\right)^3\right] \tag{4.28}$$

Remembering the relationship $\varepsilon_s = \beta\varepsilon_z$, the differential equation of the vertical distribution of sediment concentration is obtained as

$$Cw_{ss} + \beta\frac{\kappa}{3}u_* h\sqrt{\frac{h-z}{h}}\left[1-\left(\frac{h-z}{h}\right)^3\right]\frac{dC}{dz} = 0 \tag{4.29}$$

The solution of Eq. (4.29) is

$$\frac{C}{C_a} = \exp(\zeta_\beta \Omega) \tag{4.30}$$

where $\zeta_\beta = w_{ss}/(\beta\kappa u_*)$; and

$$\Omega = 0.5\ln\frac{\left[\left(\frac{h-z}{h}\right)^{0.75}+1\right]\left[\left(\frac{h-z}{h}\right)^{0.5}-1\right]^3}{\left[\left(\frac{h-z}{h}\right)^{1.5}-1\right]\left[\left(\frac{h-z}{h}\right)^{0.5}+1\right]^3} + \sqrt{3}\arctan\left[-\frac{h}{z}\sqrt{\frac{3(h-z)}{h}}\right]_{z=a}^{z} \tag{4.31}$$

4.2.5 Influence of Sediment Suspension on Velocity and Resulting Concentration

4.2.5.1 Velocity Distribution

Einstein and Chien (1955) modified the traditional logarithmic law of the velocity distribution due to the influence of sediment suspension. They divided the sediment-laden flow into two zones. The zone close to the bed, where the sediment concentration is high, referred to as *heavy-fluid zone*. The remaining portion of the flow, where the sediment concentration is relative low, has no change of fluid mass density and is called as *light-fluid zone*. The heavy-fluid zone is relatively shallow than the light fluid zone. Turbulence is created at the boundary, the heavy-fluid zone acts as a filter, and it reduces the turbulence level because the energy is spent to suspend the sediment particles in this zone.

The clear-water flow follows the logarithmic law of velocity distribution, that is

$$\frac{u}{u_*} = \frac{2.3}{\kappa} \ln\left(30.2 \frac{z}{k_s} \right) \tag{4.32}$$

where κ = von Karmans constant; and k_s = equivalent sand roughness of Nikuradse. Eq. (4.32) was derived by assuming that the turbulent or Reynolds stress is

$$\tau = \rho \varepsilon_z \frac{du}{dz} \tag{4.33}$$

In sediment-laden flow, a more reasonable velocity distribution can be obtained by the inclusion of the participation of solid particles in the exchange mechanism. Einstein and Chien (1955) derived the following relationship:

$$\tau = \left(1 + \frac{\rho_s - \rho}{\rho} C \right) \rho \varepsilon_z \frac{du}{dz} \tag{4.34}$$

Within the light-fluid zone of the small concentration, Eq. (4.34) becomes Eq. (4.33). Under these circumstances an equation similar to the clear-water equation, that is Eq. (4.32), but with different numerical constants, might be expected to apply. Experiments suggested the following relationship:

$$\frac{u}{u_*} = 17.66 + \frac{2.3}{\kappa} \ln\left(\frac{z}{35.45 k_s} \right) \tag{4.35}$$

Experiments revealed that close to the bed, whenever the local sediment concentration reaches a value of 981 N/m^3 or relative flow depth $z/h < 0.1$, Eq. (4.35) fails. In this case, the shear stress given by Eq. (4.34) can be approximated by the bed shear stress τ_0 as

$$\tau_0 = \int_0^h [\rho + (\rho_s - \rho) C] g S \, dz \tag{4.36}$$

where S = energy slope. The velocity distribution is thus obtained as

$$\frac{u}{u_*} = \frac{2.3}{\kappa} \cdot \frac{\sqrt{1 + \frac{\rho_s - \rho}{\rho} \cdot \frac{1}{h} \int_0^h C dz}}{\sqrt{1 + \frac{\rho_s - \rho}{\rho} C_a}} \ln\left(A_e \frac{z}{k_s} \right) \tag{4.37}$$

where C_a = sediment concentration at the surface of the bed layer; and A_e = constant to be determined. However, the depth-averaged velocity U can be obtained from Eq. (4.35) without introducing any significant error as

$$\frac{U}{u_*} = 17.66 + \frac{2.3}{\kappa} \ln\left(\frac{h}{96.5 k_s} \right) \tag{4.38}$$

4.2.5.2 Sediment Distribution

Without lacking of generality, Eq. (4.5) can be written as

$$\frac{\partial C}{\partial t} = -u_i \frac{\partial C}{\partial x_i} - C \frac{\partial u_i}{\partial x_i} + \frac{\partial}{\partial x_i} \left(\varepsilon_i \frac{\partial C}{\partial x_i} \right) \tag{4.39}$$

For the special case of uniform flow in x_1-direction and the concentration being constant with time, the variation in $x_3 = z$ component are considered for which $u_3 = w$, thus Eq. (4.39) reduces to

$$0 = -w\frac{\partial C}{\partial z} - C\frac{\partial w}{\partial z} + \frac{\partial}{\partial z}\left(\varepsilon_z \frac{\partial C}{\partial z}\right) \tag{4.40}$$

The rate of change of suspended matter is given by

$$0 = -w_s \frac{\partial C}{\partial z} - C\frac{\partial w_s}{\partial z} + \frac{\partial}{\partial z}\left(\varepsilon_s \frac{\partial C}{\partial z}\right) \tag{4.41}$$

where w_s = velocity of solid particle in z-direction. Similarly, for the fluid by

$$0 = -w\frac{\partial C}{\partial z} - (1-C)\frac{\partial w}{\partial z} + \frac{\partial}{\partial z}\left(\varepsilon_z \frac{\partial C}{\partial z}\right) \tag{4.42}$$

The velocity relationship can be given by

$$w_s = w - w_{ss} \tag{4.43}$$

By eliminating w_s and w from Eqs. (4.41) and (4.42), one obtains

$$[\varepsilon_s + C(\varepsilon_z - \varepsilon_s)]\frac{\partial C}{\partial z} + (1-C)Cw_{ss} = 0 \tag{4.44}$$

where ε_s and ε_z = diffusivity of solid and fluid matters, respectively. To simplify the solution, the diffusion coefficients of solid and fluid matters are assumed same, that is $\varepsilon_s = \varepsilon_z$; and thus one gets

$$\varepsilon_s \frac{dC}{dz} + (1-C)Cw_{ss} = 0 \tag{4.45}$$

The solution of Eq. (4.45) is as follows

$$\left(\frac{C}{1-C}\right)\left(\frac{1-C_a}{C_a}\right) = \left(\sqrt{\frac{1-z/h}{1-a/h}} \cdot \frac{B_s - \sqrt{1-a/h}}{B_s - \sqrt{1-y/h}}\right)^{\zeta_0} \tag{4.46}$$

where $\zeta_0 = w_{ss}/(\kappa_s B_s u_*)$; B_s = constant of integration in the velocity distribution law ($B_s \le 1$); and κ_s = constant similar to the von Karman constant.

For large sediment concentration, Eq. (4.45) should be used. If the diffusivity of solid matter is given by Eq. (4.46), one obtain

$$\frac{dC}{dz} + \left(1 + \frac{\rho_s - \rho}{\rho}C\right)(1-C)Cw_{ss}\frac{\rho}{\tau}\cdot\frac{du}{dz} = 0 \tag{4.47}$$

For small sediment concentration, as encountered in the light-fluid zone, Eq. (4.45) reduces to

$$\varepsilon_s \frac{dC}{dz} + Cw_{ss} = 0 \tag{4.48}$$

4.2.6 Suspended-Load by Diffusion Theory

4.2.6.1 Lane and Kalinske's Approach

Lane and Kalinske (1941) assumed $\varepsilon_s = \varepsilon_z$ and $\beta = 1$, Eq. (4.23) becomes

$$\varepsilon_s = \kappa u_* (h - z)\frac{z}{h} \tag{4.49}$$

The average value of ε_s along z is given by

$$\bar{\varepsilon}_s = \frac{1}{h}\int_0^h \varepsilon_s dz = \frac{\kappa u_*}{h^2}\int_0^h (h - z) z dz \tag{4.50}$$

Performing the integration of Eq. (4.50) and using the von Karman constant $\kappa = 0.41$, yields

$$\bar{\varepsilon}_s = \frac{1}{15} u_* h \tag{4.51}$$

Introducing Eq. (4.51) into Eq. (4.15), one obtains

$$\frac{C}{C_a} = \exp\left[-\frac{15 w_{ss}}{u_*}\left(\frac{z - a}{h}\right)\right] \tag{4.52}$$

The suspended-load (by weight) per unit time and width is given by

$$g_s = \int_0^h C u dz \tag{4.53}$$

Using Eq. (4.52) into Eq. (4.53), the following equation of suspended-load was suggested

$$g_s = q C_a P_L \exp\left(\frac{15 w_{ss} a}{u_* h}\right) \tag{4.54}$$

where q = flow discharge per unit width; and P_L = function of w_{ss}/u_* and relative roughness $n/h^{1/6}$, given in Fig. 4.3, where n = Manning roughness coefficient.

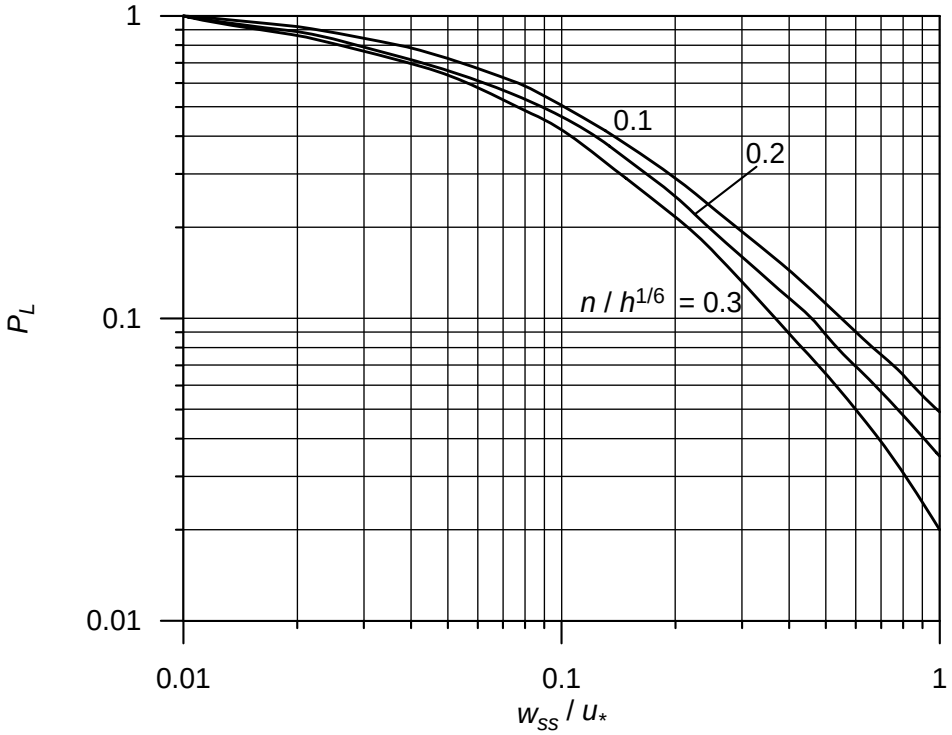

Fig. 4.3 Relationship of P_L after Lane and Kalinske (1941)

4.2.6.2 Einstein's Approach

Einstein (1950) assumed that $\beta = 1$ and $\kappa = 0.4$. Replacing the shear velocity u_* with the shear velocity due to grain roughness u'_*, yields

$$\zeta_\beta = \zeta = \frac{w_{ss}}{0.4u'_*} \tag{4.55}$$

The velocity can be expressed as

$$\frac{u}{u'_*} = 5.75\log\left(30.2\frac{z}{\Delta_k}\right) \tag{4.56}$$

where $\Delta_k = k_s/x = d_{65}/x$; and x = correction factor (see Fig. 3.3).

Substituting Eqs. (4.24) and (4.56) into Eq. (4.25), yields

$$g_s = \int_a^h C_a\left(\frac{h-z}{z}\cdot\frac{a}{h-a}\right)^\zeta 5.75u'_*\log\left(30.2\frac{z}{\Delta_k}\right)dz \tag{4.57}$$

Replacing a with $E = a/h$ and z with $z' = z/h$, one gets

$$g_s = \int_E^1 Cuhdz' = hu'_*C_a\left(\frac{E}{1-E}\right)^\zeta 5.75\int_E^1\left(\frac{1-z}{z}\right)^\zeta \log\left(\frac{30.2z}{\Delta_k/h}\right)dz \tag{4.58}$$

After simplification, Eq. (4.58) becomes

$$g_s = 5.75C_au'_*h\left(\frac{E}{1-E}\right)^\zeta\left[\log\left(\frac{30.2z}{\Delta_k}\right)\int_E^1\left(\frac{1-z}{z}\right)^\zeta dz + 0.434\int_E^1\left(\frac{1-z}{z}\right)^\zeta \ln z\, dz\right] \tag{4.59}$$

As the closed-form integration of Eq. (4.59) is impossible, Einstein (1950) expressed it as

$$g_s = 11.6C_au'_*a\left[2.3\log\left(\frac{30.2h}{\Delta_k}\right)I_1 + I_2\right] \tag{4.60}$$

where

$$I_1 = 0.216\frac{E^{\zeta-1}}{(1-E)^\zeta}\int_E^1\left(\frac{1-z}{z}\right)^\zeta dz \tag{4.61a}$$

$$I_2 = 0.216\frac{E^{\zeta-1}}{(1-E)^\zeta}\int_E^1\left(\frac{1-z}{z}\right)^\zeta \ln z\, dz \tag{4.61b}$$

The values of I_1 and I_2 were given by Einstein in graphical form in terms of E and ζ.

The flow layer right on the top of the bed, in which suspension becomes impossible, was designated by Einstein (1950) as the *bed layer*, and was found to be a thickness of $a = 2d$. The sediment within the bed layer becomes the source of the suspended-load, and then important determination of the reference concentration C_a might thus be obtained.

From the bed-load theory, the bed-load transport rate of a given size fraction i_b is i_bg_b. If the velocity with which the bed-load moves is u_b, then the weight of the particles of a given particle size per unit area is i_bg_b/u_b. The average concentration in the layer is given by

$$C_a = A_s \frac{i_b g_b}{a u_b} \tag{4.62}$$

where A_s = a correction factor (= 1/11.6). The average bed-load velocity u_b was assumed to be proportional to the shear velocity due to grain roughness u'_*. Thus, Eq. (4.62) becomes

$$C_a = \frac{1}{11.6} \cdot \frac{i_b g_b}{a u'_*} \tag{4.63}$$

The suspended-load equation for each fraction, where a bed-load function exists, is given by

$$i_s g_s = i_b g_b \left[2.3 \log\left(\frac{30.2h}{\Delta_k} \right) I_1 + I_2 \right] = i_b g_b (P_E I_1 + I_2) \tag{4.64}$$

where i_s = size fraction in suspension; and P_E = transport parameter [= $2.303\log(30.2h/\Delta_k)$].

4.2.6.3 Brook's Approach

Brooks (1963) assumed that the logarithmic velocity distribution is applicable and sediment concentration follows Eq. (4.24). He obtained

$$g_s = C_{0.5h} q \left[1 + \frac{u_*}{\kappa U} \int_E^1 \left(\frac{1-z}{z} \right)^{\zeta_\beta} dz + \frac{u_*}{\kappa U} \int_E^1 \left(\frac{1-z}{z} \right)^{\zeta_\beta} \ln z \, dz \right] \tag{4.65}$$

where q = flow discharge per unit width; and $C_{0.5h}$ = reference sediment concentration at y = 0.5h. Eq. (4.65) can be expressed in terms of a transport function T_B as

$$\frac{g_s}{q C_{0.5h}} = T_B \left(\frac{\kappa U}{u_*}, \zeta_\beta, E \right) \tag{4.66}$$

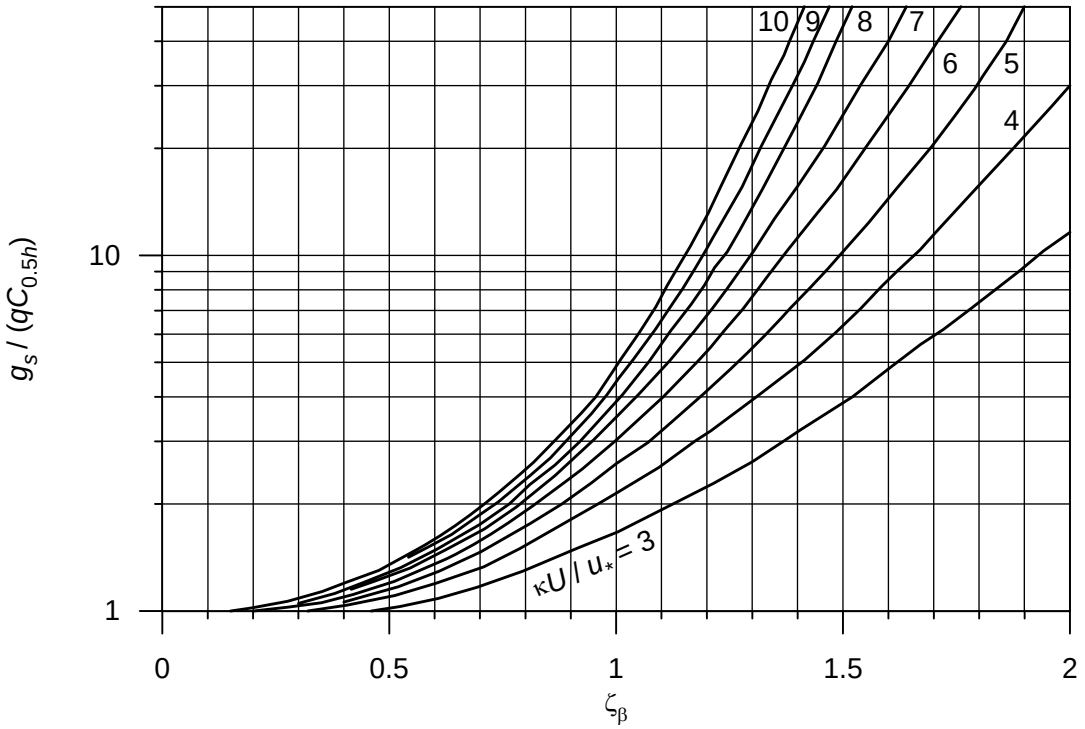

Fig. 4.4 Brook's (1963) suspended-load transport function

Taking a lower limit of integration at $u = 0$, the nondimensional reference elevation E becomes

$$E = \exp\left(-\frac{\kappa U}{u_*} - 1\right) \tag{4.67}$$

Eq. (4.66) reduces to

$$\frac{g_s}{qC_{0.5h}} = T_B\left(\frac{\kappa U}{u_*}, \zeta_\beta\right) \tag{4.68}$$

The application of this relationship is illustrated by Fig. 4.4.

4.2.6.4 Chang et al.'s Approach

Chang et al. (1965) assumed that Eq. (4.23) holds good and is written as

$$\varepsilon_s = \beta\kappa u_* h\xi(1-\xi)^{0.5} \tag{4.69}$$

where $\xi = z/h$; and $u_* = (ghS)^{0.5}$. Substituting Eq. (5.69) into Eq. (4.18), yields

$$\frac{C}{C_a} = A_1\left[\frac{\xi^{0.5}}{1-(1-\xi)^{0.5}}\right]^{\zeta_\xi} \tag{4.70}$$

In the above

$$A_1 = \left[\frac{1-(1-E)^{0.5}}{E^{0.5}}\right]^{\zeta_\xi} \tag{4.71}$$

where $\zeta_\xi = 2w_{ss}/(\beta\kappa u_*)$. The equation of suspended-load becomes

$$g_s = \int_a^h Cudz = C_a h\left(UI_3 - \frac{2u_*}{\kappa} I_4\right) \tag{4.72}$$

where I_3 and I_4 = integrals that can be given as

$$I_3 = \left[\frac{1-(1-E)^{0.5}}{E^{0.5}}\right]^{\zeta_\xi} \int_E^1 \left[\frac{\xi^{0.5}}{1-(1-\xi)^{0.5}}\right]^{\zeta_\xi} d\xi \tag{4.73a}$$

$$I_4 = \left[\frac{1-(1-E)^{0.5}}{E^{0.5}}\right]^{\zeta_\xi} \int_E^1 \left(\frac{\xi}{1-\xi}\right)^{\zeta_\xi} \left\{\ln\left[\frac{\xi^{0.5}}{1-(1-\xi)^{0.5}}\right] - (1-\xi)^{0.5} - \frac{1}{3}\right\}^{\zeta_\xi} d\xi \tag{4.73b}$$

Similar to Einstein's approach, Eq. (4.72) can be reduced to

$$g_s = \frac{h}{0.8aU}\left(UI_3 - \frac{2u_*}{\kappa} I_4\right) g_b \tag{4.74}$$

It was assumed that the velocity of the bed sediment $u_b = 0.8U$ and the thickness of the bed layer is based on DuBoys' (1879) assumption, that is

$$a = j\frac{\tau_0 - \tau_c}{(1-\rho_0)(\rho-\rho_s)g\tan\varphi} \tag{4.75}$$

where j = experimental constant (= 10); ρ_0 = porosity of sediment; τ_c = critical bed shear stress of sediment; and φ = angle of repose.

4.3 Gravitational Theory of Suspension

4.3.1 Velikanov's Theory

Velikanov (1958) proposed the gravitational theory for the vertical distribution of sediment suspension applying principle of energy conservation. He considered a unit volume of a mixture of fluid and sediment that flows from a higher position to a lower position in a unit time interval. Let E_1 and E_2 refer to the amount of energy supplied by the fluid and sediment phases, respectively; E_3 and E_4 denote the energy lost in the fluid and sediment phases to overcome frictional resistance, respectively; and E_5 stands for the amount of energy needed to maintain the suspension.

Velikanov expressed the energy balance equations as: $E_1 = E_3 + E_5$ for fluid phase; and $E_2 = E_4$ for sediment phase. For two-dimensional uniform flow, the energy terms are

$$E_1 = \rho g(1-\overline{C})\overline{u}S \tag{4.76}$$

$$E_2 = \rho_s g\overline{C}\,\overline{u}S \tag{4.77}$$

$$E_3 = -\overline{u}\frac{d\tau}{dz} = \rho\overline{u}\frac{d}{dz}[(1-\overline{C})\overline{u'w'}] \tag{4.78}$$

$$E_4 = \rho_s\overline{u}\frac{d}{dz}(\overline{C}\,\overline{u'w'}) \tag{4.79}$$

$$E_5 = (\rho_s - \rho)g(1-\overline{C})\overline{C}w_{ss} \tag{4.80}$$

where w_{ss} = fall velocity of a sediment particle in still fluid of infinite extent. In the above equations, over-bar denotes the time-averaged of a quantity. Velikanov assumed the fall velocity of a sediment particle in flowing fluid being $\overline{w} - w_{ss}$. The continuity equation for sediment passing through a unit area located at a distance z from the bed is

$$\overline{C(w-w_{ss})} = 0 \tag{4.81}$$

and the continuity equation for fluid is

$$\overline{w(1-C)} = 0 \tag{4.82}$$

If the instantaneous value is expressed as the sum of the time-averaged and the fluctuation values, the results are as follows:

$$\overline{w}\,\overline{C} - \overline{C}w_{ss} + \overline{w'C'} = 0 \tag{4.83}$$

$$\overline{w} - \overline{C}\,\overline{w} + \overline{w'C'} = 0 \tag{4.84}$$

Adding Eqs. (4.83) and (4.84) yields

$$\overline{w} = \overline{C}w_{ss} \tag{4.85}$$

It indicates that $\overline{w}$ becomes zero only for the low concentration of fine particles. Hence, in Eq. (4.80), $(1 - \overline{C})w_{ss}$ was used rather than w_{ss} to express E_5. Substituting the related energy terms into the energy balance equations, yield

$$g(1-\overline{C})\overline{u}S = \overline{u}\frac{d}{dz}[(1-\overline{C})\overline{u'w'}] + \Delta g(1-\overline{C})\overline{C}w_{ss} \tag{4.86}$$

$$g\overline{C}S = \frac{d}{dz}(\overline{C}\,\overline{u'w'}) \tag{4.87}$$

where $\Delta = s - 1$; and s = relative density of sediment particles, that is ρ_s/ρ. In Eqs. (4.86) and (4.87), $\overline{C}$, $\overline{u}$ and $\overline{u'w'}$ are unknown terms, so that an additional condition is required to solve them.

Velikanov suggested the logarithmic law of velocity distribution as

$$\overline{u} = \frac{u_*}{\kappa}\ln\left(1+\frac{z}{\Delta_v}\right) = \frac{(ghS)^{0.5}}{\kappa}\ln\left(1+\frac{\xi}{\alpha}\right) \tag{4.88}$$

where Δ_v = parameter depending on the bed roughness; and $\alpha = \Delta_v/h$. Dividing Eq. (4.86) by $\overline{u}$ and adding it to Eq. (4.87), one can express the integral form of the resulting equation as

$$\int_z^h gS\,dz = \int_z^h \frac{d}{dz}\overline{u'w'}\,dz + \Delta g w_{ss}\int_z^h \frac{(1-\overline{C})\overline{C}}{\overline{u}}\,dz \tag{4.89}$$

Thus, the following expression is obtained as

$$-gS(h-z) = \overline{u'w'} + \Delta g w_{ss}\int_z^h \frac{(1-\overline{C})\overline{C}}{\overline{u}}\,dz \tag{4.90}$$

The second term of the RHS is much smaller than the first term and can be neglected. The equation is then simplified to

$$\overline{u'w'} = -gS(h-z) \Rightarrow \frac{d\overline{u'w'}}{dz} = gS \tag{4.91}$$

For small concentration, $1 - \overline{C} = 1$ and the substitution of Eqs. (4.88) and (4.91) into Eq. (4.86) yields the differential equation for concentration distribution as

$$\frac{dC}{C} = \beta_v \frac{d\xi}{(1-\xi)\ln[1+(\xi/\alpha)]} \tag{4.92}$$

where $\beta_v = \Delta\kappa w_{ss}/[S(ghS)^{0.5}]$. Thus, the vertical distribution of sediment concentration is obtained from Eq. (4.92) as

$$\frac{C}{C_\alpha} = \exp(-\beta_v\zeta_v) \tag{4.93}$$

where

$$\zeta_v = \int_\alpha^\xi \frac{d\xi}{(1-\xi)\ln[1+(\xi/\alpha)]} \tag{4.94}$$

The most serious shortcoming of the gravitational theory is that the energy balance equation is not scientifically sound. In reality, the energy for suspension E_5 comes from the energy of turbulence, those functions as the energy loss of the flow in order to overcome resistance. Hence, in energy balance equation, that part of the dissipated energy should not be taken into account two times.

4.3.2 Suspended-Load by Gravitational Theory

4.3.2.1 Velikanov's Approach

Velikanov (1958) assumed the sediment concentration is small, that is $1 - \overline{C} = 1$, and integrated Eq. (8.86) over the flow depth as

$$\int_0^h g\bar{u}Sdz = \int_0^h \bar{u}\frac{d}{dz}\overline{u'w'}dz + \int_0^h \Delta g\overline{C}w_{ss}dz \tag{4.95}$$

In the above, $-\overline{u'w'} = \tau/\rho$. Since $\tau \sim U^2$, one gets

$$\int_0^h \bar{u}\frac{d}{dz}\overline{u'w'}dz = bU^3 \tag{4.96}$$

Therefore, Eq. (4.95) is integrated, simplified using Eq. (4.96) and rearranged to

$$\frac{b}{\lambda} + \Delta\frac{\overline{C}_{av}w_{ss}}{US} = 1 \tag{4.97}$$

where $\lambda = ghS/U^2$; and $\overline{C}_{av}$ = depth-averaged concentration. For clear-water flow, $\overline{C}_{av} = 0$, and from Eq. (4.97), one can write

$$b = \lambda_0 \tag{4.98}$$

Importantly, under certain flow conditions, the sediment concentration may reach the state of saturation, which may refer to the maximum sediment carrying capacity of the flow. In this case, one obtains

$$\lambda = \lambda_k \tag{4.99}$$

In the following, the value of the ratio λ_0/λ_k is approximately taken as constant. Substituting this ratio into Eq. (4.97) yields

$$\Delta\frac{\overline{C}_{av}w_{ss}}{US} = 1 - \frac{\lambda_0}{\lambda_k} \tag{4.100}$$

Here, $\overline{C}_{av}$ is considered to be saturated depth-averaged concentration. The depth-averaged velocity can be given by

$$U = \frac{1}{h}\int_0^h \bar{u}dz = \frac{1}{h}\int_0^h \frac{(ghS)^{0.5}}{\kappa}\ln\left(1 + \frac{z}{\Delta_v}\right)dz = c_1\frac{(ghS)^{0.5}}{\kappa} \tag{4.101}$$

where $c_1 = (1+\alpha)[\ln(1+\alpha) - 1] = f(\alpha)$. Substituting Eq. (4.101) into Eq. (4.100), yields

$$\Delta\frac{\kappa\overline{C}_{av}w_{ss}}{c_1S(ghS)^{0.5}} = 1 - \frac{\lambda_0}{\lambda_k} \tag{4.102}$$

The above equation is therefore given by $\beta_v\overline{C}_{av}/c_1 = 1 - \lambda_0/\lambda_k$ = constant. Hence, one can write

$$\overline{C}_{av} \sim \frac{c_1}{\beta_v} = \frac{\kappa^2U^3}{\Delta f^2(\alpha)ghw_{ss}} \tag{4.103}$$

The general form of the above equation is

$$\overline{C}_{av} = K\frac{U^3}{ghw_{ss}} \tag{4.104}$$

where K = constant to be determined experimentally. Researchers of the Wuhan Institute of Hydraulic and Electric Engineering (WIHEE 1981) made an extensive analysis of field data collected form different rivers and canals and concluded that Eq. (4.104) should be modified as

$$\overline{C}_{av} = K\left(\frac{U^3}{ghw_{ss}}\right)^{m_1} \tag{4.105}$$

The values of K (in kg/m^3) and m_1 are functions of $U^3/(ghw_{ss})$, as shown in Fig. 4.5.

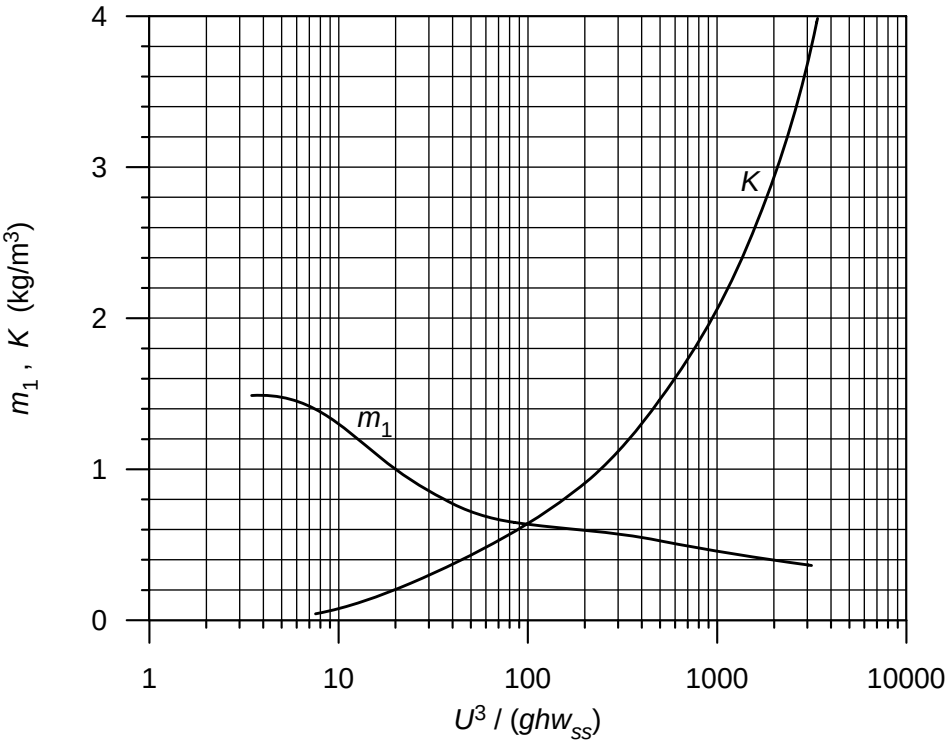

Fig. 4.5 Variations of K (in kg/m^3) and m_1 with $U^3/(ghw_{ss})$

4.4 Bagnold's Model for Suspended-load Transport

Bagnold (1966) investigated the suspended-load transport rate using the same method that he used for the bed-load transport.

In fluid, the sediment particles are known to settle with a fall velocity w_{ss}, but the centroid of the entire suspended-load can still be maintained at a certain elevation. Thus, the flow must continuously lift sediment with an upward velocity equal to w_{ss}. In the fluid column above a unit bed area, the work done (per unit time) by the turbulence to suspended sediment is equal to $W_S w_{ss}$, where W_S is the total submerged weight of suspended sediment in the column. The rate of suspended sediment load g_{ss} (in submerged weight) can be expressed as

$$g_{ss} = W_S \overline{u}_s \tag{4.106}$$

where $\overline{u}_s$ = depth-averaged velocity of the suspended-load.

The turbulent energy required to maintain the suspended sediment actually comes from the potential energy of the flow. Hence, a relationship should exist between the energy required for sediment suspension and the potential energy loss. Thus, the amount of flow potential

energy used to sustain the bed-load motion equaling the work done for sediment suspension can be expressed as

$$W_S w_{ss} = \tau_0 U(1-e_b)e_s \tag{4.107}$$

where e_b and e_s = efficiencies for bed-load and suspended-load transport, respectively. Combining Eqs. (4.106) and (4.107), one can obtain

$$g_{ss} = \tau_0 U \frac{\bar{u}_s}{w_{ss}}(1-e_b)e_s \tag{4.108}$$

Since suspended sediments move with the same velocity as the flow, one can write

$$\bar{u}_s = \frac{1}{h-a}\int_a^h Cudz \tag{4.109}$$

In the above, a refers to the lower boundary of the suspension zone to the bed. Since the velocity increases and the sediment concentration decreases with z, $\bar{u}_s$ is generally smaller than depth-averaged velocity U. If $r = \bar{u}_s/U < 1$, then Eq. (4.108) can be written as

$$g_{ss} = \tau_0 U \frac{U}{w_{ss}} r(1-e_b)e_s \tag{4.110}$$

However, the suspended-load transport rate g_s (in weight) is given by

$$g_s = \tau_0 U \frac{sU}{\Delta w_{ss}} r(1-e_b)e_s \tag{4.111}$$

Bangnold reviewed the laboratory data and obtained $r(1 - e_b)e_s = 0.01$. Thus, the suspended-load transport rate is

$$g_s = 0.01\tau_0 U \frac{sU}{\Delta w_{ss}} \tag{4.112}$$

4.5 Mixing-Length Model for Suspended-Load Transport

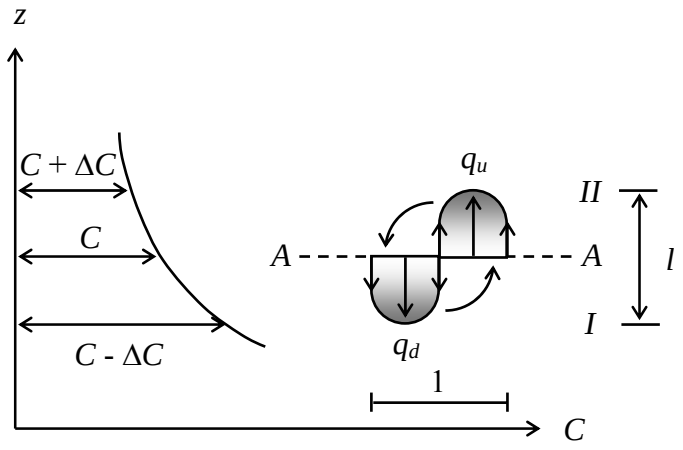

Fig. 4.6 Sediment suspension in turbulent flow

In steady flow, sediment is kept in suspension by the turbulent fluctuations. The sediment is assumed to settle relative to the surrounding fluid mass by their fall velocity. Following the

concept of the Prandtl's mixing length theory, fluid and sediment are transported from lower level *I* where the (volumetric) concentration of suspended sediment is $C - \Delta C$ up to a height level *II* where the concentration is $C + \Delta C$ (see Fig. 4.6).

The fluid (volume per unit time and area) transfers up through the section *AA* with the amount of sediment q_u, which is given by

$$q_u = (w' - w_{ss})\left(C - \frac{l}{2}\cdot\frac{dC}{dz}\right) \tag{4.113}$$

The upward transport is reciprocated by a corresponding downward transport of fluid with sediment. Analogous to Eq. (4.113), the downward sediment transport q_d is given by

$$q_d = (w' + w_{ss})\left(C + \frac{l}{2}\cdot\frac{dC}{dz}\right) \tag{4.114}$$

In case of a steady flow, q_u and q_d are equal, which yields

$$Cw_{ss} + \frac{w'l}{2}\cdot\frac{dC}{dz} = 0 \tag{4.115}$$

By assuming $w'l/2 \approx \beta\varepsilon_s l$ and using Eq. (4.23), one gets

$$Cw_{ss} + \kappa\beta u_* z\left(1 - \frac{z}{h}\right)\frac{dC}{dz} = 0 \tag{4.116}$$

Performing the integration within the limit $z = a$ to $z = h$, the vertical distribution of the concentration is obtained as

$$\frac{C}{C_a} = \left(\frac{h-z}{z}\cdot\frac{a}{h-a}\right)^{\zeta_\beta} \tag{4.117}$$

4.6 Total-Load Transport

The amount of sediment that passes through a given river reach for given conditions of the flow and boundary is termed *total-load*. Based on the mode of sediment transport, total-load is the sum of the bed-load and suspended-load. There are two general approaches to determine the total-load. The first is to estimate bed-load and suspended-load separately, and then add them together to quantify the total-load. The second is to determine the total load function directly without dividing it into bed-load and suspended-load. A sediment particle may be transported as bed-load at one time and as suspended-load at another time or location.

4.6.1 Indirect Estimation of Total-Load Transport

4.6.1.1 Einstein's Approach

Einstein (1950) advanced the bed-load and the suspended-load concept for the estimation of total-load. The bed-load and suspended-load are given by $i_b g_b$ and $i_s g_s$, respectively. Therefore, the total-load transport g_t for a given size fraction i_t is given by

$$i_t g_t = i_b g_b + i_s g_s \tag{4.118}$$

where g_b and g_s = bed-load and suspended-load transport rates, respectively; and i_b and i_s = particle size fractions of bed-load and suspended-load transport rates, respectively.

Using Eq. (4.64) into Eq. (4.118), the total-load transport g_t of a given size fraction i_t is obtained as

$$i_t g_t = i_b g_b (1 + P_E I_1 + I_2) \tag{4.119}$$

4.6.1.2 Bagnold's Modified Approach

Bagnold (1966) considered the relationship between the rate of energy available to a fluvial system and the rate of work done by the system in transporting sediment and obtained the following equation of bed-load transport rate g_b:

$$g_b = \frac{\tau_0 s}{\Delta \tan \varphi} U e_b \tag{4.120}$$

where τ_0 = bed shear stress; $\Delta = s - 1$; s = relative density of sediment particles, that is ρ_s/ρ; ρ_s = mass density of sediment; ρ = mass density of fluid; and U = depth-averaged flow velocity; and e_b = efficiency for bed-load transport. In Eq. (4.120), $\tau_0 U$ is the stream power or the power per unit area acting along the bed. The variation of e_b as given by Bagnold is shown in Fig. 4.7.

Using the expression of suspended-load transport rate g_s, the total-load transport rate g_t (= $g_b + g_s$) is obtained as

$$g_t = \frac{\tau_0 s U}{\Delta} \left(\frac{e_b}{\tan \varphi} + 0.01 \frac{U}{w_{ss}} \right) \tag{4.121}$$

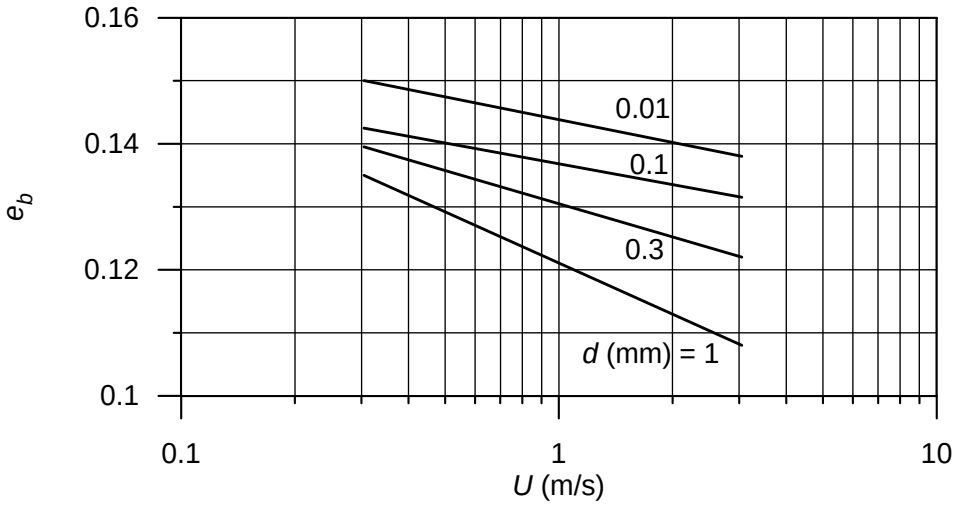

Fig. 4.7 Variation of bed-load transport efficiency e_b with U for different particle size d

4.6.2 Direct Estimation of Total-Load Transport

4.6.2.1 Graf and Acaroglu Approach

Unlike Einstein (1950), who considered the hydraulic radius due to particle roughness R_b', Graf and Acaroglu (1968) used hydraulic radius R_b, without dividing it into R_b' and R_b''. They developed a *shear intensity parameter* ψ_A as a transport criterion. It is given as

$$\Psi_A = \frac{\Delta d}{S R_b} \tag{4.122}$$

Based on a work rate concept, a *transport parameter* was established, such as

$$\Theta_A = \frac{\overline{C} U R_b}{(\Delta g d^3)^{0.5}} \tag{4.123}$$

where $\overline{C}$ = volumetric concentration of the transported particles. Using experimental data of different investigators, Graf and Acaroglu (1968) obtained the following empirical relationship between Θ_A and ψ_A:

$$\Theta_A = \frac{10.39}{\Psi_A^{2.52}} \tag{4.124}$$

4.7 Calculations

Calculation of Hydraulic Parameters:

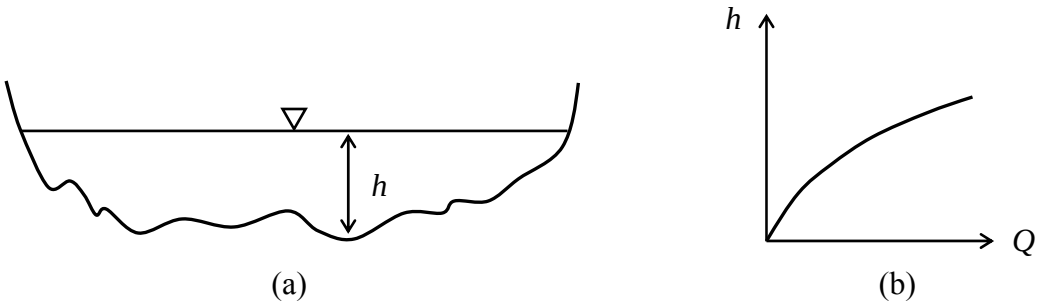

Fig. 4.8 (a) Schematic of a channel section and (b) stage discharge curve

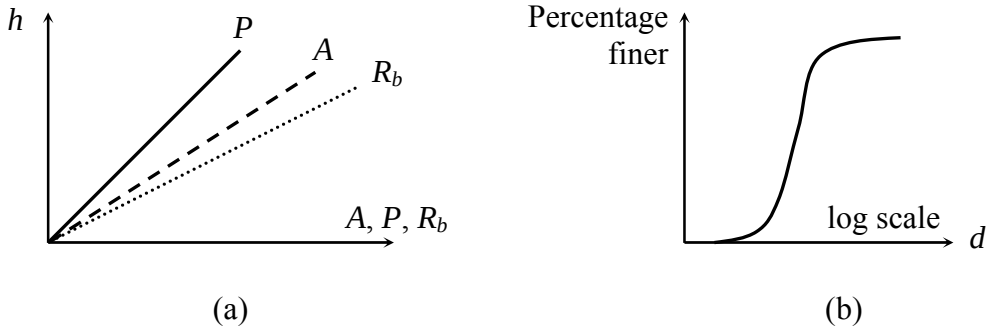

Fig. 4.9 (a) Channel characteristics curves and (b) particle size distribution curve

1. For a given channel section [Fig. 4.8(a)], the stage discharge curve (h versus Q), the channel characteristics curves (h versus area A, wetted perimeter P and hydraulic radius R_b) and the particle size distribution curve are given in Fig. 4.8(b), Fig. 4.9(a) and Fig. 4.9(b), respectively. The streamwise bed slope of the channel S is also known.
2. Assume different values of R_b' to cover the entire discharge Q_{max}.
3. Calculate $u_*' = (g R_b' S)^{0.5}$.
4. Calculate $\delta = 11.6\nu / u_*'$.
5. Find $k_s = d_{65}$ from particle size distribution curve.
6. Find x from Fig. 3.3 (curve x versus k_s/δ).

7. Calculate $\Delta_k = k_s/x$.
8. Calculate $U = u'_* \, 5.75 \log (12.27 \, R'_b/\Delta_k)$.
9. Calculate $\Psi = \Delta d_{65}/(R'_b \, S)$.
10. Find U/u''_* from Fig. 4.10 (curve U/u''_* versus Ψ).

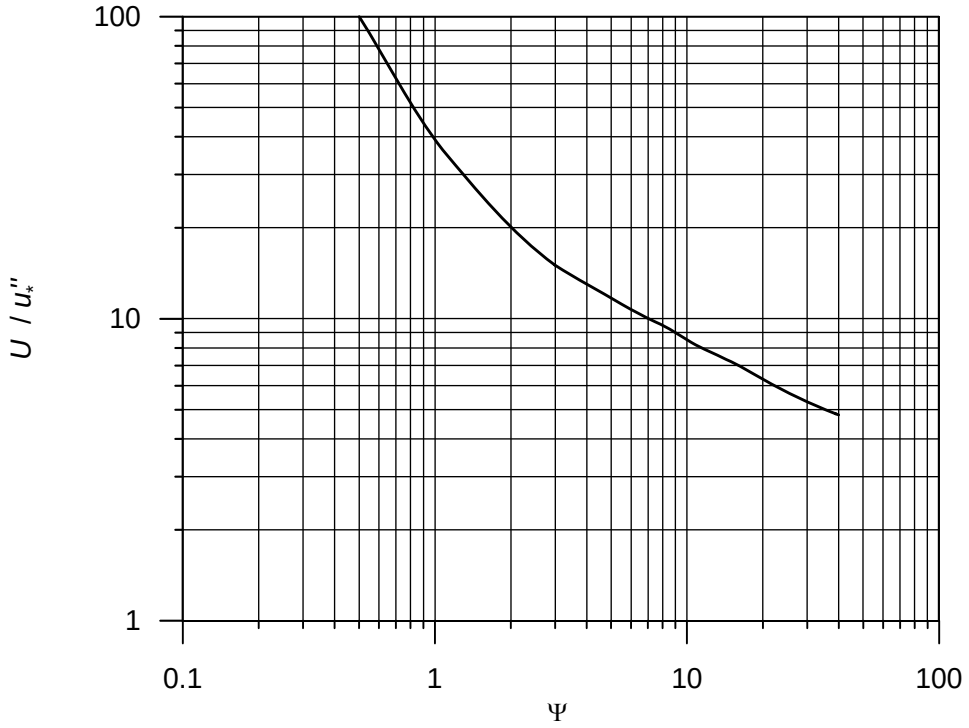

Fig. 4.10 Dependency of U/u''_* on Ψ

11. Determine u''_* (shear velocity due to channel irregularities such as bed forms).
12. Calculate R''_b from $u''_* = (g \, R''_b \, S)^{0.5}$.
13. Calculate $R_b = R'_b + R''_b$.
14. Calculate $u_* = (g \, R_b \, S)^{0.5}$.
15. Find flow depth h form channel characteristics curves [Fig. 4.9(a)].
16. Find flow area A form channel characteristics curves [Fig. 4.9(a)].
17. Find wetted perimeter P form channel characteristics curves [Fig. 4.9(a)].
18. Estimate flow discharge $Q = UA$.
19. Determine the characteristic distance X: $X(\Delta_k/\delta > 1.8) = 0.77\Delta_k$ and $X(\Delta_k/\delta < 1.8) = 1.39\delta$.
20. Determine the lift correction factor Y from Fig. 3.5.
21. Calculate $\beta_x = \log(10.6X/\Delta_k)$.
22. Evaluate $(\beta/\beta_x)^2$, with $\beta = \log(10.6)$.
23. Calculate Einstein's transport parameter P_E: $P_E = 2.303\log(30.2h/\Delta_k)$.

Calculation of Total Load:

24. The representative particle size d is known from the particle size distribution curve given in Fig 4.9(b).
25. The corresponding fraction i_b is obtained from the ordinate scale of Fig 4.9(b).
26. For d/X, find the hiding factor ξ from Fig. 3.4.
27. Calculate $\Psi_* = \xi Y \Psi(\beta/\beta_x)^2$.
28. Find Φ from Fig. 3.6 (curve Ψ_* versus Φ).
29. Calculate $i_b g_b = i_b \Phi \Delta^{0.5} \rho_s g^{1.5} d^{1.5}$.
30. Calculate $i_b G_b = (i_b g_b) P$, bed-load rate in weight per unit time for a size fraction for entire cross section.
31. Calculate $\sum i_b G_b$, bed-load rate in weight per unit time for all size fractions for entire cross section.
32. Calculate $E = a/h$ with $a = d_{65}$.
33. Calculate $\zeta = w_{ss}/(\kappa u'_*)$.
34. Find I_1 and I_2 from Eqs. (4.61a) and (4.61b) by numerical integration.
35. Calculate $i_t g_t = (1 + P_E I_1 + I_2)$.
36. Calculate $i_t G_t = (i_t g_t) P$, total-load rate in weight per unit time for a size fraction for entire cross-section.
37. Calculate $\sum i_t G_t$, total-load rate in weight per unit time for all size fractions for entire cross section.

4.8 References

Bagnold, R. A. (1966). "The flow of cohesionless grains in fluids." *Phil. Trans. Royal Soc.*, 249A, 235-297.

Bijker, E. W. (1971). "Longshore transport computations." *J. Waterways, Harbors Coastal Eng. Div., Am. Soc. Civ. Eng.*, 97(4), 687-701.

Brooks, N. H. (1963). "Calculation of suspended load discharge from velocity concentration parameters." *Proc. Federal Interagency Sediment Conf.*, US Department of Agriculture.

Chang, F. M., Simons, D. B., and Richardson, E. V. (1965). "Total bed-material discharge in alluvial channels." *Paper 1498-I*, US Geological Survey Water Supply.

Chien, N., and Wan, Z. (1999). *Mechanics of sediment transport*. ASCE Press, Virginia, USA.

DuBoys, M. P. (1879). "Etudes du regime et l'action exercée par les eaux sur un lit á fond de graviers indefiniment affouillable." *Annales des Ponts et Chaussés*, 18(Series 5), 141-195.

Einstein, H. A. (1950). "The bed-load function for sediment transportation in open channel flows." *Tech. Bulletin No. 1026*, US Department of Agriculture.

Einstein, H. A., Anderson, A. G., and Johnson, J. W. (1940). "A distinction between bed-load and suspended-load in natural streams." *Trans. Am. Geophys. Union*, 21.

Einstein, H. A., and Chien, N. (1955). "Effects of heavy sediment concentration near the bed on velocity and sediment distribution." *Inst. Eng. Res. Rep. No. 8*, University of California.

Elder, J. W. (1959). "The dispersion of marked fluid in turbulent shear flow." *J. Fluid Mech*., 5, 544-560.

Fredsøe, J., and Deigaard, R. (1992). *Mechanics of coastal sediment transport*. World Scientific Publishing Company Private Limited, Singapore.

Graf, W. H. (1971). *Hydraulics of sediment transport*. McGraw-Hill, New York.

Graf, W. H., and Acaroglu, E. R. (1968). "Sediment transport in conveyances systems (part 1)." *Bulletin Int. Assos. Sci. Hydraul.*, 13(2).

Lane, E. W., and Kalinske, A. A. (1941). "Engineering calculations of suspended sediment. *Trans. Am. Geophys. Union*, 20(3), 603-607.

Raudkivi, A. J. (1998). *Loose boundary hydraulics*. A. A. Balkama, Rotterdam, The Netherlands.

Rouse, H. (1937). "Modern conceptions of the mechanics of turbulences." *Trans. Am. Soc. Civ. Eng.*, 102, 463-543.

Vanoni, V. A. (1946). "Transport of suspended sediment by water." *Trans. Am. Soc. Civ. Eng.*, 111, 67-102.

Velikanov, M. A. (1958). *Fluvial process of rivers*. State Publishing House for Physics and Mathematics Literature, Moscow, Russia.

WIHEE. (1981). *River sedimentation engineering*. Hydraulic and Electric Press, Wuhan Institute of Hydraulic and Electric Engineering, China.

Yalin, M. S. (1972). *Mechanics of sediment transport*. Pergamon Press, Braunschweig, Germany.

Yang, C. T. (1996). *Sediment transport: theory and practice*. McGraw-Hill Book Companies, Singapore.

Chapter 5

Bed-Forms

5.1 General

When the flow over a sedimentary bed exceeds the threshold value, the bed does not remain stable but takes different features known as *bed-forms*. The shape and size of the bed-forms depends on the flow characteristics. In turn, the bed-forms significantly influence on various flow parameters. A review on bed-forms is available in Graf (1971), Yalin (1972), Yang (1996) and Fredsøe and Deigaard (1992).

5.2 Types of Bed-Forms

For the purpose of the classification of bed-forms, three flow regimes are distinguished according to the flow Froude number F [$= U/(gD_h)^{0.5}$, where U = depth-averaged flow velocity; g = acceleration due to gravity; D_h = hydraulic depth, A/T; A = flow area; and T = top width of flow]:

(1) Lower regime for $F < 1$; e.g. ripples, ripples on dunes and dunes.

(2) Transition for $F \approx 1$; e.g. washout dunes.

(3) Upper regime for $F > 1$; e.g. plane beds, antidunes, chutes and pools.

5.2.1 Ripples

Small triangular sand waves with long gradual upstream slope (approximately 6°) and short steep downstream slope (approximately 32°) are called *ripples* [Fig. 5.1(a)].

In case of fine sediments ($d_{50} < 0.7$ mm), ripples are formed, while coarse sediments usually form dunes. The wavelengths of ripples are usually shorter than 300 mm or approximately equaling $1000d_{50}$ and the heights less than 50 mm or approximately equaling $150d_{50}$. It is assumed that ripples are formed if viscous sub-layer is present when the threshold shear stress is just suppressed, while dunes are formed if the bed is hydraulically rough. The length of the ripples depends on the sediment size and the flow velocity, but is essentially independent of the flow depth. Ripples may be superposed upon the upstream side of dunes [Fig. 5.1(b)].

5.2.2 Dunes

Dunes are the bed-forms larger than ripples, whose profile is out of phase with the free surface profile [Fig. 5.1(c)]. The streamwise profile of a dune is roughly triangular with a mild upstream slope and a downstream slope approximately equal to the angle of repose. Dunes are formed in coarse sediments ($d_{50} > 0.6$ mm).

Flow separation that occurs at the crest of a dune reattaches in the trough, so that bottom rollers are formed on the lee side of a dune. Above this a zone of high turbulence exists, where a large production (and dissipation) of turbulent energy takes place. Near the zone of reattachment, the sediment particles are transported by the turbulence, even when the local bed shear stress is below its threshold value.

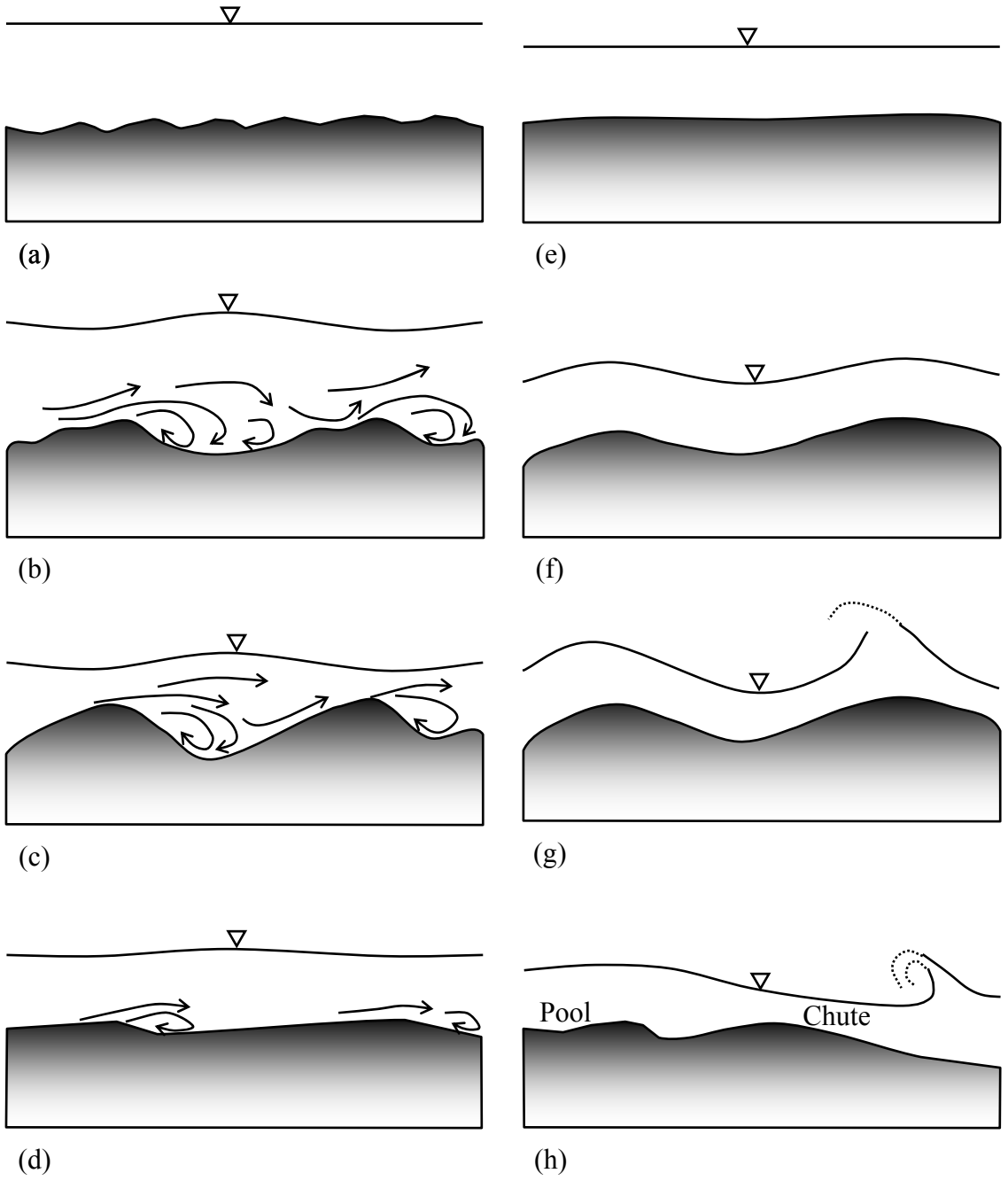

Fig. 5.1 Schematic of bed-forms: (a) Ripples; (b) ripples on dunes; (c) dunes; (d) transition or washed out dunes; (e) plane bed; (f) antidune standing waves; (g) antidune breaking wave; and (h) chutes and pools

On the upstream side of the dune, the bed shear stress drives sediment particles uphill until they pass over the crest and eventually are buried in the bed for a period. As sediment is transported from the upstream side and deposited on the lee side of a dune, the result is a slow continuous downstream migration of the dunes.

5.2.3 Transition and Plane Bed

For increased stream power (product of the velocity and the bed shear stress), the dunes tend to wash out and they become progressively longer and flatter and finally disappear [Figs.

5.1(d) and 5.1(e)]. This change from dunes to plane bed means a rather drastic reduction of both hydraulic resistance and flow depth.

5.2.4 Antidunes

In *Antidunes*, the bed and the free surface profiles are in phase [Figs. 5.1(f) and 5.1(g)]. The streamwise bed profile is nearly sinusoidal and so is free surface profile, but usually with much larger amplitude. While the flow is in downstream direction, the sand waves and free surface waves may remain stationary or move upstream or downstream. At lower Froude numbers, antidunes appear as *standing sand wave* [Fig. 5.1(f)]. However, at higher Froude numbers, the sand wave may grow becoming unstable and breaking in the upstream direction (sand waves move upstream just before breaking) [Fig. 5.1(g)]. If the latter occurs, the antidunes are destroyed, the bed becomes flat, and the formation of antidunes starts all over again.

5.2.5 Chutes and Pools

Extremely strong antidunes actively lead to *chutes* and *pools* flow, which occur at relatively large slopes with high flow velocities and sediment concentrations. They consist of large elongated heaps of sediment. Shooting flow on the heaps of sediment runs into a pool where the flow is generally tranquil [Fig. 5.1(h)].

5.3 Mechanics of Dunes

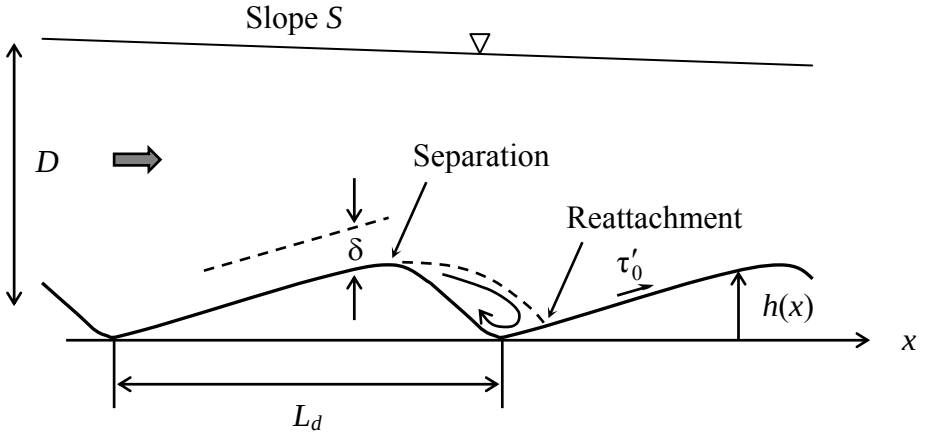

Fig. 5.2 Streamwise profiles of dunes (elongated vertical scale)

It is assumed that the bed waves are traveling at a constant velocity a without any change in shape. Under these condition the shape of the bed is described by an expression of the form

$$h = h(x - at) \tag{5.1}$$

where h = local height of the dune above an x-axis passing through the troughs (Fig. 5.2). Then, consider the bed-load of sediment q_B through two consecutive sections with unit spacing in the x-direction. The net outflow of sediment is $\partial q_B/\partial x$, which is equal to the change in bed elevation when the correction for the porosity ρ_0 of the bed sediment is taken into account. However, the change in the amount of sediment stored in suspension is ignored. Therefore, the sediment continuity equation (Exner equation) is

$$\frac{\partial q_B}{\partial x} = -(1-\rho_0)\frac{\partial h}{\partial t} \tag{5.2}$$

If Eq. (5.1) is substituted into Eq. (5.2), it becomes obvious that they are satisfied by putting

$$q_B = q_B(x) = q_0 + a(1-\rho_0)h \tag{5.3}$$

where q_0 = a constant, interpreted as the value of q_B at $h = 0$, that is at the trough the bed-load is zero. For small bed shear stress, q_0 becomes zero, because the sediment mainly moves as bed-load and so q_B becomes q_b. This transport is related to the local bed shear stress, which is negligible in the trough because of flow separation. In this case, the following relationship is obtained

$$q_b = a(1-\rho_0)h \tag{5.4}$$

In the above, it is evident that the local intensity of bed-load transport is proportional to the local height of the bed above the plane through the troughs. This indicates that the bed shear stress at the dune surface must vary from zero at the trough to a maximum at the crest.

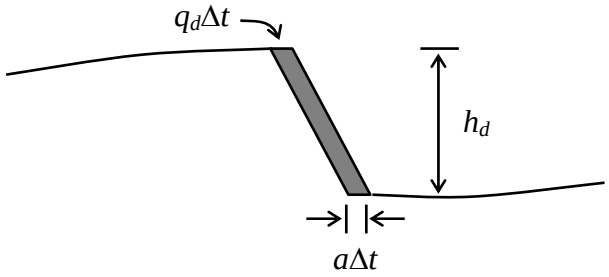

Fig. 5.3 Migration of dune front

At the front of the dune, the amount of sediment deposited is called q_d. This amount determines the migration velocity a of the dune (Fig. 5.3).

$$a = \frac{q_d}{(1-\rho_0)h_d} \tag{5.5}$$

where h_d = dune height. From Eqs. (5.3) and (5.4), it is seen that for small bed shear stress, q_d becomes same as q_b. Now, if the sediment is transported mainly as a bed-load, the shape of the bed-form can be found from Eqs. (5.4) and (5.5), combining them as

$$\frac{h}{h_d} = \frac{q_b}{q_b\big|_{\text{top}}} \tag{5.6}$$

where $q_b\big|_{\text{top}}$ = sediment transport at the dune crest level where $h = h_d$. The modified bed-load equation of Meyer-Peter due to bed slope is given by

$$q_b = 8\sqrt{\Delta g d^3}\left(\Theta - \frac{\Theta_c}{\tan\varphi}\cdot\frac{\partial h}{\partial x} - \Theta_c\right)^{3/2} \tag{5.7}$$

where d = representative particle diameter, that is median particle diameter; g = acceleration due to gravity; $\Delta = s - 1$; s = relative density of sediment particles, that is ρ_s/ρ; ρ_s = mass density of sediment; ρ = mass density of fluid; Θ = local Shields parameter, $u_*^2/(\Delta g d)$; u_* = shear velocity; Θ_c = threshold Shields parameter; and φ = angle of repose of bed sediment. Inserting Eq. (5.7) into Eq. (5.6) yields

$$\frac{1}{\tan\varphi}\cdot\frac{\partial h}{\partial x}+\left(\frac{\Theta_{top}}{\Theta_c}-1\right)\left(\frac{h}{h_d}\right)^{2/3}=\frac{\Theta}{\Theta_c}-1 \tag{5.8}$$

Due to the presence of the dunes, the local flow depth varies along the dune, which results in spatial changes to the depth-averaged flow velocity U, which varies along the dune as

$$U(D+0.5h_d-h)=q \tag{5.9}$$

where q = flow discharge per unit width. In the above equation, the undulation of the free surface due to the presence of dune is neglected. In case of dunes where the wavelength is several times the flow depth, this variation in depth-averaged flow velocity can be included in the spatial variation in bed shear stress along the dune by giving the bed shear stress as

$$\tau_0=\tau_{top}\,f\left(\frac{x}{h_d}\right)\left(\frac{U}{U_{top}}\right)^2 \tag{5.10}$$

The bed shear stress usually varies with the square of the flow velocity. Thus Eqs. (5.9) and (5.10), yields

$$\Theta_c=\Theta_{top}\,f\left(\frac{x}{h_d}\right)\left(\frac{D-0.5h_d}{D+0.5h_d-h}\right)^2 \tag{5.11}$$

5.3.1 Dune Height

The dune height can be obtained from the geometrical consideration. Thus, combining Eqs. (5.1) and (5.5), gives

$$\frac{\partial h}{\partial t}=-a\frac{\partial h}{\partial x}=-\frac{q_d}{(1-\rho_0)h_d}\cdot\frac{\partial h}{\partial x} \tag{5.12}$$

Again, combining Eqs. (5.2) and (5.12), yields

$$\frac{\partial q_B}{\partial x}=\frac{q_d}{h_d}\cdot\frac{\partial h}{\partial x} \tag{5.13}$$

Eq. (5.13) can also be written as

$$\frac{\partial \Phi_B}{\partial x}=\frac{\Phi_d}{h_d}\cdot\frac{\partial h}{\partial x} \tag{5.14}$$

where Φ_B = nondimensional sediment transport rate. In steady flow, Φ_B is a function of the Shields parameter Θ and can be written as

$$\frac{\partial \Phi_B}{\partial \Theta}\cdot\frac{\partial \Theta}{\partial \mathrm{x}}=\frac{\Phi_d}{h_d}\cdot\frac{\partial h}{\partial x} \tag{5.15}$$

At the dune crest, Eq. (5.11) is approximated by

$$\Theta=\Theta_{top}\left(\frac{D-0.5h_d}{D+0.5h_d-h}\right)^2 \tag{5.16}$$

In the above equation, the weak variation in the function f is disregarded, which is a good approximation far away from the former crest. Θ_{top} appearing in Eq. (5.16) is the Shields parameter due to the skin friction, which can be related to the averaged skin friction Θ_{av} by

$$\Theta_{av} = \Theta_{top}\left(\frac{D-0.5h_d}{D}\right)^2 \tag{5.17}$$

Now, Eq. (5.16) gives

$$\frac{\partial\Theta}{\partial x} = \frac{2\Theta_{top}}{D-0.5h_d}\cdot\frac{\partial h}{\partial x} \tag{5.18}$$

Eq. (5.18) combines with Eq. (5.14) resulting the following expression for the dune height

$$\frac{h_d}{D} = \frac{2\Phi_d}{4\Theta\dfrac{d\Phi_B}{d\Theta}+\Phi_d}, \quad \Theta = \Theta_{top} \tag{5.19}$$

In Eq. (5.19), all the quantities on the RHS must be taken at the dune top.

5.3.2 Dune Length

In case of dominant bed-load transport, the maximum bed shear stress is located around 16 times the dune height downstream from the former crest. Also, the maximum sediment transport rate, except for very small Shields parameters, occurs at the location of maximum dune height. The equation of the dune length can be obtained from Eq. (5.6) as

$$L_d = 16h_d \tag{5.20}$$

At higher bed shear stresses, where suspended sediment becomes the dominant transport mechanism, the situation becomes a little more complex because a spatial phase lag L_s is introduced between the location of the maximum bed shear stress and the location of the maximum suspended-load transport. The maximum bed-load and suspended-load transport can be estimated being located around

$$\frac{L_d}{h_d} = \frac{16q_b + \left(\dfrac{L_s}{h_d}+16\right)q_s}{q_b+q_s} \tag{5.21}$$

where q_s = suspended-load transport rate. In the above equation, the weighted mean of the influence from the bed-load and suspended-load is considered. Eq. (5.21) suggests that the influence of suspended sediment is that the dune lengthens.

5.3.3 Phase Lag of Suspended Sediment

The phase lag L_s is introduced because a sediment particle takes some time to settle after being picked up from the bed. The magnitude of L_s can be estimated from the basic equation of sediment suspension. In steady state, it reads

$$u\frac{\partial C}{\partial x} = w_{ss}\frac{\partial C}{\partial z} + \frac{\partial}{\partial z}\left(\varepsilon_s\frac{\partial C}{\partial z}\right) + \frac{\partial}{\partial x}\left(\varepsilon_s\frac{\partial C}{\partial x}\right) \tag{5.22}$$

An illustrative example of the solution of Eq. (5.22) can be obtained assuming ε_s and u to be constant over the flow depth. In uniform flow, Eq. (5.22) can be solved giving

$$\frac{C}{C_{b0}} = \exp\left(-\frac{w_{ss}z}{\varepsilon_s}\right) \tag{5.23}$$

where C_{b0} = nominal reference sediment concentration at the bed. Now the case is considered where the concentration C_{b0} varies in the flow direction, for instance, due to spatial changes in the bed shear stress. In this simplified example, ε_s and u are assumed not to vary in the x-direction. Because of the variation in C_{b0}, the vertical distribution of the suspended sediment deviates from the equilibrium profile given by Eq. (5.23). For simplicity, the vertical distribution of suspended sediment is still described by an exponential function introducing a steepness variable λ as

$$\frac{C}{C_{b0}} = \exp\left[-\frac{w_{ss}}{\varepsilon_s}(1+\lambda)z\right] \tag{5.24}$$

Introducing Eq. (5.24) into the diffusion Eq. (5.22) and integrating over the flow depth, yields

$$u\frac{\varepsilon_s}{w_{ss}}\cdot\frac{\partial}{\partial x}\left(\frac{C_{b0}}{1+\lambda}\right) = -C_{b0}w_{ss} + C_{b0}w_{ss}(1+\lambda) \tag{5.25}$$

In this derivation, it is assumed that the sediment concentration vanishes towards the free surface, and the horizontal diffusion of sediment is neglected. The variation in C_{b0} is taken to be a small perturbation, and Eq. (5.24) can then be linearized to give the following differential equation for the unknown parameter λ:

$$\frac{d\lambda}{dx} + \frac{w_{ss}^2}{u\varepsilon_s}\lambda - \frac{1}{C_{b0}}\cdot\frac{\partial C_{b0}}{\partial x} = 0 \tag{5.26}$$

This equation can be solved for a given variation in C_{b0}. As an example a periodic perturbation of C_{b0} is considered, giving a variation of

$$C_{b0} = C_0 + C_1\sin(kx) \tag{5.27}$$

Introducing Eq. (5.27) into Eq. (5.25) and using that $C_0 >> C_1$, yields

$$\frac{d\lambda}{dx} + \frac{\lambda}{L_s} - \frac{C_1 k}{C_{b0}}\cos(kx) = 0 \tag{5.28}$$

In Eq. (5.28), the length scale L_s is introduced as

$$L_s = u\frac{\varepsilon_s}{w_{ss}^2} \tag{5.29}$$

The solution to Eq. (5.26) is given by

$$\lambda = \frac{C_1 k}{C_0}\cdot\frac{L_s}{1+(kL_s)^2}[\cos(kx) + kL_s\sin(kx)] + C_2\exp(-x/L_s) \tag{5.30}$$

The vanishing transient part can be ignored, that is $C_2 = 0$. For long wavelengths of the perturbation, the nondimensional parameter kL_s is small, and Eq. (5.30) can be approximated by

$$\lambda = \frac{C_1}{C_0}\cdot kL_s\cos(kx) \tag{5.31}$$

The sediment transport rate q_s can be found as

$$q_s = \int_0^D Cudz = C_{b0}u\frac{\varepsilon_s}{w_{ss}}\cdot\frac{1}{1+\lambda} \approx C_{b0}u\frac{\varepsilon_s}{w_{ss}}(1-\lambda)$$

$$= C_0 u \frac{\varepsilon_s}{w_{ss}} \left[1 + \frac{C_1}{C_0} \sin(kx) \right] \left[1 - \frac{C_1}{C_0} kL_s \cos(kx) \right]$$

$$\approx C_0 u \frac{\varepsilon_s}{w_{ss}} \left\{ 1 + \frac{C_1}{C_0} [\sin(kx) - kL_s \cos(kx)] \right\}$$

$$\approx C_0 u \frac{\varepsilon_s}{w_{ss}} \left\{ 1 + \frac{C_1}{C_0} \sin[k(x - L_s)] \right\} \tag{5.32}$$

If the development of the sediment transport concentration profile had been neglected (that is for the quasi-uniform conditions), the suspended sediment transport rate would have been calculated as

$$q_s = \int_0^D Cudz = C_{b0} u \frac{\varepsilon_s}{w_{ss}} = C_0 u \frac{\varepsilon_s}{w_{ss}} \left[1 + \frac{C_1}{C_0} \sin(kx) \right] \tag{5.33}$$

By comparing Eqs. (5.32) and (5.33), it is seen that the development in the concentration profile causes the sediment transport rate to have a phase lag relative to the variation in the bed concentration. The phase lag is equal to L_s. As seen from Eq. (5.29) the lag distance increases with a decrease in w_{ss} and with an increase in eddy viscosity ε_s or flow velocity u.

As seen from Eqs. (5.23) and (5.29), the length scale L_s can be given by

$$L_s = z_c \frac{u\big|_{z_c}}{w_{ss}} \tag{5.34}$$

where z_c = height of the centroid of the concentration profile above the bed (= ε_s / w_{ss}); and $u\big|_{z_c}$ = average velocity at an elevation z_c. It can be expressed as

$$z_c = \frac{\int_0^D Czdz}{\int_0^D Cdz} \tag{5.35}$$

5.3.4 Flow Resistance due to Dunes

In presence of bed-forms, the resistance to the flow consists of two parts, one originating from the skin friction (or grain resistance) and other due to the expansion loss downstream of a dune crest. The latter is denoted by $\Delta h''$, and the magnitude of the loss can be estimated from the Carnot equation as

$$\Delta h'' = K \frac{(U_{cr} - U_{tr})^2}{2g} \tag{5.36}$$

where U_{cr} = average velocity at the crest; U_{tr} = average velocity at the trough; and K = coefficient due to flow geometry. The average velocities U_{cr} and U_{tr} are given by

$$U_{cr} = \frac{q}{D - 0.5h_d} \tag{5.37a}$$

$$U_{tr} = \frac{q}{D + 0.5h_d} \tag{5.37b}$$

where $q = UD$. Therefore, Eq. (5.36) becomes

$$\Delta h'' \approx \alpha \frac{U^2}{2g}\left(\frac{h_d}{D}\right)^2 \tag{5.38}$$

The total energy loss J per unit length in the streamwise direction is given by

$$J \approx J' + \frac{\Delta h''}{L_d} = J' + J'' \tag{5.39}$$

where J' = gradient due to friction. In a steady-uniform open channel flow, the total bed shear stress τ_0 is related to the energy gradient J by

$$\tau_0 = \rho g D J \tag{5.40}$$

According to Eq. (5.39), τ_0 can be split into two parts as

$$\tau_0 = \rho g D J' + \rho g D J'' = \tau' + \tau'' \tag{5.41}$$

where τ' = mean bed shear stress acting directly as a friction on the surface of the dune; and τ'' = form drag on the dune. In nondimensional form, Eq. (5.41) can be expressed as

$$\Theta = \Theta' + \Theta'' \tag{5.42}$$

where Θ = Shields parameter, $\tau_0/(\Delta g d)^{0.5}$; $\Theta' = DJ'/(\Delta d)$; and $\Theta'' = 0.5\alpha(Uh_d)^2/(\Delta g d D L_d)$.

To calculate J', an additional flow resistance equation for the skin friction is required. For this purpose, consider Fig. 5.4, where immediately downstream the dunes crest a wake like flow is formed producing large amount of turbulent energy. This is dissipated into heat further downstream and thus causing the expansion loss.

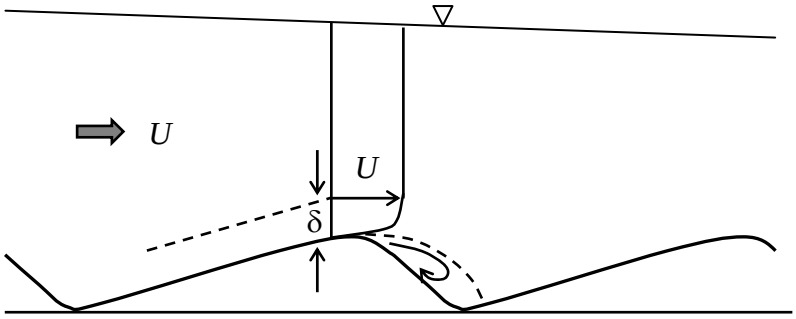

Fig. 5.4 Schematic of boundary layer developed along a dune

At the end of the trough, a boundary layer with thickness δ is developed, where the velocity gradient is large, while the velocity distribution outside this layer is uniform. Engelund and Hansen (1972) assumed that the upper flow and the boundary layer flow are independent of each other in the sense that no significant amount of energy is exchanged between them. Hence, the energy gradient of the boundary layer flow (defined as the dissipation per unit weight and discharge) is equal to that of the upper layer and that of the total flow. It is

$$J = \frac{\tau_b' U'}{\rho g U' D'} = f' \frac{\rho U^2}{2\rho g D'} = f' \frac{U^2}{2gD'} \tag{5.43}$$

where U' = average flow velocity in the boundary layer; and f' = skin friction coefficient defined by

$$\tau_b' = f' \frac{\rho U'^2}{2} \tag{5.44}$$

The expression of J is given by

$$J = f \frac{U^2}{2gD} \tag{5.45}$$

Therefore, Eqs. (5.43) and (5.45) produce

$$\frac{f'}{D'} = \frac{f}{D} \tag{5.46}$$

Eqs. (5.45) and (5.46) gives

$$\sqrt{\frac{2}{f'}} = \frac{U}{\sqrt{gD'J}} \tag{5.47}$$

The friction factor f' for the boundary layer is determined from the equation of Nikuradse as

$$\sqrt{\frac{2}{f'}} = 6 + 2.5 \ln\left(\frac{D'}{k_s}\right) \tag{5.48}$$

where k_s = equivalent sand roughness of Nikuradse. As $f = f'$ and $D = D'$, the value of the constant in Eq. (5.48) is 6. Using Eqs. (5.47) and (5.48), yields

$$\frac{U}{\sqrt{2gD'J}} = 6 + 2.5 \ln\left(\frac{D'}{k_s}\right) \tag{5.49}$$

The above equation was originally suggested by Einstein (1950), who obtained it as an analogy to his calculation of sidewall correction. Combining Eqs. (5.43) and (5.45), yields the important expression

$$\tau_b' = \rho g D' J \tag{5.50}$$

5.4 References

Engelund, F., and Hansen, E. (1972). *A monograph on sediment transport in alluvial stream*. Technical Press, Copenhagen, Denmark.

Einstein, H. A. (1950). "The bed-load function for sediment transportation in open channel flows." *Tech. Bulletin No. 1026*, US Department of Agriculture.

Fredsøe, J., and Deigaard, R. (1992). *Mechanics of coastal sediment transport*. World Scientific Publishing Company Private Limited, Singapore.

Graf, W. H. (1971). *Hydraulics of sediment transport*. McGraw-Hill, New York.

Yalin, M. S. (1972). *Mechanics of sediment transport*. Pergamon Press, Braunschweig, Germany.

Yang, C. T. (1996). *Sediment transport: theory and practice*. McGraw-Hill Book Companies, Singapore.

Chapter 6

Local Scour at Structures

6.1 General

Scour is a natural phenomenon of lowering the level of riverbeds by the erosive action of the flowing stream. The amount of reduction in the level of riverbeds below an assumed natural level is termed *scour depth*. Scour is classified as *general scour* and *local scour*.

General scour in the river occurs as a result of the change in the characteristics of the river. Based on the time taken for scour development, general scour can be categorized as *short-term scour* and *long-term scour*. *Short-term general scour* develops during a single or several closely spaced floods, while *long-term general scour* takes considerably long time, normally of the order of several years, and includes progressive degradation and lateral bank erosion. *Short-term general scour* may occur due to convergence of flow, a shift in the channel thalweg or braids within the channel, and bed-form migration. On the other hand, the *long-term general scour* may be caused by the natural changes in the catchments (e.g. channel straightening, volcanic activities, climate change etc) or by the human activities (e.g. channel alterations, streambed mining, dam / reservoir construction, and land-use changes).

In contrast, *local scour* (also termed *localized scour*) develops near the structures, due to modification of the flow field as a result of obstruction to the flow by the structures. Scour within the contracted portion of the channel, scour downstream of an apron due to submerged jets, scour below horizontal pipes, scour at bridge piers and abutments, scour at spur dikes and other river training works are the examples of local scour.

Local scour is classified as *clear-water scour* and *live-bed scour*. *Clear-water scour* occurs when the sediment is removed from the scour hole but not supplied by the approaching stream. The equilibrium scour depth is attained when the fluid induced force can no longer dislodge the sediment particles from the scour hole. On the other hand, *live-bed scour*, occurs when the scour hole is continuously fed with the sediment by the approaching stream. The equilibrium scour depth is attained over a period of time, when the rate of removal of sediment out of the scour hole equals the rate of supply of sediment into the scour hole.

This chapter summarizes the local scour at different structures including various aspects such as flow field, influence of various parameters on scour depth, design formula for the prediction of scour depth.

6.2 Scour within Channel Contractions

Channel contraction is the reduction in the width of waterways by constructing parallel sidewalls. The reduction in flow area due to channel contraction increases the flow velocity and thereby enhances the bed shear stress. As a result, the sediment bed within the channel contraction is scoured. Such local scour in the contracted zone of the channel is called *contraction scour*. Straub (1934) was the pioneer to present a simplified one-dimensional theory of the equilibrium scour in long contractions. His work was later extended and modified by Ashida (1963), Laursen (1963), Komura (1966), Gill (1981), Webby (1984), and Lim (1993). Recently, Dey and Raikar (2005, 2006) studied the scour in long contractions in gravel-beds and proposed analytical models for the estimation of scour depth under both clear-water and live-bed scour conditions.

Depending on the ratio of the length of contraction L to the approaching channel width b_1, channel contractions are designated as long or short. According to Komura (1966) and Dey and Raikar (2005), a contraction becomes long when $L/b_1 > 1$, whereas Webby (1984) considered it as $L/b_1 > 2$. Figs. 6.1(a) and 6.1(b) show a schematic of channel contraction and photograph of the scoured bed. Smith (1967) proposed the angle of upstream and downstream transitions as 12.5^o for a smooth transition to the contracted zone.

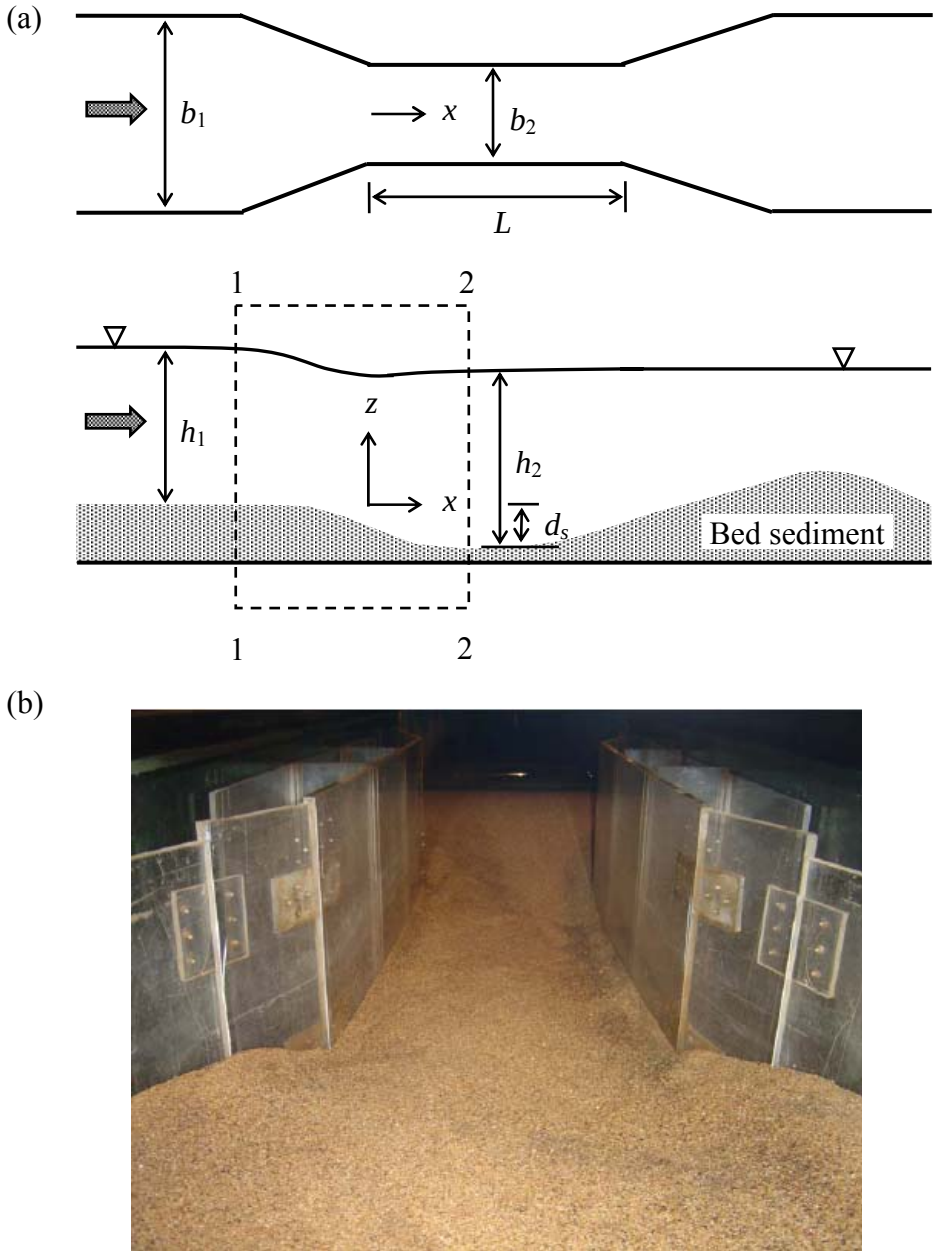

Fig. 6.1 (a) Schematic of rectangular channel contraction at equilibrium scour condition and (b) photograph showing a scoured bed

6.2.1 Flow Field within Scoured Zone of Channel Contraction

Raikar and Dey (2004) detected the flow field within the scoured zone of channel contractions by an acoustic Doppler velocimeter (ADV). The velocity vectors within a channel contraction are given in Fig. 6.2 that shows the passage of flow within the scour hole.

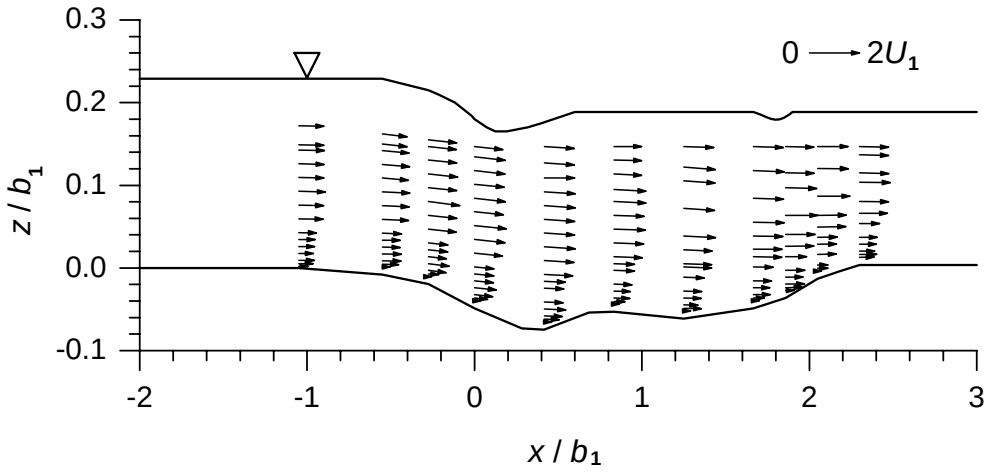

Fig. 6.2 Typical flow field within the scoured zone of a channel contraction at equilibrium

6.2.2 Influence of Various Parameters on Scour Depth

The parameters that influence the scour within channel contractions are as follows:

- Parameters relating to contraction: Channel opening ratio and channel shape.
- Parameters relating to the bed sediment: Median particle size, particle size distribution, angle of repose and cohesiveness.
- Parameters relating to the approaching flow condition: Approaching flow velocity, approaching flow depth, shear velocity and roughness.
- Parameters relating to the fluid: Mass density, viscosity, gravitational acceleration and temperature (may not be important in scour problems).

The functional relationship showing the influence of above parameters on the equilibrium scour depth d_s in a long rectangular contraction can be given as follows:

$$d_s = f_1(U_1, h_1, \rho, \rho_s, g, \nu, d_{50}, b_1, b_2, \sigma_g) \tag{6.1}$$

where U_1 = approaching flow velocity; h_1 = approaching flow depth; ρ = mass density of water; ρ_s = mass density of sediment; g = gravitational acceleration; ν = kinematic viscosity of water; d_{50} = median sediment size; b_2 = contracted width of channel; and σ_g = geometric standard deviation of the particle size distribution. In sediment-water interaction, the parameters g, ρ and ρ_s are combined into a parameter Δg (Dey and Debnath 2001; Dey and Raikar 2005); where $\Delta = s - 1$; and s = relative density of sediment, that is ρ_s/ρ. Also, it is reasonable to use the parameter channel opening ratio $\hat{b}$ (= b_2/b_1) to account for the combined effect of b_1 and b_2. In addition, the influence of kinematic viscosity ν is insignificant for a turbulent flow over rough beds (Yalin 1977). Using the Buckingham π-theorem with U_1 and b_1 as repeating variables yields

$$\tilde{d}_s = f_2(\tilde{d}, F_0, \tilde{h}, \hat{b}, \sigma_g) \tag{6.2}$$

where $\tilde{d}_s = d_s/b_1$; $\tilde{d} = d_{50}/b_1$; $F_0 = U_1/(\Delta g d_{50})^{0.5}$, that is the densimetric Froude number; and $\tilde{h} = h_1/b_1$. Dependency of nondimensional equilibrium scour depth $\tilde{d}_s$ on above nondimensional parameters studied by Dey and Raikar (2005) is as follows:

Figs. 6.3(a) - 6.3(d) show the variation of the nondimensional equilibrium scour depth $\tilde{d}_s$ with $\tilde{d}$, $\tilde{h}$, F_0 and $\hat{b}$ for uniform sediments. The equilibrium scour depth increases with an increase in sediment size for gravels [Fig. 6.3(a)]. But the curves of scour depth versus sediment size have considerable sag at the transition of sand and gravel. Also, the scour depth increases with an increase in approaching flow depth at lower depths, while it becomes independent of approaching flow depth at higher flow depths [Fig. 6.3(b)]. The scour depth reduces gradually with an increase in densimetric Froude number for larger opening ratios, whereas the trend is opposite for small opening ratios [Fig. 6.3(c)]. Further, the scour depth increases with a decrease in channel opening ratio [Fig. 6.3(d)].

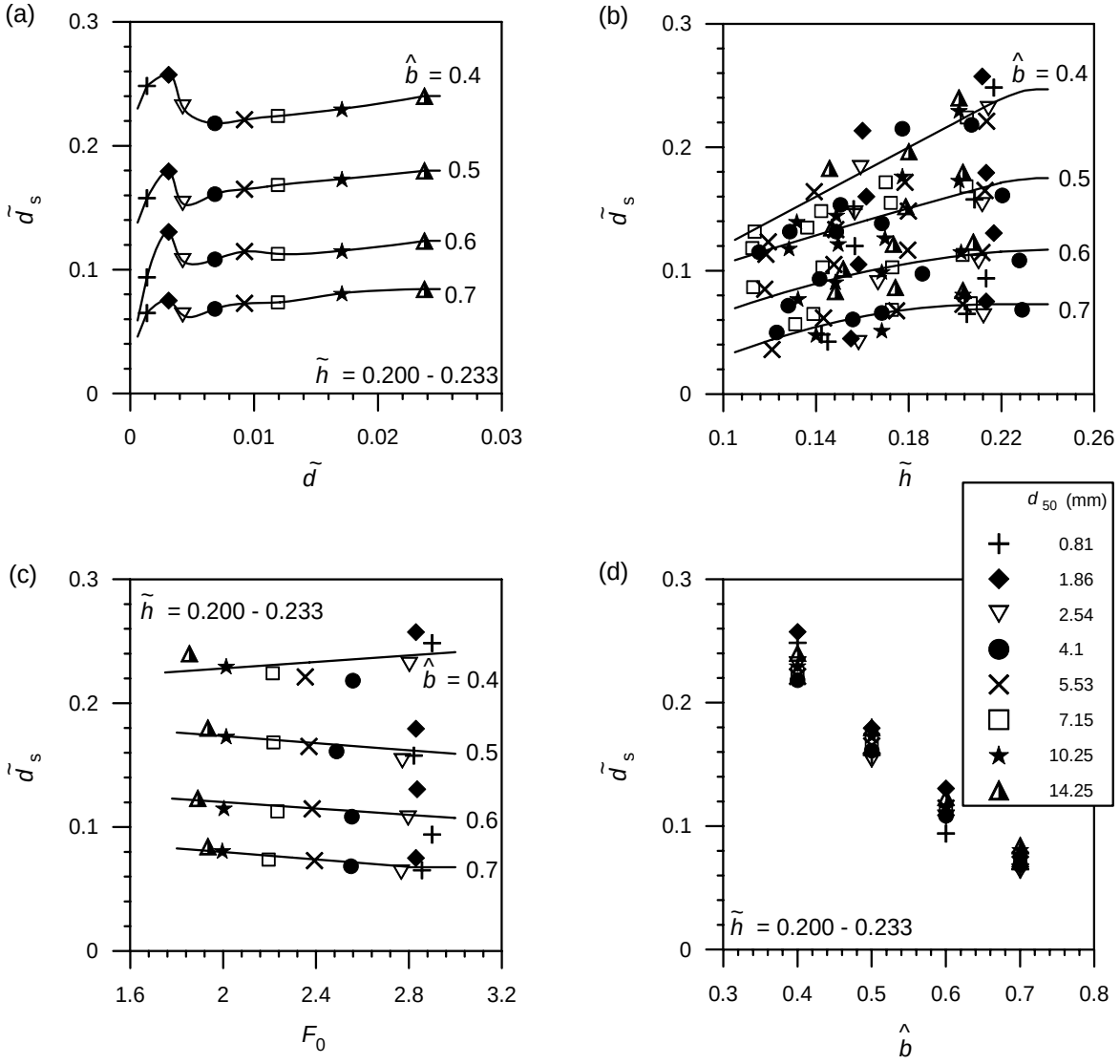

Fig. 6.3 Variations of (a) $\tilde{d}_s$ with $\tilde{d}$; (b) $\tilde{d}_s$ with $\tilde{h}$; (c) $\tilde{d}_s$ with F_0 and (d) $\tilde{d}_s$ with $\hat{b}$ (after Dey and Raikar 2005)

The effect of sediment gradation on scour depth is pronounced for nonuniform sediments, which result in reduction of scour depth due to the formation of armor-layer in the scour hole. The equilibrium scour depth $d_s(\sigma_g)$ in nonuniform sediments can be estimated in terms of geometric standard deviation σ_g of sediments using the following relationship:

$$\tilde{d}_s(\sigma_g) = K_\sigma \tilde{d}_s \tag{6.3}$$

where K_σ = coefficient due to sediment gradation. The coefficient K_σ is defined as the ratio of equilibrium scour depth in nonuniform sediment ($\sigma_g > 1.4$) to that in uniform sediment. The variation of K_σ with σ_g is given in Fig. 6.4. It is apparent from the mean curve that the scour depth in nonuniform sediment with $\sigma_g = 3$ is drastically reduced to 25% of scour depth in uniform sediment. However, the reduction of scour depth for $\sigma_g > 3$ is not influenced by the nonuniformity of sediments.

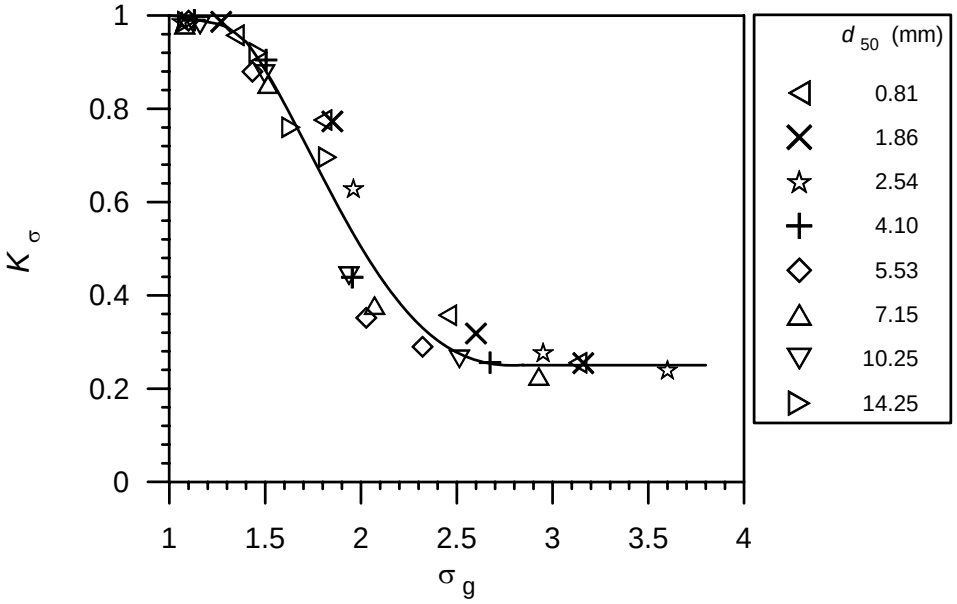

Fig. 6.4 Variation of K_σ as a function of σ_g (after Dey and Raikar 2005)

6.2.3 Laursen's Model

Laursen (1963) considered a channel contraction as shown in Fig. 6.1(a). The discharge in the channel is given by

$$Q = U_1 h_1 b_1 = U_2 h_2 b_2 \tag{6.4}$$

where h_2 = flow depth in contracted zone; and U_2 = flow velocity in contracted zone. The scour depth d_s is given by

$$d_s = (h_2 - h_1) + (1 + K)\left(\frac{U_2^2}{2g} - \frac{U_1^2}{2g}\right) \tag{6.5}$$

where K = head loss coefficient, defined as

$$K = \frac{2gh_f}{U_2^2 - U_1^2} \tag{6.6}$$

where h_f = head loss through transition. Eq. (6.5) can then be written in nondimensional form as

$$\hat{d}_s = \frac{h_2}{h_1} - 1 + \left(\frac{1+K}{2}\right) F_1^2 \left[\left(\frac{b_1}{b_2}\right)^2 \left(\frac{h_1}{h_2}\right)^2 - 1\right] \tag{6.7}$$

where $\hat{d}_s = d_s/h_1$; and $F_1 = U_1^2/gh_1$, that is the approaching flow Froude number.

When the scour depth in contracted zone reaches equilibrium, the bed shear stress becomes equal to tractive force, that is $\tau_c = 0.628 d_{50}$ (in Pa); where d_{50} in mm. The bed shear stress, in

the uncontracted zone can be estimated using the Manning equation and the Strickler's relationship for n (= Manning roughness coefficient) as

$$\tau_{01} = \frac{U_1^2 d_{50}^{0.33}}{30 h_1^{0.33}} \tag{6.8}$$

Taking the ratio of shear or tractive force in the contracted and uncontracted zones yields

$$\frac{\tau_{01}}{\tau_c} = \frac{U_1^2}{120 d_{50}^{0.67} h_1^{0.33}} \tag{6.9}$$

Similar expression can also be written for the bed shear stress in the contracted zone. Hence, the flow depth ratio h_2/h_1 can be obtained as

$$\frac{\tau_{01}}{\tau_{02}} = \left(\frac{U_1}{U_2}\right)^2 \left(\frac{h_2}{h_1}\right)^{1/3} = \frac{\tau_{01}}{\tau_c} \tag{6.10}$$

Using Eqs. (6.4) and (6.10), one can write

$$\frac{h_2}{h_1} = \left(\frac{\tau_{01}}{\tau_c}\right)^{3/7} \left(\frac{b_1}{b_2}\right)^{6/7} \tag{6.11}$$

Substituting Eq. (6.11) into Eq. (6.7), results

$$\hat{d}_s = \left(\frac{\tau_{01}}{\tau_c}\right)^{3/7} \left(\frac{b_1}{b_2}\right)^{6/7} - 1 + 1.87(1+K)\left(\frac{d_{50}}{h_1}\right)^{0.67} \left[\frac{(b_1/b_2)^{2/7}}{(\tau_{01}/\tau_c)^{6/7}} - 1\right]\left(\frac{\tau_{01}}{\tau_c}\right) \tag{6.12}$$

Neglecting the difference in the velocity heads and the loss through the transition, Eq. (6.12) reduces to

$$\hat{d}_s = \left(\frac{\tau_{01}}{\tau_c}\right)^{3/7} \left(\frac{b_1}{b_2}\right)^{6/7} - 1 \tag{6.13}$$

6.2.4 Dey and Raikar's Model

6.2.4.1 Energy and Continuity Equations

Applying the energy equation between sections 1 and 2 for the flow situation at equilibrium scour condition [Fig. 6.1(a)], one obtains

$$h_1 + \frac{U_1^2}{2g} = h_2 + \frac{U_2^2}{2g} - d_s + h_f \tag{6.14}$$

where h_f = head loss. If the contraction is gradual and smooth, the resulting head loss h_f is negligible (Graf 2003). The continuity equation is given by Eq. (6.4).

6.2.4.2 Clear-Water Scour Model

The analytical models for clear-water scour proposed by Dey and Raikar (2005) are given.

Determination of Scour Depth with Sidewall Correction:

In clear-water scour, the equilibrium scour depth d_s reaches in a long contraction, when the flow velocity U_2 in the contracted zone becomes equaling critical velocity U_c for sediments.

The flow velocity $U_2\big|_{U_2=U_c}$ in the contracted zone can be determined from the well-known equation of bed shear stress as a function of dynamic pressure. It is

$$U_2\big|_{U_2=U_c} = u_{*c}\sqrt{\frac{8}{f_b}} \tag{6.15}$$

where u_{*c} = critical shear velocity for sediment; and f_b = friction factor associated with the bed. The Colebrook-White equation, used to evaluate f_b, is given as

$$\frac{1}{\sqrt{f_b}} = -0.86\ln\left(\frac{\varepsilon P_b}{14.8A_b} + \frac{2.51}{R_b\sqrt{f_b}}\right) \tag{6.16}$$

where ε = equivalent roughness height (= $2d_{50}$); A_b = flow area associated with the bed; P_b = wetted perimeter associated with the bed (= b_2); and R_b = flow Reynolds number associated with the bed, that is $4U_2\big|_{U_2=U_c} A_b/(\nu P_b)$.

In the contracted zone, the bed is rough consisting of sediment particles and the sidewalls are smooth. Therefore, the friction factor associated with the wall f_w is considerably different from f_b. Therefore, Vanoni's (1975) method of sidewall correction is applied for the contracted zone of the channel, owing to the smooth wall and rough bed, as was done by Dey (2003a, b), where the solution for f_b was obtained from the following equations:

$$f_b = 0.316R_b\left(\frac{4U_2\big|_{U_2=U_c} A}{\nu\ P_w} - \frac{R_b P_b}{P_w}\right)^{-1.25} \tag{6.17}$$

$$\frac{1}{\sqrt{f_b}} = -0.86\ln\left(\frac{\varepsilon U_2\big|_{U_2=U_c}}{3.7\,\nu\ R_b} + \frac{2.51}{R_b\sqrt{f_b}}\right) \tag{6.18}$$

where A = total flow area of contracted zone (= h_2b_2); and P_w = wetted perimeter associated with the wall (= $2h_2$). In clear-water scour, Eq. (6.4) becomes

$$U_1h_1b_1 = U_2\big|_{U_2=U_c} h_2b_2 \tag{6.19}$$

For given data of U_1, h_1, b_1, b_2 and d_{50}, the unknowns $U_2\big|_{U_2=U_c}$, h_2, R_b and f_b can be determined numerically solving Eqs. (6.15) and (6.17) - (6.19). Then, Eq. (6.14) is used to determine equilibrium scour depth d_s as given below:

$$d_s = h_2 + \frac{U_2\big|^2_{U_2=U_c}}{2g} - h_1 - \frac{U_1^2}{2g} \tag{6.20}$$

The comparison of nondimensional equilibrium scour depths $\hat{d}_s$ computed from the analysis with the experimental data of clear-water scour is shown in Fig. 6.5(a).

Determination of Scour Depth without Sidewall Correction:

In this simplified approach, the average flow velocity in the contracted zone $U_2\big|_{U_2=U_c}$ for equilibrium scour is determined using the equation of the semi-logarithmic average velocity as

$$\frac{U_2\big|_{U_2=U_c}}{u_{*c}} = 5.75\log\frac{h_2}{2d_{50}} + 6 \tag{6.21}$$

For given data of U_1, h_1, b_1, b_2 and d_{50}, the unknowns $U_2\big|_{U_2=U_c}$ and h_2 can be obtained numerically solving Eqs. (6.19) and (6.21). Then, equilibrium scour depth d_s is determined from Eq. (6.20). The comparison of nondimensional equilibrium scour depths $\hat{d}_s$ computed from this method with the experimental data of clear-water scour is shown in Fig. 6.5(b).

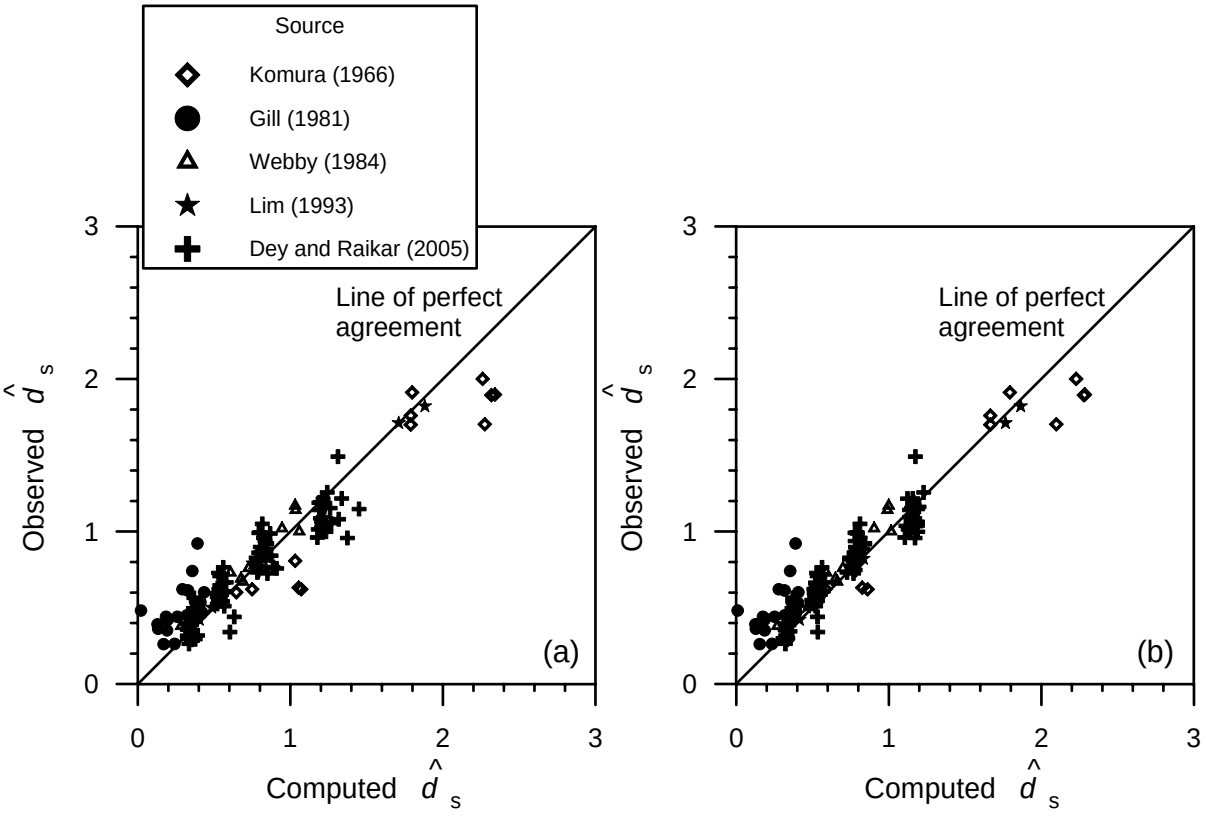

Fig. 6.5 Comparison between the measured and computed scour depths $\hat{d}_s$: (a) using clear-water scour model with sidewall correction and (b) using clear-water scour model without sidewall correction (after Dey and Raikar 2005)

6.2.4.3 Live-Bed Scour Model

Dey and Raikar (2006) proposed a live-bed scour model for the estimation of scour depth within channel contraction. In live-bed scour, the equilibrium scour depth d_s reaches, when the sediment supplied by the approaching flow into the contracted zone is balanced by the sediment transported out of the contracted zone. Thus, at equilibrium, the sediment continuity equation between sections 1 and 2 of Fig. 6.1(a) is

$$\xi\big|_{u_*=u_{*1}} b_1 = \xi\big|_{u_*=u_{*2}} b_2 \tag{6.22}$$

where ξ = bed-load transport rate of sediment. The bed-load transport rate ξ can be estimated by the formula of Engelund and Fredsøe (1976) as

$$\xi = 1.55\pi d_{50} u_* \left(1 - 0.7\frac{u_{*c}}{u_*}\right)\left[1 + \left(\frac{0.085\pi\Delta g d_{50}}{u_*^2 - u_{*c}^2}\right)^4\right]^{0.25} \tag{6.23}$$

Assuming the semi-logarithmic average velocity for approaching flow, the shear velocity u_{*1} at section 1 is obtained as

$$u_{*1} = U_1\left(5.75\log\frac{h_1}{2d_{50}} + 6\right)^{-1} \tag{6.24}$$

In the contracted zone, incorporating the semi-logarithmic average velocity in Eq. (6.4), yields

$$\frac{b_1}{b_2}\cdot\frac{h_1}{h_2} = \frac{u_{*2}}{U_1}\left(5.75\log\frac{h_2}{2d_{50}} + 6\right) \tag{6.25}$$

where u_{*2} = shear velocity in the contracted zone.

For given data of U_1, h_1, b_1, b_2 and d_{50}, the unknowns U_2 and h_2 can be determined numerically solving Eqs. (6.22), (6.23) and (6.25). Then, Eq. (6.14) is used to determine equilibrium scour depth d_s as given below:

$$d_s = h_2 + \frac{U_2^2}{2g} - h_1 - \frac{U_1^2}{2g} \tag{6.26}$$

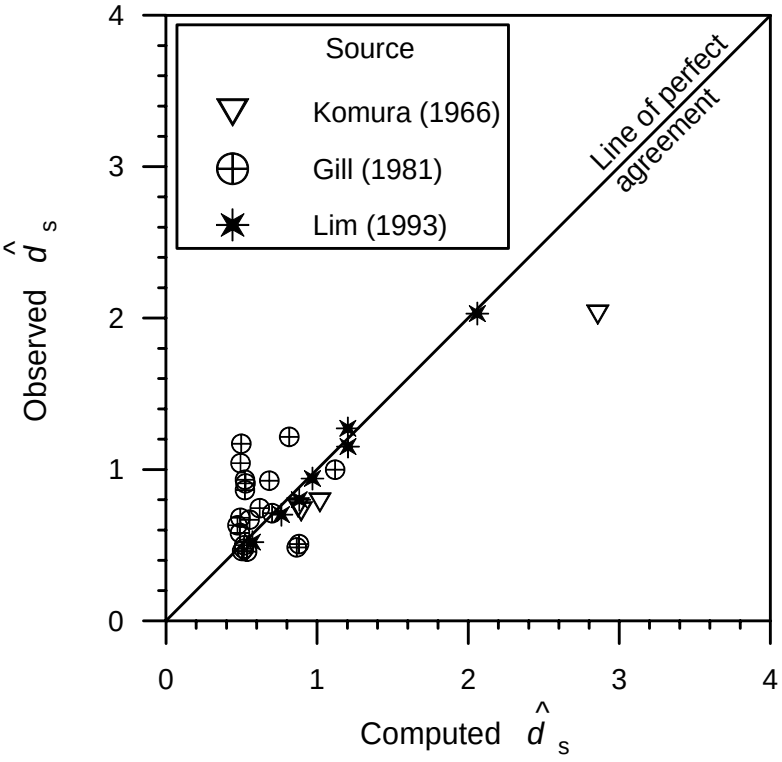

Fig. 6.6 Comparison between the equilibrium scour depths $\hat{d}_s$ computed using live-bed scour model and the experimental data (after Dey and Raikar 2006)

The comparison of nondimensional equilibrium scour depths $\hat{d}_s$ computed using the model with the live-bed scour data is shown in Fig. 6.6. It is important to mention that in case of

live-bed scour, the equilibrium scour depth fluctuates due to the passage of bed-forms over a period of time. As the present analysis does not take into account the bed-forms, the resulting equilibrium scour depth is the mean value of the instantaneous equilibrium scour depths over a period of time.

6.2.5 Comparative Study of Different Predictors of Scour Depth

Phenomena involving scour in long contractions have been studied extensively in laboratory experiments, from which a number of analytical and empirical equations have been developed to estimate the maximum equilibrium scour depth (that is design scour depth) both under clear-water and live-bed scour conditions. In general, they are based on a limited range of data. Table 1 furnishes the equations of maximum equilibrium scour depth proposed by different investigators. The comparisons of the experimental data with the scour depths computed by the equations proposed by different investigators is presented here.

Table 1. Equations of Maximum Equilibrium Scour Depth within Channel Contractions Proposed by Different Investigators

Investigator	Proposed equation	Regime
Laursen (1963)	$\hat{d}_{sm} = \hat{b}^{-0.857} - 1$	Clear-water
Komura (1966)	$\hat{d}_{sm} = 1.6F_{rc}^{0.2}\hat{b}^{-0.67}\sigma_g^{-0.5} - 1$ where $F_{rc} = U_1\big\vert_{U_1=U_c}/(gh_1)^{0.5}$.	Clear-water
	$\hat{d}_{sm} = 1.22F_{rc}^{0.2}\hat{b}^{-0.67}\sigma_g^{-0.2} - 1$	Live-bed
Gill (1981)	$\hat{d}_{sm} = 1.58\hat{b}^{-0.857} - 1$	Clear-water and live-bed
Lim (1993)	$\hat{d}_{sm} = 1.854F_0^{0.75}\hat{b}^{-0.75}\hat{d}^{0.25} - 1$	Clear-water and live-bed
Dey and Raikar (2005)	$\hat{d}_{sm} = 0.368F_{1ec}^{0.55}\hat{d}^{-0.19}\hat{b}^{-1.26}$ where $F_{1ec} = U_{1ec}/(\Delta g h_1)^{0.5}$; and U_{1ec} = excess critical approaching flow velocity	Clear-water

Note: In order to get maximum $\hat{d}_{sm}$, equations of $\hat{d}_{sm}$ are expressed for $U_1/U_c \to 1$ or $u_{*1}/u_{*c} \to 1$. For uniform sediments, geometric standard deviation σ_g is considered to be unity.

6.2.5.1 Predictors under Clear-Water Scour Condition

The comparisons between the observed scour depths and computed scour depths using different existing equations (Table 1) for clear-water scour are shown in Fig. 6.7. The equation proposed by Laursen (1963) underestimates observed scour depths to some extent being not safe for the design purpose, as a large number of data lie above the line of perfect agreement. On the other hand, the equation of Gill (1981) is very conservative (uneconomical), as all the scour data lie well below the line of perfect agreement (maximum 6 times the observed data). The equations recommended by Komura (1966), Lim (1993) and Dey and Raikar (2005) provide a reasonable estimation of scour depth in long contractions, as they envelop almost all data and over predict less than Gill's (1981) equation.

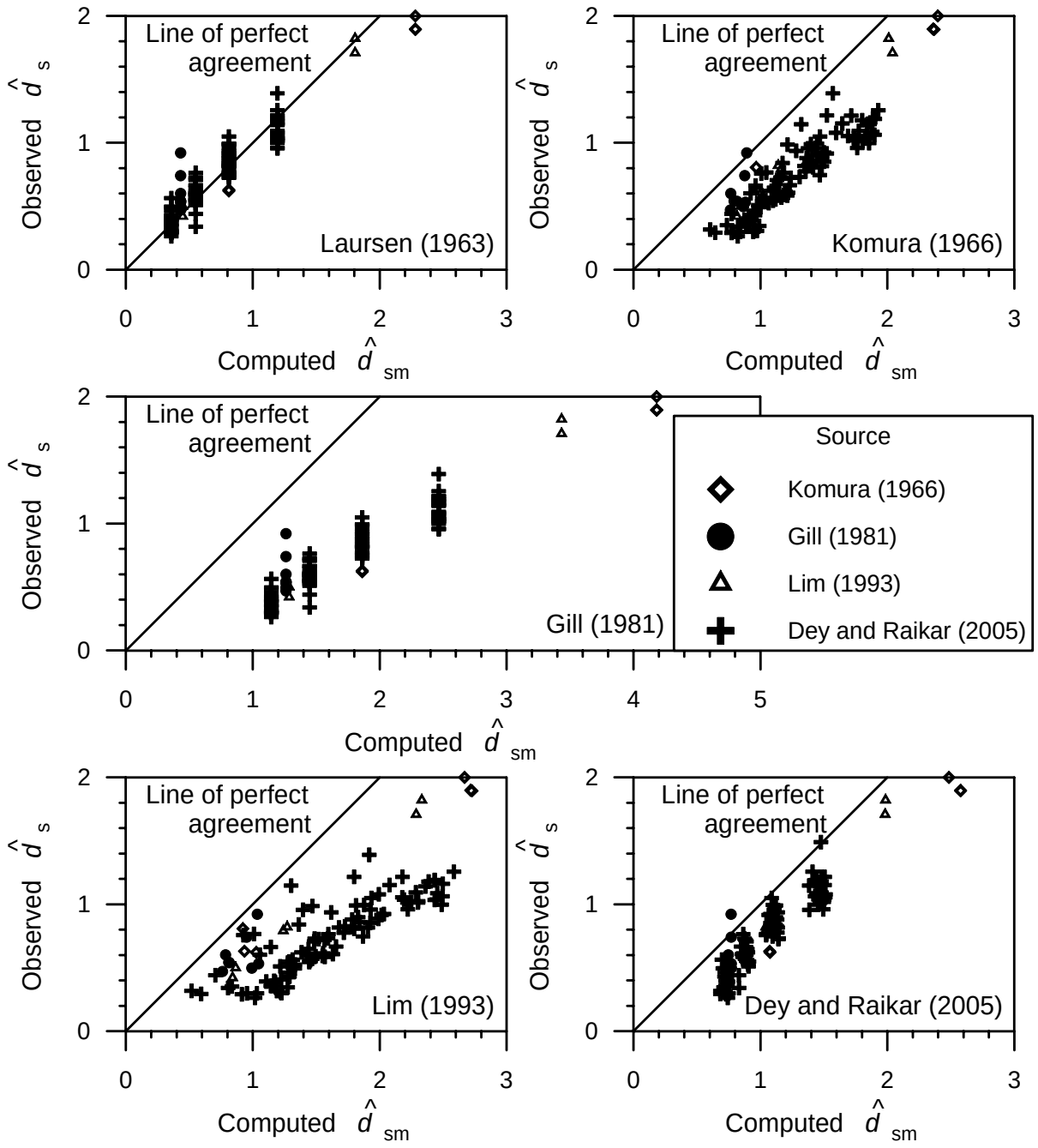

Fig. 6.7 Comparisons of the equations of maximum equilibrium scour depth $\hat{d}_{sm}$ proposed by different investigators with the experimental data for clear-water scour

6.2.5.2 Predictors under Live-Bed Scour Condition

The comparisons between the observed scour depths and the computed scour depths using different existing equations (Table 1) for live-bed scour are shown in Fig. 6.8. The equation proposed by Komura (1966) underestimates observed scour depths and is unsafe for the design purpose, because almost all data lie above the line of perfect agreement. On the other hand, the equation of Gill (1981) is uneconomical, as all the scour data lie well below the line of perfect agreement. The equation recommended by Lim (1993) provides a satisfactory estimation of scour depth in long contractions, as most of data lie along the line of perfect agreement.

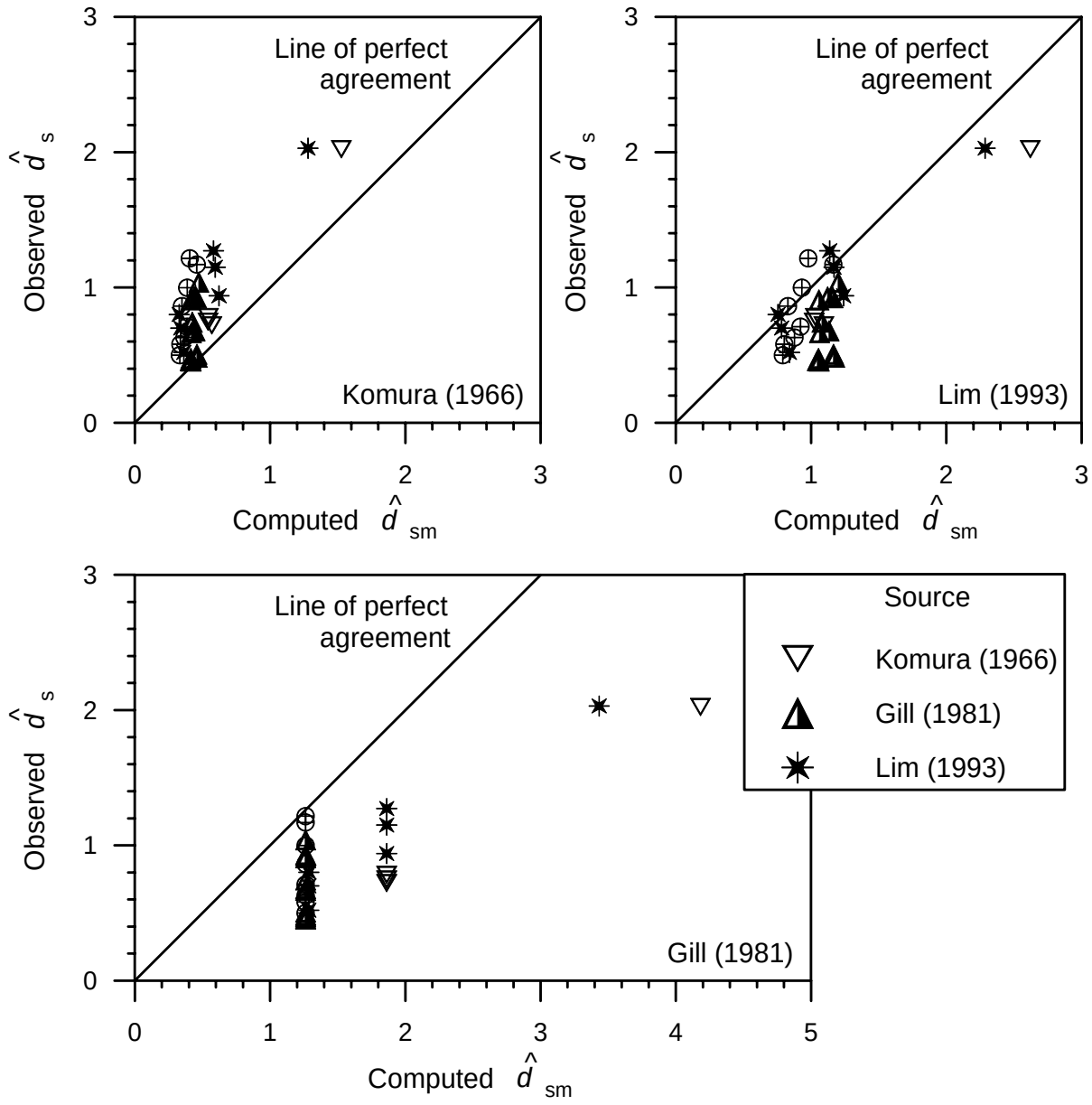

Fig. 6.8 Comparisons of the equations of maximum equilibrium scour depth $\hat{d}_{sm}$ proposed by different investigators with the experimental data for live-bed scour

6.2.6 Example

Estimate the maximum equilibrium scour depth within a long contraction for the following data:

- Approaching channel width, $b_1 = 70$ m
- Channel width at contracted zone, $b_2 = 46$ m
- Median size of sediment, $d_{50} = 2.6$ mm
- Geometric standard deviation of sediment, $\sigma_g = 2.84$
- Approaching flow depth, $h_1 = 1.8$ m
- Approaching flow velocity, $U_1 = 1.76$ m/s

For d_{50} = 2.6 mm, the critical shear velocity u_{*c} is calculated from Eq. (2.30a) – (2.30e) as 0.0429 m/s. From Eq. (6.21) replacing $U_2\big|_{U_2=U_c}$ by $U_1\big|_{U_1=U_c}$ and h_2 by h_1, the average critical flow velocity $U_1\big|_{U_1=U_c}$ corresponding to h_1 = 1.8 m is obtained as 0.884 m/s. Hence, with U_{1ec} as $U_1 - U_1\big|_{U_1=U_c}$, $F_{1ec} = U_{1ec}/(\Delta g h_1)^{0.5} = 0.164$.

Using $\hat{b} = b_2/b_1 = 0.657$ and $\hat{d} = d_{50}/h_1 = 0.00144$ in Dey and Raikar's (2005) equation given in Table 1, the value of $\hat{d}_{sm}$ is 0.8. Therefore, the maximum equilibrium scour depth d_{sm} for uniform sediment is 1.44 m.

For nonuniform sediment, with σ_g = 2.84 for which K_σ = 0.31 (obtained from Fig. 6.4), the maximum equilibrium scour depth d_{sm} is estimated as 0.447 m.

6.3 Scour Downstream of a Structure

Hydraulic structures, such as weirs, stilling basins, diversion work and sills, dams etc., are constructed in the channels and rivers in order to regulate the flow discharge in the channels. It may be for the control of flood discharge, for the generation of electricity and for other purposes. The water released from these structures impinges on the free surface of the tailwater as a jet, which is called *plunging jet*. This freely falling jet may have considerable potential to scour the downstream bed of the structures and such scour is known as *jet scour*. Scour due to jets develops very rapidly, which causes danger to the stability of the channel bed, in addition to the devastating effects on the hydraulic structures. Hence, the scour downstream of a hydraulic structure is the problem of importance to the engineers. Fig. 6.9 shows various hydraulic structures, which come under the group of this study.

The pioneering study on such type of scour was due to Schoklitsch (1932). He proposed the following empirical relationship for the scour depth for the flow over structures:

$$d_s = \frac{4.75 q^{0.57} H^{0.2}}{d_{90}^{0.32}} - h_t \tag{6.27}$$

where q = discharge per unit width; H = height between upstream and downstream water levels; d_{90} = 90% finer sediment; and h_t = tailwater depth.

Based on the dimensional analysis and using experimental data, Kotoulas (1967) developed a relationship for the equilibrium scour depth downstream of a structure. It is

$$d_s = \frac{1.9}{g^{0.35}} \left(\frac{H^{0.35} q^{0.7}}{d_{95}^{0.4}} \right) - h_t \tag{6.28}$$

where d_{95} = 95% finer sediment.

Bormann and Julien (1991) investigated the scour downstream of grade-control structures based on two-dimensional jet diffusion and particle stability and put forward the following expression for the scour depth:

$$d_s = \frac{k_b q^{0.6} U_1 \sin\theta}{(2\Delta g)^{0.8} d_{90}^{0.4}} - D_p \tag{6.29}$$

where k_b = coefficient = $3.24[\sin\varphi/\sin(\varphi + \theta)]^{0.8}$; $U_1 = (2gH)^{0.5}$, that is the jet velocity entering tailwater; D_p = drop height of grade-control structure; θ = jet angle near surface; and φ = angle of repose of bed sediment.

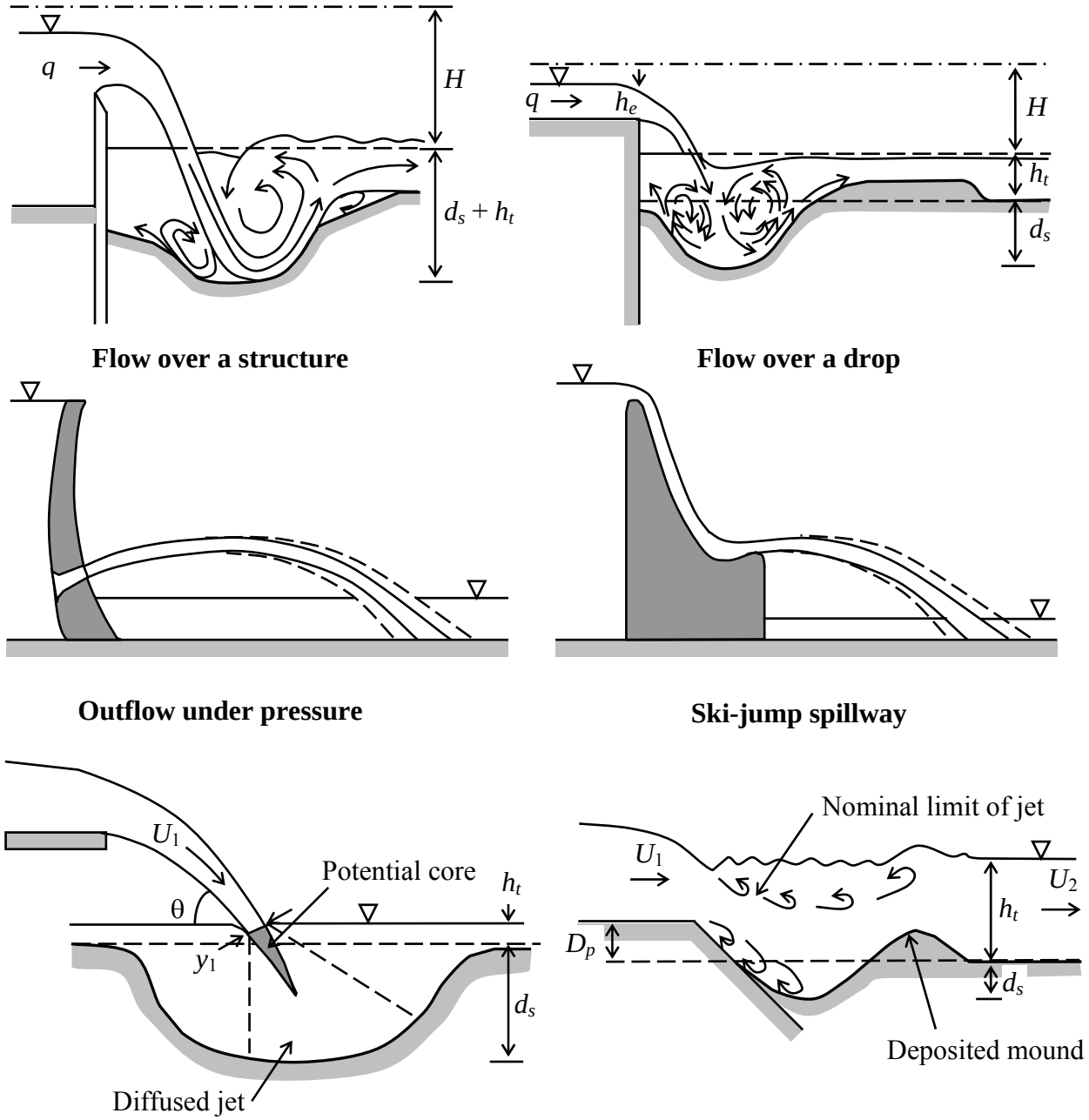

Fig. 6.9 Schematic of flow over different hydraulic structures

Fahlbusch (1994) derived the relationship to predict the equilibrium scour depth downstream of a dam as

$$d_s = \frac{20}{\lambda}\sqrt{\frac{qU_1 \sin\theta}{g}} - h_t \tag{6.30}$$

where λ = scour factor that depends on d_{90} (see Fig. 6.10).

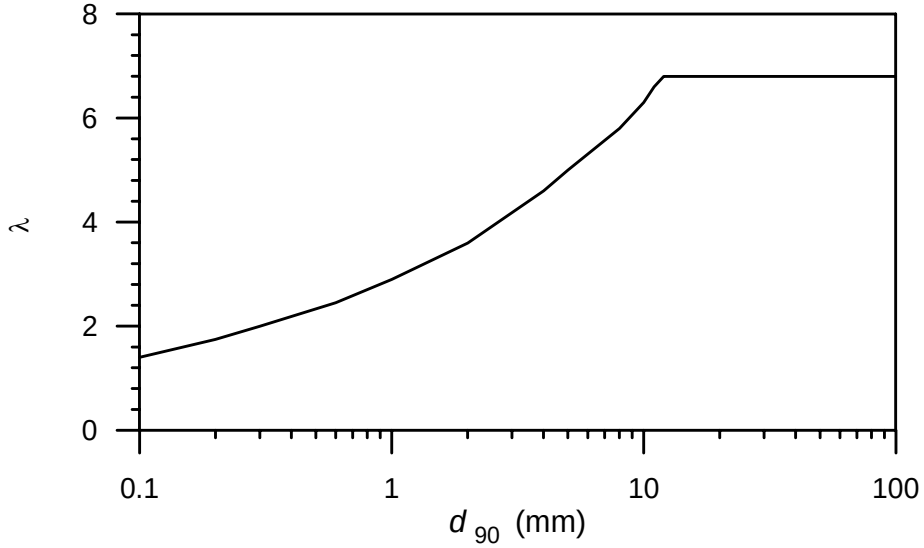

Fig. 6.10 Scour factor λ as a function of d_{90} (after Fahlbusch 1994)

Stein et al. (1993) developed an analytically equation to predict the equilibrium scour depth downstream of a head-cut. That is

$$d_s = \frac{C_d^2 C_f \rho U_1^2 y_1}{\tau_c} \sin\theta \tag{6.31}$$

where C_d = diffusion coefficient; C_f = friction coefficient; y_1 = initial jet thickness; and τ_c = critical shear stress of bed sediment.

In spite of variations in the form of equations and coefficients, the relationships predict the scour depth reasonably. Out of these equations, the scour depth relationship proposed by Schoklitsch (1932) yields excellent results (Hoffmans and Verheij 1997).

6.3.1 Scour Downstream of Two-Dimensional Culverts

Two-dimensional culverts refer to jet flow under hydraulic structures having considerable width. Many forms of jets can occur, such as free jets, submerged jets etc. Fig. 6.11 depicts different types of horizontal jets. The jets can even be vertical or inclined also. Flow through these jets has a substantial scour potential. On the other hand, the flow through circular, square and other shaped outlets is considered as three-dimensional culvert flow. These culverts are designed as cross-drains across the roadway embankments. These outlets discharge water where the tailwater depth is usually less than the diameter or the width of the outlet. Scour hole developed downstream of these culverts is three-dimensional. Sometimes, three-dimensional scour pattern also occur in which the tailwater depth is relatively high. In case of larger tailwater depths, a submerged hydraulic jump is formed and the turbulence is very high resulting in severe scouring than unsubmerged jet scour.

Rajarathnam and Berry (1977) proposed the following relationship for the equilibrium scour depth downstream of a circular culvert under submerged condition as

$$d_s = 0.4D(F_0 - 2) \qquad 2 < F_0 < 14 \tag{6.32}$$

where D = pipe diameter of circular culvert; $F_0 = U_1/(\Delta g d_{50})^{0.5}$, that is the densimetric Froude number; and U_1 = jet velocity.

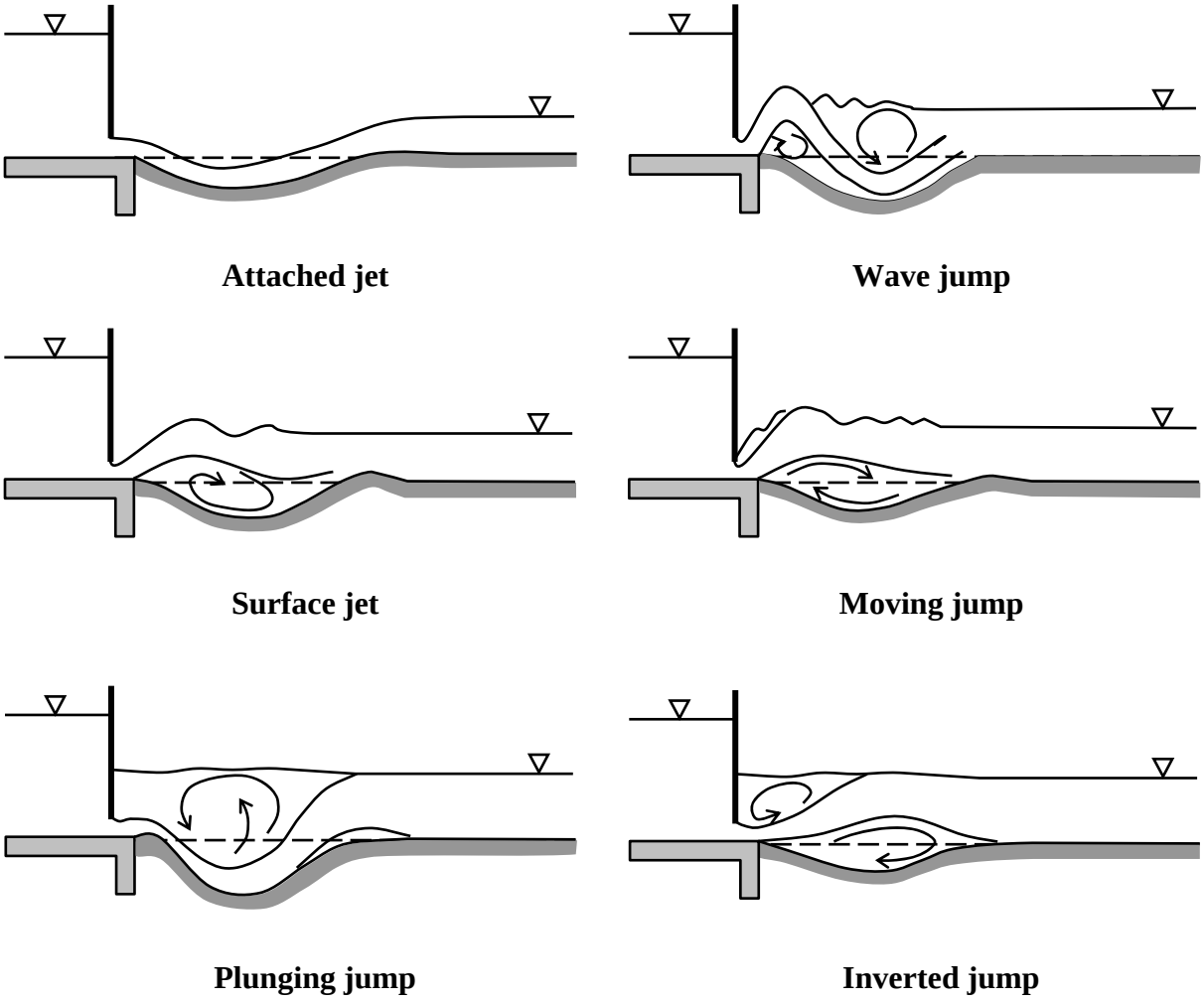

Fig. 6.11 Two-dimensional horizontal jets

Ruff et al. (1982) put forward the expression for the scour depth downstream of circular culvert. It is

$$d_s = 2.07D(Q/\sqrt{gD^5})^{0.45} \tag{6.33}$$

where Q = discharge through the culvert.

Breusers and Raudkivi (1991) obtained the following relationship for the scour depth downstream of a circular culvert, using the assumption that the maximum flow velocity in the jet never exceeds the critical flow velocity as

$$d_s = 0.08DU_1/u_{*c} \tag{6.34}$$

where u_{*c} = critical shear velocity for bed sediment.

Hoffmans (1997) developed a simple method for the estimation of maximum scour depth based on the momentum principle. It is

$$d_s = \frac{7}{\lambda}\left[\frac{Q(U_1 - U_2)}{g}\right]^{1/3} \tag{6.35}$$

It is important to mention that the above equations [Eqs. (6.32) – (6.35)] can only be used for the initial approximation of the magnitude of the equilibrium scour depth. However, the actual scour depths are to be determined by physical model studies.

6.4 Scour Downstream of an Apron due to Submerged Jets

The scouring downstream of an apron is complex in nature owing to the abrupt change of the flow characteristics on the sediment bed with time (Fig. 6.12). Scour initiates at the downstream edge of the apron when the bed shear stress exerted by the submerged jet exceeds the critical bed shear stress for the bed sediments. The evolution of the vertical dimension of scour hole is faster than the longitudinal one. In the initial stage, the suspension of sediments is the only means of sediment transport. But with the development of the vertical dimension of scour hole, the mode of sediment transport changes to a combination of suspended- and bed-loads. As the flow separation takes place at the edge of the apron having a reattachment of flow at the deepest point of the scour hole, the movement of the sediment particles is divided into two parts. Some amount of sediments moves along the downstream slope of the scour hole and ultimately goes out of the scour hole. The other part is moved back towards the upstream along the upstream slope of the scour hole by the reversed flow. The down-slope sliding and rolling movement of sediments takes place when the reversed flow becomes feeble with the development of scour hole. The upstream portion of the scour hole achieves a steep slope.

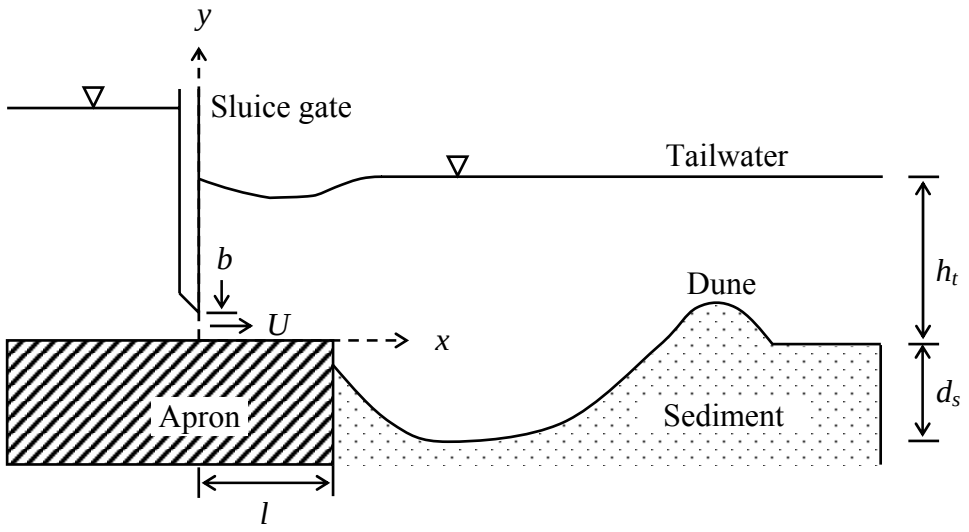

Fig. 6.12 Schematic of scour hole downstream of an apron due to submerged jet

6.4.1 Flow Field in Developing Scour Hole

Fig. 6.12 describes a schematic of scour downstream of an apron due to submerged jet issuing from a sluice opening and the coordinate system. The time-averaged velocity components are (u, v) in (x, y). The distributions of velocity vectors are represented in a normalized $\hat{x}\hat{y}$-plane at different streamwise distances $\hat{x}$ from the sluice opening; where $\hat{x}$ is x/b; $\hat{y}$ is y/b; and b is the sluice opening. Figs. 6.13(a) - 6.13(d) represent the normalized velocity vectors in submerged jets over the initial flat sediment bed, intermediate scour holes (having 0.3 and 0.8 times the equilibrium scour depth d_{se}) and equilibrium scour hole downstream of an apron detected by an acoustic Doppler velocimeter (ADV) [see Sarkar (2005)]. The magnitude and the direction of velocity vectors are $(\hat{u}^2 + \hat{v}^2)^{0.5}$ and $\arctan(\hat{v}/\hat{u})$, respectively, where $\hat{u}$ is u/U; and $\hat{v}$ is v/U; and U is the issuing jet velocity.

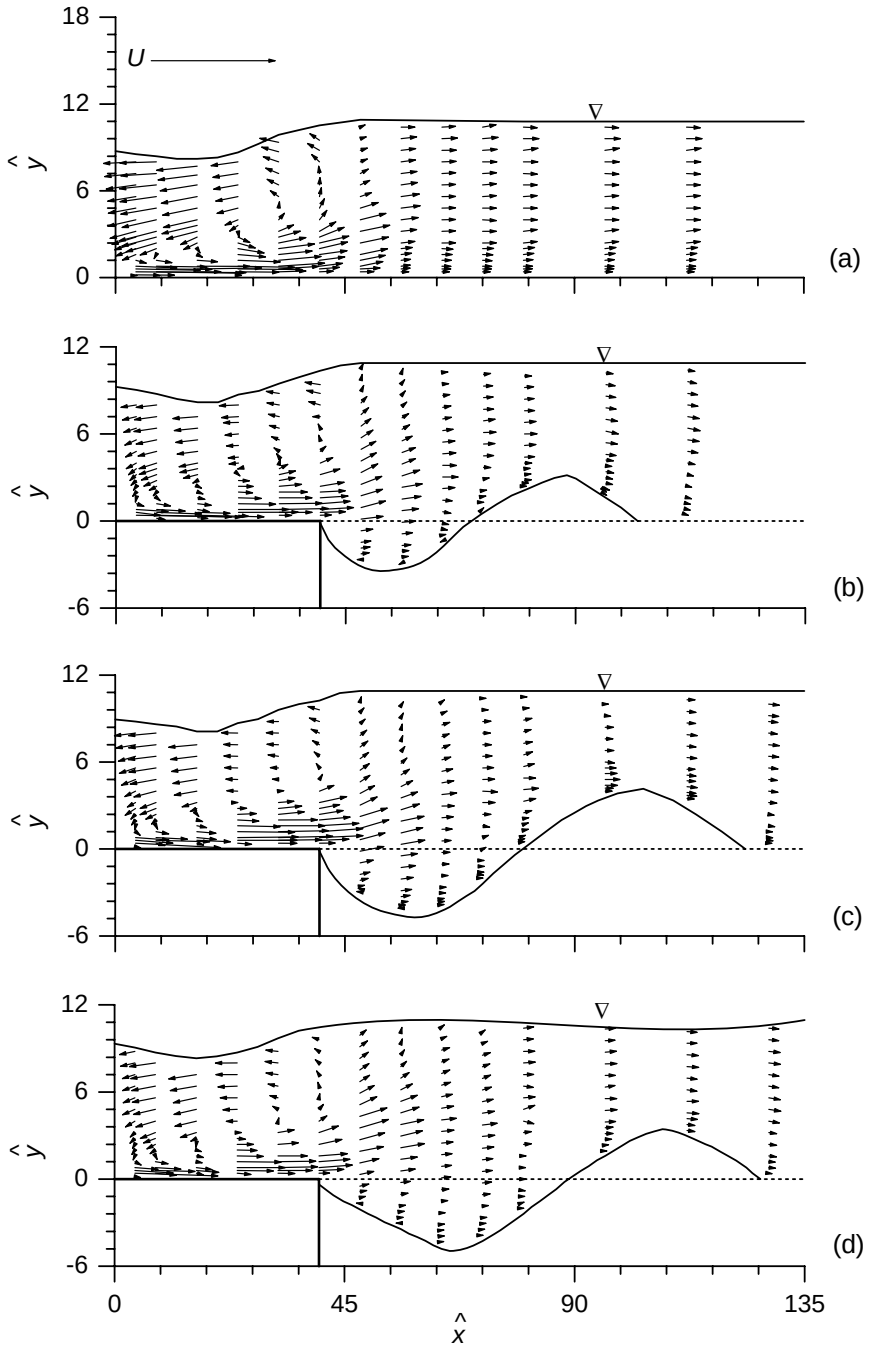

Fig. 6.13 Normalized velocity vectors for (a) flat bed condition; (b) intermediate scour hole with $0.3d_{se}$; (c) intermediate scour hole with $0.8d_{se}$ and (d) equilibrium scour depth with $d_{se} = 0.062$ m

The characteristics of the decay of jet including a vortical flow in the fully developed zone over the apron and the sediment beds (initial flat bed, intermediate scour holes and equilibrium scour hole) are apparent [Figs. 6.13(a) – 6.13(d)]. The growth rate of the boundary layer over the apron is slower than that over the scoured bed due to an increase in flow depth within the scour hole. To be more explicit, the growth rate of the boundary layer within an intermediate scour hole is less than that within equilibrium scour hole. Consequently, the rate of decay of the submerged jets is higher within the scour hole in general and with increased scour hole dimensions in particular. The reversal nature of the

velocity indicates a strong vortical flow (that is the surface roller). However, the submerged jet travels above the original bed level in the scoured zone and is attenuating in nature. On the other hand, below the original bed level in the scoured zone, the jet velocities diminish with an increase in scour hole dimension.

6.4.2 Effects of Different Parameters on Scour Depth

Experimental data of Dey and Sarkar (2006) are used in Fig. 6.14 to show the variation of nondimensional equilibrium scour depth $\tilde{d}_{se}$ (= d_{se}/b) with sediment size - sluice opening ratio $\tilde{d}$ (= d_{50}/b) for different apron lengths l and jet Froude numbers F_u [= $U/(gb)^{0.5}$]. It is evident that the equilibrium scour depth $\tilde{d}_{se}$ decreases with an increase in $\tilde{d}$. It implies that d_{se} is less for relatively coarse sediment. To be more explicit, with the development of scour hole, the bed shear stress acting on the scour hole reduces. Thus, for coarser sediments, which need relatively more critical bed shear stress to initiate motion, the equilibrium scour reaches at a lesser scour depth d_{se}. The most interesting feature of the curves is that $\tilde{d}_{se}$ decreases sharply for $\tilde{d}$ < 0.1. Then, the rate of reduction of $\tilde{d}_{se}$ falls down, becoming independent of $\tilde{d}$ for $\tilde{d}$ > 0.3. The curves also show that scour depth $\tilde{d}_{se}$ increases with a decrease in l. The submerged jet loses its erosive power through the decaying process over the apron before encountering the sediment bed. A reduction of l increases the erosive power of the jet, which exerts greater bed shear stress over the sediment bed resulting in an increase of d_{se}.

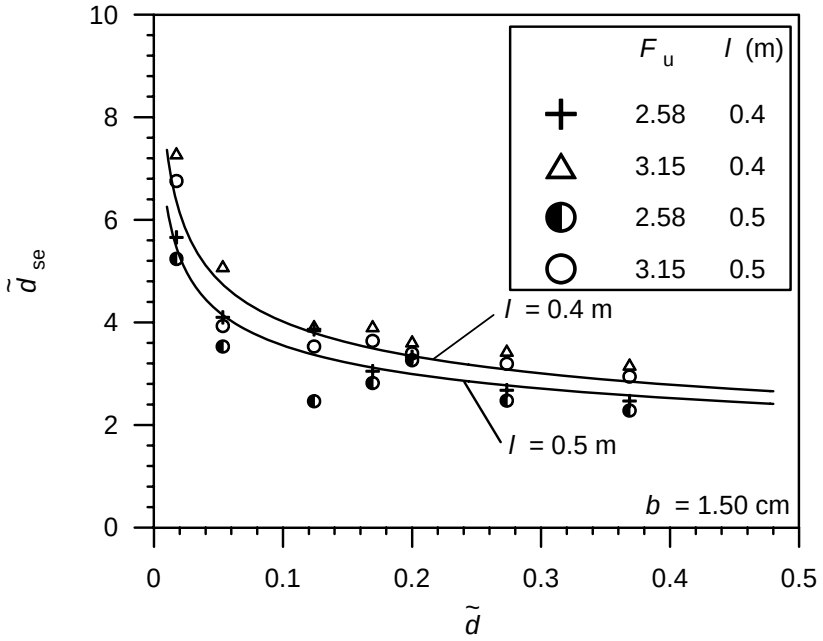

Fig. 6.14 Variation of $\tilde{d}_{se}$ with $\tilde{d}$ for different l and F_u (after Dey and Sarkar 2006)

Using the experimental data of Dey and Sarkar (2006), the dependency of $\tilde{d}_{se}$ on densimetric Froude number F_0 for different l and d_{50} is shown in Fig. 6.15. The equilibrium scour depth $\tilde{d}_{se}$ increases with an increase in F_0. As $F_0 \sim U$ and $F_0 \sim d_{50}^{-0.5}$, $\tilde{d}_{se}$ increases with an increase in U and with a decrease in d_{50}. The rate of increase of $\tilde{d}_{se}$ is more for lower

F_0, whereas for higher F_0 ($F_0 > 12$), it drops down becoming almost independent of F_0. It is also evident that for a given F_0, $\tilde{d}_{se}$ decreases with an increase in l.

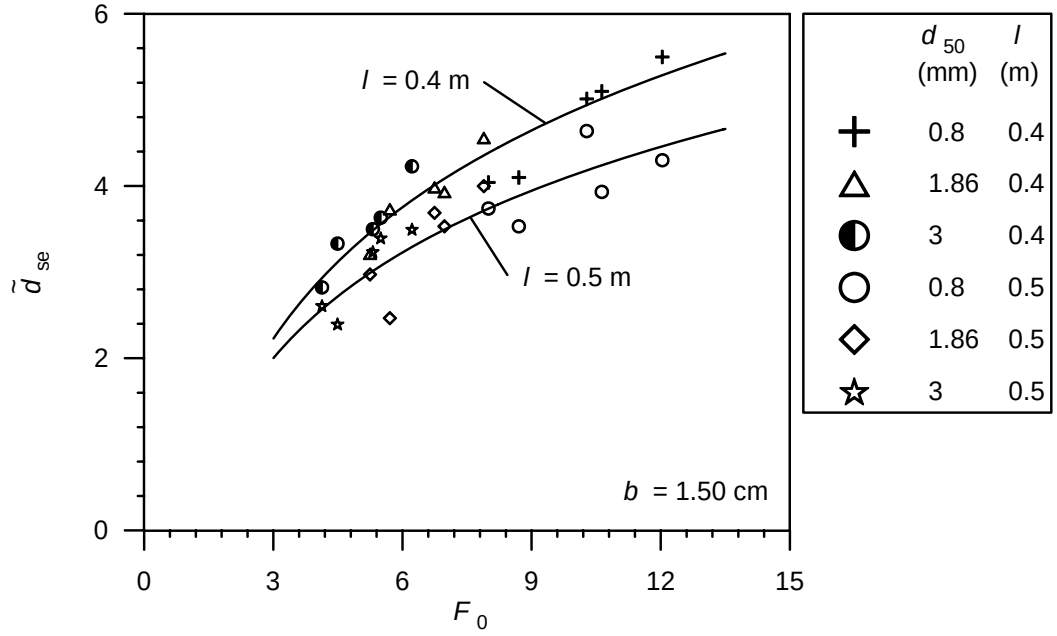

Fig. 6.15 Variation of $\tilde{d}_{se}$ with F_0 for different l and d_{50} (after Dey and Sarkar 2006)

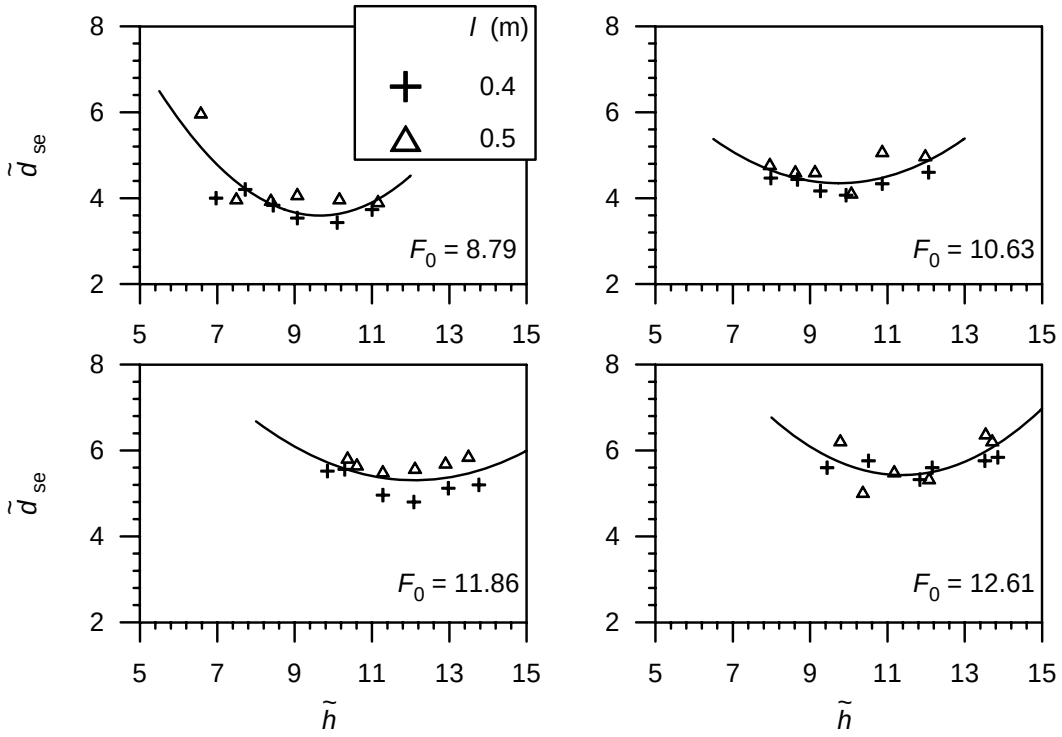

Fig. 6.16 Variation of $\tilde{d}_{se}$ with $\tilde{h}$ for different l and F_0 (after Dey and Sarkar 2006)

Fig. 6.16 depicts $\tilde{d}_{se}$ as a function of tailwater depth - sluice opening ratio $\tilde{h}$ (= h_t/b) for different l and F_0, using the experimental data of Dey and Sarkar (2006). The variation of $\tilde{d}_{se}$

with $\tilde{h}$ is sagging in nature. Hence, a critical value of tailwater depth exists corresponding to a minimum value of $\tilde{d}_{se}$.

The laboratory experimental data (Dey and Sarkar 2006) of scour depth for different sediment gradations of well-graded nonuniform sediments, tested for b = 0.15 m and l = 0.5 m, are used to plot Fig. 6.17, which shows the variation of coefficient K_σ with geometric standard deviation of particle size distribution σ_g. The sediment gradation has a pronounced influence on the scour depth. It is apparent from the mean curve drawn through the experimental data that the scour depth in nonuniform sediment having σ_g = 4 is drastically reduced to 54% of the scour depth in uniform sediment. In nonuniform sediments, a process of armoring in the scour hole commences resulting in an exposure of coarser particles due to washing out the finer fraction. The armor-layer causes a gradual increase in the effective critical bed shear stress that restricts the development of scour hole.

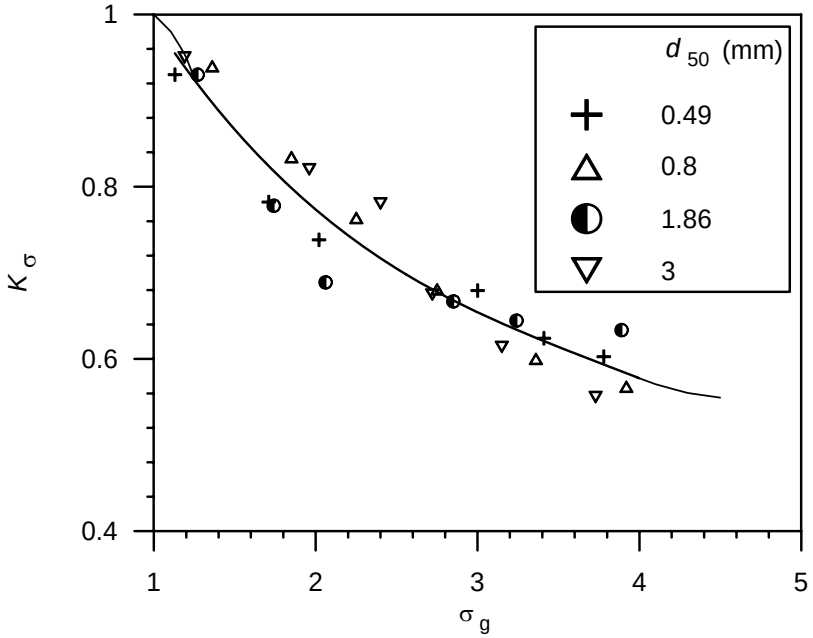

Fig. 6.17 Coefficient K_σ as a function of σ_g (after Dey and Sarkar 2006)

Dey and Sarkar (2006) proposed an equation of nondimensional maximum scour depth downstream of an apron due to submerged jets issuing from a sluice opening. It is

$$\tilde{d}_{se} = 2.59 F_0^{0.94} \tilde{l}^{-0.37} \tilde{h}^{0.16} \tilde{d}^{0.25} \tag{6.36}$$

where $\tilde{l} = l/b$. The range of applicability of the above equation is $6.57 \le \tilde{h} \le 13.85$ and $\tilde{l} > 26$.

6.5 Scour below Horizontal Pipes

Pipelines are laid on riverbeds to transport gas and crude oil and also to dispose of the wastewater. Thus, scour occurs below the pipeline under the action of flow. This may cause the suspension of pipeline along its length.

Initiation of Scour:

When a pipeline laid on an erodible bed with little embedment is subjected to strong flow, the pressure difference is set up between the two sides of the pipe. Due to this pressure difference the seepage flow takes place below the pipeline and as a result the sediment bed below the pipeline gets scoured. This is called initiation of scour. The critical condition for the initiation of scour was studied by many investigators (Sumer and Fredsøe 2002). The mechanism of the initiation of scour below the pipeline under the steady flow is presented below.

The pressure difference induced between the upstream and downstream sides of a pipe laid on a sediment bed under the action of flow exerts a seepage flow in the sand bed below the pipeline. Fig. 6.18(a) shows the pressure difference setup below a pipe. With an increase in flow velocity, a critical point is reached at which the rate of seepage flow increases more rapidly than the order of the driving pressure difference, and at the same time the surface of the sand in the immediate downstream of the pipe rises. The mixture of sediment and water breaks through the space underneath the pipe and this process is called *piping*. At equilibrium, the forces acting on an element of sediment bed of volume $\Delta x \times 1 \times 1$ are:

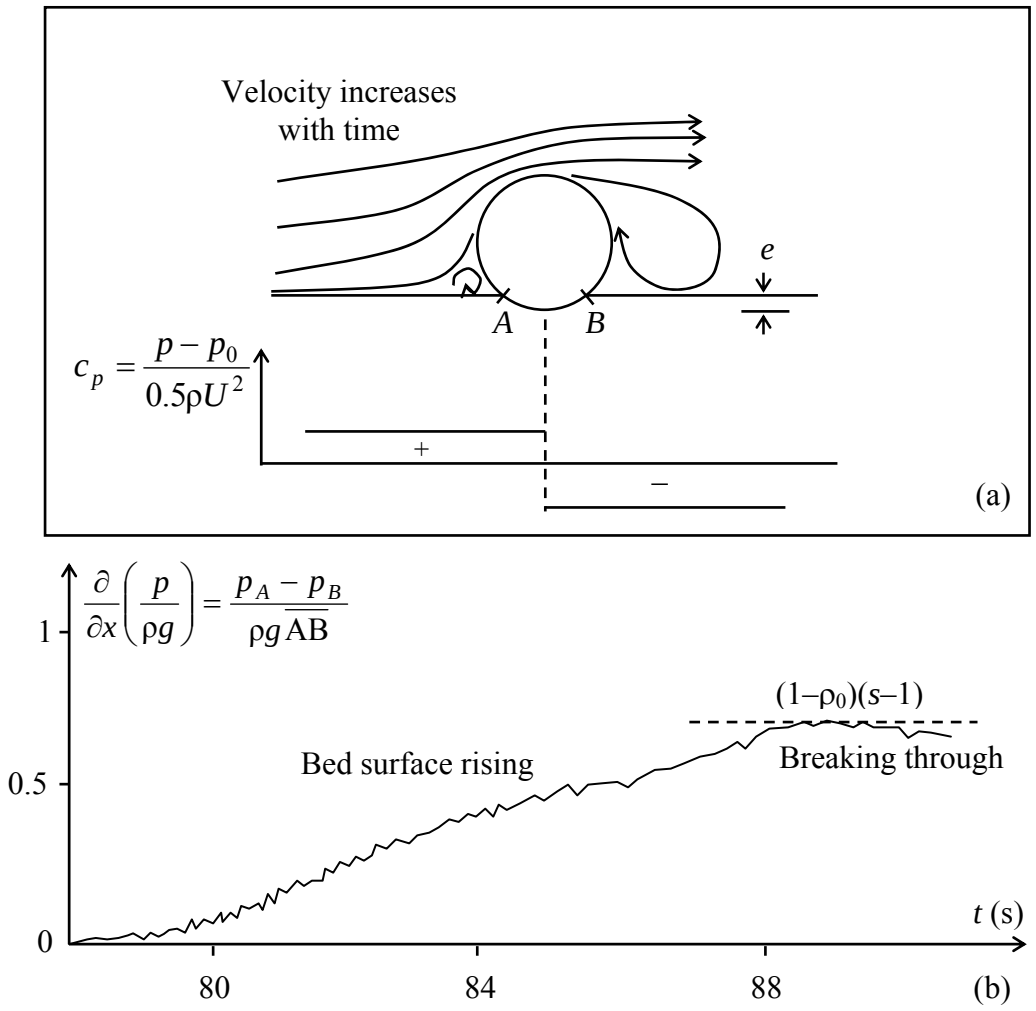

Fig. 6.18 (a) Pressure distribution and (b) time series of pressure gradient below a pipeline (after Sumer et al. 2001)

1. The seepage (driving) force P given by

$$P = \frac{\partial p}{\partial x}\Delta x \tag{6.37}$$

where p = pressure intensity; and x = distance along the perimeter of the pipe.

2. The submerged weight W of the sediment

$$W = \rho g(s-1)(1-\rho_0)\Delta x \tag{6.38}$$

where ρ_0 = porosity of sediment.

At equilibrium

$$P \geq W \tag{6.39}$$

Using Eqs. (6.37) and (6.38) into Eq. (6.39), yields

$$\frac{\partial}{\partial x}\left(\frac{p}{\rho g}\right) \geq (s-1)(1-\rho_0) \tag{6.40}$$

The time series of pressure gradient $\partial(p/\rho g)/\partial x$ measured by Sumer et al. (2001) is presented in Fig. 6.18(b). The following observations were made by Sumer and Fredsøe (2002):

1. As the flow velocity increases, the pressure gradient is enhanced (because pressure intensity is proportional to square of the velocity).
2. With an increase in pressure gradient, a critical condition is reached at which the sediment in the immediate downstream of the pipe begins to rise.
3. This stage continues for a short period (about 5 s), and subsequently, a mixture of sediment and water breaks through. At this instant, the pressure gradient exceeds the floatation gradient $(s - 1)(1 - \rho_0)$ and the sediment is continuously removed.

The initiation of scour does not occur all along the length of the pipe simultaneously, but occurs locally. Eq. (6.40) can be written in the nondimensional form as

$$\left[\frac{\partial \hat{p}}{\partial \hat{x}} \cdot \frac{U^2}{gD(s-1)(1-\rho_0)} + C\right]_{cr} \geq 1 \tag{6.41}$$

where $\hat{p} = p/\rho U^2$; $\hat{x} = x/D$; U = flow velocity at the top of the pipe; D = diameter of pipe; and C = a nondimensional term that accounts for the effect of the vortices developed in front of the pipe and in the lee wake. The terms $\partial \hat{p}/\partial \hat{x}$ and C are functions of the burial depth - pipe diameter ratio (e/D). Hence, Eq. (6.41) becomes

$$\hat{U}_{cr} \geq f\left(\frac{e}{D}\right) \tag{6.42}$$

where $\hat{U} = U^2/[gD(s\text{-}1)(1\text{-}\rho_0)]$. Eq. (6.42) is called the *criterion for the initiation of scour*. The function $f(e/D)$ is determined experimentally. It is important to mention that the function f not only depends on e/D ratio, but also on pipe Reynolds number $R = UD/\nu$ and relative roughness $\hat{k}$ (= k_s/D, where k_s = surface roughness of pipe). However, the influence of the relative roughness is negligible when change in flow regime (from subcritical to supercritical or from superctitical to transcritical) is insignificant. The variation of criterion for the initiation of scour with e/D-ratio is shown in Fig. 6.19.

After the piping process, a small gap δ ($\delta << D$) is developed between the pipe and the bed. A considerable amount of water is diverted through this gap leading to flow concentration in the gap, which enhances the shear stress acting on the bed just below the pipeline. The increase in bed shear stress is of the order of magnitude equal to three times the bed shear stress in the approaching flow. As a result, a large amount of sediment is scoured below the

pipeline. The sediment-water mixture flows in the form of violent jet. Such scour process is known as *tunnel erosion* (see Fig. 6.20). With an increase in gap size, the gap velocity decreases and the tunnel erosion seizes. This stage is followed by *lee-wake erosion*.

As a result of tunnel erosion, a dune is formed on the downstream end of the pipe, which gradually migrates further downstream. Finally, the dune disappears as the scour progresses. At this stage, the scour is governed by the lee-wake erosion, which occurs due to the vortex shedding on the downstream end of the pipe (Fig. 6.21).

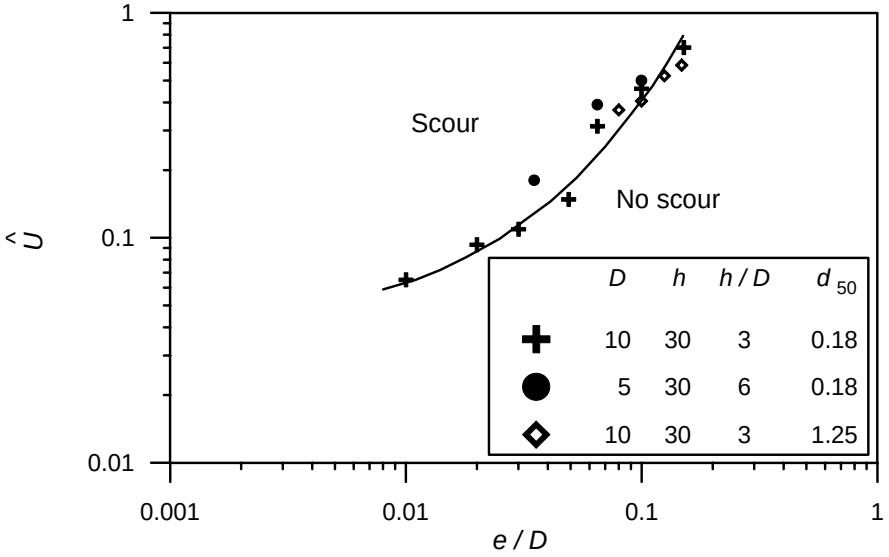

Fig. 6.19 Initiation of scour under flow (after Sumer et al. 2001)

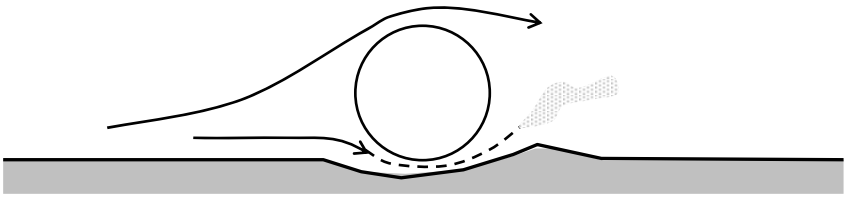

Fig. 6.20 Tunnel erosion below a pipeline

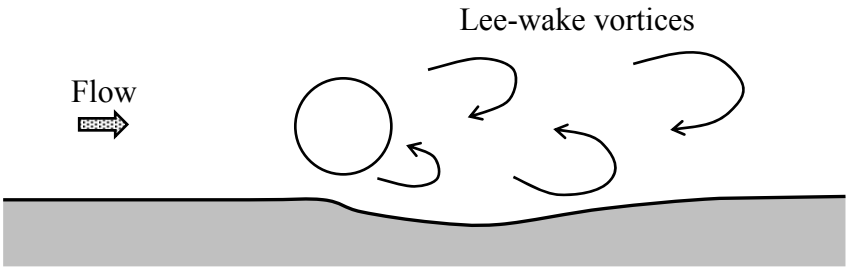

Fig. 6.21 Lee-wake erosion and vortices shedding downstream of a pipe

When the gap between the pipe and bed reaches a certain value at the end of the tunnel erosion, the vortex shedding begins. The vortices that shed from the bed of the pipe sweep the

sediment as they get convected downstream. During this period the Shields parameter Θ increases approximately by 4 times indicating the greater scour potential at the lee side of the pipe. The vortex shedding is established within the first 15 minutes and subsequently, the scour downstream end of the pipe occurs under the action of the systematic wake flow, that is an agglomeration of separation of vortices that shed from the pipe and steadily convected downstream. The equilibrium is attained when the bed shear stress below the pipe reaches the value equal to the approaching bed shear stress. Fig. 6.22 illustrates the results of typical scour test below a pipe with no initial gap and subjected to a steady flow. It shows how the scouring process evolves with time. The broken line represents the equilibrium scour profile.

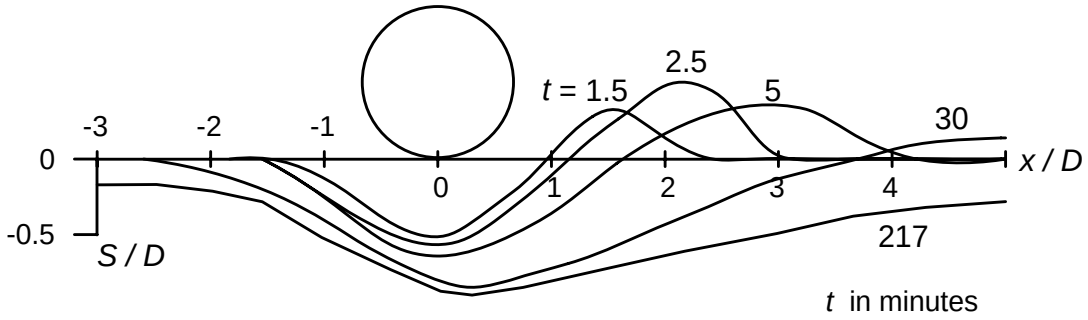

Fig. 6.22 Scour development (after Mao 1986)

Initially, the scour breaks out underneath the pipe locally, and it propagates along the length of the pipeline in both the direction. The scour hole is interrupted by stretches, called span shoulders, where the pipe gets supported. However, after a reasonable developed stage, the scour in the middle part of a scour hole can be considered as two-dimensional. The lee-wake erosion succeeds tunnel erosion in such cases.

6.5.1 Scour Depth

Many investigators have proposed the relationships for the estimation of equilibrium scour depth *S* below the pipeline. Kjeldsen et al. (1973) were the initiators to establish an empirical relationship for equilibrium scour depth under live-bed scour condition. It is

$$S = 0.972\left(\frac{U^2}{2g}\right)^{0.2} D^{0.8} \tag{6.43}$$

Eq. (6.43) can be expressed in nondimensional form as

$$\frac{S}{D} \sim \Theta^{0.2} \tag{6.44}$$

Using the dimensional analysis, the functional form for the nondimensional scour depth is

$$\frac{S}{D} = f(\hat{k}, R, \Theta) \tag{6.45}$$

The influence of $\hat{k}$ and *R* exist on the downstream flow of the pipe. For hydraulically rough pipes, the pipe Reynolds number *R* does not affect the wake flow, while for hydraulically smooth pipes, *R* has influence on the downstream vortex shedding. Fig. 6.23 presents the data plot of Kjeldsen et al. (1973), Lucassen (1984), Mao (1986) and Kristiansen (1988) on scour depth. It depicts the feeble influence of *R* on the scour depth. On the other hand, the influence of the Shields parameter Θ on scour depth *S* depends on the scour condition. In clear-water

scour, the effect of Θ on S is more pronounced, whereas in live-bed scour, S has very little variation with Θ.

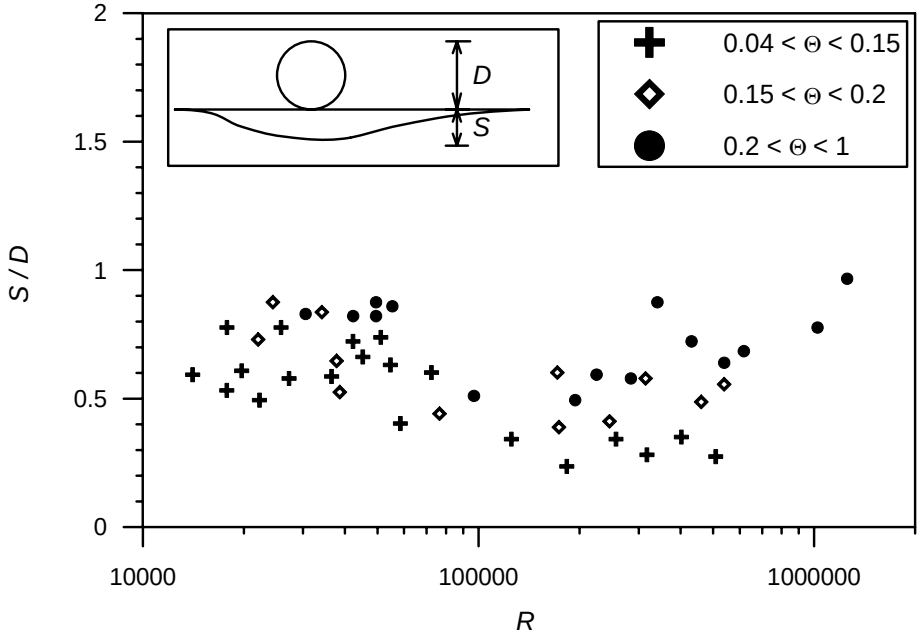

Fig. 6.23 Data of equilibrium scour depth for live-bed scour condition (after Sumer and Fredsøe 1990)

Chao and Hennessy (1972) proposed a method to evaluate the maximum scour depth below pipelines from the following equation:

$$U_{bot} = U\left[\frac{2(2H/D)^2 - (2H/D) - 1}{2(2H/D)^2 - 3(2H/D) + 1}\right] \tag{6.46}$$

where U_{bot} = average velocity in the scour hole below a pipeline; and H = scour depth measured from the pipe center.

The empirical equations proposed by Ibrahim and Nalluri (1986) for the estimation of scour depth below pipelines are

$$\frac{S}{D} = 4.706\left(\frac{U}{U_c}\right)^{0.89} F^{1.43} + 0.06 \quad \text{for clear-water scour} \tag{6.47}$$

$$\frac{S}{D} = 0.084\left(\frac{U}{U_c}\right)^{-0.03} F^{-0.16} + 1.33 \quad \text{for live-bed scour} \tag{6.48}$$

where $F = U/(gh)^{0.5}$; h = flow depth; and U_c = critical velocity for sediments.

The Dutch research group (Bijker and Leeuwestein 1984) proposed the following empirical equation of the scour depth below a submarine pipeline:

$$S = 0.929\left(\frac{U^2}{2g}\right)^{0.26} D^{0.78} d_{50}^{-0.04} \tag{6.49}$$

Eq. (6.49) includes the moderate effect of sediment size on scour depth.

Alix et al. (1999) found that the pipe Reynolds number R has negligible influence on the scour depth. In contrast, the Froude number was an important parameter that influences the scour depth. They proposed the following equation for the estimation of scour depth

$$S / D = 2F \sec h(1.7e/D) \tag{6.50}$$

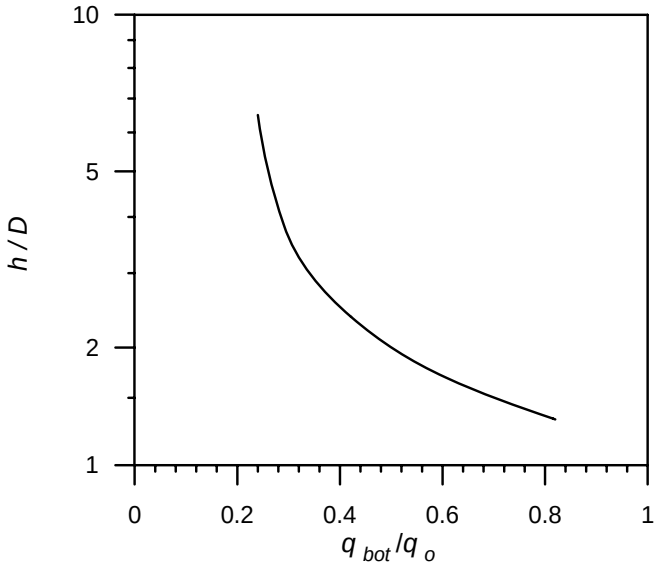

Fig. 6.24 Variation of h/D with q_{bot}/q_o (after Chiew 1991)

Chiew (1991) proposed the following iterative method to predict the scour depth below pipelines:

- For a given value of h/D, determine the unit discharge through the gap q_{bot} from Fig. 6.24, where q_o = unit discharge of the approaching flow.
- Assume a scour depth S and estimate the average velocity below the pipeline U_{bot} by

$$U_{bot} = q_{bot} / S \tag{6.51}$$

- Compute the bed shear stress in the scour hole τ_{bot} using

$$\tau_{bot} = f\rho U_{bot}^2 / 8 \tag{6.52}$$

where ρ = mass density of water; and f = friction factor to be estimated from the Moody diagram for a relative roughness (= d_{50}/S) and a Reynolds number (= $U_{bot}S/\nu$).

- Compare τ_{bot} with the critical shear stress τ_c obtained from the Shields diagram. Continue the iteration until $\tau_{bot} = \tau_c$.

The following example illustrates this method.

6.5.2 Example

Compute the maximum scour depth below a 100 mm diameter submarine pipe laid on a sediment bed of d_{50} = 0.6 mm, subjected to steady flow of 0.35 m/s with flow depth 0.4 m. Take $\nu = 0.85\times10^{-6}$ m^2/s.

For h/D = 0.4/0.1 = 4, q_{bot}/q_o is obtained from Fig. 6.24 as 0.29. Hence, q_{bot} = $0.29(0.35\times0.4) = 0.0406$ m^3/s. Assuming S = 120 mm, $U_{bot} = 0.0406/0.12 = 0.338$ m/s. For a relative roughness = 0.6/120 = 0.005 and a Reynolds number = $0.338\times0.12/(0.85\times10^{-6}) = 4.8\times10^4$, the friction factor f obtained from the Moody diagram is 0.032. Thus, the bed shear

stress in the scour hole below pipeline, $\tau_{bot} = 0.032 \times 1000 \times 0.338^2/8 = 0.457$ Pa. From the Shields diagram, for $d_{50} = 0.6$ mm, τ_c is estimated as 0.324 Pa. Therefore, τ_{bot} is greater than τ_c. With iterative procedure, the value of S that satisfy the condition of $\tau_{bot} = \tau_c$ is 141 mm. Therefore, the maximum scour depth is 141 mm.

6.6 Scour at Bridge Piers

At bridge sites, localized scour in the vicinity of piers poses a challenging problem to the hydraulic engineers. Failure of bridges due to scour at pier foundations is a common occurrence. The obstruction of the flowing stream by a bridge pier causes a three-dimensional separation of flow forming a vortex flow field around the pier (Dey et al. 1995; Dey 1995). To be more explicit, the flow separates at the upstream face of the pier as it travels by the side of the pier, creating a vortex trail, termed horseshoe vortex, which moves downstream. As a result of which local scour takes place around the pier due to the removal of bed sediments. The scour at bridge piers has been studied extensively by various researchers. Review of the important experiments and field studies was given by Breusers et al. (1977), Dargahi (1982), Breusers and Raudkivi (1991), Dey (1997a, b), Melville and Coleman (2000), Richardson and Davis (2001), and Sumer and Fredsøe (2002).

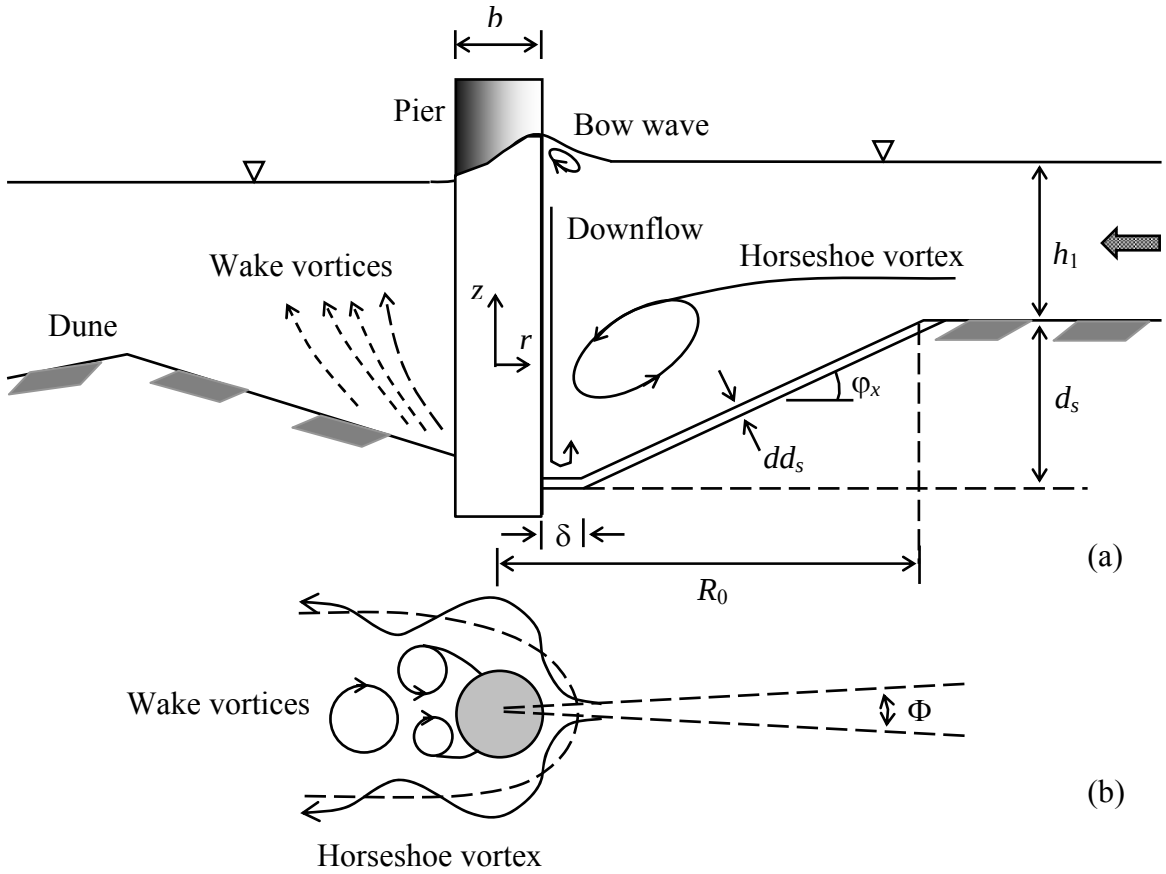

Fig. 6.25 Definition sketch showing components of flow field around a pier

6.6.1 Flow Field around Bridge Piers

The flow field around a pier is coupled with a complex three-dimensional separation of the approaching flow upstream and a periodical vortex shedding downstream of the pier. The complexity increases with the development of the scour hole. The existence of the pier in the flowing stream induces a downward negative pressure gradient normal to the approaching

flow. The boundary layer at the pier upstream gets through this pressure gradient set up by the pier, separating the flow and forming the horseshoe vortex. In addition, the other flow components developed are the downflow, wake vortex and bow wave. Fig. 6.25 shows the different components of flow field around a pier.

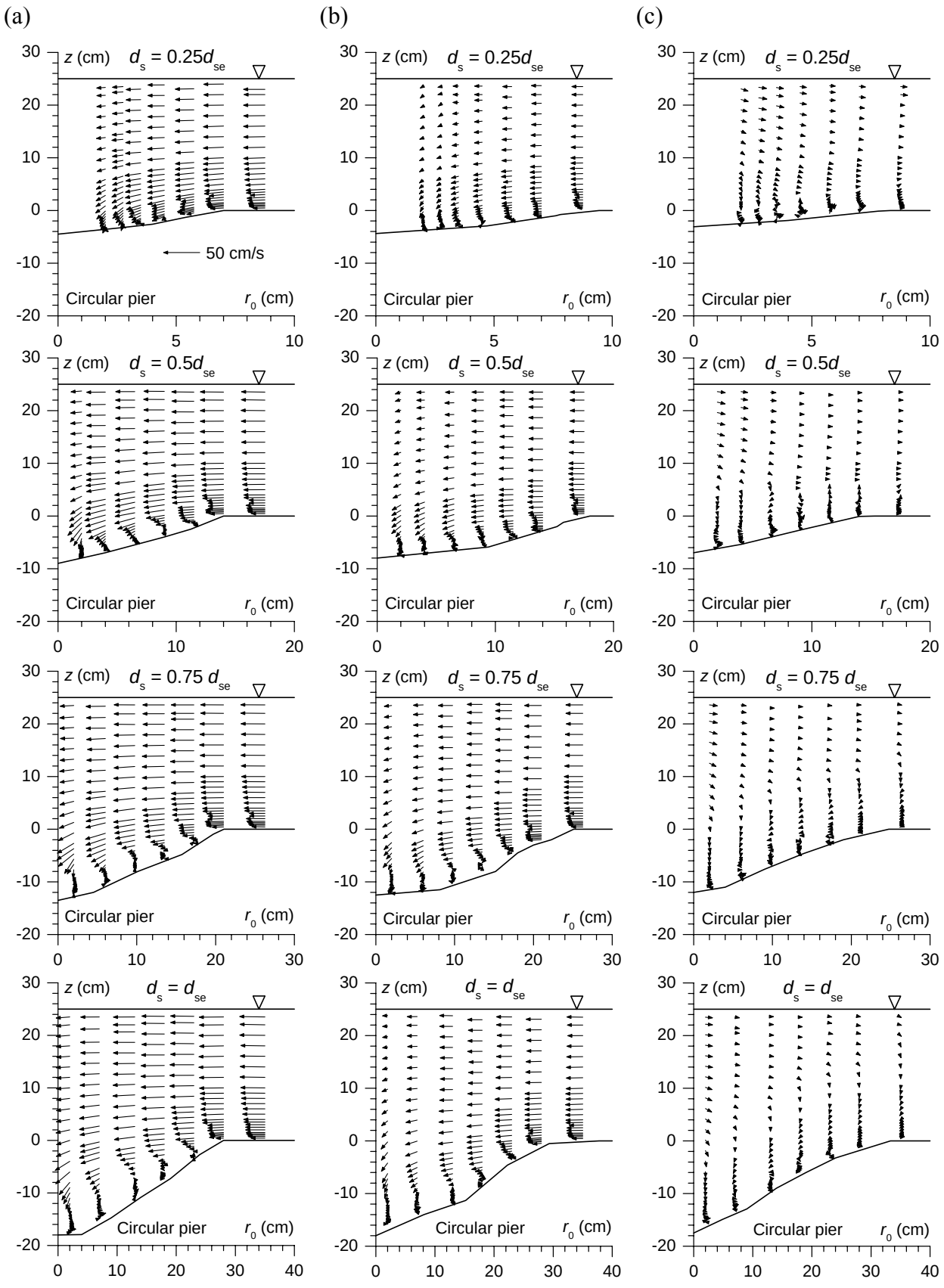

Fig. 6.26 Velocity vectors at azimuthal planes: (a) $\theta = 0^o$; (b) $\theta = 45^o$ and (c) $\theta = 90^o$ (after Raikar 2006) (In the figure, d_{se} = equilibrium scour depth; and $r_0 = r - 0.5b$)

Melville (1975), Dey et al. (1995), Ahmed and Rajaratnam (1998) and Graf and Istiarto (2002) measured the flow field within the scour hole around a circular pier. Recently, Raikar (2006) studied the characteristics of turbulent horseshoe vortex flow within the developing scour holes at cylindrical piers and presented the evolution of the horseshoe vortex during the development of a scour hole through the vector diagrams. Fig. 6.26 shows the time-averaged velocity vectors at different azimuthal planes (0^o, 45^o and 90^o with reference to the upstream axis of symmetry) for intermediate and equilibrium scour holes at a circular pier.

6.6.2 Parameters Influencing Scour Depth at Piers

Scour at piers is influenced by various parameters (Breusers et al. 1977), which are grouped as follows:

- Parameters relating to the pier: Size, shape, spacing, number and orientation with respect to the approaching flow direction.
- Parameters relating to the bed sediment: Median size, particle size distribution, mass density, angle of repose and cohesiveness.
- Parameters relating to the approaching flow condition: Approaching flow velocity, approaching flow depth, shear velocity and roughness.
- Parameters relating to the fluid: Mass density, viscosity, gravitational acceleration and temperature (may not be important in scour problems).
- Parameters relating to the time: Time of scouring for an evolving scour hole.
- Parameters relating to the unsteadiness: Passage of flood wave in rivers and waves in marine environment.

The relationship showing the influence of various parameters on the equilibrium scour depth d_s at piers can be given in functional form as follows:

$$d_s = f_1(U_1, h_1, \rho, \rho_s, g, \nu, b, d_{50}, \sigma_g, t) \tag{6.53}$$

where b = pier width; and t = time of scour. The dependency of scour depth on various parameters is given in the following subsections.

6.6.2.1 Effect of Pier Width Relative to Sediment Size on Scour Depth

Fig. 6.27 shows the variation of nondimensional equilibrium scour depth $\hat{d}_s$ (= d_s/b) as a function of $\tilde{b}$ (= b/d_{50}) for clear-water scour condition. The curves shown by continuous lines are for circular and square piers embedded in gravel-beds, obtained by Raikar and Dey (2005b), while the broken line are for circular piers in sand-beds after Ettema (1980). The curves for circular piers in gravel- and sand-beds have a similar trend, and the difference between the curves decreases with the sediment size reducing from gravel size to sand size. The salient feature of Fig. 6.27 is the equilibrium scour depth $\hat{d}_s$ relative to pier width being greater for larger pier width and smaller sediment size. The probable reason is partly attributed to the fact that the strength of the horseshoe vortex and the magnitude of downflow, being considered to be an integral part of the horseshoe vortex (Dey et al. 1995;

Dey 1995), is proportional to the pier width *b* for blunt nosed piers, resulting in a vortex flow with an enhanced scour potential (Breusers 1965). Moreover, the horseshoe vortex is stronger to excavate large volume of sediments, when the sediment size is relatively fine developing greater scour depth d_s. On the other hand, the coarser sediments make the bed more porous to allow the downflow to penetrate and dissipate its energy in the sediment bed. However, magnitude of $\hat{d}_s$ for square pier is greater than that for circular pier, because the strengths of the downflow and horseshoe vortex are greater in the case of the square pier (Tseng et al. 2000).

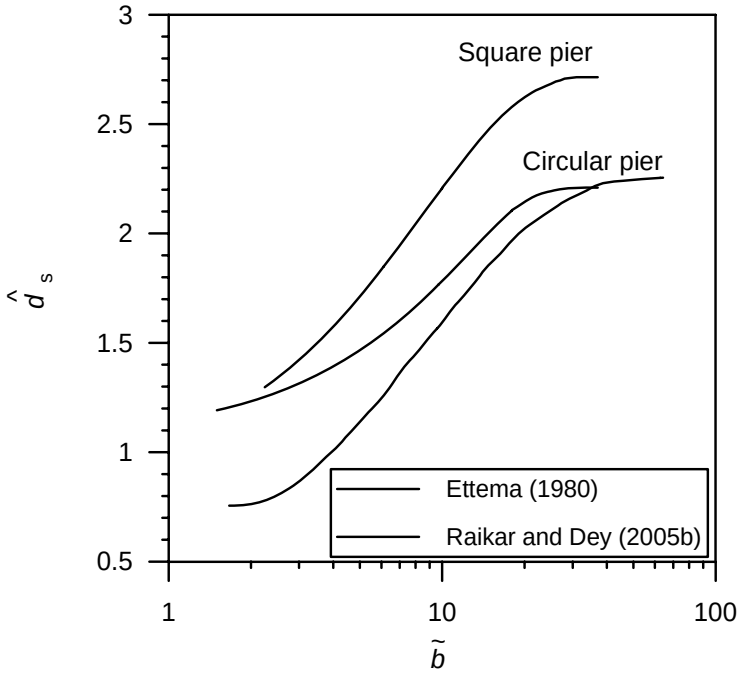

Fig. 6.27 Variation of $\hat{d}_s$ with $\tilde{b}$ for $U_1/U_c \approx 1$

6.6.2.2 Effect of Approaching Flow Depth Relative to Pier Width on Scour Depth

The dependency of $\hat{d}_s$ at circular piers for clear-water scour condition on the ratio of approaching flow depth to pier width $\hat{h}$ (= h_1/b) for different $\tilde{b}$ and d_{50} = 4.1 mm is presented in Fig. 6.28 (Raikar 2006). At small $\hat{h}$, the nondimensional equilibrium scour depth $\hat{d}_s$ increases sharply with an increase in $\hat{h}$. However, as $\hat{h}$ increases, $\hat{d}_s$ becomes almost independent of $\hat{h}$. It is evident from Fig. 6.28 that larger the $\tilde{b}$, the range of influence of flow depth is relatively small. For large *b*, scour depth d_s is essentially independent of flow depth at $\hat{h}$ being three, whereas for small *b*, $\hat{h}$ is approximately seven. This aspect may be justified that there is a little increase of horseshoe vortex strength due to an increase in flow depth beyond three and seven times of pier width for large and small pier widths, respectively. On the other hand, in case of pier scour in sands, most of the investigators stated that the influence of flow depth is insignificant for $\hat{h}$ greater than one to three (Raudkivi and Ettema 1983; Raudkivi 1986). In this context, it is pertinent to mention that it is appropriate to represent the variation of scour depth with upstream flow depth for different $\tilde{b}$. From the close examination of Fig. 6.28, it is also obvious that for the same value of h_1 (in the plots, same symbols are used), $\hat{d}_s$ increases with an increase in $\tilde{b}$, as was observed in the preceding section. For shallow flow depths, the surface roller, termed bow wave, having a

sense of rotation opposite to the horseshoe vortex, reduces the horseshoe vortex strength, resulting in a reduced scour depth.

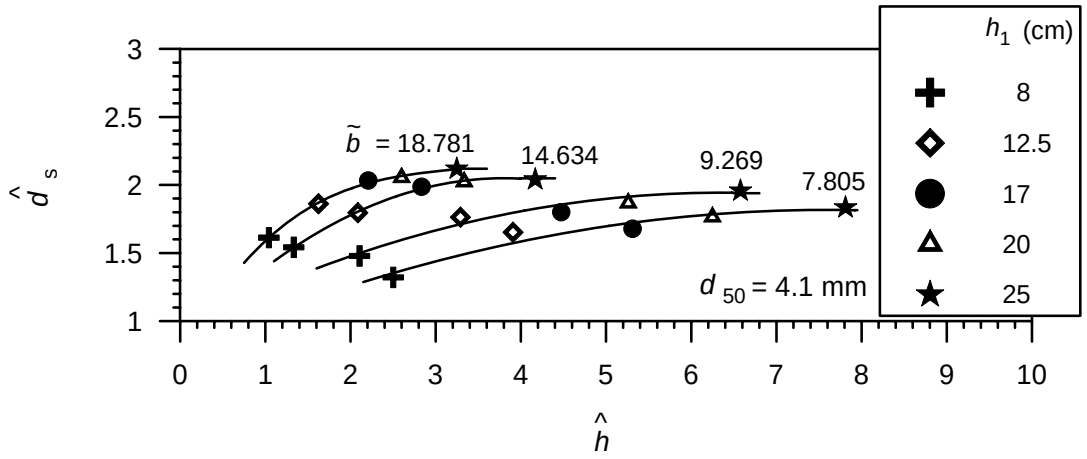

Fig. 6.28 Dependency of $\hat{d}_s$ on $\hat{h}$ for circular piers under $U_1/U_c \approx 1$ (after Raikar 2006)

6.6.2.3 Effect of Nonuniform Sediment Gradation on Scour Depth

In nonuniform sediments ($\sigma_g > 1.4$), the particle size distribution has a pronounced effect on scour depth. When the bed is comprised of nonuniform sediments, a process of armoring in the scour hole commences resulting in an exposure of coarser particles due to washing out of the finer fraction. The armor-layer thus formed gradually increases the effective critical bed shear stress, which inhibits the further growth of scour hole. Hence, the nonunifrom sediments consistently produce lower scour depths than that of the uniform sediments. The dependencies of K_σ on σ_g for circular and square piers are shown in Figs. 6.29(a) and 6.29(b). It is evident from the mean curves for scour at circular piers that the difference between Ettema's (1980) curve for sands and Raikar and Dey's (2005a) curve for gravels is considerable. For scour at circular piers in sands, Ettema's (1980) curve of K_σ versus σ_g overestimates the mean curve for gravels, having a deviation for ripple forming sands (d_{50} = 0.55 mm) at $1 < \sigma_g < 1.5$. However, for a given σ_g, coefficient K_σ for square piers is greater than that for circular piers due to stronger horseshoe vortex for square piers.

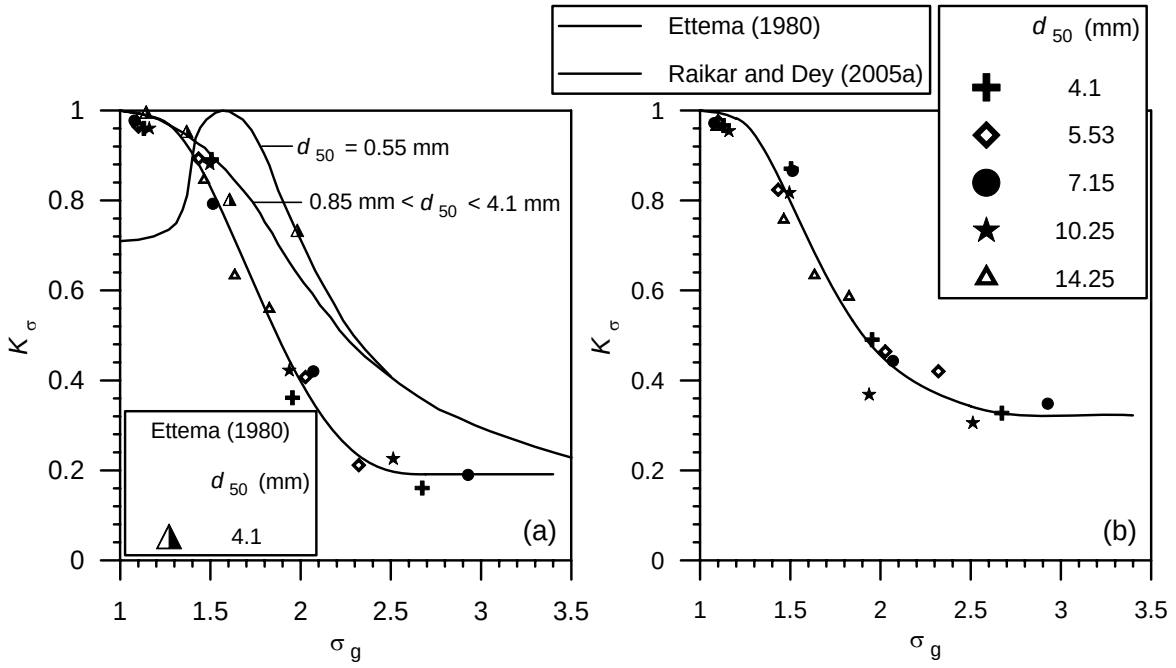

Fig. 6.29 Variation of K_σ with σ_g for $U_1/U_c \approx 1$: (a) circular piers and (b) square piers

6.6.2.4 Time-Variation of Scour Depth

The time-variation of scour depth at piers embedded in gravels studied by Raikar and Dey (2005a) is presented below:

Scour Depth in Uniform Gravels:

According to Sumer et al. (1993), the instantaneous scour depth at a pier d_{st} at time t can be represented in functional form as

$$d_{st} = d_s[1 - \exp(t/T)] \tag{6.54}$$

where T = time scale. The quantity T represents the time period during which scour depth develops substantially. The time scale T can be determined from the scour depth d_{st} versus time t diagram by estimating the slope of the tangent to the $d_{st}(t)$ curve at $t = 0$, as shown schematically in Fig. 6.30(a). The time scale can be expressed in nondimensional form as T_* [$= T(\Delta g d_{50}^3)^{0.5}/b^2$]. For pier scour, the nondimensional time scale T_* can be written in the following functional form:

$$T_* = T_*(F_b, d_{50}) \tag{6.55}$$

where F_b = pier Froude number, that is $U_1/(gb)^{0.5}$. For circular and square piers, the variations of nondimensional time scale T_* with pier Froude number F_b for different sizes of gravels are given in Figs. 6.30(a) and 6.30(b), respectively. The nondimensional time scale T_* increases with increase in F_b and u_{*c}.

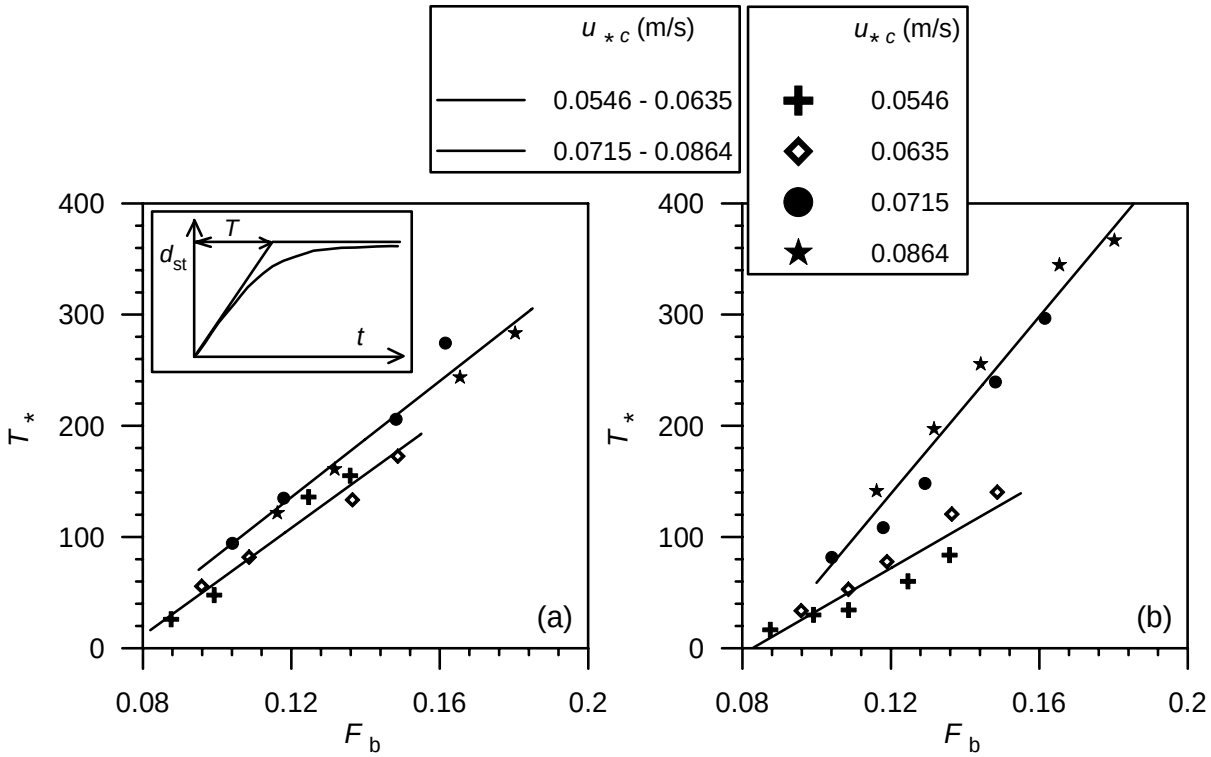

Fig. 6.30 Variation of T_* with F_b for different gravel sizes d_{50} under $U_1/U_c \approx 1$: (a) circular pier and (b) square pier (after Raikar and Dey 2005a)

Scour Depth in Nonuniform Gravels:

For nonuniform gravels ($\sigma_g > 1.4$), the nondimensional time scale T_* is represented as a function of σ_g for different u_{*c}. The nondimensional time scale T_* decrease with an increase in σ_g and u_{*c}. Due to the formation of an armor-layer at the base of the scour hole, the rate of development of scour hole reduces; and hence, the time to reach equilibrium in nonuniform gravels is lesser than that in uniform gravels. The nondimensional time scale $T_*(\sigma_g)$ for nonuniform gravels can be represented as a function of T_* for uniform gravels as

$$T_*(\sigma_g) = K_T T_* \tag{6.56}$$

where K_T = coefficient for time scale depending on the gradation of gravels. The dependencies of K_T on σ_g for circular and square piers are shown in Figs. 6.31(a) and 6.31(b), respectively.

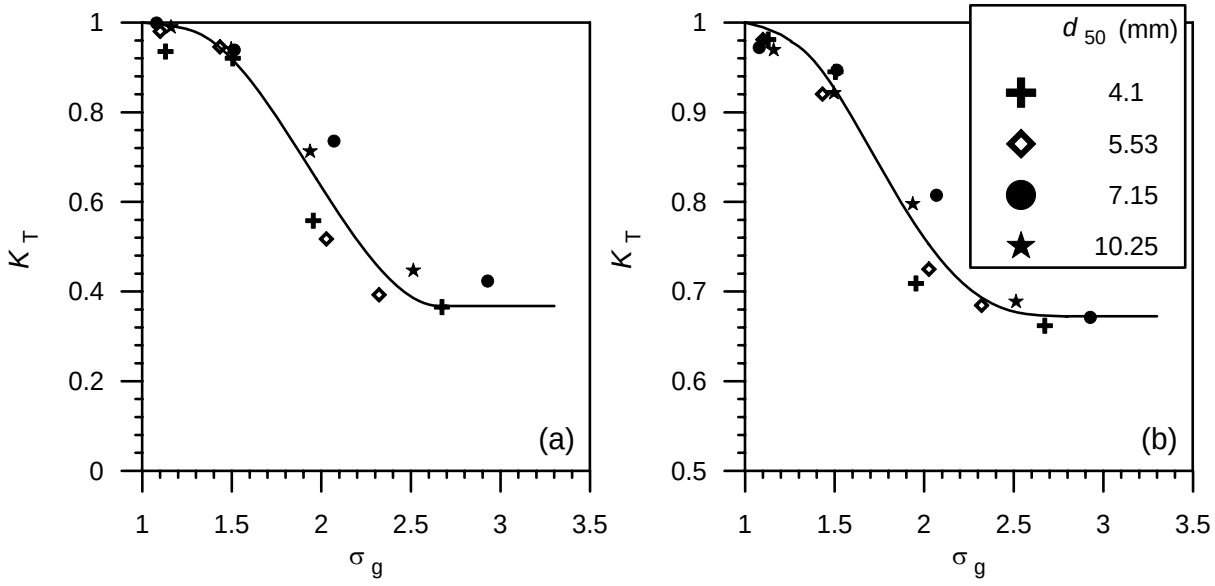

Fig. 6.31 Variation of K_T as a function of σ_g for $U_1/U_c \approx 1$: (a) circular piers and (b) square piers (after Raikar and Dey 2005a)

6.6.3 Modeling of Time-Variation of Scour Depth

An analytical model proposed by Dey (1999) to estimate the time-variation of scour depth in an evolving scour hole at cylindrical piers under clear-water and live-bed scour condition with uniform and nonuniform sediments is presented in this section.

The scour hole at a pier forms beneath the horseshoe vortex, which sinks into the hole as scouring progresses. The hydrodynamic forces (namely drag and lift forces) acting on the sediment particles owing to the vortex flow remove the bed particles and decrease with an increase in scour depth. The conical shape of the scour hole upstream makes an angle φ_x with the original bed except for the semicircular flat region having a width δ [Fig. 6.25(a)]. The sediment particles are mainly dislodged from this region by the action of the vortex and are carried downstream by the sides of the pier. The semicircular region is also fed with the sediment particles of the conical portion of scour hole upstream, as it collapses; subsequently, those particles are picked up (Dey 1991). In reality, the depletion of the bed sediment in the scour hole takes place layer by layer. However, in live-bed scour, the approaching sediment load is also added to the hole. The angle φ_x, termed *dynamic angle of repose*, was measured to be about 15% greater than the angle of repose of the bed sediment in still water (Dey et al. 1995; Melville and Raudkivi 1977).

The mathematical model of scouring process at a pier is derived from the following concepts:

a) The horseshoe vortex at the pier base upstream is the basic cause of scouring (Melville 1975).

b) Sediment particles are picked up from the flat semicircular region upstream where the maximum scour depth appears (Dey 1991).

c) The scour profiles are geometrically similar with time as scouring progresses (Dey 1991).

d) The rate of change of sediment mass in the scour hole equals the difference between the sediment mass removal rate from the scour hole and the sediment mass inflow rate by the approaching flow into the scour hole.

Figs. 6.25(a) – 6.25(b) present the sectional elevation and the top view of a typical scour hole at a cylindrical pier in time *t,* as was idealized by Dey et al. (1995). Considering a small angle Φ to the axis of symmetry of the scour hole upstream, the mass of sediment picked up from the flat semicircular region during a small interval of time *dt* is

$$dm_1 = 0.5\delta(\delta + b)\beta E dt \tag{6.57}$$

where β = factor; and *E* = sediment pick-up rate at the base of the pier in time *t.* The effective pick-up rate of sediment, that leaves the scour hole, is actually considered to be β*E.* The coefficient β is introduced for the reason that the number of sediment particles leaving the scour hole decreases with the scour depth. The sediment particles have a characteristic kinetic energy assumed proportional to $\tau_b d_e^3$. Here, τ_b is the bed shear stress in the scour hole at the pier base and d_e is the effective size of sediment. On the other hand, the potential energy of the sediment particles, corresponding to the scour depth d_{st} from the point of view of similarity of the scour profiles, is proportional to $\rho\Delta g d_e^3 d_{st}$, where d_{st} = scour depth in time *t*. The fraction of the sediment that leaves the hole is proportional to β which is, in turn, proportional to the ratio of the kinetic energy to potential energy that is $\tau_b/(\rho\Delta g d_{st})$.

The width of the flat semicircular region δ can be expressed as a fraction of the radial length of the scour hole from the pier boundary at the original bed level upstream

$$\delta = \varepsilon(R_0 - 0.5b) \tag{6.58}$$

where ε = geometric factor; and R_0 = radius of the scour hole at the original bed level upstream in time *t*. Thus, R_0 is given by

$$R_0 = \left[\frac{d_{st}}{(1-\varepsilon)}\right]\cot\varphi_x + 0.5b \tag{6.59}$$

Using Eqs. (6.58) and (6.59) into Eq. (6.57), yields

$$dm_1 = 0.58\frac{\varepsilon}{1-\varepsilon} d_{st}\cot\varphi_x\left(\frac{\varepsilon}{1-\varepsilon} d_{st}\cot\varphi_x + b\right)\times\beta E dt \tag{6.60}$$

In Eq. (6.60), the sediment pick-up rate *E* at the base of the pier due to scouring, determined using the formula of van Rijn (1984), is given as

$$E = 0.00033\rho_s(\Delta g d_e)^{0.5} d_{*e}^{0.3} T_s^{1.5} \tag{6.61}$$

where d_{*e} = particle parameter, that is $d_e(\Delta g/\nu^2)^{1/3}$; T_s = transport-stage parameter due to scour, that is $(\tau_b - \tau_{bc})/\tau_{bc}$; τ_{bc} = critical shear stress in the scour hole (= $\xi\tau_{cre}$); τ_{cre} = critical shear stress on a plane bed for the particle size of d_e; and ξ = factor depending on turbulence agitation and oscillation of horseshoe vortex.

According to Kothyari et al. (1992a), the effective size of sediment d_e, an equivalent mean size of the uniform sediment where scouring rate is same as that of the nonuniform sediment, can be determined as

$$d_e = 0.925 d_{50}\sigma_g^{0.67} \qquad \text{nonuniform sediment} \tag{6.62a}$$

$$d_e = d_{50} \qquad \text{uniform sediment} \tag{6.62b}$$

The local bed shear stress τ_b at the pier base is determined from the empirical formula given by Kothyari et al.(1992a) as

$$\tau_b = 4\tau\left[\left(\frac{2}{\pi}\right)\left(\frac{d_{st}}{d_v}\right)^2 \cos\varphi_x + 1\right]^{-0.57} \tag{6.63}$$

where τ = bed shear stress of approaching flow; and d_v = diameter of the horseshoe vortex at the beginning of scour. Kothyari et al. (1992a) proposed an empirical equation as $d_v = 0.28h_1^{0.15}b^{0.85}$. The critical shear stress, τ_{cr} that is given in the Shields diagram can be determined from the empirical formula proposed by van Rijn (1984) as

$$\tau_{cre} = \Delta\rho g d_e \Theta_{cr} \tag{6.64}$$

where Θ_{cr} = nondimensional critical shear stress or Shields parameter, that is $\tau_{cre}/(\Delta\rho g d_e)$. The relationship between Θ_{cr} and d_{*e} was given by van Rijn (1984).

In live-bed scour, when the bed shear stress of approaching flow τ exceeds its critical value for the initiation of sediment motion, the sediment particles start moving being picked up from the upstream bed at a rate of E_u. The sediment mass that is entering into the scour hole, deposits over the flat semicircular region of the scour hole by the downward flow. In this context, it is important to point out that the deposition of the approaching sediment load does not take place uniformly over the entire scour hole owing to the downward motion of the fluid towards the flat semicircular region. The flow field inside the scour hole has an upward motion along the slant bed where the sediment deposition is not possible (Dey 1995). However, the mass rate of sediment deposition in the scour hole is always less than that of sediment pick-up from the scour hole during scouring. The equilibrium prevails over a period of time when sediment deposition and pick-up rates are equal. Thus, the mass of sediment deposited over the flat semicircular region of the scour hole, in an interval of time dt, is

$$dm_2 = 0.5\,\mathrm{sgn}(T_u)\Phi\,\delta(\delta + b)E_u dt \tag{6.65}$$

where E_u = sediment pick-up rate by the approaching flow at the plane bed upstream. The function $\mathrm{sgn}(T_u)$ is

$$\mathrm{sgn}(T_u) = 1 \quad \text{for } T_u > 0 \text{ (live-bed scour)} \tag{6.66a}$$

$$\mathrm{sgn}(T_u) = 0 \quad \text{for } T_u \le 0 \text{ (clear-water scour)} \tag{6.66b}$$

where T_u = transport-stage parameter due to approaching flow, that is $(\tau - \tau_{cr})/\tau_{cr}$; and τ_{cr} = critical shear stress on the plane bed for the particle size of d_{50}. τ_{cr} can be determined from Eq. (6.64) using d_{50} in place of d_e. The function $\mathrm{sgn}(T_u)$ implies that there is no sediment supply ($dm_2 = 0$) into the scour hole under a clear-water scour condition. Using Eqs. (6.58) and (6.59), Eq. (6.65) is rewritten as

$$dm_2 = 0.5\,\mathrm{sgn}(T_u)\Phi\frac{\varepsilon}{1-\varepsilon}d_{st}\cot\varphi_x\left(\frac{\varepsilon}{1-\varepsilon}d_{st} + b\right)\times E_u dt \tag{6.67}$$

The sediment mass, picked up by the approaching flow under a live-bed scour condition, has a direct contribution towards a decrease in rate of change of scour depth in the process of its deposition in the hole. The formula given by van Rijn (1984) is also used to estimate E_u as

$$E_u = 0.00033\rho_s(\Delta g d_{50})^{0.5} d_{*50}^{0.3} T_s^{1.5} \tag{6.68}$$

where $d_{*50} = d_{50}(\Delta g/\nu^2)^{1/3}$. Applying the geometrical similarity of scour profiles with time, the depletion of the sediment mass due to an increase in scour depth dd_{st} in time dt is given by

$$dm_3 = 0.5(1-\rho_0)\rho_s\Phi\{\delta(\delta + b) + \sec\varphi_x[(R^2 - 0.25b^2) - \delta(\delta + b)]\}dd_{st} \tag{6.69}$$

where ρ_0 = porosity of sediment. Substituting Eqs. (6.58) and (6.59) into Eq. (6.69), yields

$$dm_3 = 0.5(1-\rho_0)\rho_s \Phi \frac{d_{st}}{1-\varepsilon}\left[\varepsilon \cot\varphi_x\left(\frac{\varepsilon}{1-\varepsilon} d_{st}\cot\varphi_x + b\right) + \frac{(1+\varepsilon)d_{st}\cot\varphi_x (1-\varepsilon)b}{\sin\varphi_x}\right] dd_{st} \tag{6.70}$$

The fundamental equation to describe the scouring process can be obtained from the concept of conservation of the mass of sediment as

$$dm_1 = dm_2 + dm_3 \tag{6.71}$$

Eqs. (6.60), (6.67) and (6.70) are used in Eq. (6.71) to obtain the following differential equation in nondimensional form:

$$(1-\rho_0)\left[\varepsilon\cot\varphi_x\left(\frac{\varepsilon}{1-\varepsilon}\hat{d}_{st}\cot\varphi_x + 1\right) + \frac{(1+\varepsilon)\hat{d}_{st}\cot\varphi_x + 1 - \varepsilon}{\sin\varphi_x}\right]\frac{d\hat{d}_{st}}{d\hat{t}}$$

$$= \varepsilon\cot\varphi_x\left(\frac{\varepsilon}{1-\varepsilon}\hat{d}_{st}\cot\varphi_x + 1\right) \times [\beta \hat{D}^{0.5}\varphi_p - \mathrm{sgn}(T_u)\varphi_{pu}]\tilde{b} \tag{6.72}$$

where $\hat{t} = td_{50}(\Delta g d_{50})^{0.5}/b^2$; $\hat{d}_{st} = d_{st}/b$; $\hat{D} = d_e/d_{50}$; φ_p = sediment pick-up function due to scouring, that is $E/[\rho_s(\Delta g d_e)^{0.5}]$; and φ_{pu} = sediment pick-up function for the upstream bed that is $E_u/[\rho_s(\Delta g d_{50})^{0.5}]$. Eq. (6.72) is a first-order differential equation, which can be solved by the Runge-Kutta method to determine the dependency $\hat{d}_{st}$ on $\hat{t}$. The geometric factor ε was taken as 0.1, as was observed by Dey (1991). In this analysis, ρ_0 and φ_x were assumed as 0.4 and 37 degree, respectively. Figs. 6.32(a) - 6.32(c) presents the validation of the model using the experimental data of Raudkivi and Ettema (1983) and Kothyari et al. (1992b).

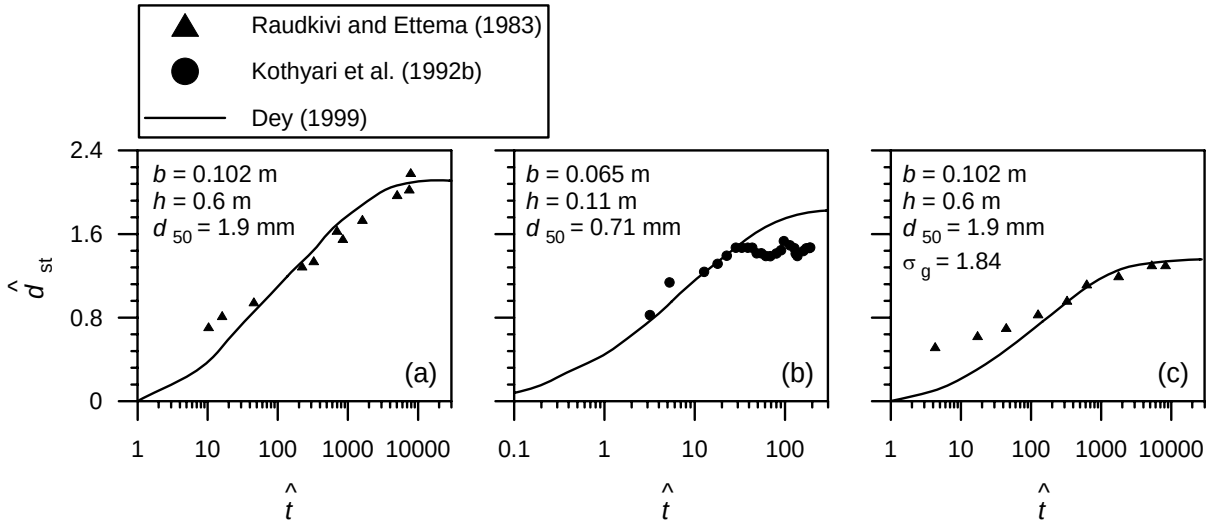

Fig. 6.32 Dependency of $\hat{d}_{st}$ on $\hat{t}$: (a) uniform sediments under clear-water scour; (b) uniform sediments under live-bed scour and (c) nonuniform sediments under clear-water scour (after Dey 1999)

Equilibrium Scour Conditions and Maximum Scour Depth:

The traditional concept of equilibrium for clear-water scour, when the local bed shear stress τ_b approaches the critical shear stress τ_{cr}, cannot be applied to strongly three-dimensional (turbulent) vortex flow situations. In reality, the sediment particles are dislodged by the fluid-induced forces under the combined effect of bed shear stress, turbulent agitation and

oscillation of the horseshoe vortex (Melville 1997; Dey and Kar 1995). Melville and Raudkivi (1977) and Dey and Bose (1994) estimated the bed shear stress τ_b, which was found to be well below the critical shear stress τ_{cr} in the scour hole when the equilibrium was reached. Thus, an equilibrium condition in pier scour can be defined when τ_b tends to $\xi\tau_{cr}$. This concept was implemented by introducing $\xi = 0.7$, as was estimated by Dey and Bose (1994). However, the above discussion refers to the case of clear-water scour, but the concept of equilibrium in live-bed scour is completely different. When the rate of sediment pick-up out of the scour hole is balanced by the incoming sediment transport rate due to the approaching flow, an equilibrium condition in a live-bed scour prevails over a period of time. However, the maximum scour depth can be estimated from Eq. (6.72), satisfying the aforementioned conditions of equilibrium scour for either condition of scouring. The value of $\beta = 0.97$ was found to give satisfactory agreement between the results obtained using the model and the experimental data reported by various investigators.

In order to determine the maximum scour depth, computation is extended up to the equilibrium scour condition for which $d\hat{d}_{st}/d\hat{t} = 0$. By incorporating it into Eq. (6.72), the following formula for maximum scour depth at piers is obtained as

$$\hat{d}_s = 0.393\left(\frac{h_1}{b}\right)^{0.15}\left\{21.28\left[\frac{\tau_0/\tau_{cr}}{1+1.02\,\mathrm{sgn}(T_u)^{0.67}\hat{D}^{0.53}T_u}\right]^{1.754} - 1\right\}^{0.5} \tag{6.73}$$

The comparison of nondimensional equilibrium scour depths $\hat{d}_s$ computed from the Dey's (1999) model with the laboratory experimental and field data reported by various investigators is shown in Fig. 6.33.

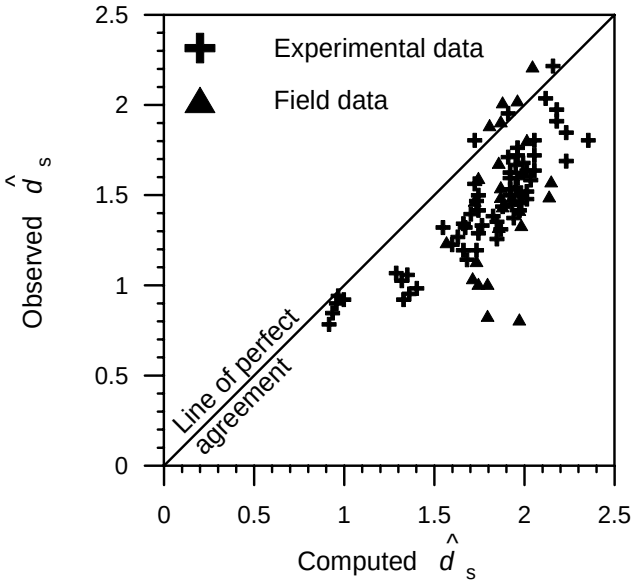

Fig. 6.33 Comparison between the equilibrium scour depths $\hat{d}_s$ computed using the model and the experimental and field data (after Dey 1999)

6.6.4 Equations of Equilibrium Scour Depth

A large number of investigators proposed empirical equations for the estimation of maximum scour depth at piers based on the model studies in laboratory experimental flumes. In general, these equations are derived from a limited range of data and are applicable to the conditions similar to those for which they are valid. Though the number of proposed equations for the

estimation of maximum scour depth is overwhelming (Dey 1997a; Melville and Coleman 2000), it is, however, difficult to confirm their adequacy for the design purposes due to limited field measurements. However, design equations proposed by Melville and Coleman (2000) and HEC18 (Richardson and Davis 2001) seem to be good.

Melville and Coleman (2000) recommended a design equation for the estimation of maximum scour depth at piers based on empirical relationships, called *K*-factors, which account for the effects of pier, flow and sediment characteristics. The maximum equilibrium scour depth d_s at a bridge pier formulated as a product of *K*-factors is given by

$$d_s = K_h K_I K_d K_s K_\alpha K_t \tag{6.74}$$

where K_h = flow depth - foundation size factor; K_I = flow intensity factor; K_d = sediment size factor; K_s = pier shape factor; K_α = pier alignment factor; and K_t = time factor. The relationships for these *K*-factors are as follows:

The *flow depth - foundation size factor* K_h is the value of $\hat{d}_s$ at a particular value of $\hat{h}$. It is obtained by the envelope curves for pier scour data as

$$K_h(b < 0.7h_1) = 2.4b \tag{6.75a}$$

$$K_h(0.7h_1 \le b < 5) = 2(h_1 b)^{0.5} \tag{6.75b}$$

$$K_h(b \ge 5h_1) = 4.5h_1 \tag{6.75c}$$

The *flow intensity factor* K_I is the ratio of scour depth at a particular flow velocity to that at the critical velocity for the bed sediment. The flow intensity factor K_I represents the effect of flow intensity on scour depth. It also accounts for the nonuniformity of sediments. It is given by

$$K_I = \frac{U_1 - (U_{ca} - U_c)}{U_c} \quad \text{for } \frac{U_1 - (U_{ca} - U_c)}{U_c} < 1 \tag{6.76a}$$

$$K_I = 1 \quad \text{for } \frac{U_1 - (U_{ca} - U_c)}{U_c} \ge 1 \tag{6.76b}$$

where U_{ca} = critical velocity for armor-layer particles.

The *sediment size factor* K_d is the ratio of $\hat{d}_s$ at a particular value of $\tilde{b}$ to that of $\tilde{b}$, where $\hat{d}_s$ becomes a maximum and beyond which there is no effect of $\tilde{b}$ on $\hat{d}_s$. It is obtained by envelope curves for pier scour data as

$$K_d(\tilde{b} \le 25) = 0.57 \log(2.24\tilde{b}) \tag{6.77a}$$

$$K_d(\tilde{b} > 25) = 1 \tag{6.77b}$$

However, for the piers embedded in gravel-beds, Raikar and Dey (2005b) proposed new sediment size factors. They are

$$K_d(\tilde{b} \le 10) = 0.25 \ln \tilde{b} + 0.363 \tag{6.78a}$$

$$K_d(10 < \tilde{b} \le 25) = 0.076 \ln \tilde{b} + 0.75 \tag{6.78b}$$

$$K_d(\tilde{b} > 25) = 1 \tag{6.78c}$$

The *shape factor* K_s is defined as the ratio of the scour depth for a particular pier shape to that for the circular piers. The shape factors K_s for different piers are given in Table 2.

Table 2 Shape Factors K_s for Piers

Pier model	Pier Shape	K_s
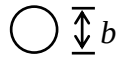	Circular	1
	Round nosed	1
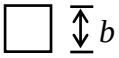	Square nosed	1.1
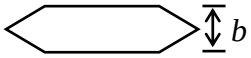	Sharp nosed	0.9

The *alignment factor* K_α is the ratio of the scour depth at an oblique pier to that at an aligned pier. In case of non-circular piers, the scour depth increases with an increase in the effective projected width of the piers. The multiplying factor K_α for rectangular pier can be obtained from the following equation:

$$K_\alpha = (b_p / b)^{0.65} \tag{6.79}$$

where b_p = projected width of rectangular pier normal to the approaching flow (= $L\sin\alpha$ + $b\cos\alpha$); α = pier orientation relative to approaching flow; and L = pier length. The curves for alignment factors proposed by Laursen and Toch (1956) are shown in Fig. 6.34.

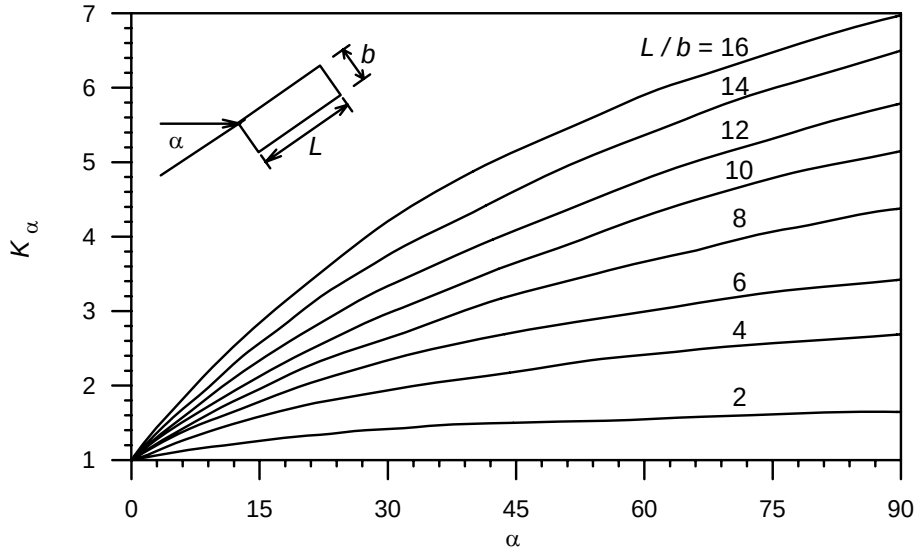

Fig. 6.34 Alignment factor K_α (after Laursen and Toch 1956)

The *time factor* K_t is the ratio of scour depth at a particular time t to the equilibrium scour depth. Its value depends on the scour condition, whether clear-water scour or live-bed scour. For live-bed scour, K_t is unity; while in clear-water scour, K_t is given by

$$K_t = \exp\left\{-0.03\left|\frac{U_c}{U_1}\ln\left(\frac{t}{t_e}\right)\right|^{1.6}\right\} \tag{6.80}$$

where t_e = time to reach equilibrium scour depth. At threshold condition ($U_1 = U_c$), t_e being maximum, when $h_1 > 6b$, is given as

$$t_e(\text{days}) = 28.96\frac{b}{U_1} \tag{6.81}$$

where b and U_1 are in m and m/s, respectively.

According to HEC18 (Richardson and Davis 2001), the scour depth at a pier in both clear-water and live-bed scour conditions is given by

$$\hat{d}_s = 2K_s K_\alpha K_{bed} K_a \left(\frac{h_1}{b}\right)^{0.35} F_1^{0.43} \tag{6.82}$$

where K_{bed} = factor for bed condition (Table 3); $F_1 = U_1/(gh_1)^{0.5}$; and K_a = factor for armoring of bed sediment. The factors K_α and K_a are furnished in Tables 4 and 5, respectively.

Table 3 Factors K_{bed} for Bed Condition

Bed condition	Dune height H (m)	K_{bed}
Clear-water scour	N/A	1.1
Plane bed and antidune flow	N/A	1.1
Small dunes	$3 > H > 0.6$	1.1
Medium dunes	$9 > H > 3$	1.1 - 1.2
Large dunes	$H \geq 9$	1.3

Table 4 Alignment Factors K_α for Piers

α (degree)	$L/b = 4$	$L/b = 8$	$L/b = 12$
0	1	1	1
15	1.5	2	2.5
30	2	2.75	3.5
45	2.3	3.3	4.3
90	2.5	3.9	5

Table 5 Armor Factors K_a

Minimum bed sediment size	K_a
$d_{50} \geq 0.06$ m	0.7

6.6.5 Example

Estimate the maximum equilibrium scour depth at bridge pier for the following data:

- Square nosed rectangular pier having b = 2 m, L = 12 m inclined at 15 degree to the approaching flow direction
- Approaching flow velocity, U_1 = 1.2 m/s
- Approaching flow depth, h_1 = 2 m
- Median size of bed sediment, d_{50} = 2 mm
- Geometric standard deviation of sediment, σ_g = 1.24

For d_{50} = 2 mm, the critical shear velocity u_{*c} is calculated from Eq. (2.30a) – (2.30e) as 0.0362 m/s. Using the equation of semi-logarithmic average velocity [U_c/u_{*c} = $5.75\log(0.5h_1/d_{50}) + 6$], the critical flow velocity U_c for h_1 = 2 m is obtained as 0.78 m/s.

The K-factors are determined using Eqs. (6.75) – (6.80) as:

1. For $b/h_1 = 2/2 = 1$ (0.7 to 5), $K_h = 2(2\times2)^{0.5} = 4$ m.
2. For $U_1/U_c = 1.2/0.78 = 1.54 > 1$ (that is live-bed scour), $K_I = 1$ and $K_t = 1$.
3. For $\tilde{b} = b/d_{50} = 2/2\times10^{-3} = 1000 > 25$, $K_d = 1$.
4. For square nosed pier, K_s = 1.1 (from Table 2).
5. From Fig. 6.34, K_α = 1.8 for $L/b = 12/2 = 6$ and $\theta = 15^o$.
6. K_σ = 1 for σ_g = 1.24 (< 1.4, that is uniform sediment).

Using Melville and Coleman's (2000) equation [Eq. (6.74)], the maximum scour depth at pier in uniform sediments is: $d_s = K_h K_I K_d K_s K_s K_t = 4\times1\times1\times1.1\times1.8\times1 = 7.92$ m.

6.7 Scour at Bridge Abutments

Scour at bridge abutments is also equally responsible for failure of bridges as scour at piers. A study of the US Federal Highway Administration in 1973 concluded that of 383 bridge failures, 25% involved pier damage and 72% involved abutment damage (Richardson et al. 1993). Macky (1990) mentioned that about 50% of total expenditure was made towards the bridge damage repairing and maintenance, out of which 70% was spent towards the abutment scour. The abutment scour has been studied extensively by various researchers (see review given by Barbhuiya and Dey 2004).

6.7.1 Flow Field around Bridge Abutments

The flow field at an abutment is complex in detail, and the complexity increases with the development of the scour hole involving separation of flow to develop three-dimensional vortex flow. Ahmed and Rajaratnam (2000) studied the flow fields at abutment placed on a planar or unscoured bed. Kwan (1988) and Kwan and Melville (1994) used the hydrogen bubble technique to measure the three-dimensional flow field in a scour hole at a wing-wall abutment. They identified a primary vortex, which is similar to the horseshoe vortex at piers, along with the downflow being the principal cause of scour at abutments. Fig. 6.35 shows the major flow components at a wing-wall abutment identified by Kwan (1988). Barbhuiya (2003) investigated the three-dimensional turbulent flow fields at vertical-wall, 45° wing-wall and semicircular abutments, placed vertically on a flat rigid bed and in stabilized erodible scoured bed, using the acoustic Doppler velocimeter (ADV). The normalized velocity vectors at different azimuthal sections (Fig. 6.36) of a 45° wing-wall abutment with a scour hole are shown in Fig. 6.37 (Dey and Barbhuiya 2006), where $\hat{x} = x/l$; $\hat{r} = r/l$; x = streamwise distance; r = radial distance; and l = abutment length transverse to flow.

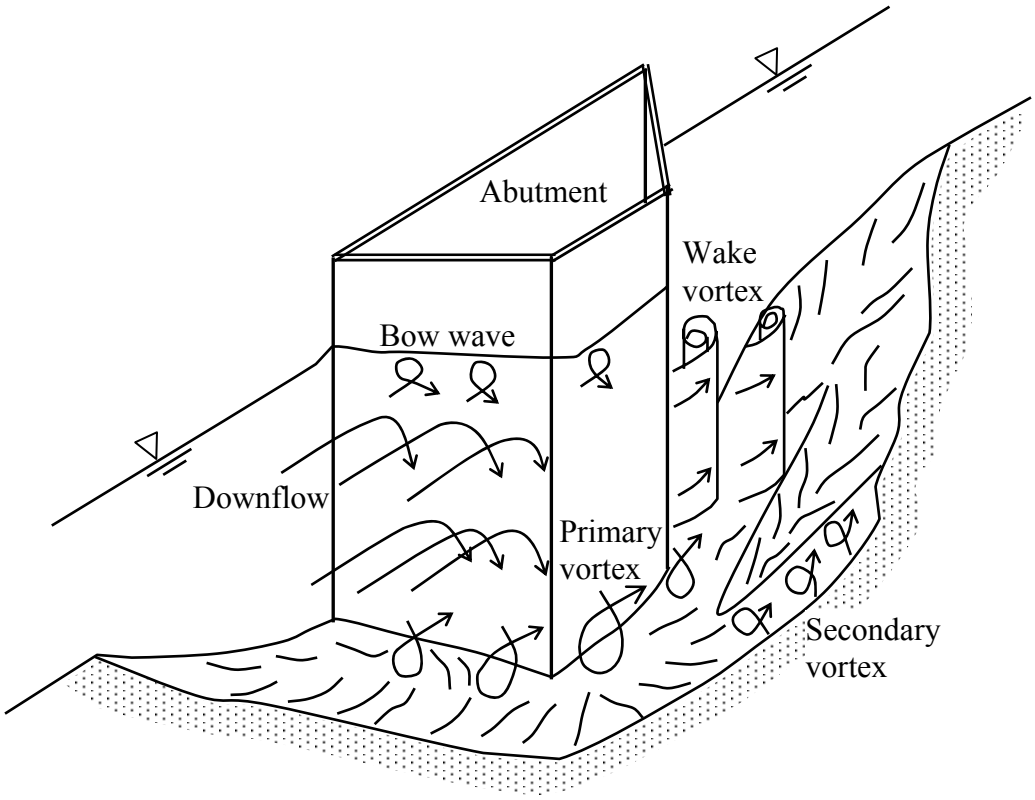

Fig. 6.35 Schematic of flow field at an abutment after Kwan (1988)

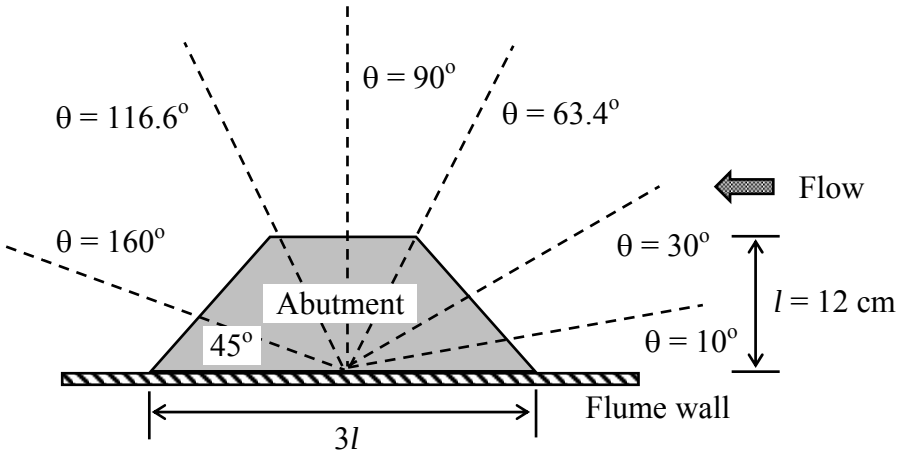

Fig. 6.36 Sections of flow measurements at 45° wing-wall abutment (after Dey and Barbhuiya 2006)

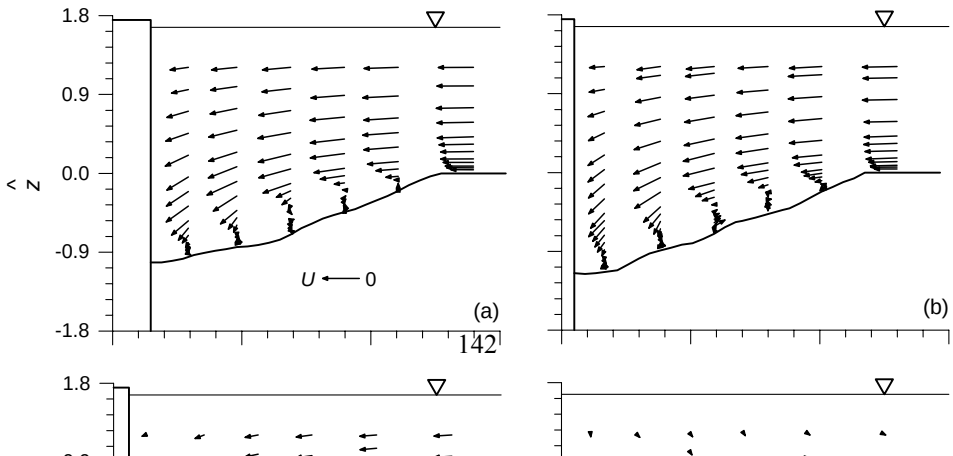

Fig. 6.37 Normalized velocity vectors at azimuthal sections of a 45° wing-wall abutment after Dey and Barbhuiya (2006): (a) θ = 10°; (b) θ = 30°; (c) θ = 63.4°; (d) θ = 90°; (e) θ = 116.6° and (f) θ = 160°

6.7.2 Parameters Influencing Scour Depth at Abutments

Parameters involved in the scour phenomenon at abutments can be grouped as follows:

- Parameters relating to the abutment: Size, shape, spacing, number and orientation with respect to the approaching flow direction.
- Parameters relating to the bed sediment: Median size, particle size distribution, mass density, angle of repose and cohesiveness.
- Parameters relating to the approaching flow condition: Approaching flow velocity, approaching flow depth, shear velocity and roughness.
- Parameters relating to the fluid: Mass density, viscosity, gravitational acceleration and temperature (may not be important in scour problems).
- Parameters relating to the geometry of channel: Width, cross-sectional shape and slope.
- Parameters relating to the time: Time of scouring for an evolving scour hole.
- Parameters relating to the unsteadiness: Passage of flood wave in rivers and waves in marine environment.

The relationship showing the influence of various parameters on the equilibrium scour depth d_s at abutments can be given in functional form as follows:

$$d_s = f_1(U_1, h_1, \rho, \rho_s, g, \nu, l, d_{50}, \sigma_g, t) \tag{6.83}$$

The dependency of scour depth on various parameters studied by Dey and Barbhuiya (2004a) is given below:

6.7.2.1 Effect of Abutment Length - Sediment Diameter Ratio on Scour Depth

The variation of nondimensional equilibrium scour depth $\hat{d}_s$ (= d_s/l) at abutments in sand-beds as a function of $\tilde{l}$ (= l/d_{50}) under clear-water scour condition is given in Fig. 6.38(a), which shows that $\hat{d}_s$ decreases with an increase in $\tilde{l}$ (Dey and Barbhuiya 2004a). The trend is almost opposite to pier scour. Also, Fig. 6.38(a) shows that $\hat{d}_s$ is greater for smaller abutment length and coarser sediment size. The probable reason is attributed to the fact that the substantial increase of approaching flow velocity U_1 to maintain the clear-water scour condition for a coarser sediment size increases the strength of the primary vortex and the downflow to a great extent, resulting in a vortex flow with an enhanced scour potential. On the other hand, $\hat{d}_s$ is independent of $\tilde{l}$ for larger abutment length and finer sediment size. However, the curves of different abutments show that for a given $\tilde{l}$, the magnitude of $\hat{d}_s$ for vertical-wall abutment is greater than that for other types of abutments, whereas $\hat{d}_s$ for 45° wing-wall is marginally higher than that for semicircular abutments. Recently, Raikar and Dey (2005b) studied the influence of gravels on scour depth at abutments. The variation of $\hat{d}_s$ with $\tilde{l}$ for the 45° wing-wall and vertical-wall abutments is presented in Fig. 6.38(b).

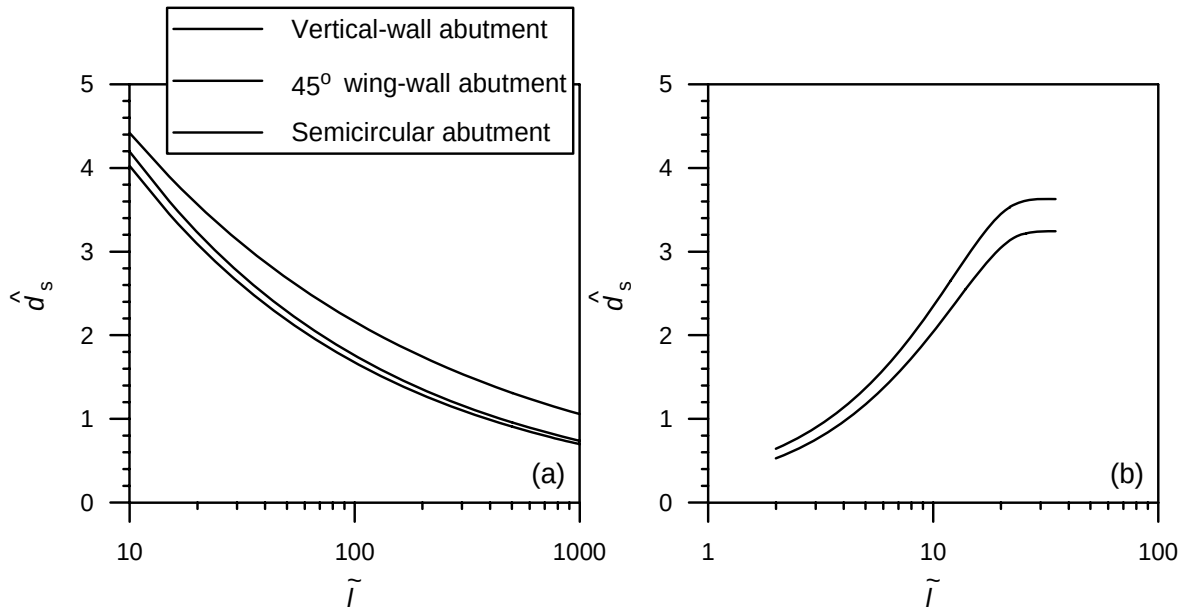

Fig. 6.38 Variation of $\hat{d}_s$ with $\tilde{l}$ for $U_1/U_c \approx 1$: (a) in sand-beds (after Dey and Barbhuiya 2004a) and (b) in gravel-beds (after Raikar and Dey 2005b)

6.7.2.2 Effect of Approaching Flow Depth - Abutment Length Ratio on Scour Depth

The dependency of $\hat{d}_s$ at 45° wing-wall abutments for clear-water scour condition on approaching flow depth - abutment length ratio $\hat{h}$ (= h_1/l) for different $\tilde{l}$ and d_{50} = 0.26 mm is presented in Fig. 6.39 (Dey and Barbhuiya 2004a). At small $\hat{h}$, the nondimensional equilibrium scour depth $\hat{d}_s$ increases significantly with an increase in $\hat{h}$, while $\hat{d}_s$ becomes

almost independent of $\hat{h}$, as $\hat{h}$ increases. However, the variation of $\hat{d}_s$ with $\hat{h}$ has similar trend as that of pier scour case (see Fig. 6.28). It is obvious from Fig. 6.39 that larger the abutment length, the range of influence of flow depth is smaller. For large l, scour depth d_s is essentially independent of flow depth at $\hat{h}$ being two, whereas for small l, $\hat{h}$ is approximately six. This aspect may be justified that there is a little increase of strength of primary vortex due to an increase in flow depth beyond two and six times of abutment length for large and small abutment sizes, respectively. From the close examination of Fig. 6.39, it is also apparent that $\hat{d}_s$ decreases with an increase in $\tilde{l}$, as was observed in the preceding section. For shallow flow depths, the surface roller, termed bow wave, having a sense of rotation opposite to the primary vortex, helps to reduce the strength of primary vortex, resulting in a reduced scour depth.

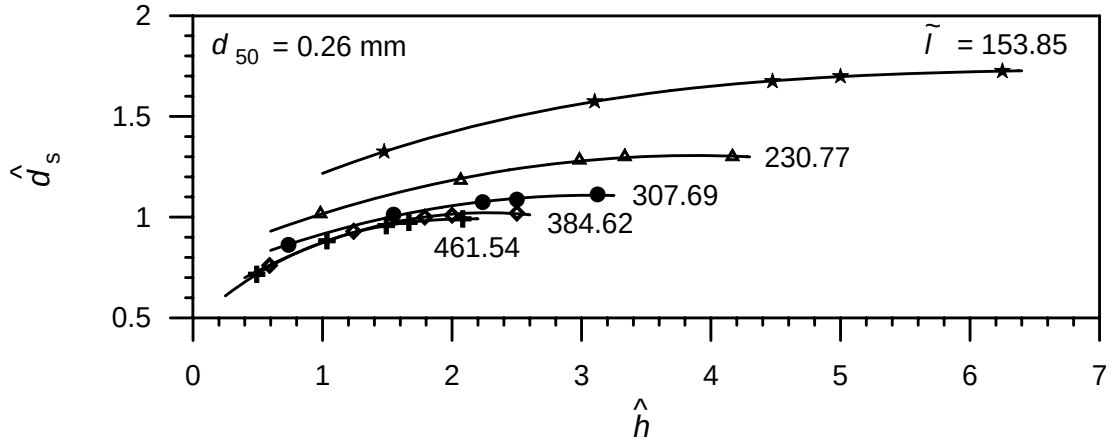

Fig. 6.39 Dependency of $\hat{d}_s$ on $\hat{h}$ for 45° wing-wall abutments for $U_1/U_c \approx 1$ (after Dey and Barbhuiya 2004a)

6.7.2.3 Effect of Sediment Gradation on Scour Depth

As discussed in section 6.6.2.3, the particle size distribution σ_g of sediments also has a pronounced influence on the scour depth at abutments. Nonuniform sediments ($\sigma_g > 1.4$) consistently produce lower scour depths than that in uniform sediments due to formation of armor-layer within the scour hole. The equilibrium scour depth $d_s(\sigma_g)$ at abutments embedded in nonuniform sediments can be obtained by multiplying the equilibrium scour depth at abutments in uniform sediments by the coefficient K_σ [as shown in Eq. (6.3)]. The variations of K_σ with σ_g for vertical-wall, 45° wing-wall and semicircular abutments are given in Fig. 6.40. It is apparent from the curves drawn for different abutments that the scour depth in nonuniform sediment with $\sigma_g = 3.5$ is drastically reduced to 20% of scour depth in uniform sediment. However, the reduction of scour depth for $\sigma_g > 3.5$ is not influenced by the nonuniformity of sediments. In Fig. 6.40, the curves of different abutments show that for a given σ_g, coefficient K_σ for vertical-wall abutment is slightly greater than that for other types of abutments.

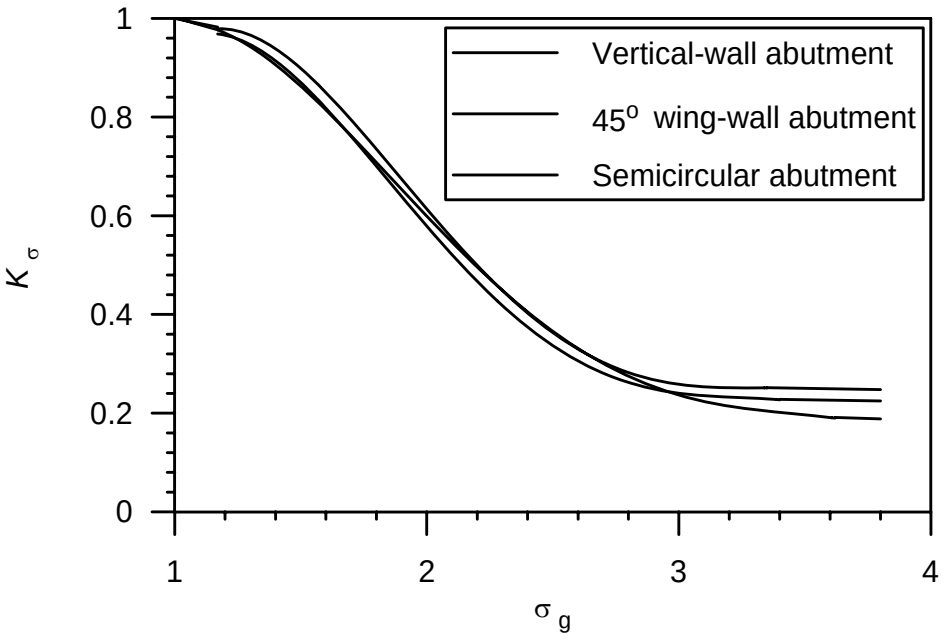

Fig. 6.40 Variation of K_σ as a function of σ_g for abutments under $U_1/U_c \approx 1$ (after Dey and Barbhuiya 2004a)

6.7.2.4 Time-Variation of Scour Depth

Scour Depth in Uniform Sediments:

Dey and Barbhuiya (2004a) studied the time-variation of clear-water scour at different sizes of vertical-wall, 45° wing-wall and semicircular abutments embedded in various uniform sediment sizes. The nondimensional instantaneous scour depth $\hat{d}_{st}$ at an abutment is represented in functional form as

$$\hat{d}_{st} = f(\hat{t}, \tilde{l}) \tag{6.84}$$

where $\hat{d}_{st} = d_{st}/l$; d_{st} = instantaneous scour depth at time t; $\hat{t} = S_l/(R_l \tilde{l})$, that is the nondimensional time; $S_l = Ut/l$, that is the Strouhal number; and $R_l = Ul/\nu$, that is the abutment Reynolds number. The variation of nondimensional instantaneous scour depth $\hat{d}_{st}$ with nondimensional time $\hat{t}$ for 45° wing-wall of different $\tilde{l}$ is presented in Fig. 6.41. The resulting trend is a family of nearly parallel lines. The instantaneous scour depth $\hat{d}_{st}$ decreases with an increase in $\tilde{l}$. To be more explicit, $\hat{d}_{st}$ decreases with an increase in l and with a decrease in d_{50}. It implies that for a given value of $\hat{d}_{st}$, larger the abutment length l, a longer time it takes to reach $\hat{d}_{st}$.

Scour Depth in Nonuniform Sediments:

In nonuniform sediments ($\sigma_g > 1.4$), the nondimensional instantaneous scour depth $\hat{d}_{st}$ at abutments is represented as a function of $\hat{t}$ and σ_g for different d_{50}. For 45° wing-wall abutments, the variation of nondimensional instantaneous scour depth $\hat{d}_{st}$ with nondimensional time $\hat{t}$ for different σ_g and d_{50} = 1.86 mm is shown in Fig 6.42. The results show for each sediment size d_{50}, a significant reduction of scour depth with an increase in

nonuniformity of sediment, which is given by the geometric standard deviation σ_g. The rate of development of scour hole reduces due to formation of an armor-layer at the base of the scour hole and hence, the equilibrium scour depth in nonuniform sediments diminishes. It is apparent that in the initial stage, the rate of scouring is rapid.

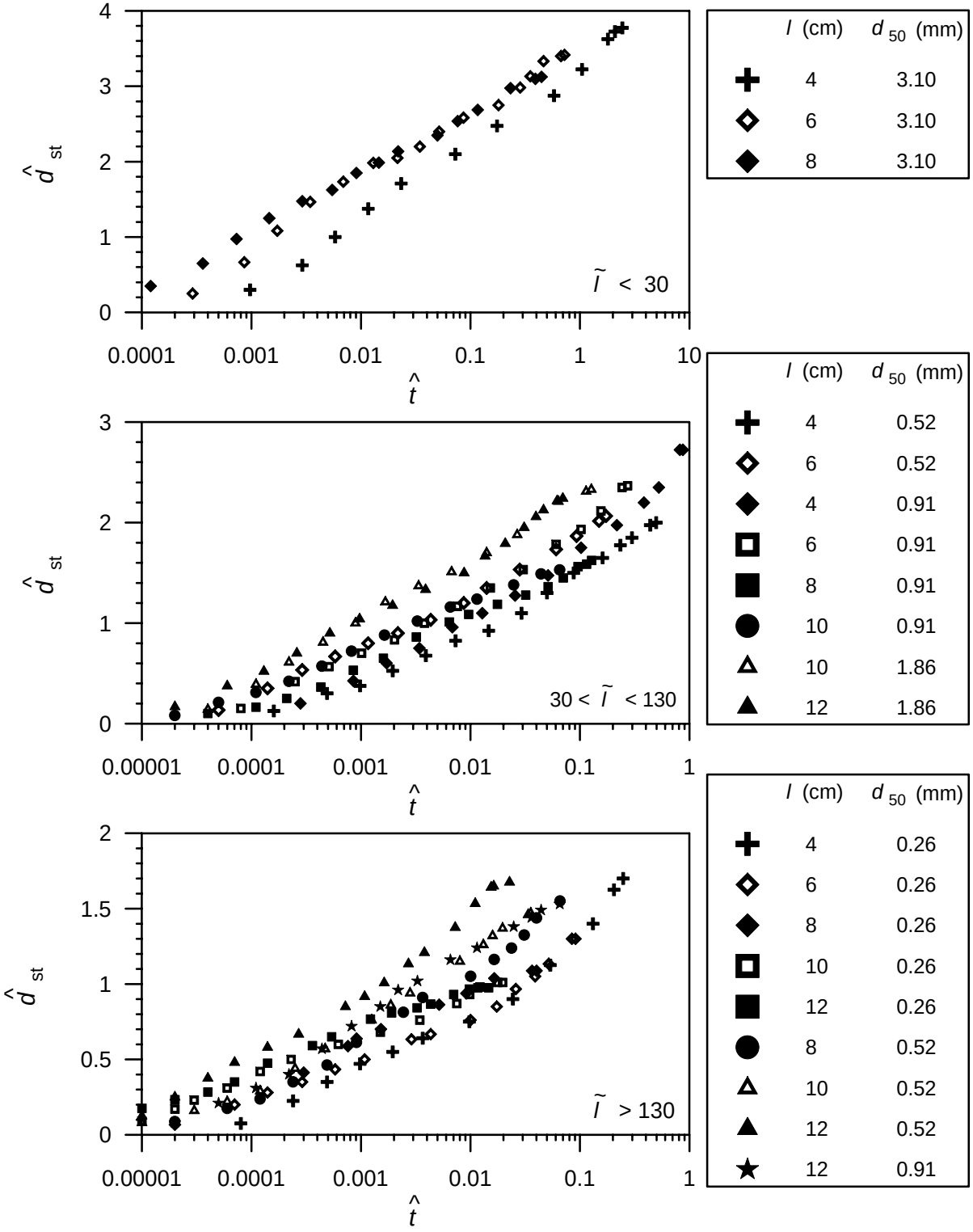

Fig. 6.41 Variation of $\hat{d}_{st}$ as a function of $\hat{t}$ for 45° wing-wall abutments in uniform sediments for $U_1/U_c \approx 1$ (after Dey and Barbhuiya 2004a)

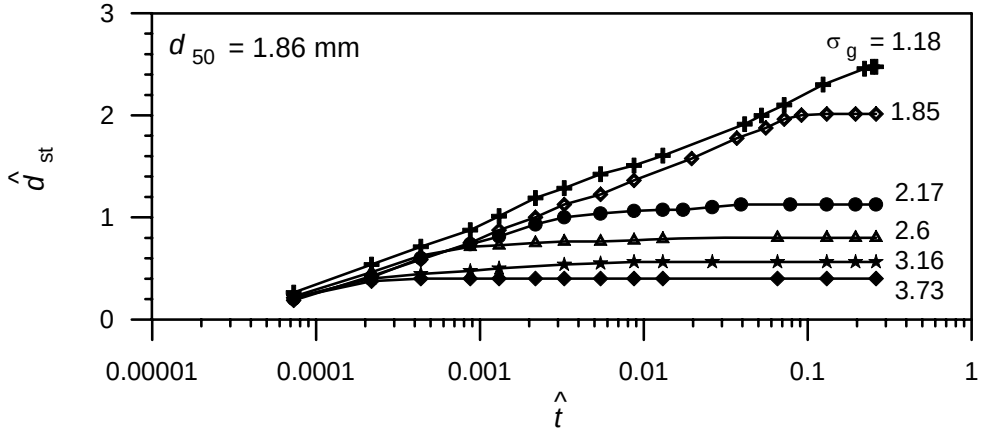

Fig. 6.42 Variation of $\hat{d}_{st}$ with $\hat{t}$ for different σ_g and d_{50} = 1.86 mm for 45° wing-wall abutments under $U_1/U_c \approx 1$ (after Dey and Barbhuiya 2004a)

6.7.3 Equations of Equilibrium Scour Depth

As the number of proposed equations for the estimation of maximum scour depth at abutments is overwhelming (Barbhuiya and Dey 2004), their application is limited to the conditions similar to those for which they are valid. The design approach recommended by Melville and Coleman (2000) for the estimation of maximum scour depth at abutments based on empirical relationship, called *K*-factors, which account for the effects of abutment, flow and sediment characteristics, seems to be good and is given. The maximum equilibrium scour depth d_s at a bridge abutment is given by

$$d_s = K_h K_I K_d K_s K_\alpha K_G K_t \tag{6.85}$$

where K_h = flow depth - foundation size factor; K_I = flow intensity factor; K_d = sediment size factor; K_s = abutment shape factor; K_α = abutment alignment factor; K_G = channel geometry factor; and K_t = time factor. The relationships for *K*-factors are given as follows:

The *flow depth - foundation size factors* K_h for abutments scour are

$$K_h(l < h_1) = 2l \tag{6.86a}$$

$$K_h(h_1 \le l < 25h_1) = 2(h_1 l)^{0.5} \tag{6.86b}$$

$$K_h(l < h_1) = 10h_1 \tag{6.86c}$$

The *flow intensity factor* K_I given by Eqs. (6.76a) and (6.76b) for the case of pier scour is also applicable for the abutment scour.

The *sediment size factor* K_d, which is same as in pier scour, given by Eqs. (6.77a) and (6.77b) is also applicable for the estimation of scour depth at abutments in sands. However, for the abutments in gravels, Raikar and Dey (2005b) proposed new sediment size factors as

$$K_d(\tilde{l} \le 10) = 0.514 \ln \tilde{l} - 0.273 \tag{6.87a}$$

$$K_d(10 < \tilde{l} \le 25) = 0.098 \ln \tilde{l} + 0.682 \tag{6.87b}$$

$$K_d(\tilde{l} > 25) = 1 \tag{6.87c}$$

The *shape factor* K_s is defined as the ratio of the scour depth for a particular abutment shape to that for the vertical-wall abutments. The values of shape factors K_s for different shapes of abutments are given in Table 6.

Table 6 Shape Factors K_s for Abutments

Abutment model	Abutment shape	K_s
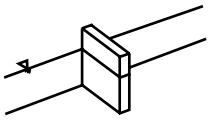	Vertical-wall	1
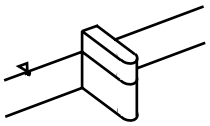	Semicircular ended	0.75
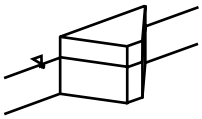	45° wing-wall	0.75
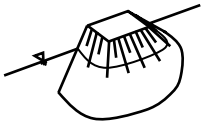	Spill-through with slope horizontal : vertical	
	0.5 : 1	0.6
	1 : 1	0.5
	1.5 : 1	0.45

For long abutments (abutment length / upstream flow depth > 1), the values of *alignment factor* K_α are given in Table 7.

Table 7 Alignment Factors K_α for Long Abutments

α (degree)	30	45	60	90	120	135	150
K_α	0.9	0.95	0.98	1	1.05	1.07	1.08

For short abutments, the values of alignment factor K_α^* are

$$K_\alpha^*(l \geq 3h_1) = K_\alpha \tag{6.88a}$$

$$K_\alpha^*(h_1 < l < 3h_1) = K_\alpha + (1 - K_\alpha)(1.5 - 0.5b/h_1) \tag{6.88b}$$

$$K_\alpha^*(l \leq h_1) = 1 \tag{6.88c}$$

The *channel geometry factor* K_G is defined as the ratio of the scour depth at an abutment to that at the same abutment in the equivalent rectangular channel. In case of rectangular channels, the channel geometry factor K_G = 1. However, for abutments in compound channels, K_G depends on the position of the abutment in the compound channel. The equation of K_G is

$$K_G = \sqrt{1 - \left(\frac{l^*}{l}\right)\left[1 - \left(\frac{h_1^*}{h_1}\right)^{5/3}\left(\frac{n}{n^*}\right)\right]} \tag{6.89}$$

where l^*= abutment length spanning the flood channel; h_1^* = flow depth in the flood channel; and n and n^* = Manning roughness coefficient in the main and flood channels, respectively.

The *time factor* K_t is the ratio of scour depth at a particular time t to the equilibrium scour depth. Its value depends on the scour condition, whether clear-water scour or live-bed scour. For live-bed scour, K_t is unity; while in clear-water scour, K_t is given by

$$K_t = 0.1\frac{U_c}{U_1}\ln\left(\frac{t}{t_e}\right)+1 \tag{6.90}$$

where the expressions for t_e can be given by

$$t_e(\text{days}) = 25h_1/U_1 \qquad \text{for } l \geq 1.2h_1 \tag{6.91}$$

$$t_e(\text{days}) = 20.83\,l/U_1 \qquad \text{for } l < 1.2h_1 \tag{6.92}$$

HEC18 (Richardson and Davis 2001) recommends Froehlich's (1989) equation of the live-bed scour at abutments for the estimation of maximum scour depth. It is

$$\frac{d_s}{h_1} = 2.27K_sK_\alpha\left(\frac{l}{h_1}\right)^{0.43}F_r^{0.61}+1 \tag{6.93}$$

where $F_r = U_e/(gh_1)^{0.5}$; $U_e = Q_e/A_e$; Q_e = flow rate obstructed by the abutment and approach embankment; and A_e = flow area of the approaching cross-section obstructed by the embankment. The values of shape factors K_s are furnished in Table 8, while the alignment factor K_α can be obtained from Fig. 6.43.

Table 8 Shape factors K_s for Abutments

Abutment shape	K_s
Vertical-wall abutment	1
Vertical-wall abutment with wing walls	0.82
Spill-through abutment	0.55

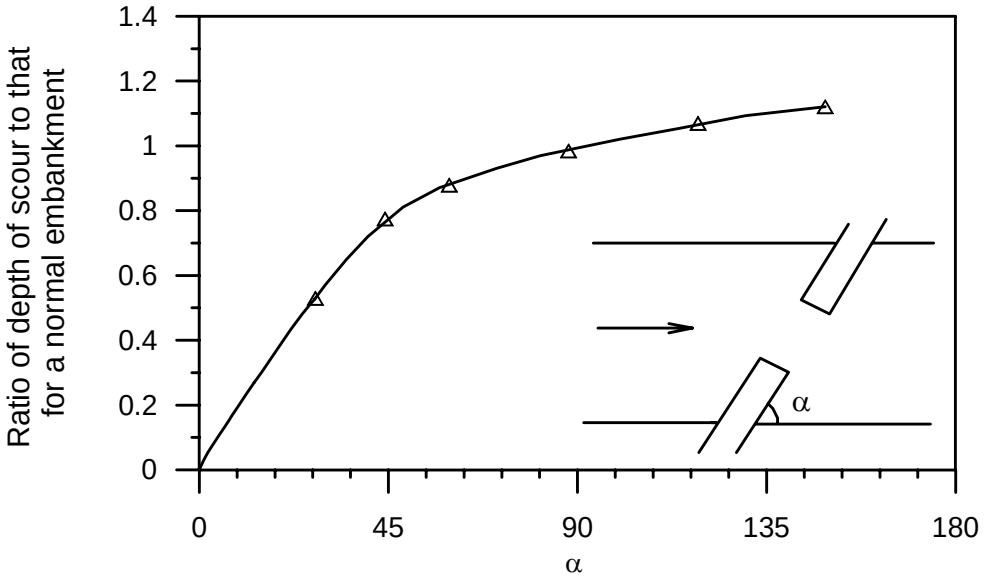

Fig. 6.43 Alignment factors K_α for abutments (after HEC18)

6.7.4 Example

Determine the maximum equilibrium scour depth at an abutment for the following data:

- Wing-wall abutment having l = 12.5 m inclined at 60^o to the approaching flow direction
- Approaching flow velocity, U_1 = 1.1 m/s
- Approaching flow depth, h_1 = 8 m
- Median size of bed sediment, d_{50} = 2.3 mm
- Geometric standard deviation of sediment, σ_g = 1.14
- Manning roughness coefficient, n = 0.02 SI units
- Channel geometry, l^* = 110 m, h_1^* = 2 m and n^* = 0.04

For d_{50} = 2.3 mm, the critical shear velocity u_{*c} is calculated from Eq. (2.30a) – (2.30e) as 0.0397 m/s. Using the equation of semi-logarithmic average velocity [U_c/u_{*c} = $5.75\log(0.5h_1/d_{50}) + 6$] the critical flow velocity U_c corresponding to h_1 = 8 m is obtained as 0.98 m/s.

The K-factors are:

1. For l/h_1 = 12.5/8 = 1.563 > 1 (that is a long abutment), using Eq. (6.86b), K_h = $2(12.5\times8)^{0.5}$ = 20 m.
2. For U_1/U_c = 1.1/0.98 = 1.125 >1 (live-bed scour condition), using Eq. (6.76b) K_I = 1 and corresponding K_t = 1.
3. For $\tilde{l}$ = $l/d_{50} = 12.5/2.3\times10^{-3}$ = 5434.78 > 25, using Eq. (6.77b) K_d = 1.
4. For wing-wall abutment, K_s = 0.75 (from Table 6).
5. For $\alpha = 60^o$, K_α = 0.98 (from Table 7).
6. From Eq. (6.89), K_G = 0.405.
7. For σ_g = 1.14 < 1.4 (that is uniform sediment), K_σ = 1.

Using Melville and Coleman's (2000) equation [Eq. (6.85)], the maximum scour depth at wing-wall abutment in uniform sediments is: d_s = $K_hK_IK_dK_sK_\alpha K_GK_t$ = $20\times1\times1\times0.75\times0.98\times0.405\times1$ = 5.95 m.

6.8 Scour in Armored Beds

In the upper reaches, riverbeds are commonly composed of a mixture of different sizes of sands and gravels. Under the varied stream flow velocities, a process of armoring on the riverbeds commences resulting in an exposure of coarser particles due to washing out of the finer fraction. The armor-layers of concern are those where the structure is embedded in a sand-bed overlain by a layer of gravels, formed owing to the sorting of riverbed sediments. The armor-layer extends the magnitude of critical flow velocity for the motion of bed particles, sustaining an extended clear-water scour condition up to the limiting stability of surface particles, as shown in Fig. 6.44. As a consequence of the surface particles at critical condition, a considerably larger scour depth develops in an armored bed (unless a secondary armor-layer developed within the scour hole is compact enough to prevent further scouring) than in a bed of uniform sediments. The scour within channel contractions, at bridge piers and at abutments embedded in armored beds studied by different investigators are presented here.

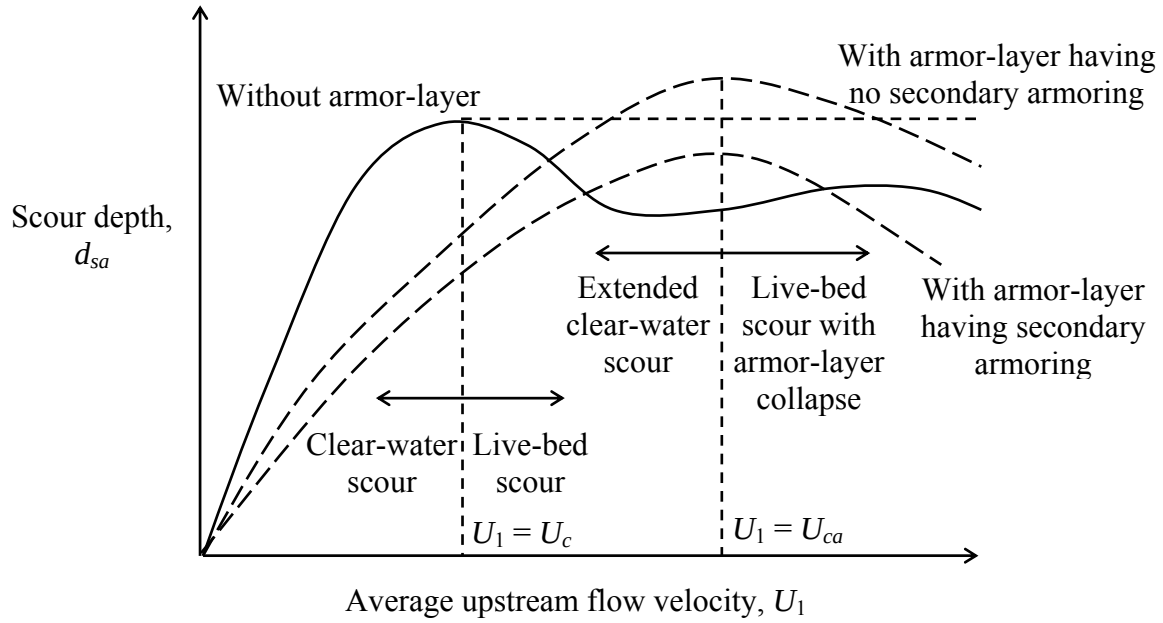

Fig. 6.44 Effect of armor-layer on scour depth as a function of upstream flow velocity

6.8.1 Scour within Channel Contractions in Armored Beds

Raikar and Dey (2006) [also in Raikar (2006)] investigated scour within channel contractions in sand-bed with a thin surface-layer of gravels. They reported that the scour depth (relative to the approaching flow depth) within long contractions with surface-layers increases with an increase in surface-gravel to bed-sand size ratio $\tilde{d}_g$ (= d_g/d_{50}; where d_g = median size of surface-gravels; and d_{50} = median size of bed-sand) and with a decrease in channel opening ratio $\hat{b}$. On the other hand, the scour depth within a channel contraction with a surface-layer of gravels is greater than that without surface-layer for the same bed sediments and flow condition.

When the flow velocity in the contracted zone of channel reaches the critical velocity U_{ca} for the gravels in the surface-layer, the gravel-layer is scoured, exposing the bed-sand to the flow velocity, which is far greater than the critical velocity U_c of bed-sand. Consequently, the bed-sand in the contracted zone scours considerably. With an increase in scour depth in the contracted zone, the flow velocity in the contracted zone decreases. As the flow velocity approaches the value of critical velocity for the bed-sand, scour within the contraction ceases and the equilibrium of the scour hole is attained. However, at equilibrium, the original surface-layer of gravels remains intact in the upstream bed of uncontracted channel. In the contracted zone, the scoured gravel particles of the surface-layer are distributed in a scattered and loose manner. Fig. 6.45 displays the photograph of the equilibrium scour hole within a long contraction with a gravel-layer.

The variation of nondimensional scour depth $\hat{d}_{sa}$ (= d_{sa}/h_1; where d_{sa} = equilibrium scour depth in armored bed) versus $\tilde{d}_g$ for the bed-sand of d_{50} = 1.86 mm under $U_1/U_{ca} \approx 1$ (that is maximum limit of clear-water scour) is shown in Fig. 6.46(a). Fig. 6.46(a) demonstrates that $\hat{d}_{sa}$ increases with an increase in $\tilde{d}_g$. Also, it depicts a significant increase in scour depth $\hat{d}_{sa}$ with a decrease in channel opening ratio $\hat{b}$.

Fig. 6.45 Photograph showing equilibrium scour within a long contraction with a thin gravel-layer

Fig. 6.46(b) displays the variations of the ratio of scour depth within long contractions with surface-layers to those of scour depth within long contractions in un-layered bed-sands $\tilde{d}_{sa}$ (= d_{sa}/d_s; where d_s = scour depth within long contractions in un-layered uniform sands) with $\tilde{d}_g$ for different values of $\hat{b}$ and d_{50} = 1.86 mm under approaching flow close to the maximum limit of clear-water scour. The scour depth ratio $\tilde{d}_{sa}$ increases with an increase in $\tilde{d}_g$. As the value of $\tilde{d}_{sa}$ is greater than unity, scour depths within long contractions with surface-layers of gravels are always greater than those in uniform bed sediments (un-layered beds).

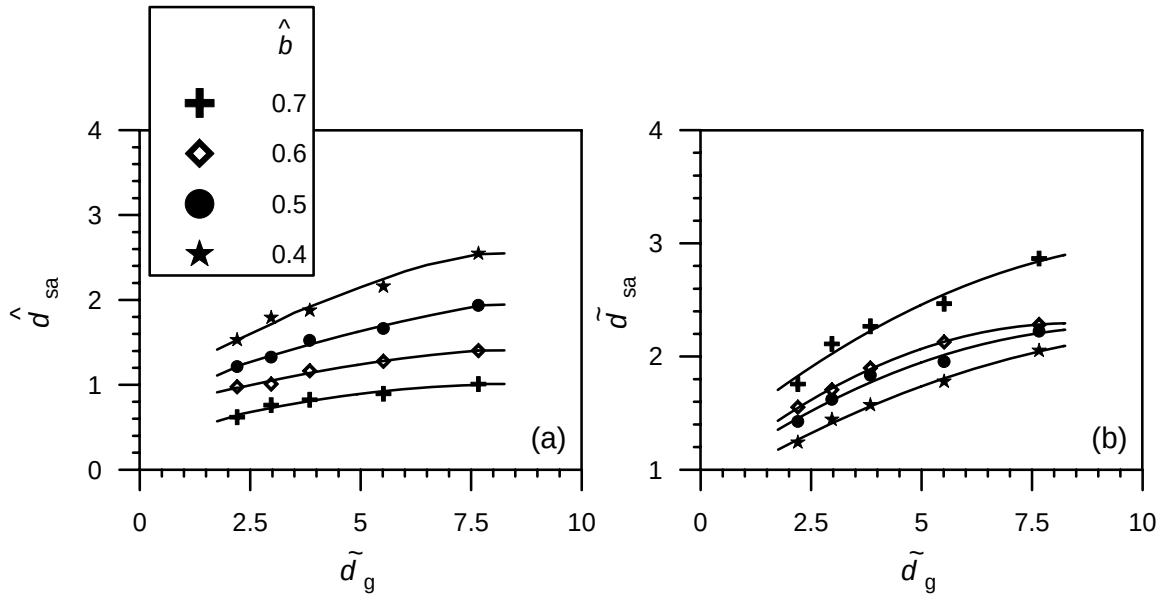

Fig. 6.46 (a) Variations of scour depth $\hat{d}_{sa}$ with $\tilde{d}_g$ for different $\hat{b}$ and d_{50} = 1.86 mm and (b) Variations of scour depth $\tilde{d}_{sa}$ with $\tilde{d}_g$ for different $\hat{b}$ and d_{50} = 1.86 mm (after Raikar and Dey 2006)

Further, the maximum equilibrium scour depth within a long contraction with gravel-layer d_{sa} was computed using the energy and continuity equations [using Dey and Raikar's (2005) clear-water scour model without sidewall correction]. The comparison of nondimensional equilibrium scour depths $\hat{d}_{sa}$ computed using the model with the experimental data is shown in Fig. 6.47.

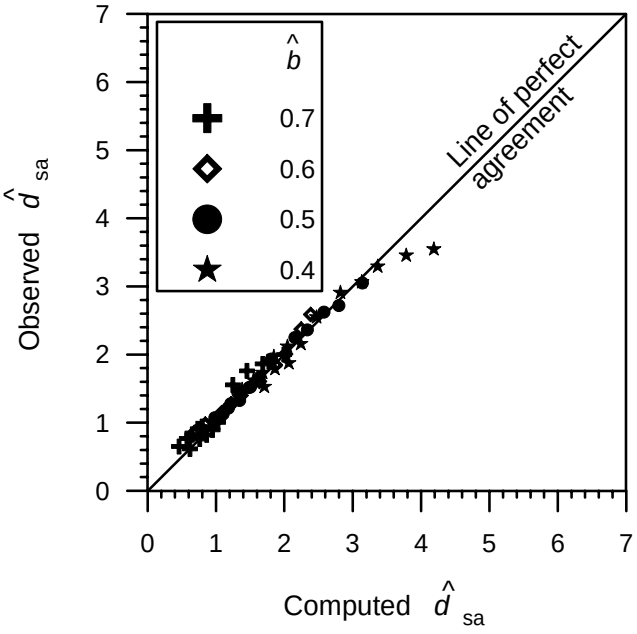

Fig. 6.47 Comparison between the equilibrium scour depths $\hat{d}_{sa}$ computed using clear-water scour model (Dey and Raikar 2005) and the experimental data of Raikar and Dey (2006)

6.8.2 Scour at Bridge Piers in Armored Beds

Ettema (1980) and Raudkivi and Ettema (1985) studied scour at piers in thin armor-layer and stratified beds. Thickness of stratified bed is more than that of natural armor-layer thickness. Froehlich (1995) reported that the natural armor-layer thickness being one to three times the armor particle sizes. Recently, Raikar (2006) studied the scour at piers embedded in a bed of uniform sands of median size d_{50} overlain by a thin armor-layer of uniform gravels of size d_g. The thickness of armor-layers was twice the armor-gravel size. The influences of various parameters on scour depth along with the design equation for maximum scour depth at bridge piers embedded in armor-layers was reported by Raikar (2006).

6.8.2.1 Classification of Scour Hole and Scouring Process

For the approaching flow velocities U_1 nearly equaling the critical velocity U_{ca} for armor particles ($U_1/U_{ca} \approx 0.9$), three different cases of idealized topography of scour holes were identified [Figs. 6.48(a) – 6.48(c)], depending on the pier width, flow depth and ratio of armor-gravel to bed-sand size $\tilde{d}_g$. The salient features of three cases of scour hole are given below:

Case 1 The scour hole in the vicinity of a pier develops through the armor-layer removing the sand from the bed underneath. The armor-layer remains intact around the perimeter of the scour hole [Fig. 6.48(a)].

Case 2 The scour hole in the vicinity of a pier forms through the armor-layer having relatively more extension of scour hole in the upstream. The armor-layer disintegrates over a short distance downstream. However, the armor-layer remains intact around the upstream perimeter of the scour hole [Fig. 6.48(b)] [same as "case b" in Raudkivi and Ettema (1985)].

Case 3 The scour hole in the vicinity of a pier develops collapsing the armor-layer over a considerable distance upstream. On the other hand, the armor-layer washed out completely downstream. However, the armor-layer exists in the far upstream perimeter of the scour hole in the form of a large arc [Fig. 6.48(c)] [same as "case c" in Raudkivi and Ettema (1985)].

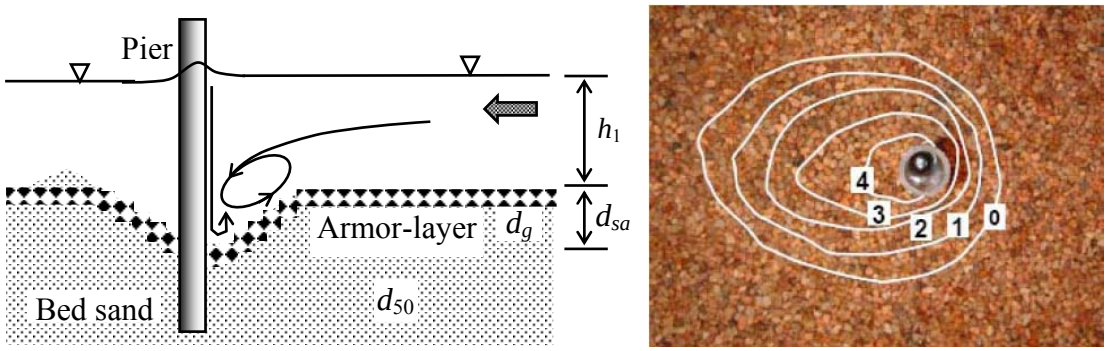

(a)

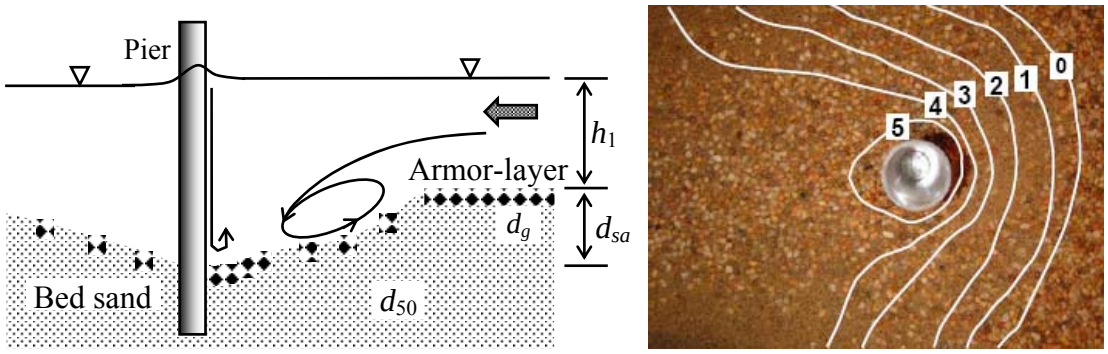

(b)

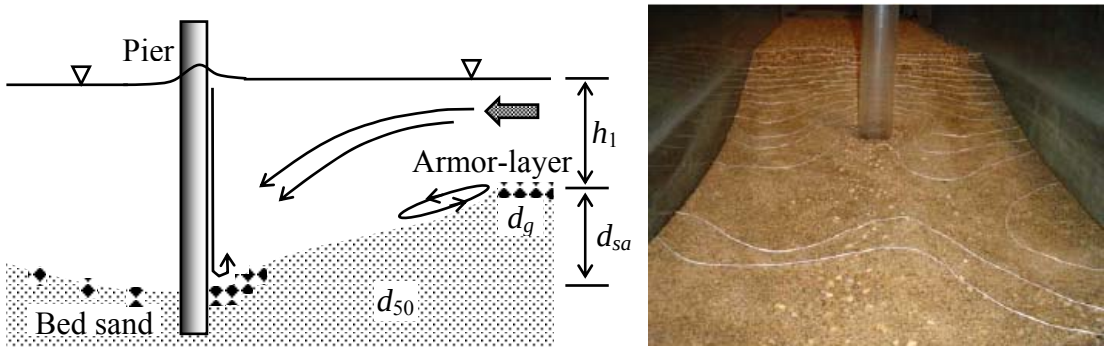

(c)

Fig. 6.48 Schematic of scour holes at pier in armored beds: (a) case 1, (b) case 2 and (c) case 3 (after Raikar 2006)

According to Raikar (2006), in case 1 [Fig. 6.48(a)], at the initial stage the scour took place through the armor-layer removing the bed-sands rapidly. A compact secondary armor-layer having one-grain thickness of gravel, which covered the scour hole almost fully, was gradually developed within the scour hole, offering resistance towards the entrainment of bed-sands and inhibiting the progress of further scouring. The original armor-layer remained unbroken around the perimeter of the scour hole. This case prevailed for a small pier width. Because a small pier width was unable to induce strong downflow and horseshoe vortex in front of the pier to disintegrate and entrain the armor-gravels to downstream of the pier. Also, smaller flow depths favored to occur case 1. In case 2 [Fig. 6.48(b)], the scour hole in the vicinity of a pier formed through the armor-layer having an extension of scour hole in the upstream. This was the stage when armor-layer started collapsing in the upstream by the joint action of the downflow and the horseshoe vortex. The upstream portion of the scour hole shifted further upstream as a result of flow separation at the upstream edge of the scour hole forming a vortex flow. However, the scour at the pier base took place due to the downflow along the upstream face of the pier. In the upstream, the secondary armor-layer was rather loose in general; though adjacent to the pier it was well compact. On the other hand, in the downstream, the original armor-layer disintegrated over a short distance without noticeable secondary armoring within the scour hole. However, the original armor-layer remained intact around the upstream perimeter of the scour hole. In case 3 [Fig. 6.48(c)], when the scour hole was developed disintegrating the armor-layer up to some distance in the upstream and completely in the downstream. The secondary armor-layer was mainly concentrated to the lower portion of the scour hole at the upstream base of the pier. The scour hole extended over a considerable distance upstream, where the original armor-layer existed in the form of a large arc at the extremity of the scour hole. Instead of a conical shaped scour hole, a streamwise curved shaped scour hole (almost two-dimensional, as an effect of flume side-walls) prevailed in this case. (In the field, the influence of the scour hole on that at neighboring piers may result in a curved shaped scour hole with an overlapping of scour holes at the pier sides.) At the far upstream of the scour hole, scour took place as if the sand-bed were scoured downstream of a rigid platform. However, scour near pier occurred solely by the action of downflow along the upstream face of the pier. A large pier width was capable to induce sufficiently strong downflow and horseshoe vortex to dislodge the armor-gravels to the pier downstream. In addition, a relatively large flow depth helped to occur case 3. In fact, case 2 is the transition of case 1 and case 3.

6.8.2.2 Effect of Armor-Layer on Scour Depth

The variations of nondimensional equilibrium scour depth $\hat{d}_{sa}$ (= d_{sa}/b) with $\tilde{d}_g$ for different flow depths h_1 and widths b of circular piers is shown in Fig. 6.49. The nondimensional equilibrium scour depth $\hat{d}_{sa}$ decreases with an increase in $\tilde{d}_g$. The decreasing rate of scour depth $\hat{d}_{sa}$ is very rapid for $\tilde{d}_g$ < 5, 7 and 12 for bed-sands of d_{50} = 2.54 mm, 1.86 mm and 0.81 mm, respectively. But the influence of $\tilde{d}_g$ on $\hat{d}_{sa}$ is less prominent for $\tilde{d}_g$ > 5, 7 and 12 in bed-sands of d_{50} = 2.54 mm, 1.86 mm and 0.81 mm, respectively. In latter case, the secondary armor-layer within the scour hole controls the development of scour hole. On the other hand, scour depth $\hat{d}_{sa}$ decreases with an increase in bed-sand size d_{50} and with a decrease in upstream flow depth h_1 and pier width b. For particular values of $\tilde{d}_g$, d_{50} and h_1,

the scour depth $\hat{d}_{sa}$ increases with an increase in pier width b. For a given value of $\tilde{d}_g$, case of scour changes depending on flow depth h_1 and pier width b.

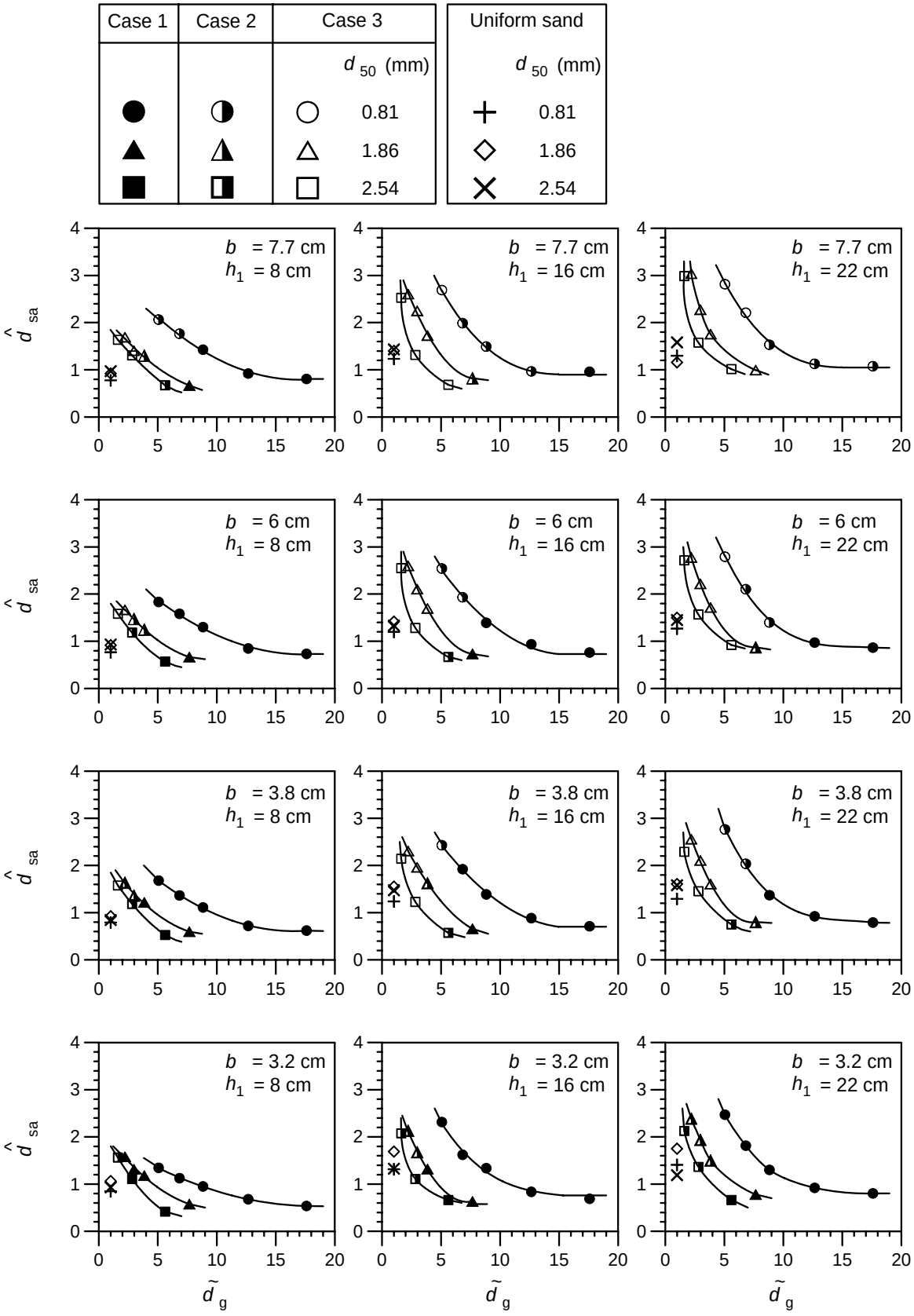

Fig. 6.49 Variation of scour depth $\hat{d}_{sa}$ with $\tilde{d}_g$ for different h_1 and b of circular piers under $U_1/U_{ca} \approx 1$ (after Raikar 2006)

Also, the data plots at $\tilde{d}_g = 1$ corresponds to $\hat{d}_{sa}$ in un-layered bed-sands. A close observation of Fig. 6.49 shows that the nondimensional scour depth increases with a sequence of case 1, case 2 and case 3. As there is no sediment supply from upstream, greater nondimensional scour depths occur in cases 2 and 3.

When the armor-gravel size is marginally larger than the bed-sand size, larger scour depth is developed due to the bed-sand having a smaller U_c than U_{ca} of armor-gravels. In such condition, case 3 occurs. On the other hand, if the armor-gravel size is considerably larger than the bed-sand size (case 1), in the beginning of scour process, the secondary flow induced by the pier dislodges the armor-gravels in the form of a shear failure. After a while, a secondary armor-layer within the scour hole develops and the secondary flow is then unable to entrain the secondary armor-gravels, but the winnowing of bed-sands through the interstices of secondary armor-gravels increases the scour depth slightly. Further, the comparison of the scour depth reveals that in case 1, the scour depth in armored beds is lesser than that in un-layered beds, as the surface of the scour hole is shielded by the secondary armor gravels. In contrast, in case 3, the scour depth in armored beds is greater than that in un-layered beds, since the secondary armor gravels are scattered within the scour hole.

6.8.2.3 Maximum Equilibrium Scour Depth

It is recognized that case 2 and case 3 are the major threat of scour at piers in armored beds. Thus, the equations of maximum equilibrium scour depth d_{sa} at a pier in an armored bed for case 2 and case 3, obtained using the experimental data of Raikar (2006), can be given by

$$\hat{d}_{sa} = 0.16 K_s F_{ca}^{1.33} \tilde{b}^{1.14} \hat{h}^{0.52} \tilde{d}_g^{-0.93} \qquad \text{for case 2} \qquad (6.94a)$$

$$\hat{d}_{sa} = 0.14 K_s F_{ca}^{0.78} \tilde{b}^{1.07} \hat{h}^{0.6} \tilde{d}_g^{-0.95} \qquad \text{for case 3} \qquad (6.94b)$$

where $F_{ca} = U_{ca}/(\Delta g b)^{0.5}$; $\tilde{b} = b/d_{50}$; and $\hat{h} = h_1/b$. The classification of the different cases of scour holes can be determined from Table 9.

Table 9 Classification of Scour Holes in Armored Beds (after Raikar 2006)

	Circular pier			Square pier		
β	Case 1	Case 2	Case 3	Case 1	Case 2	Case 3
0.128	$\eta \geq 6.25$	$2.78 < \eta < 6.25$	$\eta \leq 2.78$	$\eta \geq 8.33$	$1.33 < \eta < 8.33$	$\eta \leq 3.33$
0.1	$\eta \geq 2.56$	$1.54 < \eta < 2.56$	$\eta \leq 1.54$	$\eta \geq 3.57$	$1.96 < \eta < 3.57$	$\eta \leq 1.96$
0.063	$\eta \geq 1.35$	$0.71 < \eta < 1.35$	$\eta \leq 0.71$	$\eta \geq 1.70$	$0.97 < \eta < 1.70$	$\eta \leq 0.97$
0.053	$\eta \geq 0.60$	$\eta < 0.60$		$\eta \geq 0.79$	$\eta < 0.79$	

Note: $\beta = b/B$ and $\eta = \tilde{d}_g / \hat{h}$.

Determination of Maximum Equilibrium Scour Depth:

For the given values of pier width b, pier spacing B, armor-gravel size d_g, bed-sand size d_{50} and flow depth h_1, the appropriate case of scour hole can be determined from Table 9. Then, using Eqs. (6.94a) and (6.94b) for the appropriate case, the maximum equilibrium scour depth d_{sa} can be evaluated.

6.8.3 Scour at Bridge Abutments in Armored Beds

Dey and Barbhuiya (2004b) studied the development of clear-water scour at short abutments ($l/h_1 < 1$), namely vertical-wall, 45° wing-wall and semicircular, embedded in a bed of relatively fine uniform sediment overlain by an armor-layer of coarser sediment.

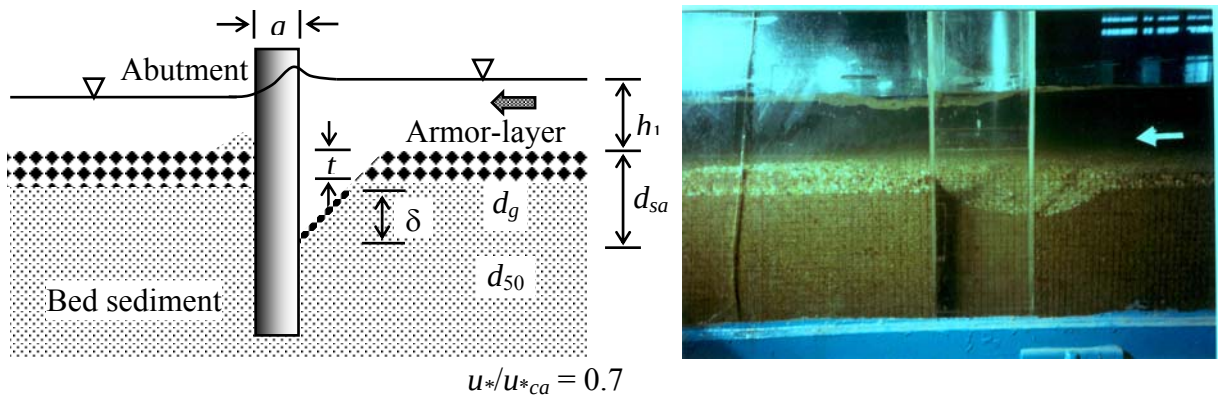

(a)

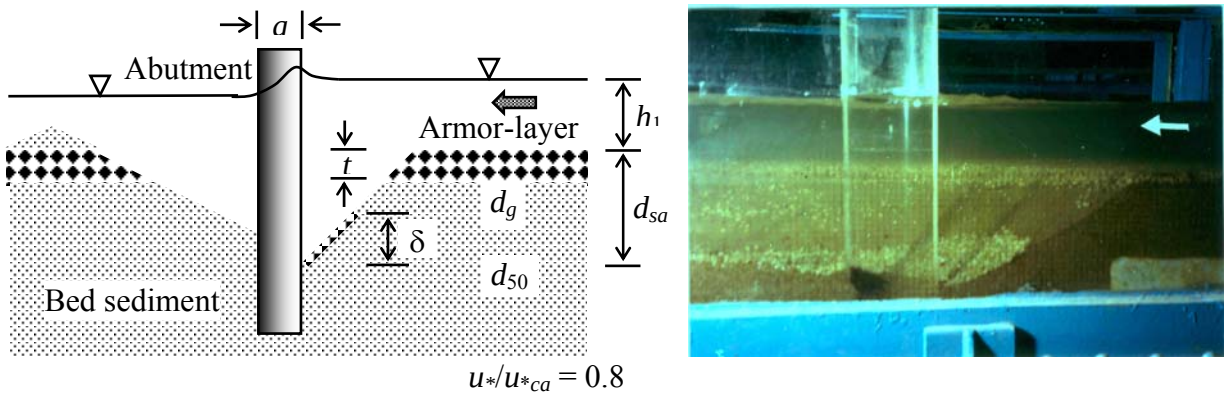

(b)

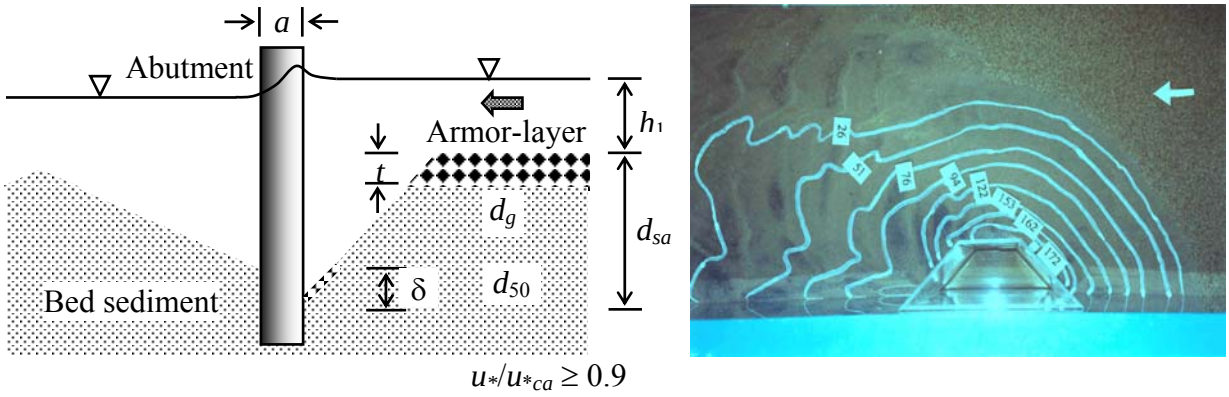

(c)

Fig. 6.50 Schematic of scour holes at abutments in armored beds: (a) case 1, (b) case 2 and (c) case 3 (after Dey and Barbhuiya 2004b)

6.8.3.1 Classification of Scour Hole and Scouring Process

Depending on the approaching flow conditions, following three topography of scour holes are classified [Figs. 6.50(a) – 6.50(c)]

Case 1 The scour hole at an abutment develops through the armor-layer in the upstream mainly. The scour hole does not extend beyond the downstream edge of the abutment. The armor-layer remains intact in the downstream of the abutment and around the upstream perimeter of the scour hole [Fig. 6.50(a)].

Case 2 The scour hole at an abutment forms through the armor-layer in the upstream and downstream. The armor-layer remains intact in the downstream of the scour hole and around the upstream perimeter of the scour hole [Fig. 6.50(b)].

Case 3 The armor-layer disintegrates over a long distance downstream but remains intact around the upstream perimeter of the scour hole [Fig. 6.50(c)].

According to Dey and Barbhuiya (2004b), case 1 was observed for the approaching flow condition $u_*/u_{*ca} = 0.7$. For $d_g > 2$ mm, a secondary armor-layer, which covered the scour hole either fully or partially, developed offering resistance towards the entrainment of bed sediment and restricting the progress of further scouring to a great extent [Fig. 6.50(a)]. But, no significant secondary armor-layer was found for $d_g < 2$ mm. With an increase in magnitude of approaching flow velocity, the scour hole extended beyond the downstream edge of abutments without disintegrating armor-layer in the downstream of the scour hole. Case 2 prevailed for the approaching flow condition $u_*/u_{*ca} = 0.8$. For $d_g > 2$ mm, a secondary armor-layer, which covered almost half portion of the scour hole, developed posing relatively less resistance to the progress of scouring [Fig. 6.50(b)]. When the approaching flow condition became close to the critical condition of the armor-layer particles, that is $u_*/u_{*ca} \geq 0.9$, case 3 was observed with completely disintegrating armor-layer in the downstream of the scour hole. The secondary armor-layer, for $d_g > 2$ mm, was mainly concentrated to the lower portion of the scour hole near the upstream base of abutments [Fig. 6.50(c)].

6.8.3.2 Effect of Armor-Layer on Scour Depth

Fig. 6.51 depicts the variations of scour depth $\hat{d}_{sa}$ (= d_{sa}/l) at 45° wing-wall abutments with $\tilde{d}_g$ for different $\hat{h}$ (= h_1/l), u_*/u_{*ca}, and $\hat{t}$ (= t/d_g; where t = thickness of armor-layer), showing the smooth curves drawn through the plotted points [data of Dey and Barbhuiya (2004b)] to have a clear idea of the dependency of different parameters on $\hat{d}_{sa}$. In Fig. 6.51, two points are plotted in some plots for the same value of $\tilde{d}_g$ due to different $\hat{t}$ resulting in different values of $\hat{d}_{sa}$. In general, the scour depth $\hat{d}_{sa}$ for $\hat{t} < 2$ (shown by the broken line curves) is greater than that for $\hat{t} > 2$ (shown by the firm line curves). Because more sediment particles are supplied by a relatively thick armor-layer into the scour hole to form a secondary-armor layer resulting in a lesser scour depth for the same value of $\tilde{d}_g$. The scour depth $\hat{d}_{sa}$ decreases with an increase in $\tilde{d}_g$ up to $\tilde{d}_g$ = 4-5, and then $\hat{d}_{sa}$ increases with further increase in $\tilde{d}_g$ to form a second peak of the curve at $\tilde{d}_g$ = 6-7. Thereafter, $\hat{d}_{sa}$ again decreases up to $\tilde{d}_g$ = 9, and then $\hat{d}_{sa}$ gradually increases at a feeble rate. In general, scour depths $\hat{d}_{sa}$ for $\tilde{d}_g > 9$ (ripple forming sediments) are less than that for $\tilde{d}_g < 9$. It confirms, as

was shown by Ettema (1980), and Raudkivi and Ettema (1983, 1985), that the clear-water scour depth in ripple forming sediments is less than that in sediments, which do not form ripples. The formation of secondary armor-layer resists the rate of increase of $\hat{d}_{sa}$ with an increase in $\tilde{d}_g$ for $\tilde{d}_g > 9$. Further, the increase in scour depth $\hat{d}_{sa}$ with an increase in $\hat{h}$ and u_*/u_{*ca} is observed. It is important to mention that the scour depth in armored beds is significantly greater than that in uniform sediments.

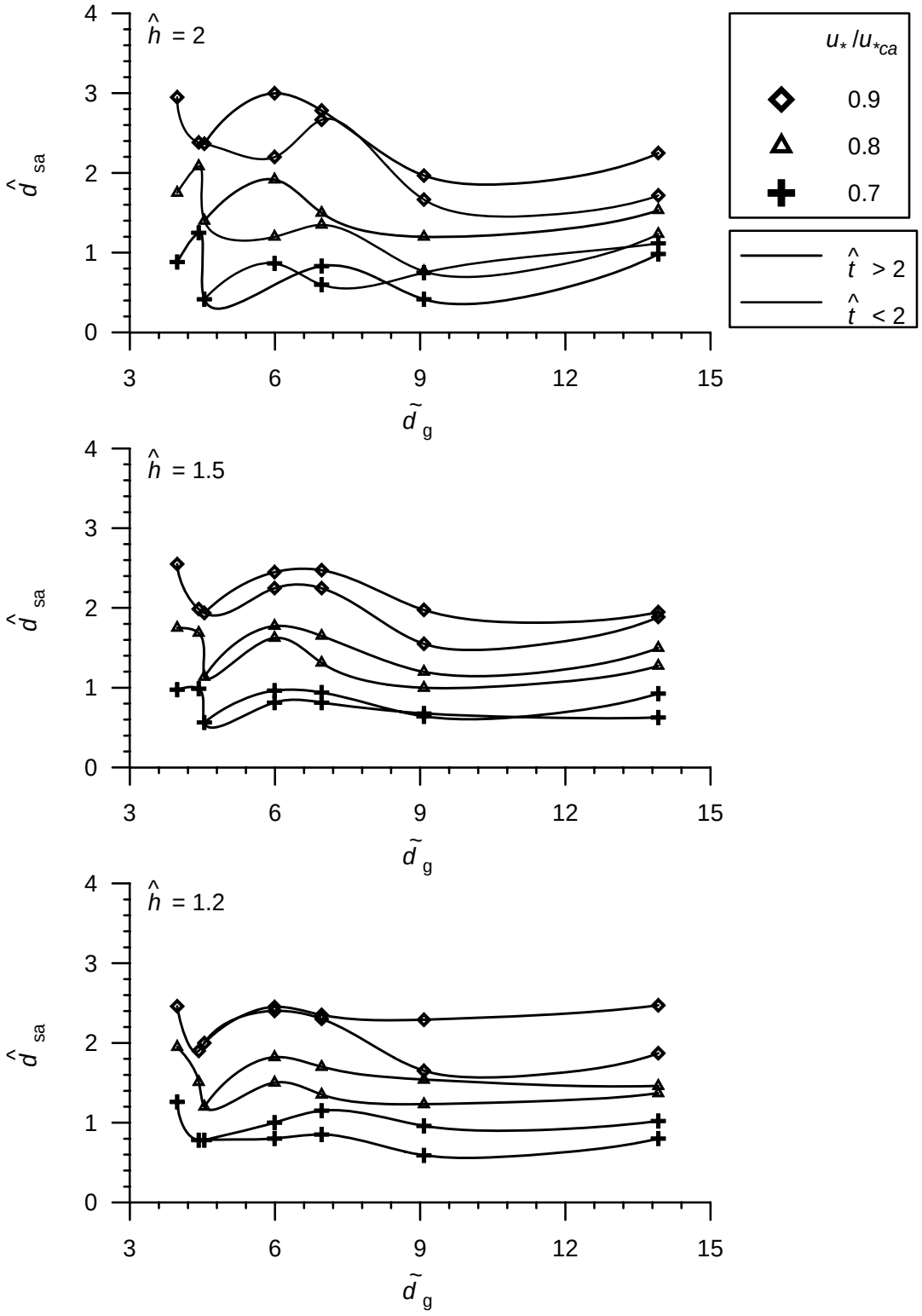

Fig. 6.51 Variations of scour depth $\hat{d}_{sa}$ with $\tilde{d}_g$ for different $\hat{h}$, $\hat{t}$, and u_*/u_{*ca} for 45° wing-wall abutments (after Dey and Barbhuiya 2004b)

6.8.3.3 Maximum Equilibrium Scour Depth

The equations for maximum equilibrium scour depths for different abutments obtained by regression analysis of the experimental data of Dey and Barbhuiya (2004b) are

$$\hat{d}_{sam} = 4.42F_{ca}^{0.266}\hat{h}^{0.195}\hat{t}^{-0.147}\hat{d}_g^{-0.117} \quad \text{for vertical-wall} \quad (6.95a)$$

$$\hat{d}_{sam} = 5.28F_{ca}^{0.266}\hat{h}^{0.207}\hat{t}^{-0.306}\hat{d}_g^{-0.211} \quad \text{for } 45^o \text{ wing-wall} \quad (6.95b)$$

$$\hat{d}_{sam} = 3.582F_{ca}^{0.185}\hat{h}^{0.165}\hat{t}^{-0.151}\hat{d}_g^{-0.135} \quad \text{for semicircular} \quad (6.95c)$$

where $\hat{d}_{sam} = d_{sam}/l$; and $F_{ca} = U_{ca}/(\Delta g l)^{0.5}$, that is the critical abutment Froude number.

6.9 References

Ahmed, F., and Rajaratnam, N. (1998). "Flow around bridge piers." *J. Hydraul. Eng.*, 124(3), 288-300.

Ahmed, F., and Rajaratnam, N. (2000). "Observations on flow around bridge abutment." *J. Eng. Mech.*, 126(1), 51-59.

Alix, T., Moncada, M., and Julián, A. P. (1999). "Scour below pipeline in river crossings." *J. Hydraul. Eng.*, 125(9), 953-958.

Ashida, K. (1963). "Study on the stable channel through constrictions." *Annual Report*, Disaster Prevention Research Institute, Kyoto University, July, 312-327 (in Japanese).

Barbhuiya, A. K. (2003). "Clear water scour at abutments." *PhD thesis*, Indian Institute of Technology, Kharagpur, India.

Barbhuiya, A. K., and Dey, S. (2004). "Local scour at abutments: a review." *Sadhana, Proc. Indian Acad. Sci.,* 29(Oct.), 449-476.

Bijker, E. W., and Leeuwestein, W. (1984). "Interaction between pipeline and the seabed under the influence of waves and current." *Seabed Mechanics, Proc. Symp. IUTAM/IUGG*. International Union of Theoretical and Applied Mechanics / International Union of Geology and Geophysics, 235-242.

Bormann, N. E., and Julien, P. Y. (1991). "Scour downstream of grade-control structures." *J. Hydraul. Eng.*, 117(5), 579-594.

Breusers, H. N. C. (1965). "Scour around drilling platforms." *IAHR Bulletin Hydraul. Res.*, 19, 276.

Breusers, H. N. C., Nicollet, G., and Shen, H. W. (1977). "Local scour around cylindrical piers." *J. Hydraul. Res.*, 15(3), 211-252.

Breusers, H. N. C., and Raudkivi, A. J. (1991). *Scouring*. IAHR Hydraulic Structures Design Manual, Vol. 2, A. A. Balkema, Rotterdam, The Netherlands.

Chao, J. L., and Hennessy, P. V. (1972). "Local scour under ocean outfall pipeline." *J. Wat. Poll. Control Fed.*, 44(7), 1443-1447.

Chiew, Y. M. (1991). "Prediction of maximum scour depth at submarine pipelines." *J. Hydraul. Eng.*, 117(4), 452-466.

Dargahi, B. (1982). "Local scouring around bridge piers - a review of practice and theory." *Bull. No. 114*, Hydraulic Laboratory, Royal Institute of Technology, Stockholm, Sweden.

Dey, S. (1991). "Clear water scour around circular bridge piers: a model." *PhD thesis*, Indian Institute of Technology, Kharagpur, India.

Dey, S. (1995). "Three-dimensional vortex flow field around a circular cylinder in a quasi-equilibrium scour hole." *Sadhana, Proc. Indian Acad. Sci.,* 20(Dec.), 871–885.

Dey, S. (1997a). "Local scour at piers, part I: a review of development of research." *Int. J. Sediment Res*., 12(2), 23-46.

Dey, S. (1997b). "Local scour at piers, part II: bibliography." *Int. J. Sediment Res.*, 12(2), 47-57.

Dey, S. (1999). "Time-variation of scour in the vicinity of circular piers." *J. Wat. Maritime Eng.*, *Proc. Inst. Civ. Eng.*, 136(June), 67-75.

Dey, S. (2003a). "Incipient motion of bivalve shells on sand beds under flowing water." *J. Eng*. *Mech.*, 129(2), 232-240.

Dey, S. (2003b). "Threshold of sediment motion on combined transverse and longitudinal sloping beds." *J. Hydraul*. *Res.*, 41(4), 405-415.

Dey, S., and Barbhuiya, A. K. (2004a). "Clear water scour at abutments." *J. Wat. Management*, *Proc. Inst. Civ. Eng.*, 157(June), 77-97.

Dey, S., and Barbhuiya, A. K. (2004b). "Clear water scour at abutments in thinly armored beds." *J. Hydraul. Eng.*, 130(7), 622-634.

Dey, S., and Barbhuiya, A. K. (2006). "Clear water scour at abutments in thinly armored." *J. Hydraul. Res*, 44, in press.

Dey, S., and Bose, S. K. (1994). "Bed shear in equilibrium scour around a circular cylinder embedded in loose bed." *Appl. Math. Modelling*, 18(5), 265-273.

Dey, S., Bose, S. K., and Sastry, G. L. N. (1995). "Clear water scour at circular piers: a model." *J. Hydraul. Eng*., 121(12), 869-876.

Dey, S., and Debnath, K. (2001). "Sediment pickup on streamwise sloping beds." *J. Irrig. Drain. Eng.,* 127(1), 39-43.

Dey, S., and Kar, S. K. (1995). "Bed shear in evolving scour at a cylinder: a theoretical approach." *Int. J. Sediment Res.*, 10(1), 13-31.

Dey, S., and Raikar, R. V. (2005). "Scour in long contractions." *J. Hydraul. Eng*., 131(12), 1036-1049.

Dey, S., and Raikar, R. V. (2006). "Live-bed scour in long contractions." *Int. J. Sediment Res*., 21(1), in press.

Dey, S., and Sarkar, A. (2006). "Scour downstream of an apron due to submerged horizontal jets." *J. Hydraul. Eng*., 132(3).

Engelund, F., and Fredsøe, J. (1976). "A sediment transport model for straight alluvial channels." *Nordic Hydrol.*, 7, 293-306.

Ettema, R. (1980). "Scour at bridge piers." *Report No. 216*, School of Engineering, University of Auckland, Auckland, New Zealand.

Fahlbusch, F. E. (1994). "Scour in rock riverbeds downstream of large dams." *Int. J. Hydropower Dams,* 1(4), 30-32.

Froehlich, D. C. (1989). "Local scour at bridge abutments." *Proc., Nat. Conf. Hydraul. Eng.*, ed. M. A. Ports, ASCE, New Orleans, 13-18.

Froehlich, D. C. (1995). "Armor-limited clear-water contraction scour at bridges." *J. Hydraul. Eng.*, 121(6), 490-493.

Gill, M. A. (1981). "Bed erosion in rectangular long constriction." *J. Hydraul. Div.*, *Am. Soc. Civ. Eng.*, 107(3), 273-284.

Graf, W. H. (2003). *Fluvial hydraulics*. John Wiley and Sons, Chichester, England.

Graf, W. H., and Istiarto, I. (2002). "Flow pattern in the scour hole around a cylinder." *J. Hydraul. Res.*, 40(1), 13-20.

Hoffmans, H. N. C. (1997). "Jet scour in equilibrium phase." *J. Hydraul. Eng.*, 124(4), 430-437.

Hoffmans, G. J. C. M., and Verheij, H. C. (1997). *Scour manual*. A. A. Balkema, Rotterdam, The Netherlands.

Ibrahim, A., and Nalluri, C. (1986). "Scour prediction around marine pipelines." *Proc. 5th Int. Symp. Offshore, Mech. Arctic Eng.*, Tokyo, Japan, 679-684.

Kjeldsen, S. P., Gjørsvik, O., Bringaker, K. G., and Jacobsen, J. (1973). "Local scour near offshore pipelines." *Proc. 2nd Int. Conf. Port Ocean. Eng. Under Arctic Conditions*, University of Iceland, 308-331.

Komura, S. (1966). "Equilibrium depth of scour in long constrictions." *J. Hydraul. Div.*, *Am. Soc. Civ. Eng.*, 92(5), 17-37.

Kothyari, U. C., Garde, R. J., and Ranga Raju, K. G. (1992a). "Live-bed scour around cylindrical bridge piers." *J. Hydraul. Res.,* 30(5), 701-715.

Kothyari, U. C., Garde, R. J., and Ranga Raju, K. G. (1992b). "Temporal variation of scour around circular bridge piers." *J. Hydraul. Eng.,* 118(8), 1091-1106.

Kotoulas, D. (1967). "Das Kolkproblem unter besonderer Berücksichtigung der Faktoren Zeit und Geschiebemischung im Rahmen der Wildbachverbauung." *Dissertation*, *Prom. 3983*, Technischen Hochschule Zürich, Switzerland.

Kristiansen, Ø. (1988). "Current induced vibrations of pipelines on a sandy bottom." *PhD thesis*, University of Trondheim, Trondheim, Norway.

Kwan, T. F. (1988). "A study of abutment scour." *Report No. 451*, School of Engineering, University of Auckland, Auckland, New Zealand.

Kwan, T. F., and Melville, B. W. (1994). "Local scour and flow measurements at bridge abutments." *J. Hydraul. Res.*, 32(5), 661-673.

Laursen, E. M. (1963). "An analysis of relief bridge scour." *J. Hydraul. Div.*, *Am. Soc. Civ. Eng.*, 89(3), 93-118.

Laursen, E. M., and Toch, A. (1956). "Scour around bridge piers and abutments." *Bulletin No. 4,* Iowa Highway Research Board.

Lim, S. Y. (1993). "Clear water scour in long contractions." *J. Wat. Maritime Eng.*, *Proc. Inst. Civ. Eng.*, 101(June), 93-98.

Lucassen, R. J. (1984). "Scour underneath submarine pipelines." *Report No. PL-4 2A*, Netherlands Marine Tech. Res., Netherlands Industrial Council for Oceanography, Delft University of Technology, Delft, the Netherlands.

Macky, G. H. (1990). "Survey of roading expenditure due to scour." *C. R. 90.09*, Department of Scientific and Industrial Research, Hydrology Center, Christchurch, New Zealand.

Mao, Y. (1986). "The interaction between a pipeline and an erodible bed." *Series Paper No. 39*, Institute of Hydrodynamics and Hydraulic Engineering, Technical University of Denmark (DTU), Lyngby, Denmark.

Melville, B. W. (1975). "Scour at bridge sites." *Report No. 117*, School of Engineering, University of Auckland, Auckland, New Zealand.

Melville, B. W. (1997). "Pier and abutment scour: integrated approach." *J. Hydraul. Eng*., 123(2), 125-136.

Melville, B. W., and Coleman, S. E. (2000). *Bridge scour*. Water Resources Publications, Fort Collins, Colorado, USA.

Melville, B. W., and Raudkivi, R. J. (1977). "Flow characteristics in local scour at bridge piers." *J. Hydraul. Res*., 15(4), 373-380.

Raikar, R. V. (2006). "Characteristics of flow over gravel-beds and scour within contractions and at piers." *PhD Thesis*, Indian Institute of Technology, Kharagpur, India.

Raikar, R. V., and Dey, S. (2004). "Flow field in scoured zone of channel contractions." *Int. J. Sediment Res*., 19(4), 292-311.

Raikar, R. V., and Dey, S. (2005a). "Clear-water scour at bridge piers in fine and medium gravel-beds." *Can. J. Civil Eng.*, 32(4), 775-781.

Raikar, R. V., and Dey, S. (2005b). "Scour of gravel beds at bridge piers and abutments." *J. Wat. Management*, *Inst. Civ. Eng.*, 158(Dec.), 157-162.

Raikar, R. V., and Dey, S. (2006). "Pier scour and thinly layered-bed scour within a long contraction." *Can. J. Civil Eng.*, 33, in press.

Rajarathnam, N., and Berry, B. (1977). "Erosion by circular turbulent wall jets." *J. Hydraul. Res.*, 15(3), 277-289.

Raudkivi, A. J. (1986). "Functional trends of scour at bridge piers." *J. Hydraul. Eng*., 112(1), 1-13.

Raudkivi, A. J., and Ettema, R. (1983). "Clear water scour at cylindrical piers." *J. Hydraul. Eng*., 109(3), 338-350.

Raudkivi, A. J., and Ettema, R. (1985). "Scour at cylindrical bridge piers in armored beds." *J. Hydraul. Eng*., 111(4), 713-731.

Richardson, E. V., and Davis, S. R. (2001). "Evaluating scour at bridges." *HEC18 FHWA NHI-001*, Federal Highway Administration, US Department of Transportation, Washington, DC.

Richardson, E. V., Harrison, L. J., Richardson, J. R., and Davies, S. R. (1993). "Evaluating scour at bridges." *Publ. FHWA-IP-90-017,* Federal Highway Administration, Washington, DC.

Ruff, J. F., Abt, S. R., Mendoza, C., Shaikh, A., and Kloberdanz, R. (1982). "Scour at culvert outlets in mixed bed materials." *Report FHWA/RD-82/011*, Colorado State University, Fort Collins, Colorado.

Sarkar, A. (2005). "Scour downstream of an apron and characteristics of submerged horizontal jet over rough and sudden changes from smooth to rough beds." *PhD thesis*, Indian Institute of Technology, Kharagpur, India.

Schoklitsch, A. (1932). "Kolkbildung unter Überfallstrahlen." *Die Wasserwirtschaft*, 24, 341-343.

Smith, C. D. (1967). "Simplified design for flume inlets." *J. Hydraul. Div., Am. Soc. Civ. Eng.*, 93(6), 25-34.

Stein, O. R., Julien, P. Y., and Alonso, C. V. (1993). "Mechanics of jet scour downstream of a headcut." *J. Hydraul. Res.*, 31(6), 723-738.

Straub, L. G. (1934). "Effect of channel contraction works upon regimen of movable bed streams." *Trans. Am. Geophys. Union*, Part 2, 454-463.

Sumer, B. M., Christiansen, N., and Fredsøe, J. (1993). "Influence of cross section on wave scour around piles." *J. Waterw., Port, Coastal, Ocean Eng.,* 119(5), 477-495.

Sumer, B. M., and Fredsøe, J. (1990). "Scour below pipelines in waves." *J. Waterw., Port, Coastal, Ocean Eng.,* 116(3), 307-323.

Sumer, B. M., and Fredsøe, J. (2002). *The mechanics of scour in the marine environment.* World Scientific Publishing Company Private Limited, Singapore.

Sumer, B. M., Truelsen, C., Sicmann, T., and Fredsøe, J. (2001). "Onset of scour below pipelines and selfburial." *Coastal Eng.*, 42(4), 213-235.

Tseng, M. H., Yen, C. L., and Song, C. S. (2000). "Computation of three-dimensional flow around square and circular piers." *Int. J. Numerical Methods Fluids*, 34(3), 207-227.

van Rijn, L. C. (1984). "Sediment transport, part I: bed-load transport." *J. Hydraul. Eng.*, 110(10), 1431-1456.

Vanoni, V. A. (1975). "Sedimentation Engineering." *ASCE Manual No. 54*. ASCE, New York.

Webby, M. G. (1984). "General scour at contraction." *RRU Bulletin 73*, National Roads Board, Bridge Design and Research Seminar, New Zealand, 109-118.

Yalin, M. S. (1977). *Mechanics of sediment transport*. Pergamon Press, New York, NY.